TRW Defense &
Space System Group
One Space Park
Redondo Beach, CA 90278

Final Report

Space Power Distribution System Technology

Volume 1 Reference EPS Design

TRW Report Number 34579-6001-UT-00

March 1983

Contract NAS8-33198

Prepared for
George C. Marshall Space Flight Center
National Aeronautics and Space Administration
Marshall Space Flight Center, Alabama 35812

TRW Defense &
Space System Group
One Space Park
Redondo Beach, CA 90278

TRW

Final Report

Space Power Distribution System Technology

Volume 1 Reference EPS Design

TRW Report Number 34579-6001-UT-00

March 1983

Contract NAS8-33198

Prepared for
George C. Marshall Space Flight Center
National Aeronautics and Space Administration
Marshall Space Flight Center, Alabama 35812

FOREWORD

This report documents in three volumes the work performed by TRW Electronics and Defense Sector, Redondo Beach, California, for George C. Marshall Space Flight Center (NASA/MSFC), Huntsville, Alabama, under contract NAS8-33198 (TRW Sales Number 34579).

Volume 1, "Reference EPS Design," summarizes the work under Task 1, System Design and Technology Development; Volume 2, Autonomous Power Management, summarizes the work under Task 2, Power Management Subsystem Development; and Volume 3, Test Facility Design, summarizes the work under Task 3, AMPS Test Facility. This final report is submitted in compliance with the contract statement of work and covers the entire period of performance from 1978 December 05 through 1982 March 31.

These three tasks were structured to define, develop, and demonstrate technology for autonomous management of complex multi-hundred-kilowatt electrical power subsystems for orbital spacecraft. Initially, a conceptual design of a reference electrical power subsystem was developed from spacecraft level life cycle cost analyses of 1985-86 technology for solar array, energy storage, power distribution, shuttle transportation, and orbital drag makeup propulsion (Volume 1). This reference electrical power subsystem was subsequently utilized to quantify the benefits of the power management approach and to demonstrate the power management subsystem concept (Volume 2). It is important to recognize that the resultant power management technology (strategies and hardware) has application to a broad spectrum of electrical power systems and is independent of power level, distribution voltage and form (ac or dc), payload type, spacecraft mission, and orbital parameters.

This study was managed for TRW by Charles Sollo of the Electrical Power Systems Laboratory, and for NASA/MSFC by Jim Graves of the Power Branch. The principal contributors for this technical study task and preparation of this report volume include D. Kent Decker, Marshall D. Cannady, John E. Cassinelli, Bertrand F. Farber, Charles Lurie, Gerald W. Fleck, Jack W. Lepisto, Alan Massner, and Paul F. Ritterman. Their participation is gratefully acknowledged.

CONTENTS

CONTENTS (Continued)

CONTENTS (Continued)

ILLUSTRATIONS

ILLUSTRATIONS (Continued)

ILLUSTRATIONS (Continued)

ILLUSTRATIONS (Continued)

ILLUSTRATIONS (Continued)

TABLES

TABLES (Continued)

TABLES (Continued)

1. INTRODUCTION

In the past, electrical power subsystems have usually been custom-designed for the spacecraft and satellites they serve. Tradeoffs and analyses leading to their definition have usually been directed toward the solution of specific design problems and constrained by the exigencies of project schedules and budgets. Only occasionally have there been opportunities to study space electrical power subsystems at a general level, and rarely with requirements imposed for Shuttle-era operation. The challenges faced by the system designer are threefold:

1) He must deal with many new technical problems that will develop as electrical subsystems are scaled from a few kilowatts to hundreds of kilowatts.

2) He must design for a manned environment and utility-type application - not only from the viewpoints of safety and in-orbit operation and maintenance, but also with an understanding that the orbiting base will likely have many uses throughout its life and consequently the power system must thus be adaptable to ever-changing payload requirements and evolving mission objectives.

3) He must design a system that is cost effective considering the Shuttle availability for resupply and replacement.

This task focuses upon developing the methodology for achieving minimum life cycle costs for a 250-kilowatt electrical power system in low earth orbit including the interactions with other subsystems, for example, thermal control, orbital altitude maintenance, and Shuttle transportation.

The electrical power subsystem represents a significant part of the cost, mass, and volume of the intrinsic space platform or space station. The solar array and energy storage components are major contributors to each of these parameters, and studies are underway to reduce their specific costs ($/W, $/Wh). This study focuses on minimizing the life cycle cost of the electrical power subsystem including the contributions of power source configuration, distribution topology, thermal support, orbital maintenance, resupply and replacement, and Shuttle transportation in addition to the basic solar array and energy storage costs.

This study task analyses, from a cost and technology viewpoint, the multi-hundred-kilowatt electrical power aspects of a mannable space platform in low earth orbit (LEO), initially operational circa 1988, with a technology readiness of 1985-1986. At the projected orbital altitudes Shuttle launch and servicing are technically and economically viable. Power generation is specified as photovoltaic consistent with projected NASA planning. The cost models and trades are based upon a zero interest rate (the government taxes concurrently as required), constant dollars (1980), and costs derived in the first half of 1980. Space platform utilization of up to 30 years is evaluated to fully understand the impact of resupply and replacement as satellite missions are extended. Such lifetimes are potentially realizable with Shuttle servicing capability and are economically desirable.

2. EXECUTIVE SUMMARY

One of the important elements in the design of low earth orbit space platforms and stations is minimum life cycle cost. The electrical power subsystem represents a significant part of the cost, mass, and volume of the intrinsic space platform. The solar array and energy storage components are major contributors to each of these parameters, and programs are underway to reduce their specific costs ($/W, $/Wh) and mass. This study task focuses on minimizing the life cycle cost of the electrical power subsystem including the contributions of power source configuration, distribution topology, thermal support, orbital altitude maintenance, resupply and replacement, and Shuttle transportation in addition to the basic solar array and energy storage costs.

This study analyzes, from a cost and technology viewpoint, the multi-hundred-kilowatt electrical power aspects of a mannable space platform (Figure 2-1) in low earth orbit (LEO), 100 to 400 nautical miles. At these orbital altitudes, Shuttle launch and servicing are viable. A technology readiness date of 1986 and initial operation in 1988 are specified in the work statement. Power generation is specified as photovoltaic consistent with projected NASA planning. The cost models and trades are based upon a zero interest rate (the government taxes concurrently as required), constant dollars (second quarter of 1980), and costs derived during the first half of 1980. Space platform utilization of up to 30 years is evaluated to fully understand the impact of resupply and replacement as the life of multipurpose satellite missions is extended. Such lifetimes are potentially realizable with Shuttle servicing capability and are economically desirable.

2.1 MULTICHANNEL POWER SUBSYSTEM

The space platform concept supports diverse, varying, and potentially many combinations of payloads. The tentative power requirements of identified potential payloads range from several hundred watts for scientific experiments to over 100 kilowatts for material processing (furnaces).

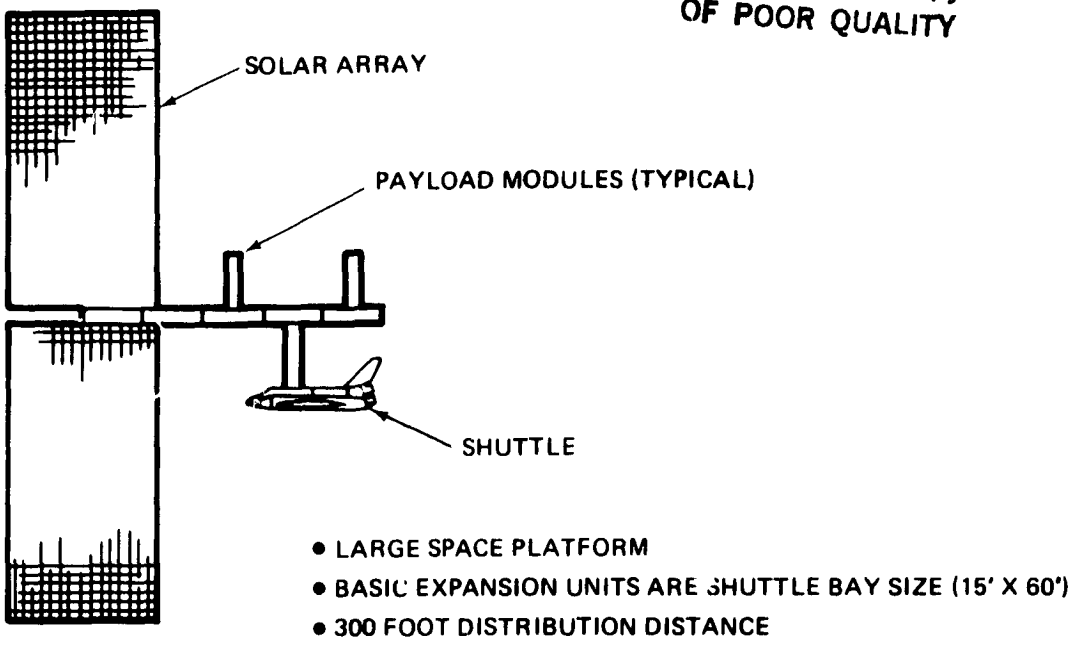

Figure 2-1. 250 kW Spacecraft Concept

However, these payload power requirements are the sum of many smaller equipment power demands generally ranging from 100 to 2000 watts. Hence, a multi-hundred-kilowatt electrical bus is not required to support these loads. Several lower power buses having 10- to 20-kilowatt capacity are suitable, provided the aggregate power of these smaller buses supports the total payload complement. This fact, coupled with the practical limitations in the foreseeable future on the size of energy storage components (battery cell capacity), directs the study reference design toward the multichannel concept for the electrical power subsystem.

The reference electrical power subsystem is configured as seventeen 16.7-kilowatt channels (Figure 2-2) to support 250 kilowatts of payload power demand and 25 kilowatts of housekeeping equipment -- predominantly liquid coolant pumps in the thermal subsystem. Each channel includes one 160-cell, 150-ampere-hour, nickel-hydrogen battery for energy storage in support of a 36-minute eclipse at full power (275 kilowatts). Each channel consists of one primary power bus that is electrically isolated from the other channels (no tie connections), but all channels utilize a common power return path. These isolated power channels are integrated into a cohesive operating utility by the Power Management Subsystem (Volume 2).

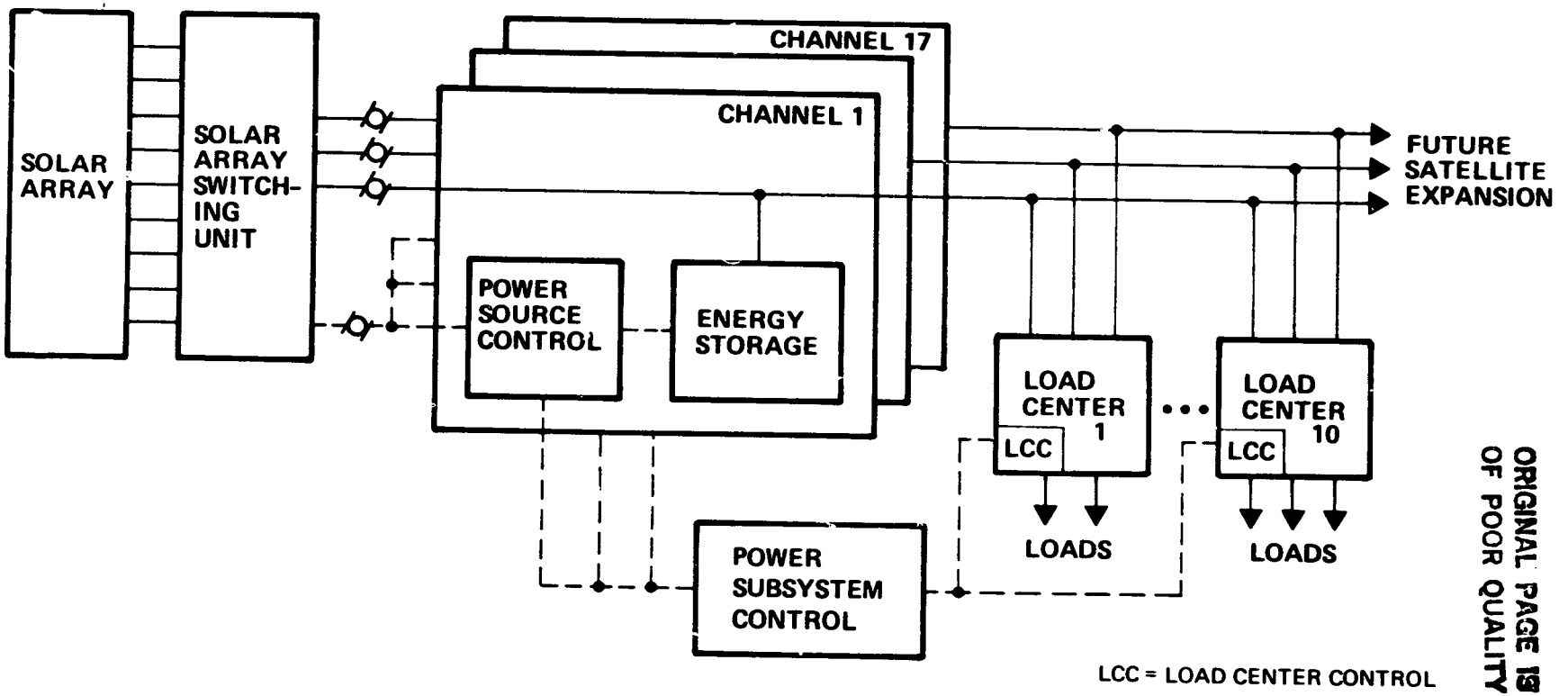

ORIGINAL PAGE IS OF POOR QUALITY

GENERATION – CASSEGRAIN CONCENTRATOR SOLAR ARRAY
ENERGY STORAGE – NICKEL-HYDROGEN BATTERY (160, 150-AH CELLS)
BATTERY CHARGER – SOLAR ARRAY SWITCHING UNIT
REGULATION – 220 ± 20 VOLTS (BATTERY CHARACTERISTICS)
POWER TRANSMISSION – DIRECT CURRENT AT SOURCE VOLTAGE
POWER DISTRIBUTION – DIRECT CURRENT AT SOURCE VOLTAGE
POWER PROCESSING – AS NEEDED WITHIN EACH PAYLOAD OR LOAD CENTER
CHANNEL QUANTITY – DEFINED BY BATTERY CAPACITY (17)
RELIABILITY – FAIL OPERATIONAL, FAIL SAFE
GRACEFUL CAPACITY DEGRADATION WITH FAILURES
LIFE – INDEFINITE; REPLACE FAILED UNIT AT NEXT SERVICE OPPORTUNITY

Figure 2-2. Multichannel Reference Electrical Power System Design

Power is generat . by a Cassegrain concentrator solar array composed of miniature elements. This solar array concept is selected for its projected cost advantage -- 30 $/W manufacturing cost. The generated power is controlled and allocated to the respective power channels by a solar array switching unit (SASU) in accordance with the needs of the payloads and batteries. This switching unit connects sufficient solar array segments to each power channel primary bus to provide the load power demand and the battery charging current of that channel. The Power Management Subsystem (PMS) monitors the loads, batteries, and solar array, and selects the appropriate switch closures to produce the desired solar array output current to each channel -- payload current plus desired battery charging current. The bus voltage therefore fluctuates from the low extreme of 200 volts at end of battery discharge to the upper extreme of 240 volts at end of recharge. Power transmission and distribution are at the power source voltage which is regulated by the voltage characteristics of the directly connected battery.

Multikilowatt space platform payloads are typically composed of several smaller individual loads in the range of 100 to 2000 watts each. Hence, power source buses of multi-hundred-kilowatt capacity are not required to support individual loads. The distribution approach developed herein incorporates 17 power source channels, each supported by a single, nickel-hydrogen battery with each power source channel forming a main distribution bus (Figure 2-2). Further, by providing alternate connecting options of each load to several main distribution buses, direct paralleling of the power source channels is not required (Figure 2-3). Parallel operation of batteries (without isolation by secondary power converters) is avoided, and redundancy is enhanced without adding power source capacity and incurring its cost. For very high power loads, power may be drawn from several power channels by paralleling the outputs of several programmable power processors (Figure 2-3). Reverse power flow is thereby precluded, and programmable power drain from the multiple source channels is attainable. Transformer isolation can be added to these processors if desired.

ORIGINAL PAGE IS
OF POOR QUALITY

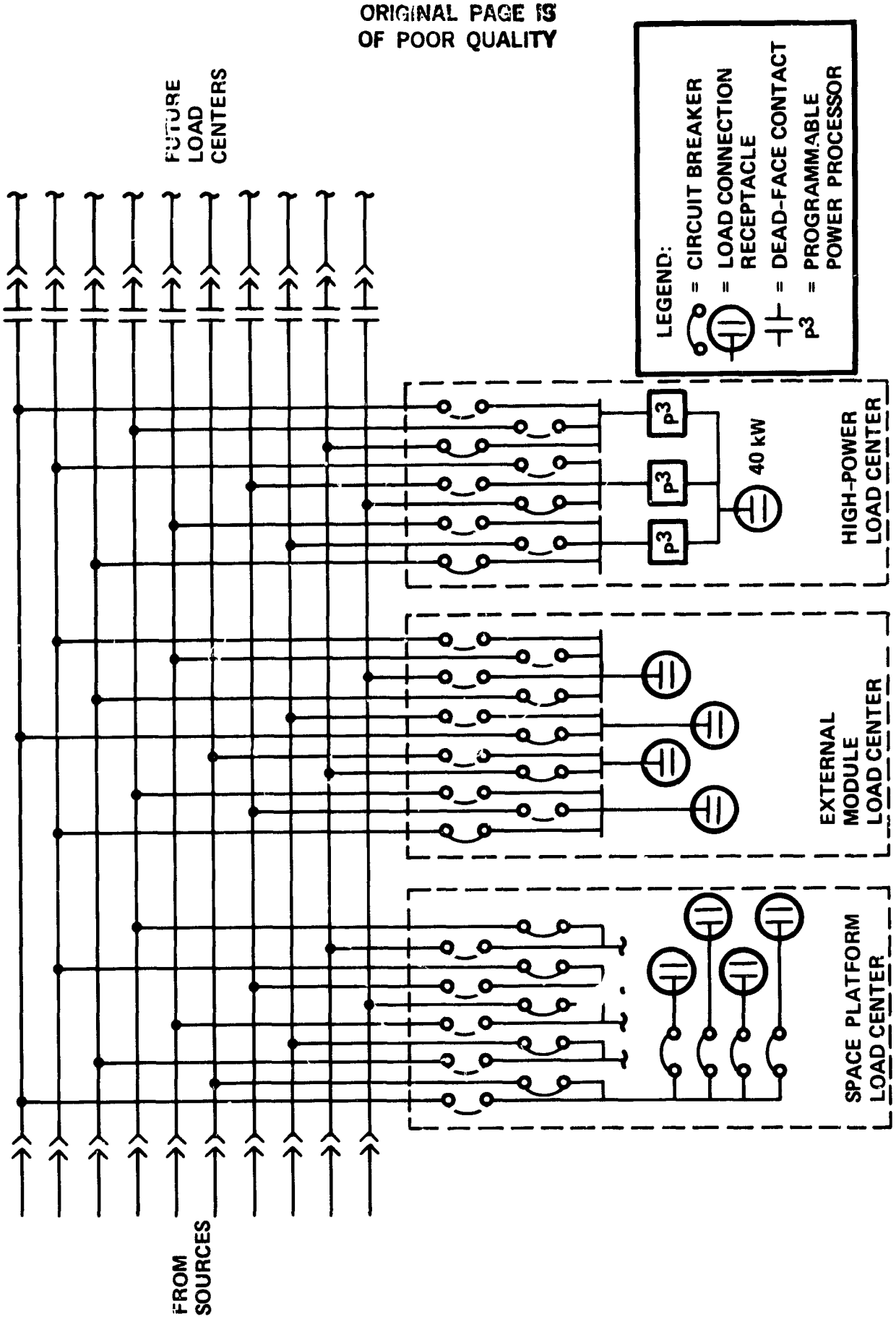

Figure 2-3. Power Distribution Concept

OGR.

2.2 ENERGY STORAGE SELECTION

Three energy storage concepts were compared based upon life cycle system costs and weights:

1) Nickel-cadmium batteries

2) Nickel-hydrogen batteries

3) Fuel cell plus electrolysis units.

In this comparison, the thermal support, solar array support, and altitude maintenance support for each energy storage concept is considered and included. The thermal equipment (heat exchangers and radiators) for waste heat dissipation from the energy storage units is identified and included. The solar array area required for the charging of each energy storage concept is also identified and included, but the solar array area providing direct support of the load during sunlight is not included. The solar array output is regulated to provide the energy storage charging needs as determined and controlled by the Power Management Subsystem. In addition, propulsion fuel, which is necessary to counteract the solar array drag and thereby maintain orbital altitude, is included.

The energy storage capacity is sized (Table 2-1) based upon a 250-kilowatt payload, a 36-minute eclipse (150 kWh), a nominal system voltage of 220 or 270 volts, and an appropriate depth of discharge. Optimum cost depth of discharge is applied for the nickel-cadmium (49 percent) and nickel-hydrogen (33 percent) batteries. A 200 kWh reactant supply is provided with the fuel cell plus electrolysis concept in order to provide some contingency reserve capacity (33 percent).

No spare battery redundancy is provided in the nickel-cadmium and nickel-hydrogen concepts. Loss of one battery can be accommodated by a temporary 6 percent increase in load on each of the remaining batteries. The battery depth of discharge will increase correspondingly from 33 to 35 percent for nickel-hydrogen; from 49 to 52 percent for nickel-cadmium. For the fuel cell plus electrolysis concept, only four fuel cell stacks and five electrolysis stacks are required. Loss of one unit would increase the load on the remainder by 33 and 25 percent, respectively. Hence, one additional fuel cell stack and one additional electrolysis stack is included in the basic power plant complement for reliability/redundancy needs to assure initial "fail operational" redundancy.

Table 2-1. Energy Storage Sizing Parameters
(250 kW Payload)

Parameter	Nickel Cadimum	Nickel Hydrogen	Fuel Cell Plus Electrolysis Unit≠
Energy Storage (Wh)	306,000	450,000	200,000
Depth of Discharge (%)	49	33	75
Average Life (yr)	2.75	7	4.6 (Stacks) 1.1 (Pumps)
Cell Size	100 Ah	150 Ah	270 amperes (Fuel Cells) 342 amperes (Electrolysis Units)
Cells/Unit	170	160	308 (Fuel Cells) 135 (Electrolysis Units)
Nominal Voltage (volts)	220	220	270
Unit Quantity	15	15	5 Fuel Cells* 6 Electrolysis Units*
Heat Losses (kW)	38**	32**	79 (Sunlight) 231 (Eclipse)
Temperature (°C)	0	0†	40/75
Input Power (kW)	229	220	430
Specific Weight (Wh/lb)	10	25	35††
Weight			
Initial (lb)	30,600	18,000	5,775
Replacements (lb)	334,000	77,000	38,700
Costs			
Initial (M$)	20.4	19.1	14.3
Replacements (M$)	223	82	87
Development (M$)	~1	<5	>50

*One unit added for reliability

**90-minute average

†Not optimized

††Not scalable

≠Data from GE report ECOS-12.

Comparison of the system level costs and weights of these energy storage options shows the nickel-hydrogen energy storage to be both the lightest and cheapest overall for a 30-year mission (Table 2-2). Initially, the three technologies are very close (Figures 2-4 and 2-5), and nickel-cadmium is competitive if the mission duration is sufficiently short to preclude resupply. The fuel-cell-plus-electrolysis technology would provide the lightest energy storage except for the extra propulsion fuel used to preclude the orbital decay in low earth orbit. The orbital decay produced by solar array drag reduces significantly for higher orbital altitudes. However, higher orbital altitudes significantly increase the total transportation cost of resupply, payload delivery and retrieval, and personnel transfer over an extended duration mission (e.g., 30 years). Optimum altitudes (Figure 2-6) appear to be near 215 nautical miles (400 kilometers. Hence, the nickel-hydrogen battery is chosen for energy storage of the reference electrical power system for the late 1980s. Advancement in fuel cell plus electrolysis unit system efficiency will change the supporting solar array and orbital altitude maintenance fuel sizing, weight, and costs. Therefore periodic review of this trade is warranted.

2.3 ELECTRICAL CONDUCTORS

Analysis of electrical conductor sizing for multikilowatt power transfer indicates the use of large cross-section copper conductors as the cost effective approach to minimum life cycle costs. As a by-product, regulation is improved, and distribution losses are reduced. In addition, the use of optimum conductor sizing in conjunction with a 300- to 500-foot distribution distance leads to direct energy distribution at the generation voltage of 220 $\pm$20 volts, direct current. Distribution costs are inversely proportional to voltage, but are sufficiently low at 220 volts for transmission distances of the order of 300 feet so that conversion costs to provide higher transmission voltages are not recovered.

The cost for electrical power transmission is composed of the conductor cost plus the incremental cost of power generation and energy storage to supply the transmission losses and of thermal control to dissipate these losses. In addition, the power conversion equipment must be increased to handle the increased electrical load due to these losses. As conductor size is increased, transmission losses decrease, and an optimum design

Table 2-2. Energy Storage Comparisons
(30-Year Duration)

Parameters	Nickel Cadmium	Nickel Hydrogen	Full Cell Plus Electrolysis
System Costs (M$)			
Energy Storage	243	101	101
Solar Array	18	18	35
Altitude Maintenance	53	51	99
Thermal Support	6	5	6
Recurring Cost	320	175	241
Development	1	5	50
Total	321	180	291
System Weight (lb)			
Energy Storage	364,600	95,000	44,500
Solar Array	14,700	14,100	27,600
Altitude Maintenance	108,800	104,500	214,700
Thermal Support	3,100	2,600	5,200
Total	491,200	216,200	282,000

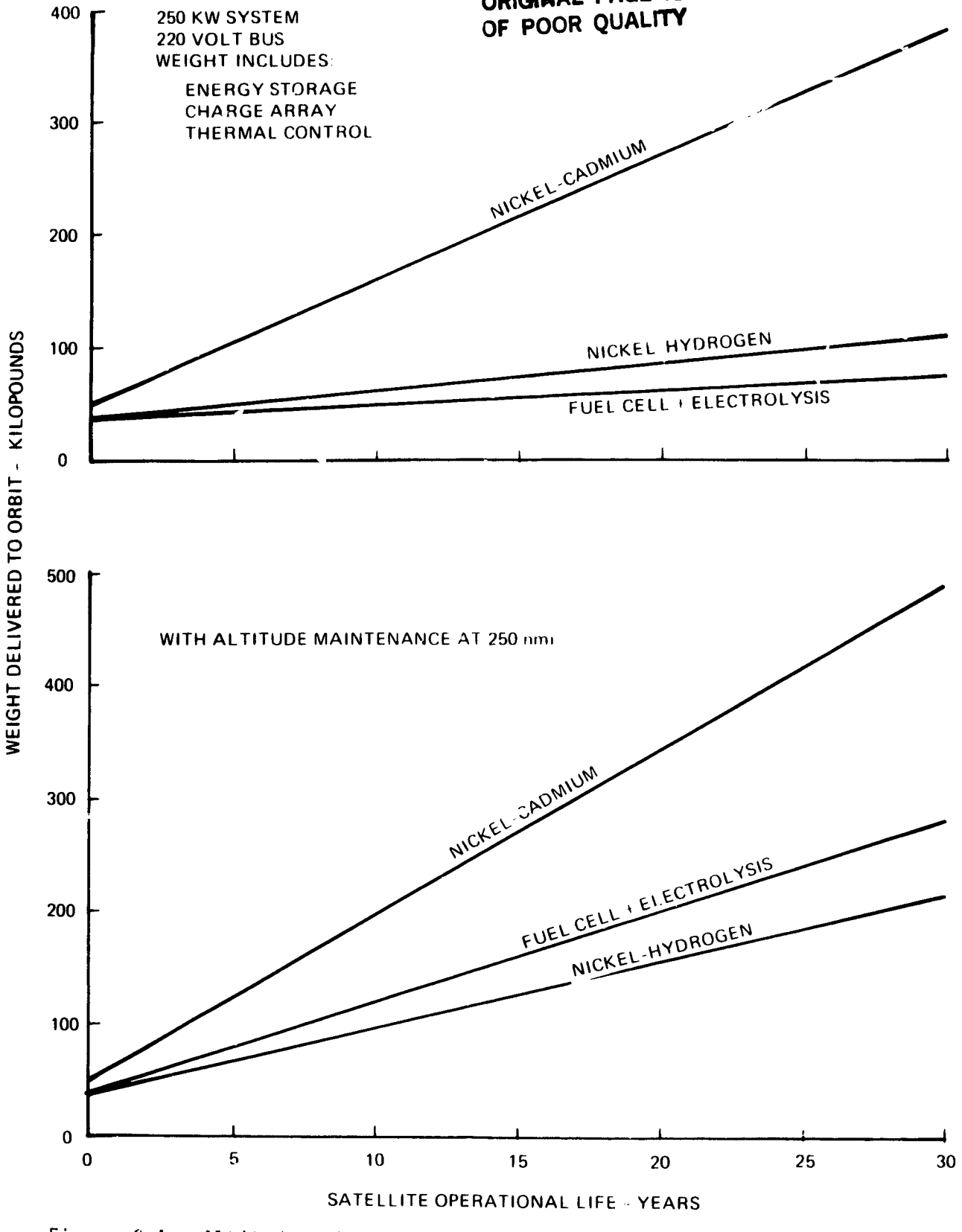

Figure 2-4. Altitude Maintenance Drives Energy Storage Weight Comparison

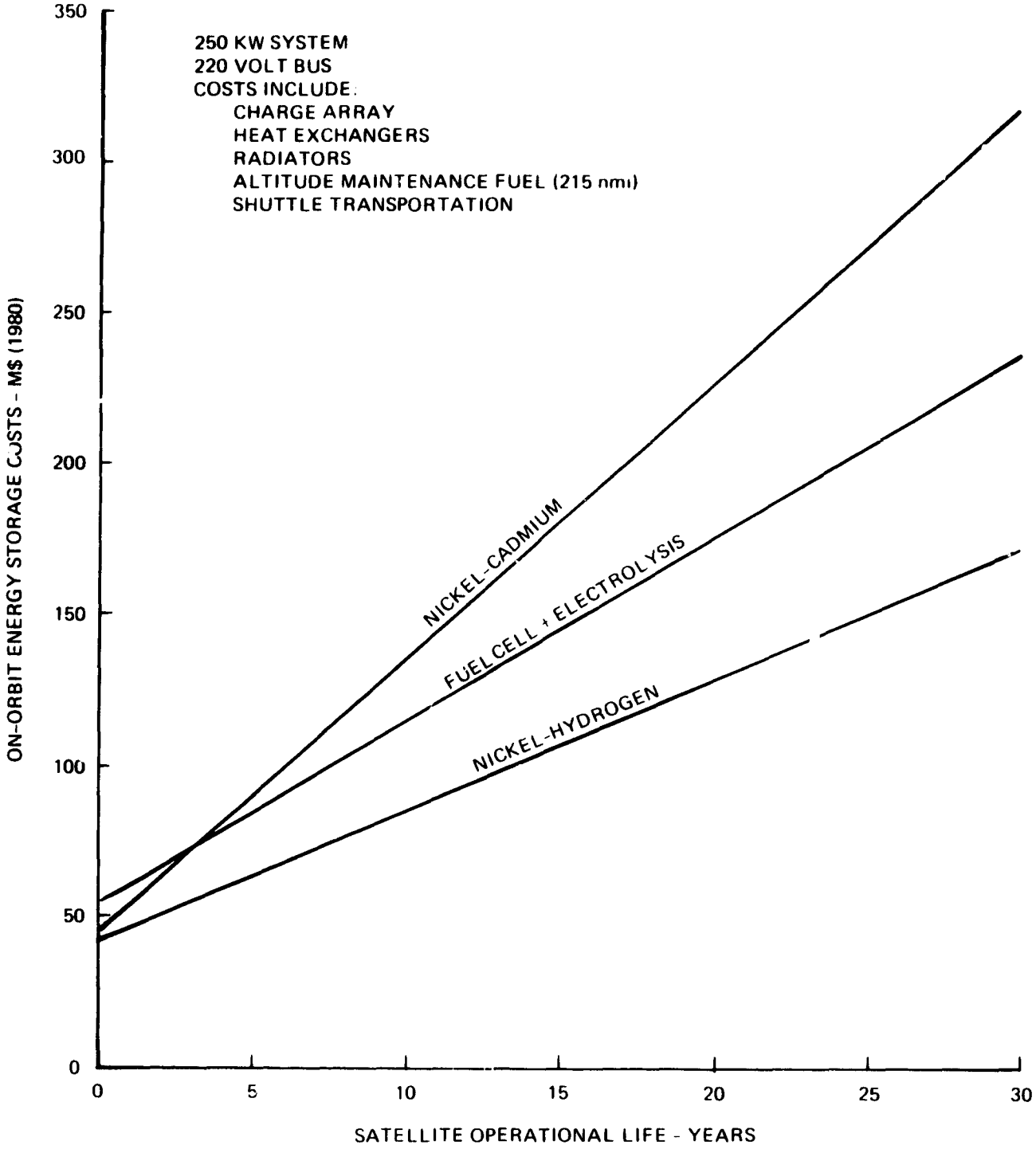

Figure 2-5. Nickel-Hydrogen is Lowest Cost Energy Storage System

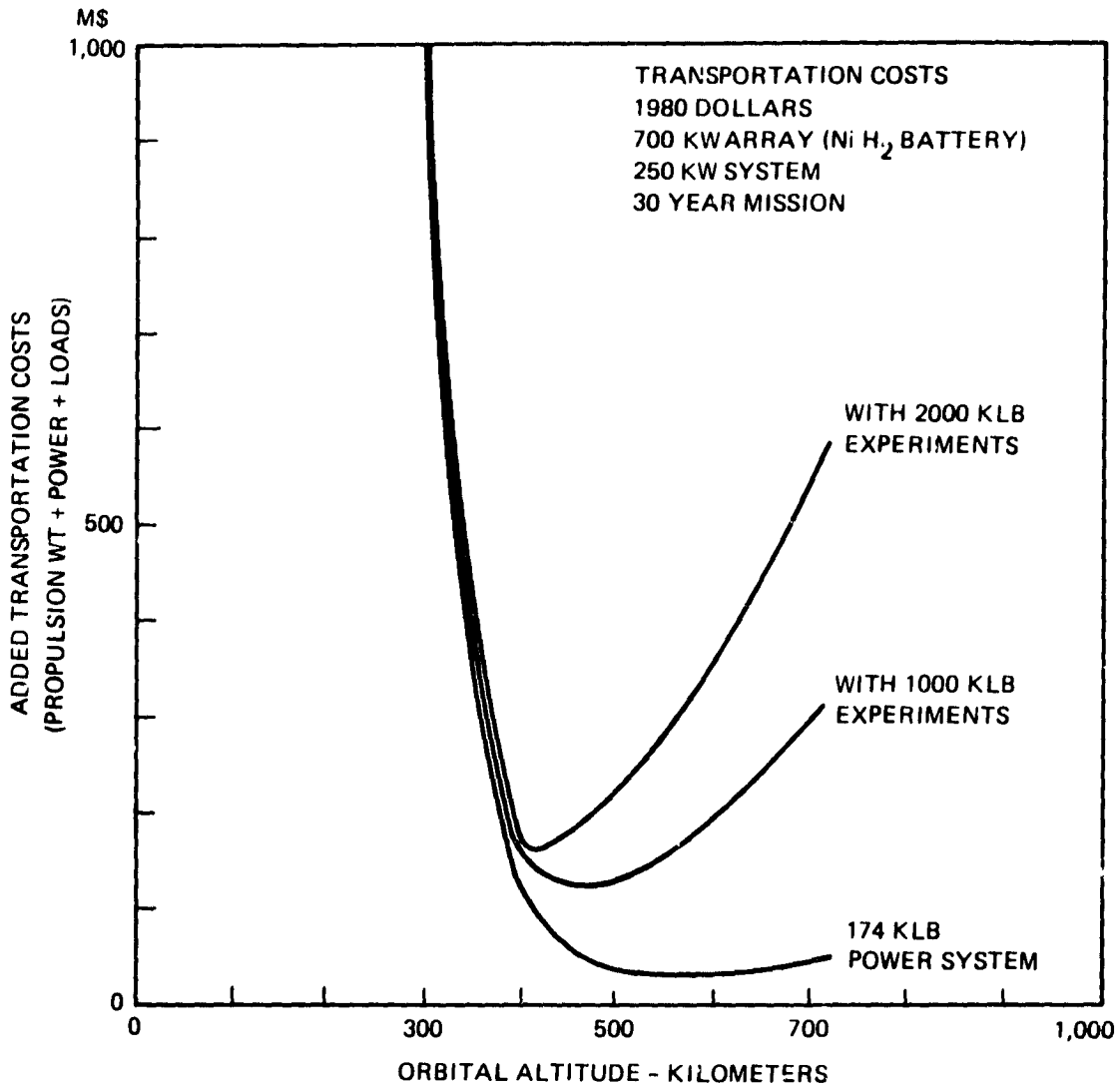

Figure 2-6. Optimum Altitude Near 400 km (215 nmi)

point exists. Surprisingly, the optimum conductor cross-sectional area is not dependent upon the distance of transmission nor upon regulation. Also, optimum conductor area is typically considerably larger than conductors sized for regulation requirements and thermal constraints.

The cost for electrical power transmission is the sum of five relatable cost terms:

$$C_{trans} = C_{wire} + C_{power\Delta} + C_{energy\Delta} + C_{thermal\Delta} + C_{conversion\Delta}$$

Each of these terms is complex but is related to the parameters of the transmission conductor under consideration (Appendix D). For simplification, the thermal and conversion incremental cost terms are neglected as a rigorous analysis has shown them to be insignificant compared to the solar array (power) and battery (energy) incremental cost terms. Differentiating with respect to conductor area, setting the result equal to zero, and solving yields the optimum-cost cross-sectional area (A_0) for transmission conductors:

$$A_0 = \frac{P}{V\varepsilon_2}\sqrt{\frac{\rho[\text{factor}]}{\sigma(C_{MW} + C_L)}}$$

where:

A_0 = conductor cross sectional area

σ = density

ρ = resistivity

P = payload power

V = transmission voltage

ε_2 = the efficiency of transmission to service (payload) power conversion

C_{ML} = Manufacturing cost of wire, \$/16

C_L = launch cost of wire weight, \$, 16

[factor is a constant for each specific application].

Note that the optimum-cost cross-sectional area (A_0) is independent of the transmission line distance! Further A_0 is directly related to the transmitted payload power (P) and inversely related to the transmission voltage (V) and transmission-to-service (payload) conversion efficiency (ε_2). With a transmission conductor of optimum-cost cross section (A_0), total transmission costs are directly related to transmission distance (ℓ), and inversely related to transmission voltage (Figure 2-7):

$$C_{trans} = 2 \frac{P\ell}{V\varepsilon_2} \sqrt{\rho\sigma(C_{MW} + C_L)} \cdot [factor]$$

The transmission cost is directly relaced to the factor $\sqrt{\rho\sigma(C_{MW} + C_L)}$. These are parameters of the conductor material (except for C_L). The comparison of conductor materials (Table 2-3), such that the factor $\sqrt{\rho\sigma(C_{MW} + C_L)}$ is minimized, indicates copper as the baseline conductor material. Pure aluminum conductors have a potential cost savings of 15 percent. This saving is not realizable due to electrical termination considerations for pure aluminum. Aluminum alloy is slightly more costly than copper due to the significantly increased resistivity of the alloy. However, utilizing aluminum structure of the satellite for power return offers a potential cost savings of 50 percent, an expected realizable cost savings of 40 to 45 percent, and warrants careful consideration.

2.4 ELECTRICAL TRANSMISSION AND DISTRIBUTION

Transmission and distribution of electrical power is at the battery voltage (220 ±20 volts) in the reference concept. Higher voltage alternatives employing up and down conversion (Table 2-4) do not provide a clear economic payback nor technical advantage. The life cycle cost for optimum cross-sectional conductors is only 5 M$ at the 200-volt transmission level. This low cost is due to the relatively short transmission distances (on the order of 300 feet) for the hypothesized space platform. The potential saving in conductor cost is, therefore, small (2-3 M$) compared to the added cost of source or central power conversion equipment including its power loss support (solar array, battery, thermal) - 5 M$ initially, 13 M$ over 30 years. Regulation at the payload is improved substantially (from 10 to 1.4 percent) with central power conversion. Potentially, regulation

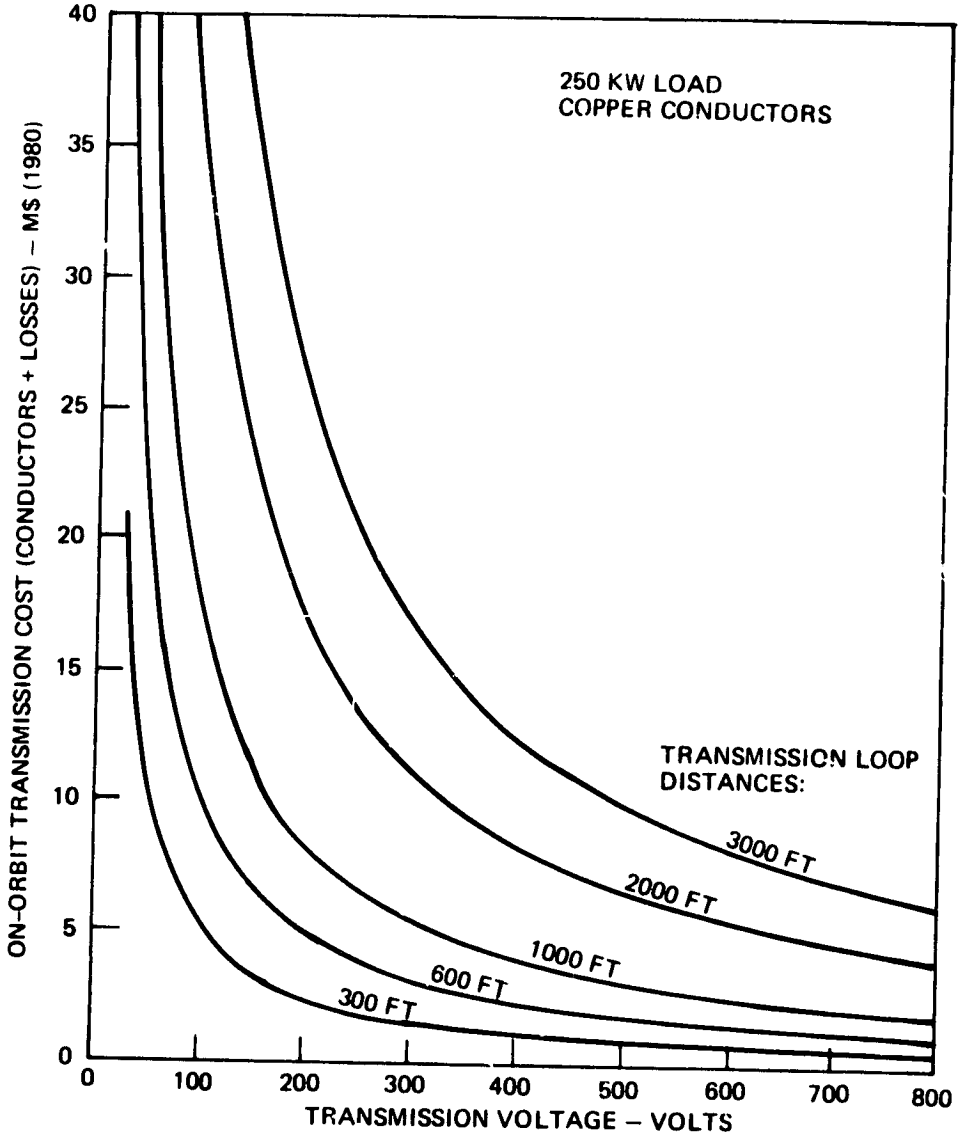

Figure 2-7. Costs Approximate 5 M$ with 220 ±20 Volt Transmission

could be avoided in the payloads. However, practical considerations, such as on/off control, overload protection, and fault isolation, suggest avoiding payload regulation is difficult to realize. A 30-year saving of 10 M$ in payload regulators is necessary to break even — possible, but highly uncertain, and a poor return on the initial investment. Hence, direct energy transmission at the source voltage, with payload power conversion added only as needed, is the economical approach.

Alternating current distribution at the common power frequencies of 60 and 400 hertz and at previously used spacecraft power frequencies of 1200, 1600, and 2400 hertz, in comparison to direct current distribution with dc-to-dc conversion at 10 to 250 kilohertz, is also unattractive. Alternating current conversion equipment is heavier, typically less efficient with sinusoidal wave form, and requires greater attention to electromagnetic compatibility than the direct current counterpart. Hence, transmission and distribution with alternating current at common power frequencies is costlier than the rejected central power conversion direct

GR.

Table 2-3. Reference Transmission Conductors are Copper

Conductor Material	Resistivity ρ μ ohm ft	Density σ lb/ft^3	Manufacturing Cost C_{MW} \$/lb	Relative Cost $\sqrt{\rho\sigma(C_{MW} + C_L)}$
Aluminum, pure	0.087	168	446	115
Aluminum alloy	0.130	174	431	142
Copper	0.056	555	135	136
Magnesium	0.146	108	695	135
Silver	0.0522	651	165	146
Sodium	0.138	60.2	1250	119
Solder	0.492	551	136	402

C_L = 462 \$/lb, Shuttle Launch Cost

$$C_{MW} = \frac{\text{Bus Bar Cost + Installation Costs}}{\text{Bus Bar Weight}} = 135 \text{ \$/lb for copper}$$

Table 2-4. Source Voltage Transmission is Cheaper (250 kW, 300 Feet)

Parameter	Source Voltage		Central Conversion	Source Conversion
Source Voltage	100 V	200 V	200 V	200 V
Transmission Voltage	100 V	200 V	600 V	600 V
Peak Power	Battery Limited		Converter Limited	Converter Limited
Reliability	Source		Source - Converter	Source - 3 Conversions
Switch Gear	Medium Voltage		High Voltage	High Voltage
Losses	$I^2R = L$	L/2	L/6 + Converter Losses	L/6 + Conversion Losses
Conductor:				
Area	3.6 sq in	1.8 sq in	0.6 sq in	0.6 sq in
Weight	4600-8370 pounds	2,?0-4160 pounds	770 - 1400 pounds	770 - 1400 pounds
On-Orbit Cost (with losses)	6 - 10M$	3 - 5 M$	1 - 2 M$	1 - 2 M$
Conversion Costs:				
Initial	-	-	5 M$	8 M$
Life Cycle (with losses)	-	-	13 M$	18 M$
Total Transmission Cost	6 - 10 M$	3 - 5 M$	14 - 15 M$	19 - 20 M$
Regulation at Payloads	±11.6 percent	±10.3 percent	±1.4 percent	±1.4 percent
Payload Conversion	Include Preregulators		No Preregulators (difficult to prevent)	No Preregulators (difficult to prevent)

current conversion approach. Alternating current transmission and distribution at typical power frequencies is, therefore, also rejected in favor of the reference direct current transmission at the power source (generation and energy storage) voltage.

Regulation of the main distribution buses is determined by the inherent battery characteristics for the reference power subsystem. Active electronic regulation of these main distribution buses does improve central regulation at the payload from 11-13 to 1.8-3.6 percent. However, central regulation introduces added equipment and losses, and this increases the costs for the solar array, energy storage, and thermal control in addition to the cost of the central regulators. Payback for this regulation improvement is questionable. The costs must be saved in simpler payload power conversion (no preregulators), and this may be difficult to realize in practice.

2.5 TRANSMISSION VOLTAGE

Higher transmission and distribution voltages improve many of the parameters of the electrical power system:

a) Conductor size is reduced, $A_o = K_1 P/V$

b) Voltage regulation is improved, $\Delta V/V = K_2 \ell/V$

c) Power loss is reduced, $P_\ell = K_3 P\ell/V$

d) Channel capacity is increased, $P_c = K_4 V$

e) Transmission costs are reduced, $C_t = K_5 P\ell/V$

where P = rated power, ℓ = transmission length, and V = transmission voltage.

The importance of achieving increased channel capacity through higher power source voltages is often overlooked. Greater energy storage per channel reduces the quantity of channels for a given power level. Hence, the power source switch gear and ultimately power management software complexity are reduced. These also reduce the cost of a high-power multichannel system. Therefore, higher voltage is desirable, and the highest practical voltage, consistent with constraints, is selected as: 220 $\pm$20 volts.

Three major concerns limit the selection of increasingly higher voltages: personnel safety, semiconductor technology, and plasma interactions.

The selected operational voltage of 220 ±20 volts is in a comfortable range with benign plasma interaction, suitable semiconductor components under development, and acceptable personnel hazard. Further, this 220-volt level is sufficiently high to recover most of the transmission cost savings obtainable from a higher transmission voltage (Figure 2-7) at the anticipated distances of 300 feet for the 250-kilowatt power subsystem. That is, the transmission voltage of 220 ±20 volts for the reference power subsystem with transmission distances up to 300 feet (600-foot loop) is beyond the knee of the curve (Figure 2-7), and cost savings are substantially diminished as voltages are further increased.

2.6 TECHNOLOGY DEVELOPMENT

The economic cost (manufacturing, test, launch, operation, and resupply) of spacecraft electrical power production and distribution is high: 103 M$ initially, rising to 230 M$ at 30 years (Figure 2-8). This converts to 400 to 900 $/W of installed end-of-life capacity. Energy storage, solar array, and thermal control are the major contributors to these high costs. Lower electrical power costs require improvements in manufacturing efficiency and cell life and reduction in weight (launch cost) for nickel-hydrogen batteries, reduction in packaging volume (launch cost) and improved manufacturing efficiency for solar arrays, reduction in thermal radiator weight (launch cost), and extension of thermal pump life. Significant economic benefits remain in these areas but typically require commensurate investment.

Three major areas of technology development required for the 250-kilowatt power system are in progress:

1) Cassegrain mini-concentrator solar array, NAS8-34131

2) Solar array switching unit, NAS3-22656

3) Power subsystem management, NAS8-33198, NAS8-34539.

The development of the 150-ampere-hour nickel-hydrogen cell is also needed to reduce energy storage costs.

Additional development is required in support of power distribution technology to attain adequate switch gear, protection devices, high-power slip rings or roller rings, high-current connectors, and high-power

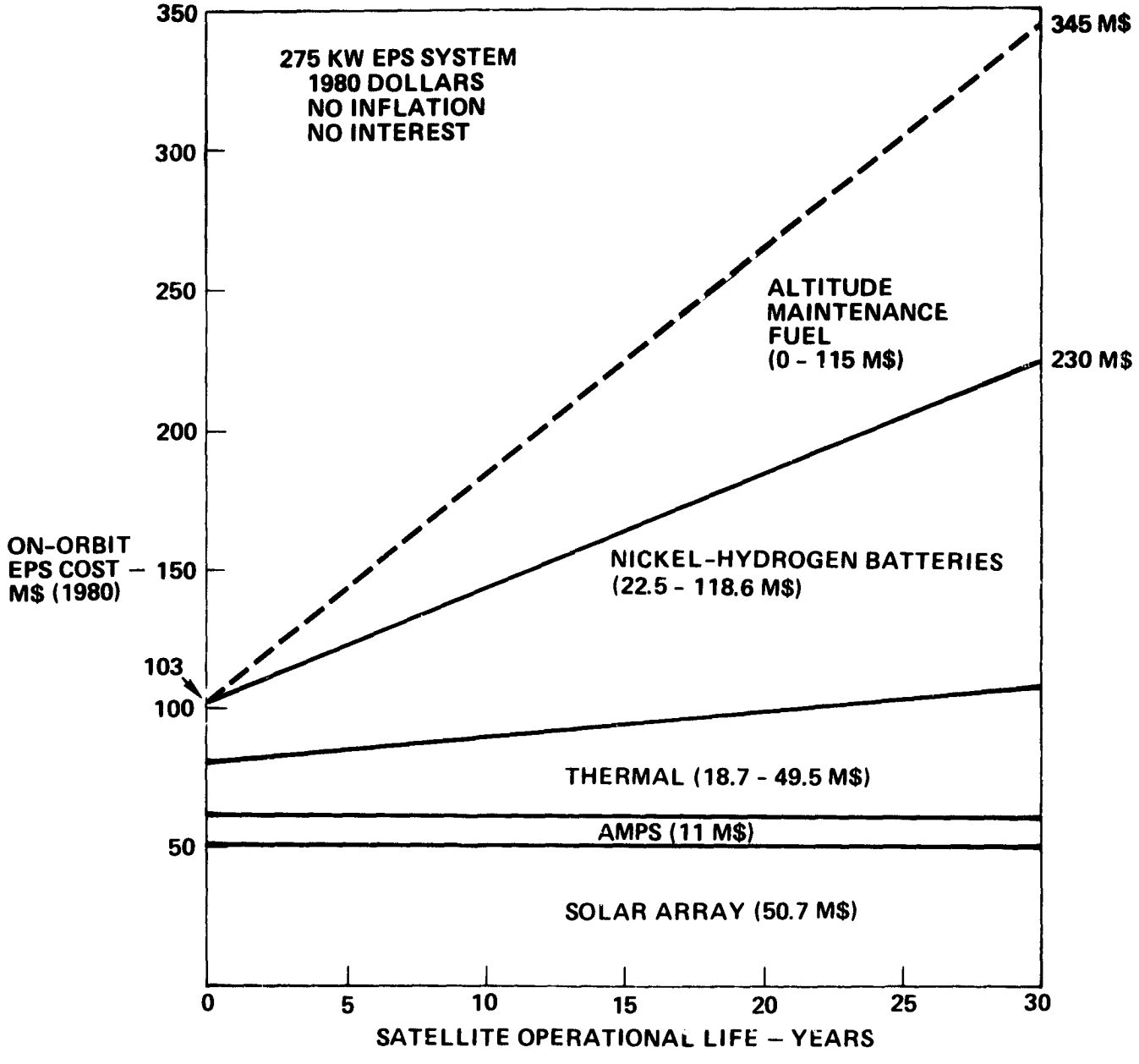

Figure 2-8. Batteries Dominate Life-Cycle Cost

converters (1-16 kW) for conversion from the 220 ±20 volt distribution voltage. In addition, the large quantity of equipment and the utility character of multi-hundred-kilowatt space platform power systems require automated power management techniques involving both the equipment and the management strategies (algorithms) to operate the system. Their development is being addressed under a contract extension to this Space Power Distribution System Technology study contract.

Technology improvements yield payback in the form of lower costs for future programs. Assessing this payback and comparing it to the development cost of the respective technology improvement provides an investment yardstick to judge the relative merits of otherwise confusing sets of peformance data. Potential technology payback from improvements in specific performance parameters is addressed with a series of graphs produced to identify the potential system value (cost savings) for these performance improvements of the major electrical subsystem components (solar array, energy storage, power distribution processing) and thermal control pumps. These graphs do not purport to identify specific technology methods to achieve performance improvements, but instead are a tool to evaluate differing, and often confusing, proposals for performance improvement. The results, summarized in Figure 2-9, indicate that energy storage remains the major contributor to electrical subsystem costs. Similar graphs for technology specific payback in manufacturing costs, reduced weight, and increased life are presented in Section 10 for the solar arrays, energy storage, power conversion, and thermal pumps as a guide to cost effective comparisons of competing technological improvement proposals.

2.7 CONCLUSIONS

The reference, cost-optimized, multichannel approach developed herein for the spacecraft electrical power subsystem enables realization of multi-hundred-kilowatt power levels in low earth orbit by the end of the century. This power subsystem configuration provides inherent solar array, energy storage, and power transmission redundancy at very low cost. However, 17 channels with the corresponding complexity are required for a 250-kilowatt system. Management of such a system by terrestrial control groups becomes

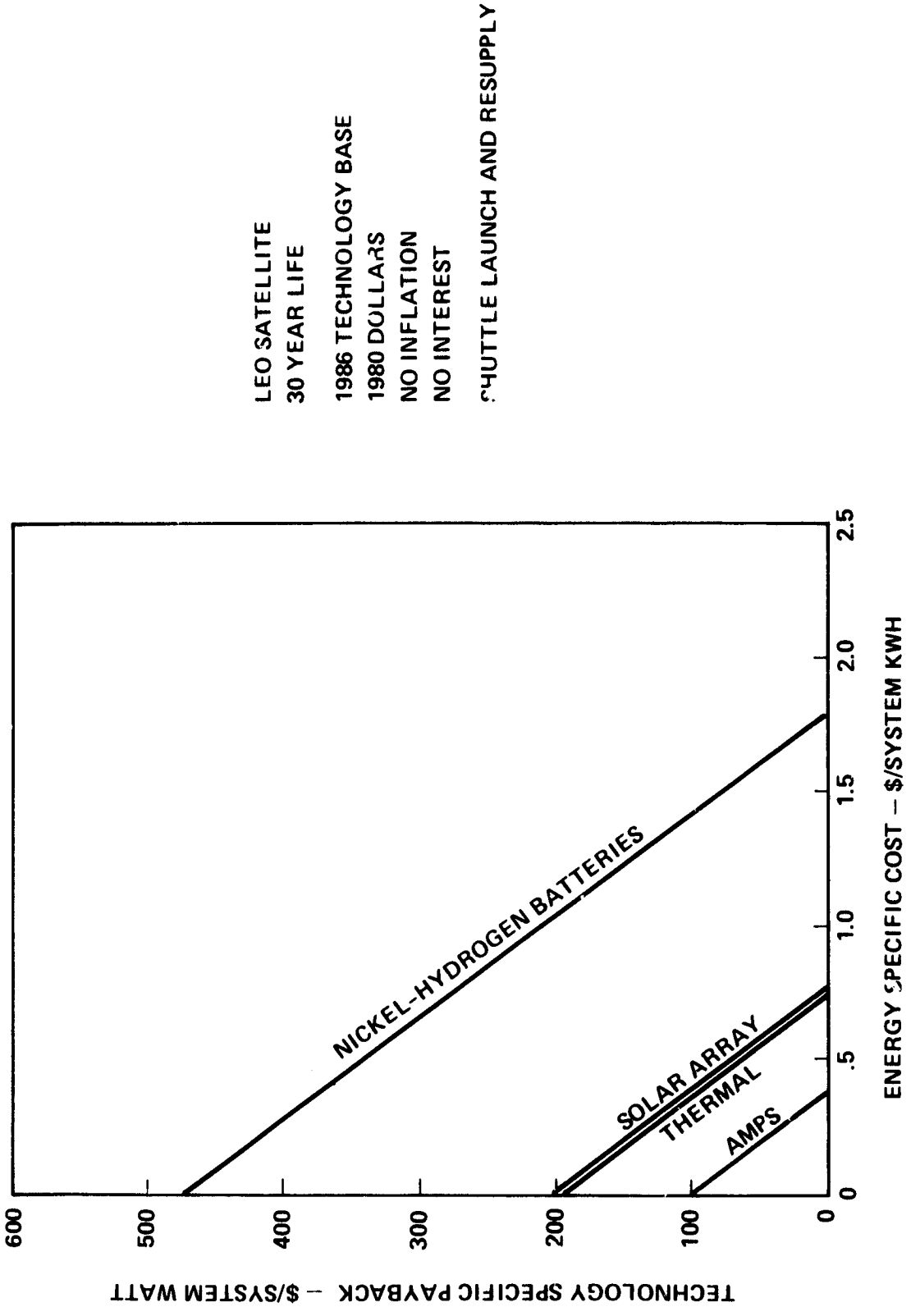

Figure 2-9. Major Cost Reduction Is Possible from Energy Storage Technology Improvements

burdensome and costly due to the large number of power system configuration and load management options available. This is solved by incorporating automated, on-board power subsystem management.

The advantages of this approach are many. Large power system ratings are became possible with modest power level components that are presently under development or that can be developed by 1988. Graceful degradation is inherent, and the necessity for added capacity (solar array and energy storage) for power source redundancy is precluded. Further, the power levels for new switch gear development are reduced, direct paralleling of batteries is avoided, and great flexibility is inherent to provide significant load isolation of payload types and for improved power quality and for fault isolation and correction.

The power source and transmission voltage levels are selected based upon cost optimizations. Higher voltages reduce costs, and at the 220 $\pm$20-volt level, a balance is achieved between the additional benefits to be realized from higher power source and transmission voltages and the technology development costs for higher-voltage solar arrays with acceptable plasma interaction losses and degradation. Direct current distribution is selected over alternating current distribution, based upon the unnecessary added complexity and cost of conversion from the direct current power sources and the elimination of successive, inefficient power conversion and control.

3. STUDY FOCUS

A set of guidelines are provided in the statement of work (Appendix A) to focus the study on the technology issues associated with an order of magnitude larger electrical power subsystem in support of multi-purpose, multimission satellite platforms in the next decade. Certain assumptions are also implicit with these guidelines. In addition, constraints are applied to the study to focus on technology issues rather than interesting, but distracting, mission issues and cost accounting practices.

3.1 GUIDELINES

The objectives of Task 1 are to generate a reference design for an electrical power subystem (EPS) and to assess the technology status and identify deficiencies. The statement of work (Appendix A) directs a 250-kilowatt, photovoltaic power system for a low earth orbiting satellite, with a technology readiness of 1985-1986 and an initial operational capability in 1988, as the focus for the technology issues. These guidelines are summarized in Table 3-1:

Table 3-1. Study Guidelines

1) 250 Kilowatt Payload Power
2) Solar Array Power Generation
3) Low Earth Orbit Mission
4) 1985-1986 Technology Readiness
5) 1988 Initial Operational Capability

3.2 ASSUMPTIONS

The 250-kilowatt electrical power subsystem is assumed to provide electrical power to a multimission, multipayload satellite such as a manned space station or an unmanned space platform. Also, a "man rated" redundancy level is assumed to be applicable to both satellite missions because certain payload operations, such as docking, and satellite servicing require intimate association with the Shuttle.

The 1988 initial operational capability and the low earth orbit missions imply application of the Shuttle transportation system for launch and any subsequent servicing, resupply, or refurbishment. Shuttle transportation costs, derived in Appendix B, are applied parametrically in the study analyses to optimize trade selections based upon total cost and to assess payoff potential for technology development. Shuttle costs are both weight and volume computed, but weight is normally the applicable factor:

462 $/pound	(1,016 $/kilogram)
2,830 $/cubic foot	(100,000 $/cubic meter)

These transportation costs increase 33 percent for Shuttle flights shared with another Shuttle user. However, the satellite size and payload complement implied with a 250-kilowatt power level suggest the full Shuttle capability can be utilized for each delivery to the satellite. Shared transportation scenarios are therefore precluded.

3.3 CONSTRAINTS

In addition to the guidelines and assumptions, certain constraints are applied to focus the study on the pertinent technological parameters affecting electrical power subsystem cost, performance, and near-term readiness. These constraints (Table 3-2) provide a consistent, uniform, and rational set of rules for the relevant and continually surfacing issues of mission duration, orbital parameters, redundancy level, and applicable interest and inflation rates.

Table 3-2. Study Constraints

1) 30-Year Satellite Mission
2) LEO ≈ 160 Nautical Mile, 28.5-Degree Inclination
3) Fail Operational, Fail Safe Redundancy
4) No Interest, i = 0
5) 1980 Dollar Base

3.3.1 Mission Duration

A 30-year satellite mission is chosen in order to develop more fully the resupply, refurbishment and servicing costs for the utility-type electrical power subsystem associated with a space platform or space station in low earth orbit. This 30-year period entails replacement of most power equipment and is representative of the operational goals implied with a satellite capable of supporting payloads aggregating 250 kilowatts. This long mission duration (30 years) develops a clearer understanding of the cost impact associated with various resupply, refurbishment, and servicing options.

3.3.2 Orbital Parameters

Low earth orbit (LEO) was interpreted for this study to mean an eastward launch from Kennedy Space Center (KSC), Florida, into a circular orbit at 160 nautical miles with the resultant 28.5 degree orbital inclination. This is the typical Shuttle launch from KSC and delivers the nominal Shuttle cargo weight into orbit (LEO). These orbital parameters are utilized in the study to define the applicable Shuttle transportation costs for initial and resupply transportation to orbit (Appendix B). Other orbits incur essentially the same total cost per launch, but greater specific transportation charges ($/pound) become applicable due to a reduction of the deliverable cargo weight into other orbits (Figure 3-1).

3.3.3 Redundancy

The 250-kilowatt power subsystem is expected to support a satellite, space platform, or space station capable of manned operation. As such, manned redundancy constraints of "fail operational, fail safe," as a minimum, are imposed on the power subsystem concepts of this study. These constraints require the power subsystem to sustain a major failure and continue the mission operation and to sustain a second major failure and still have sufficient capability to maintain the safety of the personnel onboard. This redundancy is considered a minimum to be applied in this study. Actual redundancies attained appear to be much greater.

3.3.4 Interest Rate

A major goal of this study is to reduce the cost of electrical power generation, distribution, and management for satellites. As such, the

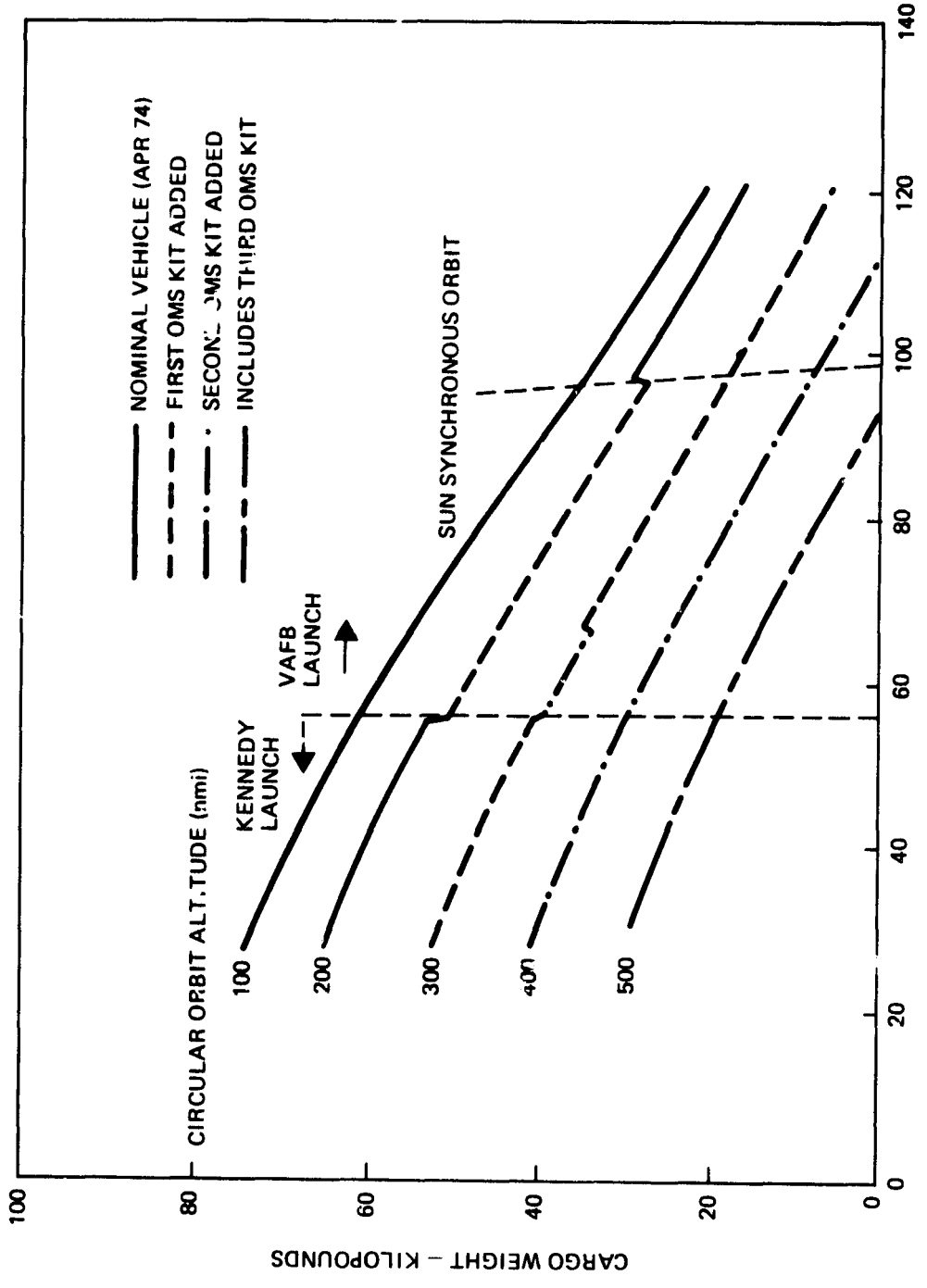

Figure 3-1. Shuttle Cargo Weight Per Launch Decreases for Higher Orbital Altitude - Delivery and Inclinations

major evaluation criteria of candidate selections, equipment options, and configuration alternatives is cost. Cost is associated with each of the many phases of a program such as development, design, qualification, fabrication, test, and initial deployment. These phases may stretch over the better part of a decade for deployment of a satellite utilizing a 250-kilowatt electrical power subsystem. In addition, operational costs, including replacement, refurbishment, and servicing, occur over subsequent decades. Correct engineering economic analyses require proper discounting of future cost reductions versus near term investments. This discount is typically the interest rate for borrowed capital to a private entrepreneur appropriately applied to the duration of the return on the investment alternative. Government interest rates historically have approximated 1 percent or less during protracted periods of little or no inflation (periods with a continuing net surplus budget). Present long-term government interest rates include this typical 1 percent interest plus an inflation charge associated with the generally perceived inflation rate. [Inflation is separately addressed in Section 3.3.5.] A zero interest rate is applied in this study rather than 1 percent for simplicity. A modest aggregate error of 16 percent is potentially introduced for 30-year elements; less for shorter periods (only 3 percent for 5 years). However, the cost accuracy attainable in this study does not allow rational decisions on such a fine distinction (16 percent) between alternatives. Hence, this simplifying assumption is acceptable and does not invalidate the conclusions of this study.

R.

3.3.5 Inflation

The "dollar" is presently an ever shrinking measure of economic value due to inflationary pressures (expansion of the money supply). Engineering decisions involving economic alternatives extending over protracted periods for payback require a consistent measurement base for economic value - a "constant value" dollar. Consequently, the costs herein (near term and far) are quoted in first-quarter 1980 dollars and are based upon pricing developed during the first quarter of 1980 (1Q1980).

Costs, when stated in current dollars of later years, will be numerically larger than quoted herein depending upon the cost of living index

and/or the labor rates prevailing for the date of cost incurrence. Projections of these indices are conjecture and dependent upon individual perceptions of what "inflation" may become. The constant dollar approach of this study avoids the ambiquity and unnecessary complexity in long-term cost projections inherent with "current" dollar measuring.

3.3.6 Life Cycle Cost

Most equipment will wear out or fail one or more times during a 30-year period and must be replaced. Equipment replacement occurs at intervals defined by the reliability statistic of mean-time-to-failure and the dispersion about this mean. As subsequent replacements occur, the time dispersion in equipment failure becomes greater (Figure 3-2) and approaches a linear rate eventually.

To address life cycle cost, these equipment replacements must be included in total cost. Costs, for these replacements, are incurred concurrently for Shuttle transportation, but earlier for manufacturing and testing the replacement unit. To address life cycle costs, these replacement costs are linearized with time as a ratio of equipment cost to equipment life (Figure 3-3).

Replacement equipment is assumed to cost the same as new or initial equipment when expressed in constant dollars. No allowance or saving is included herein for refurbishment of previously returned equipment. Such refurbishment is presumed to cost virtually the same as new equipment when the quality assurance requirements for "man rated" application are applied. That is, the cost to fully disassemble, inspect and test each component and/or subassembly, remachine worn surfaces, replace faulty or out of tolerance parts, recalibrate, reassemble, and acceptance test is considered to be as expensive as manufacturing new equipment. Furthermore, to do less during refurbishment, potentially entails a shorter mean life and a consequently greater replacement rate for refurbished equipment. Hence, in this study the cost of newly manufactured equipment is also applied for replacements.

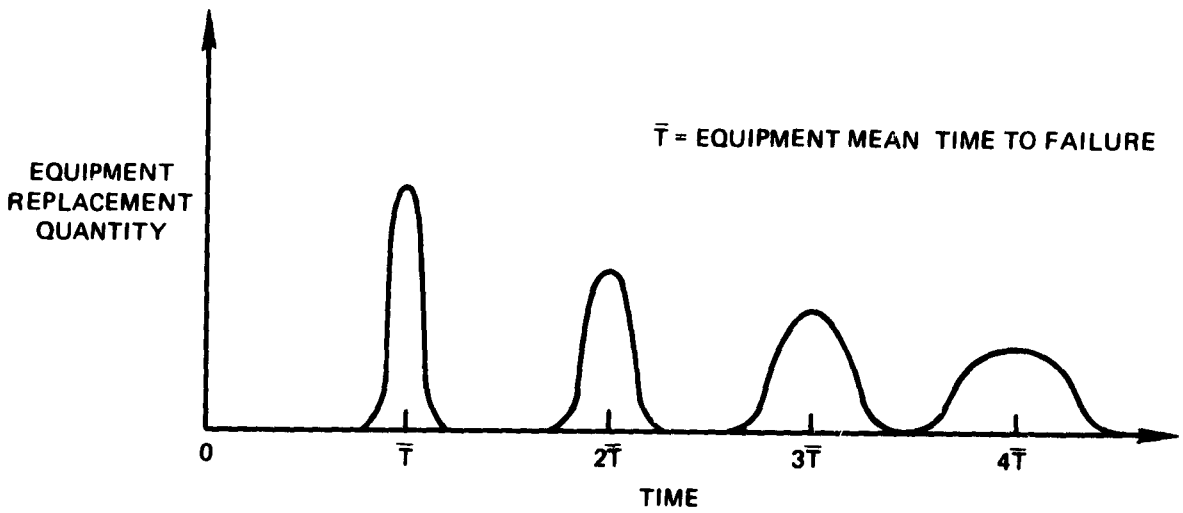

Figure 3-2. Dispersion of Equipment Replacement Occurs with Time

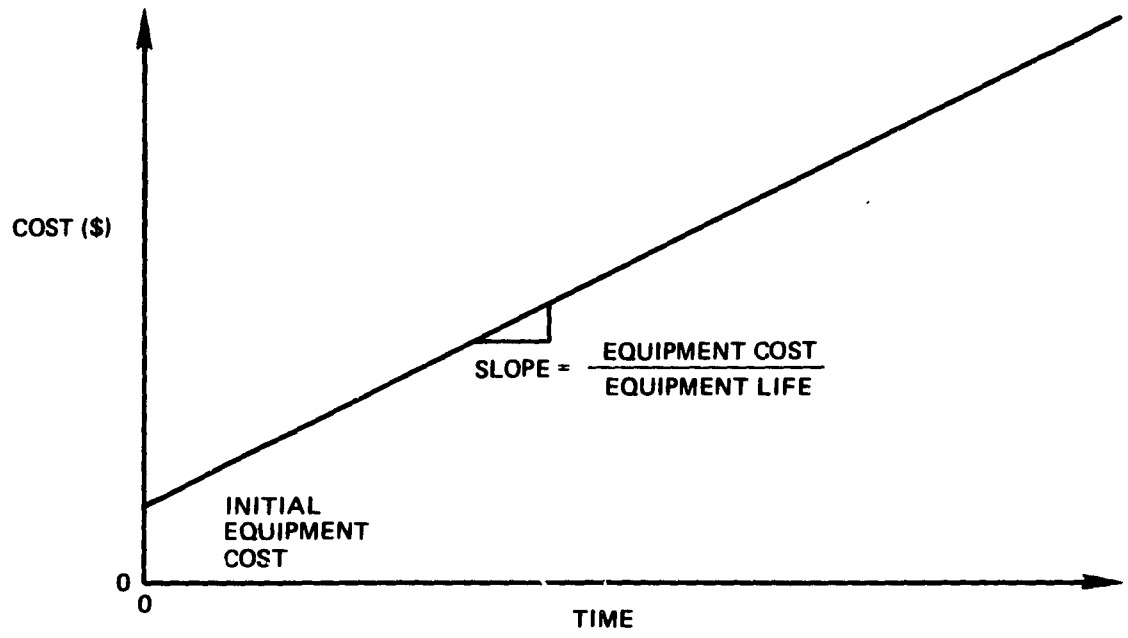

Figure 3-3. Life Cycle Costs Linearly Increase with Time

4. SOLAR ARRAY ANALYSIS

In recognition of the lead time required to develop the technology necessary for the production of low-cost multikilowatt solar array systems, NASA/MSFC awarded a series of study contracts in March 1979 for the definition of design approaches that offer the potential of meeting an array system recurring cost goal of 30 $/W. TRW, Rockwell International, and Lockheed Missiles and Space each received a study contract and performed analyses and evaluations of many diverse solar array concepts. These studies are applicable to the power levels covered by this Space Power Distribution System Technology Study. The solar array studies matured in the first quarter of 1980 concurrent with the needs of this Space Power Distribution System Technology Study, and their final briefing documents and subsequent final reports are utilized as the basis for solar array candidates, analyses, and evaluations in this study to select a cost effective solar array concept.

4.1 SOLAR ARRAY SELECTION

The three solar array study contracts concluded with predicted specific costs for each identified design approach (Table 4-1). Based on the results of these studies, NASA/MSFC awarded exploratory development contracts to TRW to pursue the high concentration ratio miniature Cassegrain concentrator (CR=125)* and to Rockwell International to pursue

*Four different values for concentration ratio (CR) may be quoted for a Cassegrain mirror system. They are appropriately quoted herein depending upon the relevant comparison or design feature under discussion. The four CR values for the TRW Cassegrain miniconcentrator are:

CR = 163, the unblocked geometric concentration ratio of the circular aperture to the illuminated solar cell area.

CR = 150, the geometric concentration ratio considering the aperture blockage due to the secondary mirror.

CR = 125, the effective geometric concentration ratio considering secondary mirror blockage and aperture truncation into a square pattern for packaging.

CR = 100, the effective light concentration ratio considering secondary mirror blockage, packaging truncation, and reflectance losses of 10 percent at each mirror surface.

Table 4-1. Identified Specific Costs

Manufacturer	Array	Cell	Cost ($/W)
TRW (Reference 4-1)	Planar	6x6 cm Silicon	96
	Miniconcentrator	4x4 mm Silicon	30
Rockwell International (Reference 4-2)	Planar	5x5 cm Silicon	74
	V-Trough	5x5 cm Silicon	57
	Pyramidal Cone	5x5 cm Silicon	58
	Cassegrain	2x2 cm Silicon	105
Lockheed Missiles and Space (Reference 4-3)	Planar	Silicon	393
	Low Concentration	Silicon	484
	Low Concentration	Gallium-arsenide	326
	High Concentration	Gallium-arsenide	736

the low concentration ratio truncated pyramidal concentrator (CR=5). The low concentration ratio approach is perceived to be the lower risk approach, while the TRW high concentration approach offers the lowest specific cost projection (by a factor of 2 or more) of the proposed solar array concepts. Of these two approaches, the TRW concentrator array utilizing miniature Cassegrain concentrator facets (Figure 4-1) is selected for the array reference design of the Space Power Distribution System Technology Study predicated primarily upon the potential for lower recurring cost. In addition, this approach is similar in thickness and method of deployment of its panels to that of present planar solar arrays with honeycomb substrates.

This Cassegrain miniconcentrator solar array concept offers other advantages. The reflector design and backside radiator plate provide some inherent shielding from the environmental fluences. This reduces the solar cell degradation rates, the consequent beginning of life oversizing of the array, and hence array cost.

The projected areal power density of the miniconcentrator array at 150 W/m^2 is significantly greater than that of planar or low concentration ratio arrays (typically 100 to 120 W/m^2) and is achievable with present 20 percent efficient gallium arsenide solar cells. Hence, a miniconcentrator array is considerably smaller in gross area (67 to 80 percent of the planar array, Figure 4-2) has proportionately less drag in low earth orbit, requires less propulsion fuel for altitude maintenance, and thereby incurs

Figure 4-1. Cassegrain Concentrator Solar Array Concept

ORIGINAL PAGE IS
OF POOR QUALITY

Figure 4-2. Planar Array Concept

lower fuel costs. This fuel reduction can become a significant cost saving for long-duration (30-year) missions in low earth orbit (lower than 225 nautical miles).

The miniconcentrator approach is very receptive to technology improvements in solar cell efficiency, but it does not require low-cost, large-area cell production to attain low array cost. The cell material utilized in the miniconcentrator concept is 100-fold less than the comparable planar array, and 30 times less than the typical low concentration arrays (effective CR = 3.3). Cell costs are only 5 percent of the miniconcentrator array cost. Hence, technology improvements in cell efficiency can be immediately utilized without a cell-cost reduction program, yet little increase in solar array specific cost is incurred. Total system costs may be further reduced with a more expensive but more efficient cell: solar array area is reduced, drag is reduced, fuel is reduced, and the related costs are reduced accordingly.

GR.

The weight of the miniconcentrator concept is greater than other approaches (Table 4-2). A specific power of 31 W/kg is projected with

Table 4-2. TRW Miniconcentrator and Planar Array Weight Comparison (756 kW BOL)

Item	Miniconcentrator Concept		Planar Concept	
	(kg)	(lb)	(kg)	(lb)
Blanket	17,185	37,890	6,100	13,400
Substrates	(12,655)	(27,900)	(775)	(1,700)
Solar Cells	(40)	(90)	(2,090)	(4,600)
Optical Elements	(4,490)	(9,900)	-	-
Coverglass	-	-	(1,590)	(3,500)
Adhesives	-	-	(820)	(1,800)
Stiffeners/Internal Hinges	-	-	(455)	(1,000)
Miscellaneous	-	-	(365)	(800)
Harness	908	2,000	900	2,000
Support	2,810	6,200	2,280	5,000
Launch Structure, Cradle	3,630	8,000	1,320	4,000
Totals	24,533	54,090	10,600	24,400
Shuttle Cargo Capability*	29,480	65,000	29,480	65,000
Weight Margin, Full Bay	4,947	10,910	18,880	40,600

*160 nautical miles, 28-degree orbital inclination.
( ) = Subtotals for Blanket

plastic and metal parts. Composite materials potentially increase the attainable specific power to 45 W/kg, but are more expensive. For a 250-kilowatt payload mission requiring a 690-kilowatt solar array, the lower cost 31 W/kg approach is adequate.

The Shuttle cargo bay physical configuration (15-foot diameter by 60 feet long, 10,600 cubic feet) allows the volumetric stowage of 756 kilowatts per launch for the mini-concentrator array. This array with launch structure weighs only 54,000 pounds, well under the rated weight capacity of the Shuttle for KSC launches:

Orbit Inclination (deg)	Delivery Altitude (nmi)	Payload Weight (lb)
28.5	215	65,000
56.0	215	55,000

Hence, the transportation charges are on cargo bay physical length utilization, rather than weight. Further weight reduction does not affect the transportation cost.

Polar orbit launchs from Vandenburg Air Force Base reduce the Shuttle cargo delivery weight to approximately 35,000 pounds (90-degree inclination, 215 nautical miles). This limits the array size to 493 kilowatts with the 31-W/kg solar array construction. The composite material construction at 45 W/kg allows a 716-kilowatt array to be delivered to orbit (90 degrees x 220 nmi). This is sufficient to support a 690-kilowatt array for a 250-kilowatt payload capability.

4.2 TRW STUDY

TRW performed a study for NASA/MSFC (Reference 4-1) which led to the definition of a solar array concept (Figure 4-1) utilizing multiple, miniature concentrator facets each having a very high geometric concentration ratio (CR = 163). This concept projects a specific cost of 30 dollars per watt (Table 4-3) and eliminates or reduces many of the disadvantages inherent in other approaches to high concentration ratios. For example, the miniature concentrator element overcomes the thermal and deployment problems associated with large-size high-concentration concepts. The radiator is passive, has approximately the same area as the entrance aperture of the concentrator, and produces a cell nominal operating temperature

Table 4-3. 30 $/W Solar Array Recurring Cost is Achievable

Items	1982 Technology			Projected 1987 Technology		
	Unit Cost ($)	Array Cost (K$)	Specific Cost ($/W)	Unit Cost ($)	Array Cost (K$)	Specific Cost ($/W)
Blankets						
Solar Cells, 4 x 4 mm	1	1,900	3.8	2.25	4,300	5.7
Heat Sinks	1	1,900	3.8	0.25	500	0.7
Substrate Frames, Substrates, Optical Parts, Miscellaneous	3.30	6,150	12.3	1.00	1,900	2.5
Material		1,450	2.9		1,450	1.9
Harnesses		3,200	6.4		3,200	4.3
Labor	9.30	17,500	35.0	2.20	4,150	5.5
Subtotal		31,100	64.2		15,500	20.7
Structures						
Masts/Canisters	175,000/	600	1.2	175,000/	600	0.8
Strong Backs	124,000	2,850	5.7	125,000	2,850	3.8
Labor		3,500	7.0		3,500	4.7
Subtotal		6,950	13.9		6,950	9.3
Totals		39,050	78.1		22,450	30.0

of approximately 80°C. Deployment is similar to that of a planar array (Figure 4-2). The optical components of each concentrator facet are arranged in a small (1.8 x 1.8 inch aperture), shallow (0.5 inch thick), Cassegrain configuration and consist of three elements (Figure 4-3):

1) A paraboloidal primary reflector

2) A hyperboloidal secondary reflector

3) A conical tertiary reflector (light catcher cone).

The inclusion of the light catcher cone in the optical path provides essentially a 3-degree half-angle tolerance to off-pointing errors (Figure 4-4). Performance parameters of the resulting miniconcentrator array is compared to a planar array in Table 4-4.

The primary mirror is manufactured from either molded, high-temperature plastic or electroformed metal. Its front surface is highly polished and vacuum coated with high-reflectance metalization and protective heat-emitting dielectric layers. The secondary mirror, similarly made, is suspended by a spider above the primary mirror and blocks approximately 10 percent of the incoming light. The light-catcher cone is also highly reflective.

The geometric concentration ratio is 163. Allowing for a nominal 90 percent reflectivity of each of the two mirrors (normal incidence), 10 percent blockage by the secondary mirror and spider, and 10 percent spillage, the effective, or net light concentration ratio is approximately 100. The concentrator collector packing density at the panel level is 90 percent. The result is a two order of magnitude reduction in the solar cell material required with this concept compared to a planar array. Mass reproducible reflector parts replace the large-area solar cell. Only a 4 by 4 millimeter cell is required for each facet. (A substantial increase in potential manufacturing yield and efficiency realization is possible with 4 by 4 millimeter cells versus the 5 by 5 centimeter or larger solar cell blanks needed for other approaches.) Consequently, solar cell cost is reduced to about 5 percent of typical low concentration array manufacturing cost. This low component of array cost also allows the cost effective

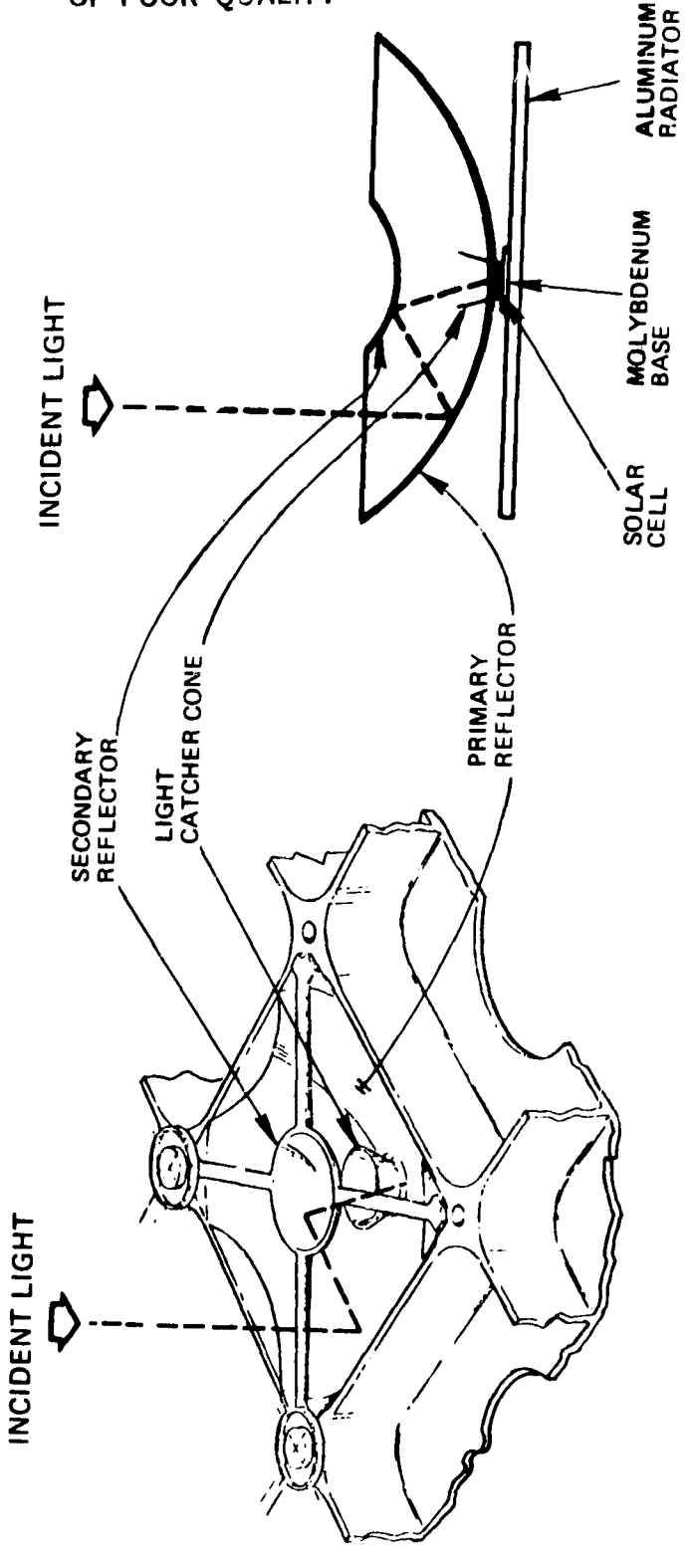

Figure 4-3. Cassegrain Miniconcentrator Concept

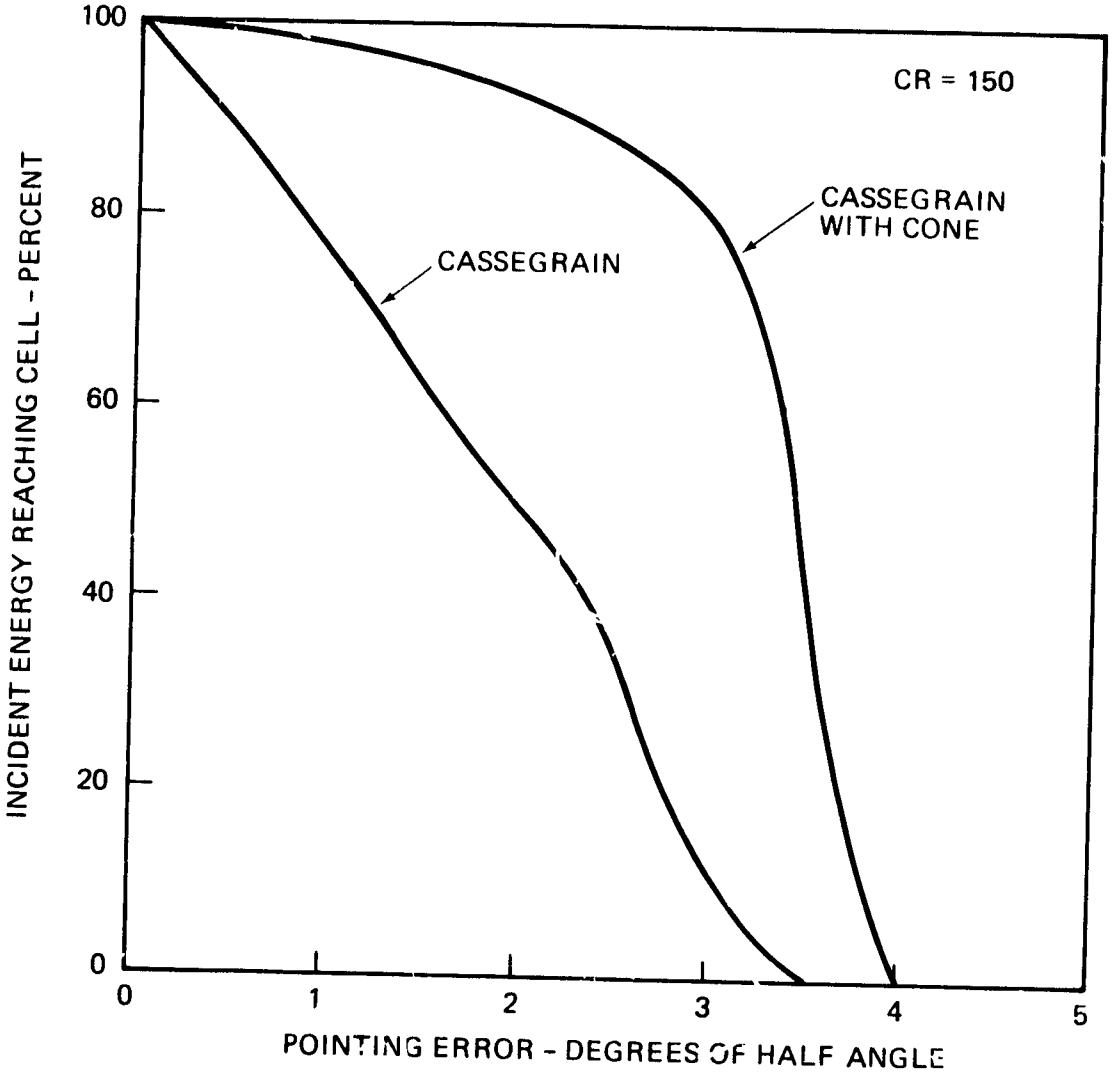

Figure 4-4. Light Catcher Cone Enhances Pointing Tolerance of Cassegrain Miniconcentrator

Table 4-4. Electrical Performance Comparison of Solar Array Concepts

Parameter	Miniconcentrator		Planar	
Technology Readiness Year	1982	1987	1982	1987
Concentration Ratio (Geometric)	160	160	1	1
Cell Efficiency at 28°C (%)	20	30	14	16
Cell Type	Si or GaAs	Tandem Junction	Si	
Cell size (cm x cm)	0.4 x 0.4	0.4 x 0.4	6 x 6	10 x 10
Number of Solar Cells	1,894,400	1,894,400	1,094,000	424,430
Cell Temprature (°C)	80	80	80	80
Optical Efficiency (%)	73	73	100	100
Average Panel Output (W)	840	1256	653	746
Harness and Wiring Efficiency (%)	95	95	95	95
Array Output, BOL (kW)	511	766	595	680
Array Specific Output (W/kg)	20.8	31.2	56.1	64.1
Array Specific Cost ($/W)	78.1	30.0	95.6	46.0

utilization of expensive, but highly efficient, solar cells without significant recurring array cost penalties (Figure 4-5). Furthermore, the required capitalization cost to mass produce large-area, high-efficiency solar cells is avoided.

4.3 ROCKWELL INTERNATIONAL STUDY

A perceptively low-risk technology approach to concentrator arrays is to use the maximum amount of existing planar array techniques. The Rockwell study epitomizes this approach by adding panels to the sides of a planar module to increase the solar flux density on the cells and thereby

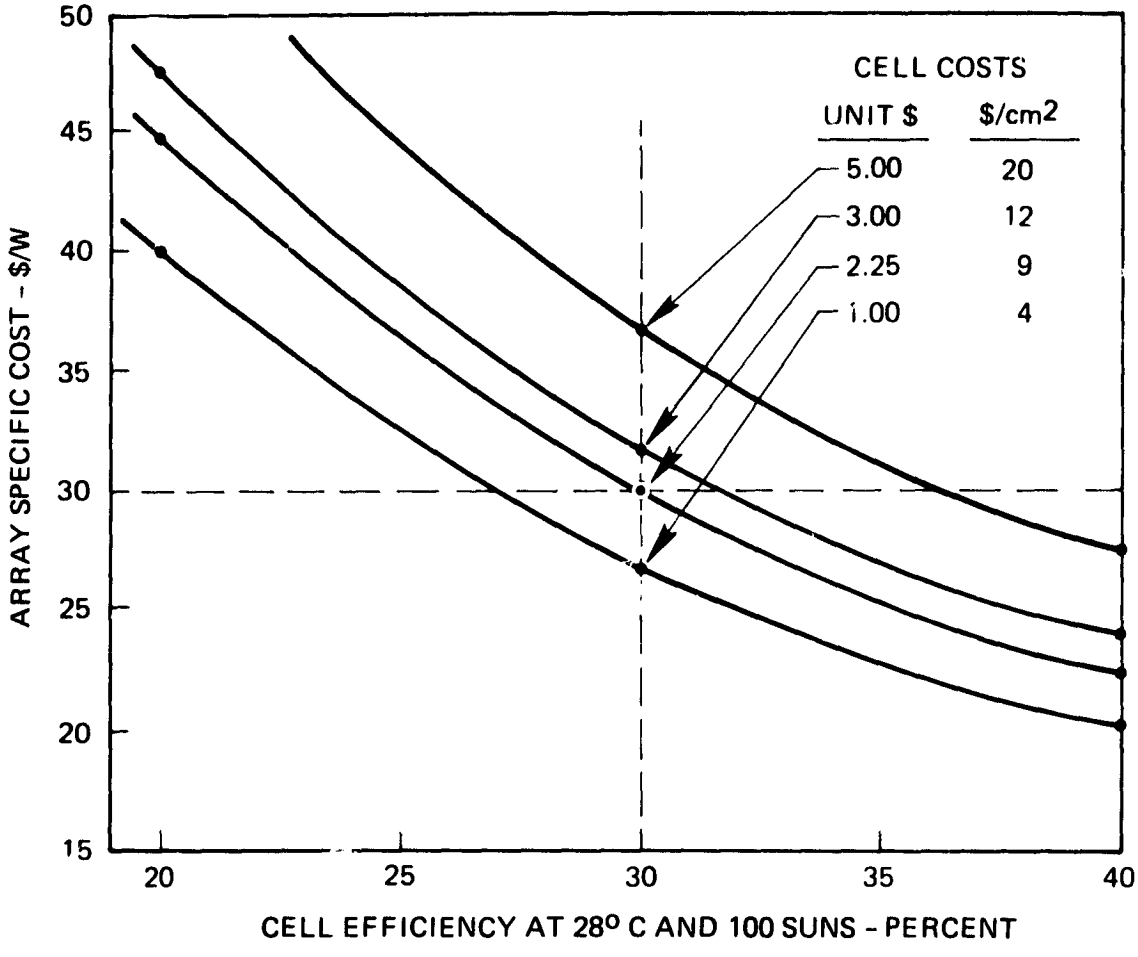

Figure 4-5. Cassegrain Miniconcentrator Can Effectively Utilize Expensive, High-Efficiency Cells

improve their cost effectiveness. Two of these design concepts project low recurring costs for solar arrays in the mid-to-late 1980s and have reasonable development requirements:

1) Large area (5 by 5 cm) silicon solar cells in a V-trough concentrator with a geometric concentration ratio of 2 (Figure 4-6)

2) Gallium arsenide solar cells (2 by 4 cm) in a pyramidal cone concentrator with a geometric concentration ratio of 6 (Figure 4-6).

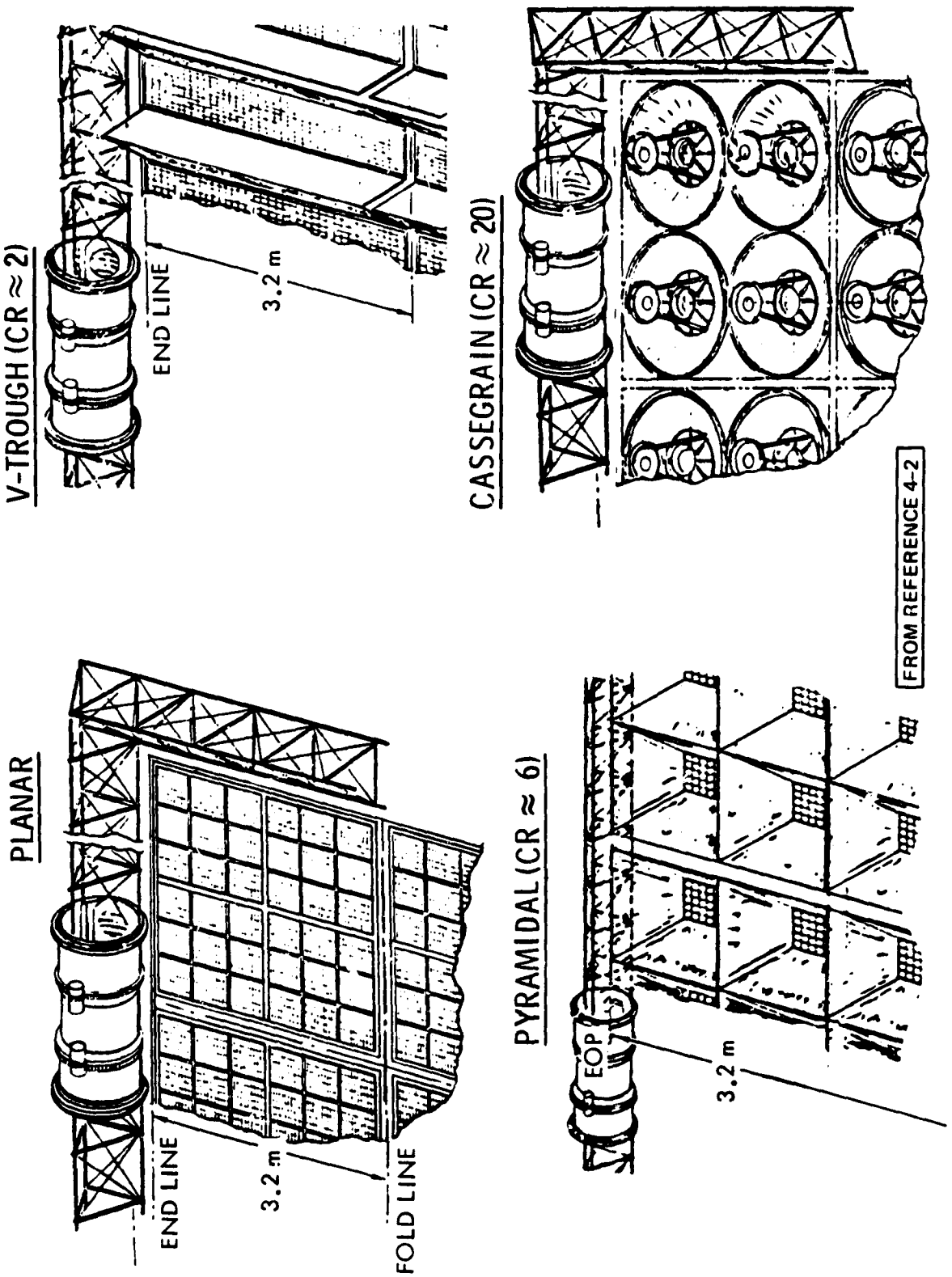

Figure 4-6. Rockwell International Solar Array Concepts

The cost estimates for either configuration project a recurring solar array cost in the range of 55 to 60 dollars per watt. Other design concepts, including various geometric concentration configurations and solar cell types, were also analyzed and evaluated in this Rockwell International study, but these other design concepts project significantly greater costs for the late 1980s (Figure 4-7). For example, the large scale Cassegrain concentrator (CR = 20) utilizing 2 x 4 cells and heat pipes is more expensive than the alternatives.

The truncated pyramidal concentrator (Figure 4-7) projects excellent reduction of array costs combined with modest technology risk. This configuration has been selected by NASA/MSFC for exploratory development. Techniques for low cost manufacturing of panels with minimum on-orbit degradation is the focus of this initial technology program.

The geometric concentration ratio of the truncated pyramidal concentrator is six. A loss of approximately 15 percent by absorption in the reflectors and a loss of another 8 percent for reflected light not reaching the cells produces an equivalent sunlight concentration ratio of 4.6 at the cells. A 0.020-inch thick aluminum radiator approximately twice the area of the cells is projected to be cost effective and acts as the substrate for the cells. The effective cell tempreature is calculated at 120°C and indicates the need for a high-temperature, high-flux cell with this array design.

4.4 ORBITAL MAINTENANCE

Each of the three solar array studies (References 4-1, 4-2, and 4-3) addresses an orbital servicing approach for maintaining solar array output considering the degradation caused by natural radiation and thermal cycling. Each study came to the same conclusion: size the beginning of life solar array to accommodate the predicted degradation caused by radiation exposure and random interconnect failures from thermal cycling. This initial oversizing is more cost effective than subsequent solar array blanket replacement or additions to maintain the desired power output level. Consequently, the solar array for this Space Power Distribution System Technology Study is designed for a beginning-of-life power (690 kilowatts) that accommodates the projected degradation over 30 years (20

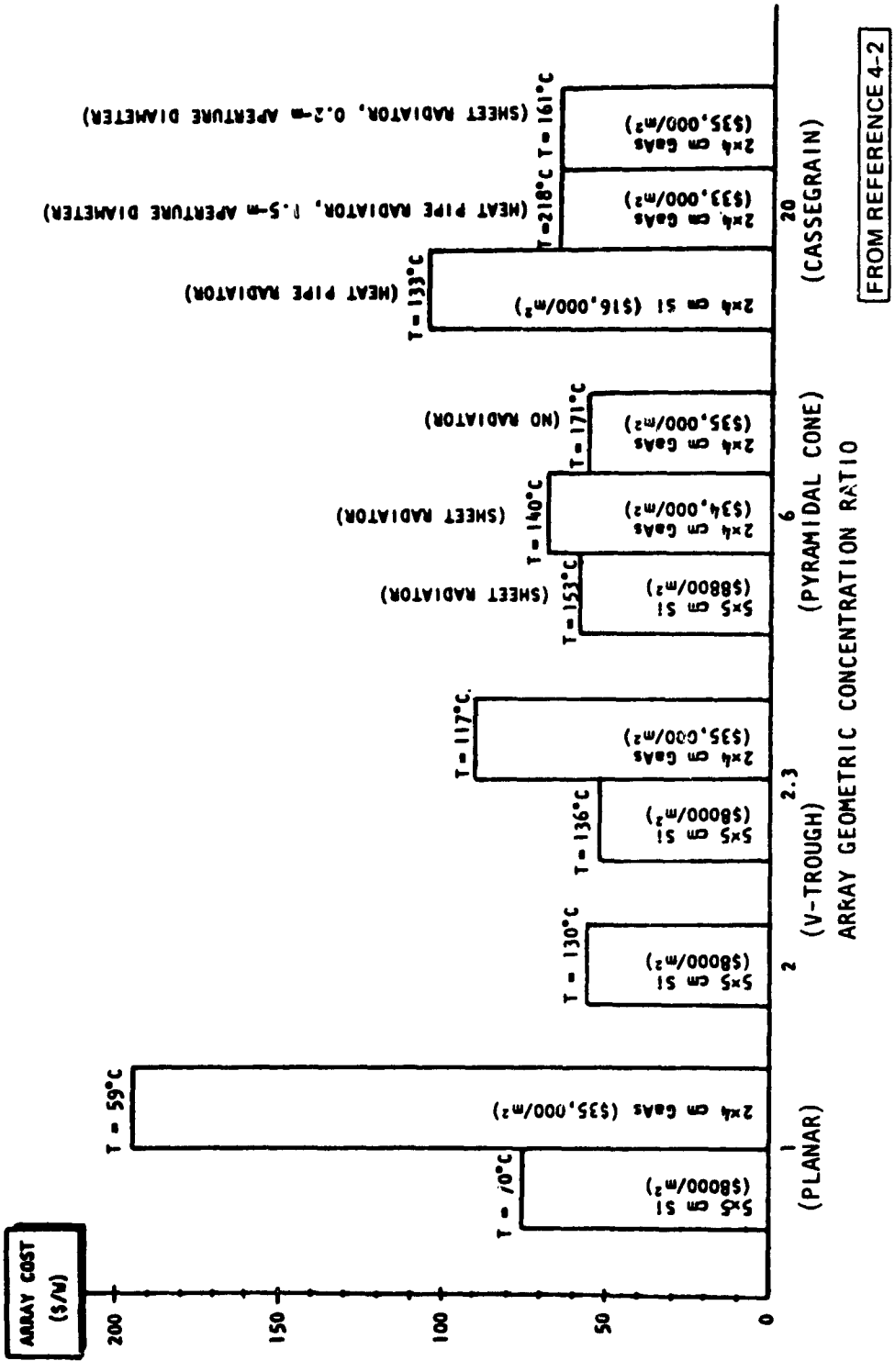

Figure 4-7. Rockwell International Comparison of Various Array Configurations

percent). (End-of-life power requirements are 550 kilowatts). However, the solar array concept for a 250-kilowatt power system is envisioned to allow unscheduled servicing (replacement of damaged blankets or panels) to accommodate unforeseen major damage to any significant portion of the solar array.

4.5 SOLAR ARRAY DEGRADATION

Two classes of phenomena reduce the solar array electrical power capability with time.

1) Component performance degradation such as reflector surface deterioration, coverglass and adhesive darkening, cell radiation degradation, etc.

2) Random loss of components, such as broken cells, joint failures, etc.

The degradation effects are due to exposure to the natural environment of trapped protons and electrons, ultraviolet radiation, micrometeorites, etc. These degradation effects are a continuous process and do not result in catastropic loss of array power. In general this overall performance deterioration rate slows with time, based upon experience from low earth orbital satellites with 8 to 10 years of operation.

Component failures, are due to meteorite collision, thermal cycling, etc., and incrementally degrade array performance in discrete steps by removing one cell in a series string and rendering that string inoperative. These component failures are considered to occur generally at random throughout an array and are, therefore, treated parametrically. Failure bit rates of 0.1 to 1.0 occur with present solar array technology. The effect of these rates on the concentrator array are tabulated in Table 4-5. A bit rate is a linear failure rate of 10^{-9} part failures per hour of operation of the part. For example, a 1.0 bit rate applied to the 1,894,400 cells of a 766 kilowatt miniconcentrator array at year three (26,298 hours) yields 50 failed parts:

$$(1.0 \times 10^{-9}) \times (1{,}894{,}400 \text{ cells}) \times (26{,}298 \text{ hours}) = 49.8 \text{ failures}$$

These 50 failures spread adversely across the array could cause 50 of the 3678 strings in the array to become inoperative, and result in a worst-case 1.4 percent power loss (Table 4-5).

A 20 percent, 30-year degradation point is selected for the performance of the TRW miniconcentrator solar array (Figure 4-8). The natural environment degradation is significantly ameliorated by the inherent shielding of the Cassegrain reflector elements. A 0.1-bit failure rate is assigned to the random failures (primarily cell interconnects). This failure rate is based upon the projection of a national program to develop solar cell interconnect welding during the interim years (1982-86), and upon the expected construction and assembly of the 4 by 4 millimeter solar cells providing a more benign interface for electrical interconnect joining. Hence, the 30-year end-of-life (EOL) solar array power capability is projected at 80 percent of the beginning-of-life (BOL) power.

Table 4-5. Typical Failure Rates Suggest 30-Year Operation

Array	Failure Rate	No. Failed Parts			Percent Array Power Loss		
	(Bits)	Yr 3	Yr 10	Yr 30	Yr 3	Yr 10	Yr 30
Planar	0.1	1	4	11	0.1	0.5	1.5
	1.0	11	37	112	1.5	5.0	15.0
Concentrator	0.1	5	15	50	0.1	0.4	1.4
	1.0	50	150	500	1.4	4.1	13.6

Figure 4-8. Cassegrain Array Degradation is Modest

A 20 percent, 30-year degradation point is selected for the performance of the TRW miniconcentrator solar array (Figure 4-8). The natural environment degradation is significantly ameliorated by the inherent shielding of the Cassegrain reflector elements. A 0.1-bit failure rate is assigned to the random failures (primarily cell interconnects). This failure rate is based upon the projection of a national program to develop solar cell interconnect welding during the interim years (1982-86), and upon the expected construction and assembly of the 4 by 4 millimeter solar cells providing a more benign interface for electrical interconnect joining. Hence, the 30-year end-of-life (EOL) solar array power capability is projected at 80 percent of the beginning-of-life (BOL) power.

Table 4-5. Typical Failure Rates Suggest 30-Year Operation

Array	Failure Rate (Bits)	No. Failed Parts			Percent Array Power Loss		
		Yr 3	Yr 10	Yr 30	Yr 3	Yr 10	Yr 30
Planar	0.1	1	4	11	0.1	0.5	1.5
	1.0	11	37	112	1.5	5.0	15.0
Concentrator	0.1	5	15	50	0.1	0.4	1.4
	1.0	50	150	500	1.4	4.1	13.6

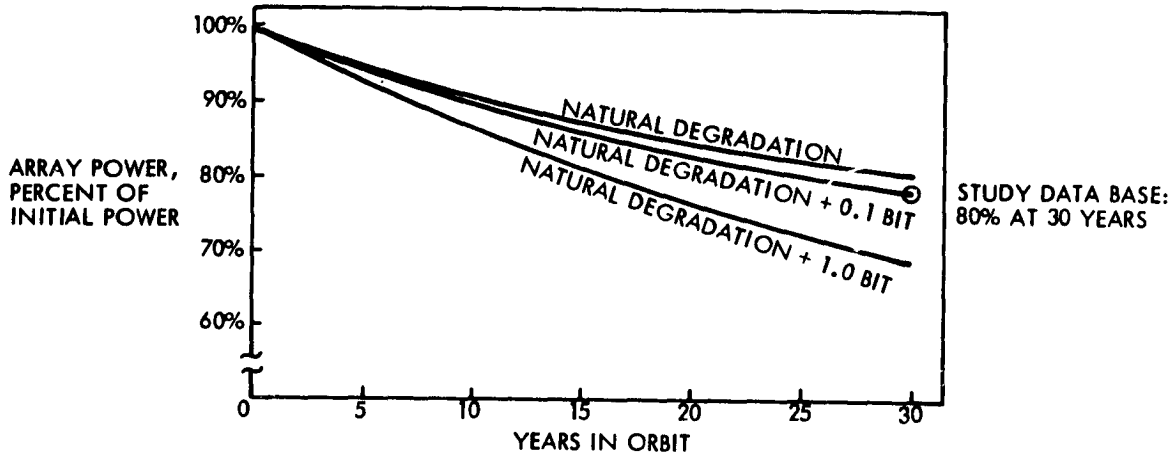

Figure 4-8. Cassegrain Array Degradation is Modest

5. ENERGY STORAGE ANALYSIS

Three energy storage technologies are considered in this study:

1) Nickel-cadmium batteries

2) Nickel-hydrogen batteries

3) Fuel cells plus electrolysis units

Nickel-cadmium batteries are the industry standard for satellite energy storage in electrical power subsystems. Nickel-hydrogen batteries are under continuing development, and initial flight application in operational systems is imminent. Fuel cells, utilizing hydrogen and oxygen reactants, have been employed on the Gemini, Apollo, and Shuttle vehicles. Only these three energy storage concepts are sufficiently developed for consideration, in scaled-up versions, for a 250-kilowatt application with a 1985-86 technology readiness requirement. Other concepts, such as secondary lithium batteries, nuclear sources, and flywheel energy storage, are not considered viable for the 1985-86 technology readiness requirement.

The comparative data for the three energy storage technologies are developed in Sections 5.2, 5.3 and 5.4. This data is based upon information received during the first quarter of calendar year 1980 and upon the life cycle cost optimization techniques developed during the study. Significant new information may affect the conclusions of this study. Therefore, periodic review of these trades is recommended.

The nickel-hydrogen battery is selected as the reference energy storage concept for application to the 250-kilowatt electrical power subsystem in low earth orbit for the purposes of this study. Nickel-hydrogen is both the lightest weight and lowest cost on a life cycle basis when the supporting parameters for solar array area, drag makeup fuel, and thermal radiator area are considered. Also, the inherent modularity and building-block size of cells and batteries makes nickel-hydrogen technology applicable to a wide range of power requirements (15 to 500 kilowatts).

Nickel-cadmium batteries are heavier and more costly than nickel-hydrogen except for short-term missions wherein battery replacement does not occur (typical of present fixed-payload low-power satellites). The fuel cell plus electrolysis unit concept is a close contender to nickel-hydrogen in cost, and is lower in weight, when only energy storage equipment is considered. Hence, the fuel cell plus electrolysis unit concept may become attractive as higher fuel cell plus electrolysis efficiencies are achieved such that the supporting requirements for solar array area and drag makeup fuel are reduced.

5.1 ENERGY STORAGE COMPARISON

The three energy storage concepts (nickel-cadmium, nickel-hydrogen, and fuel cell plus electrolysis) are compared based upon the simplified electrical power system configuration of Figure 5-1. In this configuration, thermal support and solar array support for each energy storage concept are considered and included. The thermal equipment (heat exchangers and radiators) needed to dissipate waste heat from the energy storage equipment is identified and included. The solar array area required to charge each energy storage concept is also identified and included, but the solar array area for direct support of the load during sunlight is not included. The solar array output is regulated in order to provide the charging voltage and current requirements of the energy storage units as determined and controlled by the power management subsystem.

The energy storage parameters of the three concepts are tabulated for comparison in Table 5-1. These parameters are developed in Sections 5.2, 5.3, and 5.4 of this report. To compare these concepts, the energy requirement of 150 kWh is defined by the 250-kilowatt payload and a 36-minute eclipse. The installed nameplate battery capacity is based upon this energy requirement and the appropriate depth of discharge for each battery chemistry. The optimum depth of discharge is applied to attain minimum energy storage costs and leads to energy storage nameplate capacity of 306 kWh for nickel-cadmium at 49 percent depth of discharge; 450 kWh at 33 percent depth of discharge for nickel-hydrogen.

A 200 kWh reactant supply is applied to the fuel cell plus electrolysis unit concept. This 200-kWh reactant storage is selected to provide a modest energy margin for contingency and represents an engineering judgment of a suitable energy reserve. This is consistent with the potential reserve (deeper depth of discharge) in the two battery candidates, though of a lower value (only 50 kWh). The resulting depth of discharge is equivalent to 75 percent:

$$\frac{\text{150 kWh usage}}{\text{200 kWh storage}} = \text{75 percent depth of discharge}$$

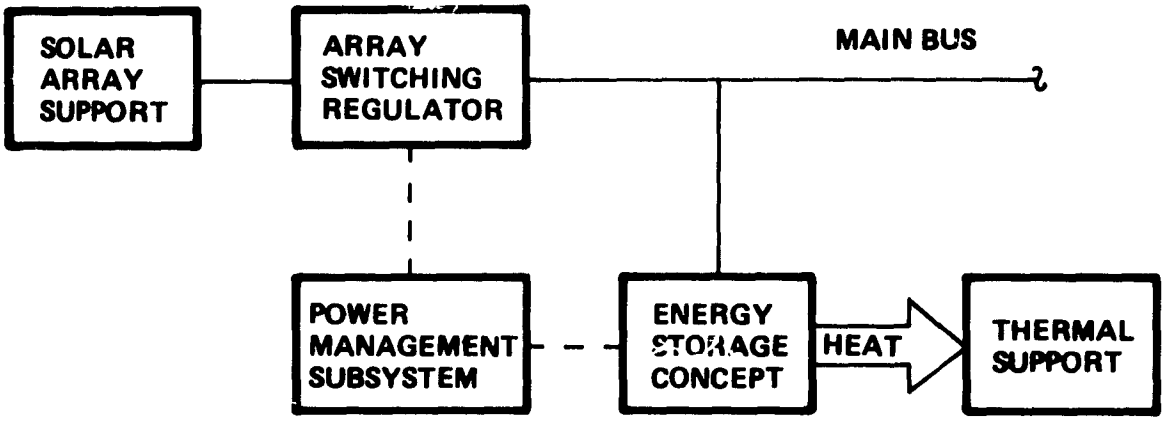

ENERGY STORAGE: Ni-Cd BATTERIES
Ni-H_2 BATTERIES
FUEL CELL + ELECTROLYSIS

SOLAR ARRAY: SIZED FOR CHARGING SUPPORT ONLY

ARRAY SWITCHING REGULATOR: REGULATES FOR ENERGY STORAGE NEEDS

POWER MANAGEMENT SUBSYSTEM: PROVIDES CHARGING CONTROL

THERMAL SUPPORT: HEAT EXCHANGERS (COLD PLATES)
RADIATOR AREA

Figure 5-1. EPS for Energy Storage Comparison

Table 5-1. Energy Storage Parameters
(250-Volt System, 250-kW Payload, 36-Minute Eclipse)

Parameter \ Concept	Nickel-Cadimum	Nickel-Hydrogen	Fuel Cell + Electrolysis Unit
Energy Storage	306,000 Wh	450,000 Wh	200,000 Wh
Depth of Discharge	49%	33%	75%
Average Life	2.75 yr	7 yr	4.6 yr (stacks) 1.1 yr (pumps)
Cell Size	100 Ah	150 Ah	270 A (FC) 342 A (EU)
Cells/Unit	170	160	308 (FC) 135 (EU)
Unit Quantity	15	15	5 Fuel Cells (1) 6 Elec. Units (1)
Heat Losses	38 kW (2)	32 kW (2)	79 kW (Sunlight) 231 kW (Eclipse)
Temperature	0°C	0°C (3)	40/75°C
Input Power (Sunlight)	229 kW	220 kW	430 kW
Specific Energy	10 Wh/lb	25 Wh/lb	35 Wh/lb (4)
Weight: Initial	30,600 lb	18,000 lb	5,775 lb
Replacements (6)	334,000 lb	77,000 lb	38,700 lb
Costs: Initial (5)	20.4 M$	19.1 M$	14.3 M$
Replacement(5)	223 M$	82 M$	87 M$
Development	~1 M$	<5 M$	>50 M$

Notes: (1) One unit added for reliability
(2) 90-minute average
(3) Not optimized
(4) Not scalable
(5) Includes shutle transportation costs to 160 nmi orbit; excludes support costs of Table 5-2
(6) For 30-year life cycle.

Tankage and reactants are sized accordingly for 200 kWh, and the reactant storage weight calculated at 1347 pounds (40 percent of the 3367 pounds for 500 kWh storage of the General Electric study, Table 5-9 of Section 5.4). Reactant storage for 500 kWh provided in the General Electric tabulation would increase the orbital system weight by 2020 pounds, increase the tankage volume, and increase the Shuttle transportation costs of reactant tankage by $6-10M (based on Shuttle payload bay length utilization charges) over that shown in the comparison tabulation (Table 5-1).

No battery redundancy is provided in the nickel-cadmium and nickel-hydrogen concepts. Loss of one battery out of 15 can be accommodated by a temporary 7 percent increase in load on each of the remaining 14 batteries. This represents an increase in the depth of discharge to 53 percent for nickel-cadmium batteries and to 35 percent for nickel-hydrogen batteries. For the fuel cell plus electrolysis concept, only four fuel cell stacks and five electrolysis stacks are required (Table 5-9). Loss of one unit would increase the load on the remainder by 33 percent and 25 percent respectively. Hence, one additional fuel cell stack and one additional electrolysis stack is included in the basic powerplant complement for redundancy needs to assure initial "fail operational" redundancy.

The specific energy values for each battery concept are developed in Sections 5.2 and 5.3. Energy storage weights are scaled from these values for the initial equipment complement. The weight of replacements is defined from this initial complement, battery mean life, and satellite life:

$$\text{Replacement weight} = \text{initial weight} \times \frac{\text{Satellite life}}{\text{Battery mean life}}$$

The specific energy value for the fuel cell plus electrolysis concept is not scalable. This value is calculated by dividing the total available energy storage by the initial system weight:

$$\frac{200{,}000 \text{ Wh}}{5{,}776 \text{ lb}} = 34.6 \text{ Wh/lb}$$

Greater energy storage requires only more reactants and tankage, but not additional powerplants (fuel cells or electrolysis units). Hence, this specific energy is a point value and not applicable to other size systems (either power or energy).

Specific energy values, while useful to calculate battery weights for an energy storage complement, do not consider replacement frequency (equipment life) nor cost. However, life cycle weight and cost including replacements as well as the initial equipment complement must be considered. The weight and cost values of Table 5-1 relate only to the energy storage equipment. For valid comparisons, weight and cost considerations of the supporting subsystems (solar array, thermal control, and orbital altitude maintenance) are developed and compared (Table 5-2). They reflect the input power and heat rejection requirements for each energy storage concept.

The solar array support parameters are based upon the identified charging power requirements (Table 5-1), a 95 percent efficiency for regulation and transmission, and a 20 percent total array degradation over the 30-year life in low earth orbit (160 to 220 nautical miles). The solar array costs are based upon the projected 30 $/watt manufacturing cost for the TRW Cassegrain mini-concentrator solar array and a Shuttle Payload bay capability of 958 kilowatts of array per launch.

The thermal support parameters are based upon the identified waste heat load of each energy storage concept, their operating temperature requirements, and the specific parameters of 5.53 kg/m^2 and 886 $\$/ft^2$ for radiators. Battery heat exchangers (cold plates) are defined based upon 9.6 kilograms per kilowatt of heat removal and $20,000 per module of approximately 20 cells. Fuel cell and electrolysis unit heat exchanger weights are identified in the General Electric tabulation (Table 5-9). Launch costs are based upon the weights obtained and the Shuttle transportation cost of 462 $/pound.

The propulsion fuel requirements for orbital altitude maintenance are based upon the size of the charging solar array for each energy storage concept, a 30-year mission, a 215-nautical-mile orbital altitude*, and a

*Orbital altitude optimization at 215 nautical miles is addressed in Appendix C.

Table 5-2. Energy Storage Support Parameters
(30-Year Life Cycle)

Concept Parameter	Nickel Cadimum	Nickel Hydrogen	Fuel Cell + Electrolysis Unit
Solar Array:			
Power (1)	301 kW	289 kW	566 kW
Manufacturing Cost	9.0 M$	8.7 M$	17.0 M$
Launch Cost (2)	9.4 M$	9.1 M$	17.7 M$
Area	21,600 ft^2	20,700 ft^2	40,600 ft^2
Weight (3)	14,700 lb	14,100 lb	27,600 lb
Altitude Maintenance:			
Solar Array Power	301 kW	289 kW	566 kW
Fuel Weight	108,800 lb	104,500 lb	204,700 lb
Fuel Launch Cost (4)	50.3 M$	48.3 M$	94.6 M$
Thermal Control:			
Heat Losses	38 kW	32 kW	79/231 kW
Weight			
Heat Exchangers	800 lb	680 lb	513 lb
Radiator (5)	2,300 lb	1,940 lb	4,646 lb
Manufacturing Cost			
Heat Exchangers (6)	2.4 M$	2.4 M$	220 K$
Radiator	1.8 M$	1.5 M$	3.6 M$
Launch Cost (4)	1.4 M$	1.2 M$	2.4 M$

Notes: (1) Beginning of life, based on 20 percent degradation over 30 years
(2) Based on volume requirements (958 kW/Shuttle)
(3) At 45 W/kg (20.5 W/lb)
(4) At 462 $/lb
(5) Pumped liquid radiators, 5.53 kg/m^2
(6) At $20,000 per unit

propellant requirement of 9.9 pounds per day for 300 kilowatts of solar array. Propellant manufacturing costs are miniscule compared to the Shuttle transportation cost of 462 $/pound for the propellant and are therefore neglected.

Comparisons of life-cycle cost and weight for the energy storage concepts (Table 5-3), which include the support elements as well as the energy storage equipment, show the nickel-hydrogen battery concept to have the lowest life cycle weight and cost for long-term missions in low earth orbit. The energy storage equipment costs are similar (101 M$) for the nickel-hydrogen batteries and the fuel cell plus electrolysis units. However, the low efficiency of the fuel cell plus electrolysis concept, compared to that of nickel-hydrogen batteries, requires approximately twice the solar array area for energy storage charging. This results in a 17 M$ cost difference for solar array support. In addition, the increased solar array area for the fuel cell plus electrolysis concept incurs proportionately greater drag and requires an additional 100,000 pounds of altitude maintenance fuel over 30 years. The added fuel requirement further increases the cost difference by 46 M$ further in favor of nickel-hydrogen. The high development costs experienced to date with fuel cell systems support the addition of another 45 M$ to this cost difference. Hence, the nickel-hydrogen battery is selected as the lowest cost, and incidentally lightest weight, energy storage concept for low earth orbit applications.

The solar array costs in the comparison (Table 5-3) are based upon realization of a manufacturing cost of 30 $/watt with the TRW Cassegrain mini-concentrator array. Present solar array costs for planar arrays are an order of magnitude higher (300 to 500 $/watt). Comparison of the energy storage concepts using a solar array specific cost of 300 $/watt (Table 5-4) increases the solar array cost difference between the nickel-hydrogen and fuel cell plus electrolysis concepts to 91.7 M$ from 17 M$. Nickel-hydrogen is then a clear economic choice for low earth orbit even if altitude maintenance fuel becomes negligible. Consequently, the nickel-hydrogen selection becomes even more cost favorable if the solar array cost reduction goals are not met (Table 5-4).

Table 5-3. Energy Storage Comparison
(250-kW System, LEO, 30-Year Life Cycle)

Concept Parameter	Nickel-Cadmium	Nickel-Hydrogen	Fuel Cell + Electrolysis Unit
System Costs (1980$):			
Energy Storage	243 M$	101 M$	101 M$
Solar Array[1]	18	18	35
Altitude Maintenance	50	48	95
Thermal Support	6	5	6
Recurring Cost[2]	317 M$	172 M$	237 M$
System Weight (pounds):			
Energy Storage	364,600 lb	95,000 lb	44,500 lb
Solar Array	14,700	14,100	27,600
Altitude Maintenance[3]	108,800	104,500	204,700
Thermal Support	3,100	2,620	5,200
Total	491,200 lb	216,220 lb	282,000 lb

Note: (1) Based on 30 $/W manufacturing costs plus Shuttle launch costs (Table 5-2).

(2) Delivered to a 160 nautical mile orbit; totals are 328, 177, and 243 M$ respectively for delivery to a 215 nautical mile orbit

(3) Fuel weight based upon a 215 nautical mile orbit.

Table 5-4. Present Solar Array Costs Suggest Nickel-Hydrogen (250-kW System, LEO, 30-Year Life Cycle)

Concept Parameter	Nickel-Cadmium	Nickel-Hydrogen	Fuel Cell + Electrolysis Unit
System Costs (1980$):			
Energy Storage(1)	243 M$	101 M$	101 M$
Solar Array(2)	100	96	188
Altitude Maintenance(3)	-0-	-0-	-0-
Thermal Support	6	5	6
Recurring Cost	349 M$	202 M$	295 M$
System Weight (pounds):			
Energy Storage	364,600 lb	95,000 lb	44,500 lb
Solar Array	14,700	14,100	27,600
Altitude Maintenance(3)	-0-	-0-	-0-
Thermal Support	3,100	2,620	5,200
Total	382,400 lb	111,720 lb	77,300 lb

Note: (1) Includes Shuttle launch charges for delivery to 160 nautical mile orbit.

(2) Based on 300 $/W manufacturing costs plus the Shuttle launch costs from Table 5-2.

(3) Assumes altitude maintenance fuel is negligible.

The costs associated with two of the support elements for energy storage (solar arrays and altitude maintenance fuel) each may be greater than the cost of the energy storage elements (solar arrays in Table 5-4, and altitude maintenance fuel in Table 5-3). The sizing of these support elements and hence their cost, is an inverse function of the efficiency of the energy storage system. Hence, technology improvements and design optimizations that provide major improvement in the efficiency of the fuel cell plus electrolysis unit concept will significantly reduce the total life cycle cost of the fuel cell plus electrolysis unit concept (energy storage and support elements). Sufficient improvement in this efficiency can make fuel cell plus electrolysis units cost competitive with nickel-hydrogen batteries. Periodic review of this trade is therefore warranted.

For short term missions, in which replacement is not involved, the nickel-cadmium battery is an appropriate energy storage selection. The initial equipment cost is comparable to the other concepts, and development costs are minimal.

Nickel-cadmium and nickel-hydrogen battery performance parameters are similar. Consequently, nickel-cadmium technology provides an alternative that allows additional time for nickel-hydrogen battery development. A nickel-cadmium battery can be installed for the initial energy storage equipment and subsequently replaced with nickel-hydrogen, provided that the larger volume requirement for nickel-hydrogen is included in the initial design.

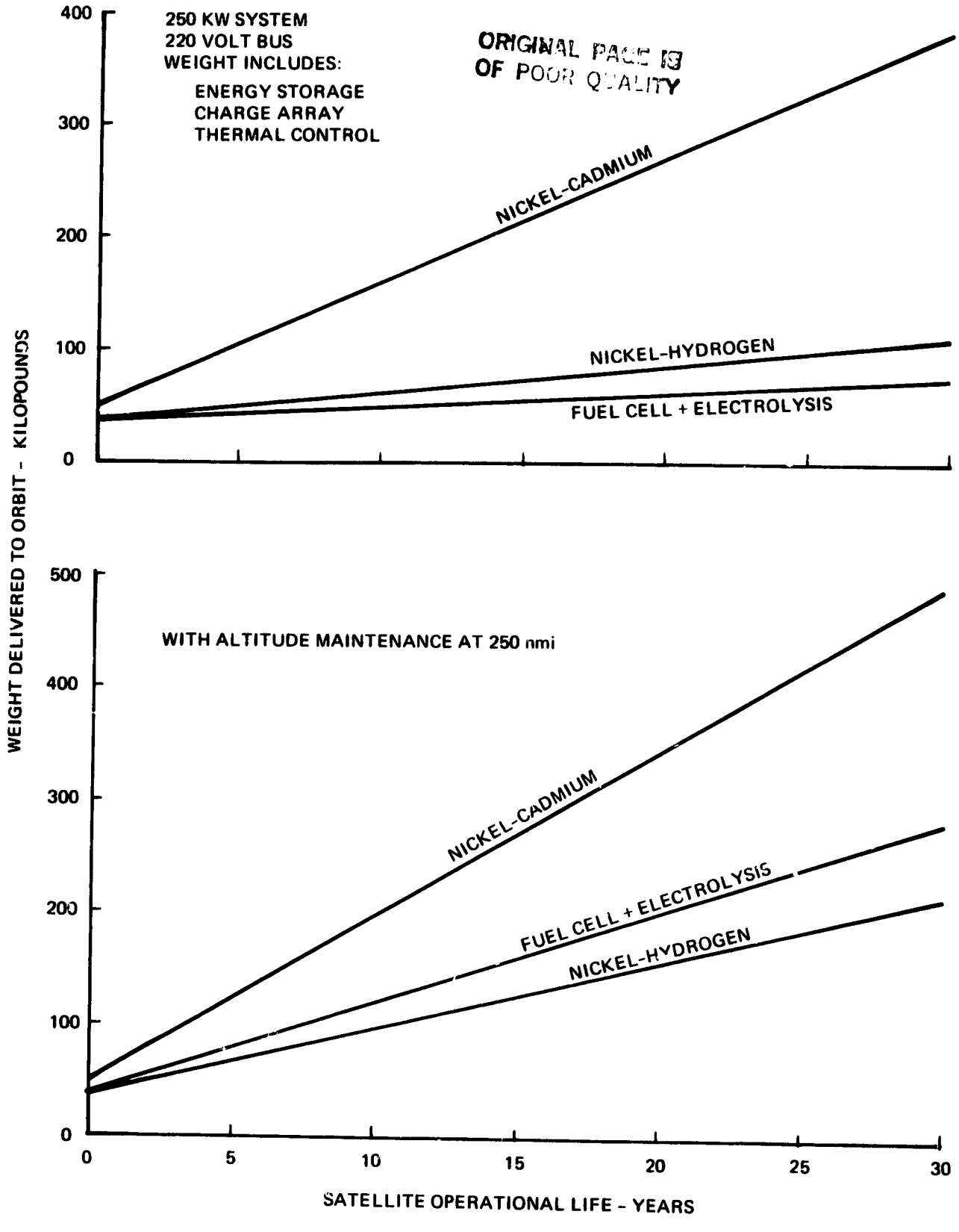

Figure 5-2. Altitude Maintenance Drives Weight Comparison

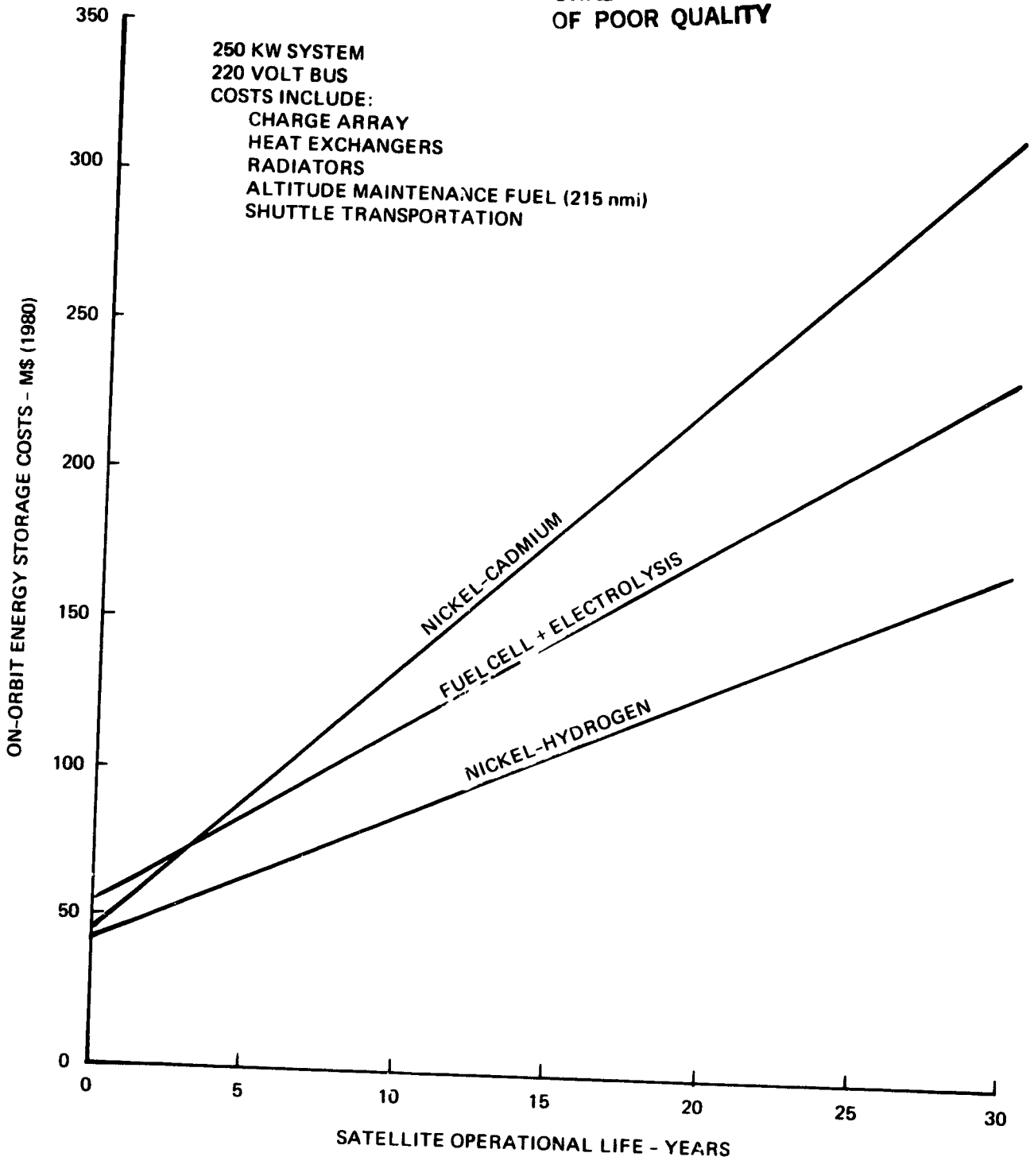

Figure 5-3. Nickel-Hydrogen Is Lowest Cost Energy Storage

5.2 NICKEL-CADMIUM BATTERY PARAMETERS

This analysis bounds and documents the life cycle cost of nickel-cadmium (Ni-Cd) batteries as applied to a 250-kilowatt power subsystem in low earth orbit. The data developed herein is utilized in the cost comparison of nickel-cadmium batteries, nickel-hydrogen batteries, and hydrogen-oxygen fuel cell plus electrolysis units to select the cost-effective energy storage method for a 250-kilowatt power subsystem.

The nickel-cadmium battery costs developed herein range from 23.5 to 11 million dollars (M$) for the initial battery complement of a 250-kilowatt power subsystem. These costs represent present technology and projectable improvements, respectively. These costs expand to 279 and 68 M$ for battery wearout and replacement over a 30-year operational period of the 250-kilowatt power subsystem.

The wide range of cost projections is due to the large uncertainty in projecting battery life (cycle life versus depth of discharge and battery life versus cell data) and the leverage that battery life has on both initial and 30-year battery costs. This life uncertainty is compounded by the variety of power utilization scenarios (load profiles) applicable to the system. In addition, the resupply scenario and redundancy requirements and the orbital altitude selection (160 nautical miles) also affect these battery costs. A significant operational research effort is required to examine these aspects, as they appear to have as great an impact on nickel-cadmium battery costs as technology improvements. However, the intent herein is to bound the range and evaluate the sensitivity of costs attributable to nickel-cadmium batteries rather than define the exact costs and specific design parameters of a nickel-cadmium battery system.

5.2.1 Capacity

A 250-kilowatt electrical power subsystem, powered by a solar array, requires energy storage to provide power during the typical eclipse in a low earth orbit. The energy storage to supply the 250 kilowatt payload is 153,333 Wh:

$$\text{Payload energy} = \frac{PT_1}{60} = \frac{250{,}000 \times 36.8}{60} = 153{,}333 \text{ Wh}$$

where P is the payload power demand and T_1 the eclipse time in minutes (36.8 minutes for 160 nautical-mile orbit).*

This payload energy must be increased for battery sizing by the losses incurred in the transmission conductors and the intervening power conversion equipment. The required battery energy is determined by multiplying the payload energy by the reciprocals of the efficiencies for the transmission conductors (ε_T), the battery to transmission line voltage power conversion equipment (ε_D), and the transmission line to service voltage power conversion equipment (ε_2). Assuming a 0.95 efficiency factor for each of these losses, the required capacity is increased to 178,840 Wh:

$$\text{Utilized energy} = \frac{PT_1}{60} \times \frac{1}{\varepsilon_D} \frac{1}{\varepsilon_2} \frac{1}{\varepsilon_T} = \frac{153,333}{0.95 \times 0.95 \times 0.95} = 178,840 \text{ Wh}$$

Installed battery capacity will be even greater due to the allowable depth of discharge (D) applied to the system to produce adequate life:

$$\text{Battery capacity} = \frac{\text{utilized energy}}{\text{depth of discharge}} = \frac{178,840}{D} \text{ Wh}$$

Typical depths of discharge for nickel-cadmium (Ni-Cd) batteries presently range from 15 to 25 percent of nameplate capacity for low earth orbit applications. Greater depth of discharge will be addressed herein to identify a cost effective approach.

*A 160 nautical mile orbit is addressed herein as a worst case for eclipse duration and for the ratio of eclipse to sunlight durations. Eclipse duration varies little (34.8 to 36.8 minutes) between 160 nautical miles and 2000 nautical miles. However, in a 160 nautical mile orbit, the drag on the large solar array area (two football fields) will require considerable reactant propellant to maintain the orbit. Higher orbits reduce the drag and the propellant requirement but impose a reduced Shuttle payload capability and increase Shuttle transportation specific costs (dollars per pound of payload). Optimization of the orbit altitude for reduced propellant consumption but increased Shuttle transportation costs is addressed in Appendix C.

5.2.2 Cell Size

The major supplier in the United States of nickel-cadmium (Ni-Cd) cells for spacecraft applications is General Electric (GE). Eagle Picher Industries is a possible alternative. Yardney Electric Corporation and SAFT America Incorporated have ceased production of spacecraft nickel-cadmium cells. SAFT (France) produces space-rated nickel-cadmium cells for European programs. Consequently, GE data will be utilized for the present technology baseline of nickel-cadmium cells.

GE produces prismatic space-rated cells in capacities of 2 to 100 Ah. Larger cells are possible, but the present equipment to manufacture plate material limits the size of conventional cell designs to approximately 150 Ah. Elongated cells with multiple terminals and headers but with a single plate pack have been proposed to attain larger capacities (e.g., the 200 Ah cell of Reference 5-1). However, these designs were not translated into hardware. Physical data is available from GE on a 100-Ah cell (Figure 5-4), and this cell is utilized for the baseline design point for nickel-cadmium batteries. This cell weighs 8.85 pounds which produces an energy density of 13.6 Wh per pound:

$$\frac{100 \text{ Ah} \times 1.2 \text{ volts}^*}{8.85 \text{ pounds}} = 13.6 \text{ Wh/lb (cell)}$$

Battery energy density is, therefore, projected at 12 Wh/lb based on a 13 percent allowance for the battery framing (end plates, thermal base, tie rods, electrical connections):

$$\frac{100 \text{ Ah} \times 1.2 \text{ volts}^*}{8.85 \text{ lb} \times 1.13} = 12 \text{ Wh/lb (battery nameplate density)}$$

5.2.3 Battery Cost

GE 100-Ah cells cost approximately $2,000 each (circa 1980) in large quantities (Figure 5-5). Cell prices are projected to be relatively linear with capacity in the 50 to 150 Ah range as cell price appears to increase

*See Section 5.2.6 for the derivation of average discharge voltage.

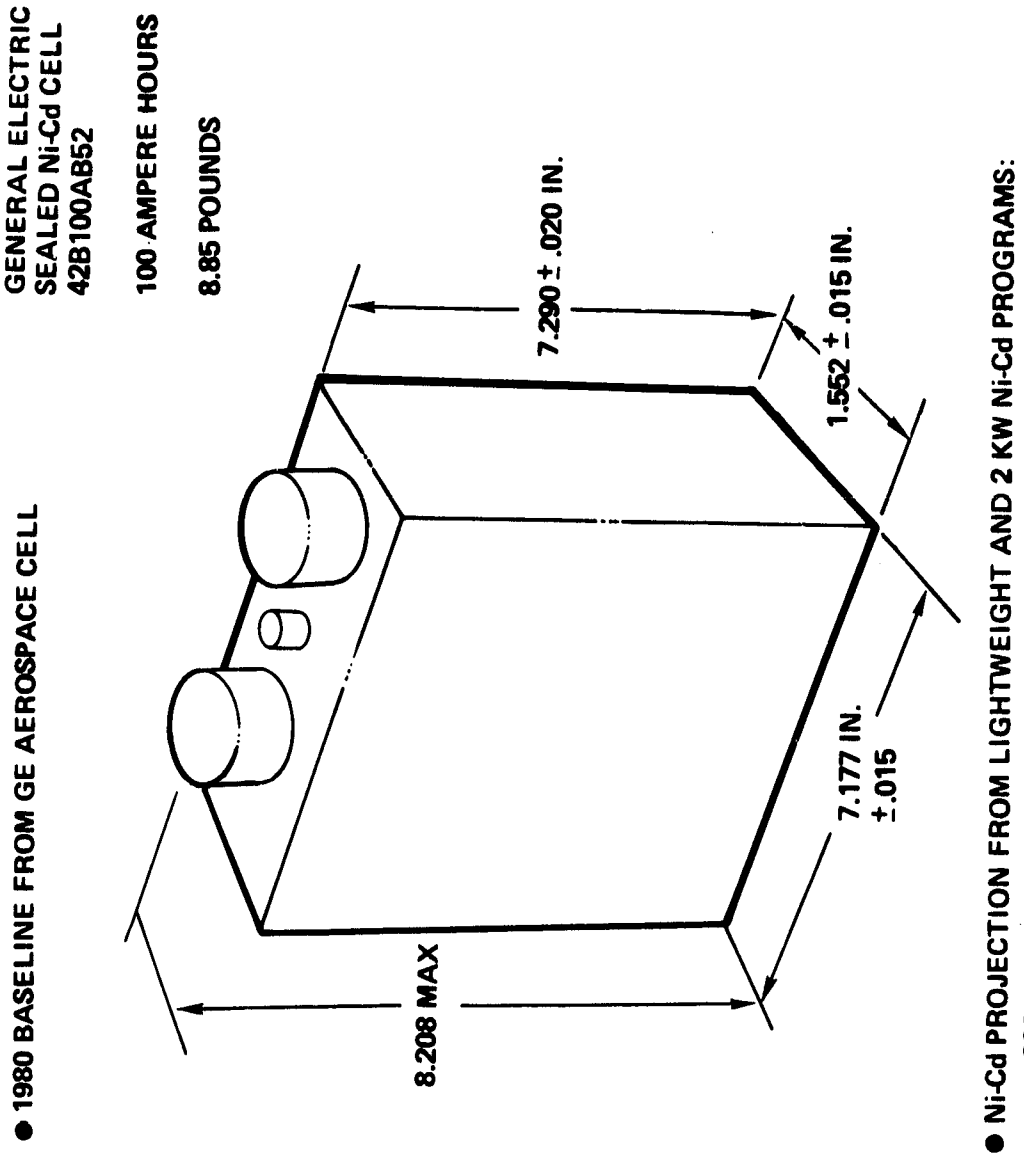

Figure 5-4. Baseline 100-Ah Nickel-Cadmium Cell

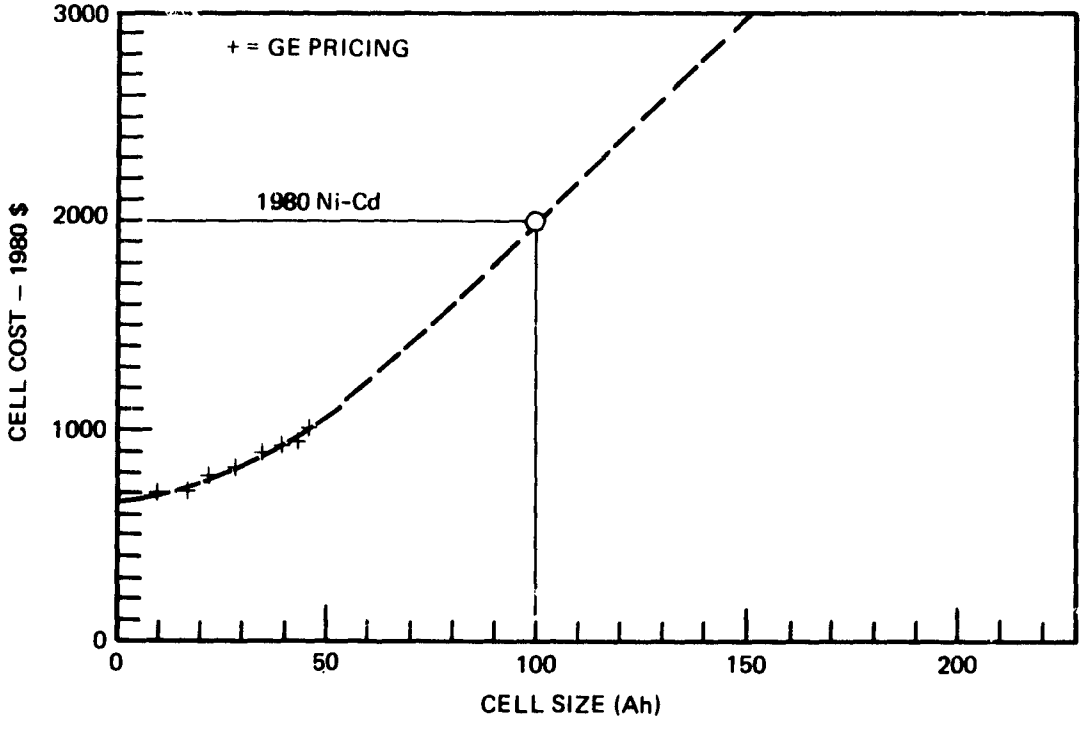

Figure 5-5. Nickel-Cadmium Cell Cost Projection

linearly with capacity for presently available sizes. This may be a pricing policy rather than being due to a significant cost component (e.g., plate material) directly related to cell ampere-hour capacity. Container, assembly, and test costs keep the cost of smaller capacity cells from linearly scaling to zero. Cell procurement costs are then 16.7$/Wh and 227 $/lb.

Assuming a nominal battery discharge voltage of 200 volts and a 1.2-volt per cell average discharge voltage, 167 series-connected cells per battery is the baseline design point. Each battery is presumed to be assembled (electrically connected) from several smaller battery modules of 28 cells each to facilitate handling during resupply (23 x 16 x 10-inch modules of 280 pounds). Aerospace ground equipment (AGE) is required for terrestrial handling, but this size is small enough to handle in zero gravity. (A 168-cell battery is 1680 pounds and potentially 123 by 16 by 10 inches.) Costs for module frames are estimated at $22,400/module of 28 cells and are projected by multiplying present satellite battery frame costs ($5,000) by the ratio of the surface areas (machining costs). This yields an $800/cell cost for packaging into battery modules ($22,400/28 cells = $800/cell).

Manufacturing and acceptance tests for present satellite batteries (22, 15-Ah cells) cost approximately $40,000 per battery. This value is also the projected cost for larger batteries as the tests are automated and are not dependent upon the quantity of cells in a battery. Hence, a 168-cell battery would have essentially the same $40,000 test cost. This yields a cost increment of $238/cell for battery testing. (Cell testing is included in the cell procurement cost.)

Summing the cell procurement cost, the battery module framing cost, and the battery testing cost yields an energy storage cost per cell of $3,200 ($2,000 + 800 + 238 = $3,038). This value is applicable to a rather large range in the cell quantity, i.e., it is applicable to cell lots of 500 cells or more -- provided the cells are 100-Ah hour size. Specific manufacturing costs for nickel-cadmium batteries are then $25.7/Wh of name-plate capacity and $304/lb.

Adding these derived manufacturing costs to the launch costs of 462 $/lb and 38.5 $/Wh (nameplate) yields total specific energy costs delivered on orbit for nickel-cadmium batteries of 766 $/lb and 64.2 $/Wh. Launch cost, at 60 percent of these totals, is the dominant contributor to total costs (Figure 5-6).

5.2.4 Depth of Discharge

Typically, nickel-cadmium batteries have been operated at a low depth of discharge, approximately 15 percent or less, for unmanned, non-repairable satellites in low earth orbits (approximately a 90 minute orbital period). This depth of discharge was necessary to attain the long cycle life required to meet minimum calendar-life goals. Loss of the battery subsystem meant replacing the entire satellite. Hence, low depth of discharge to attain adequate life was utilized, and redundant equipment to accommodate an early failure was provided.

The Shuttle Transportation System (STS) provides the opportunity to replace batteries periodically, as is necessary, without the penalty of replacing the remainder of the power system or satellite. However, the Shuttle transportation cost is large, 462 or 615 $/lb (dedicated or shared launch, Appendix B). Initial weight and cost are reduced by using a greater depth of discharge, but this reduces potential battery life and increases the resupply incidence and cost. Hence, an optimization exists for selecting the cost effective depth of discharge.

Cycle life decreases with increasing depth of discharge and temperature (Figure 5-7). Presuming batteries are kept at 0°C, experience indicates a mean cell cycle life ranging from 28,000 to 10,000 cycles for the range of 10 to 60 percent depth of discharge, respectively (Reference 5-2). As a first approximation, cell mean life is directly projected as battery life for replacement rate and cost calculations.

The relationship of depth of discharge and cycle life is not expressible simply in algebraic form. Therefore, a set of tabulated calculations (Table 5-5) is employed to identify the cost minimum -- 40 to 50 percent depth of discharge at 0°C. This depth of discharge significantly reduces the initial battery costs over a conventional selection of 15 to 25 percent

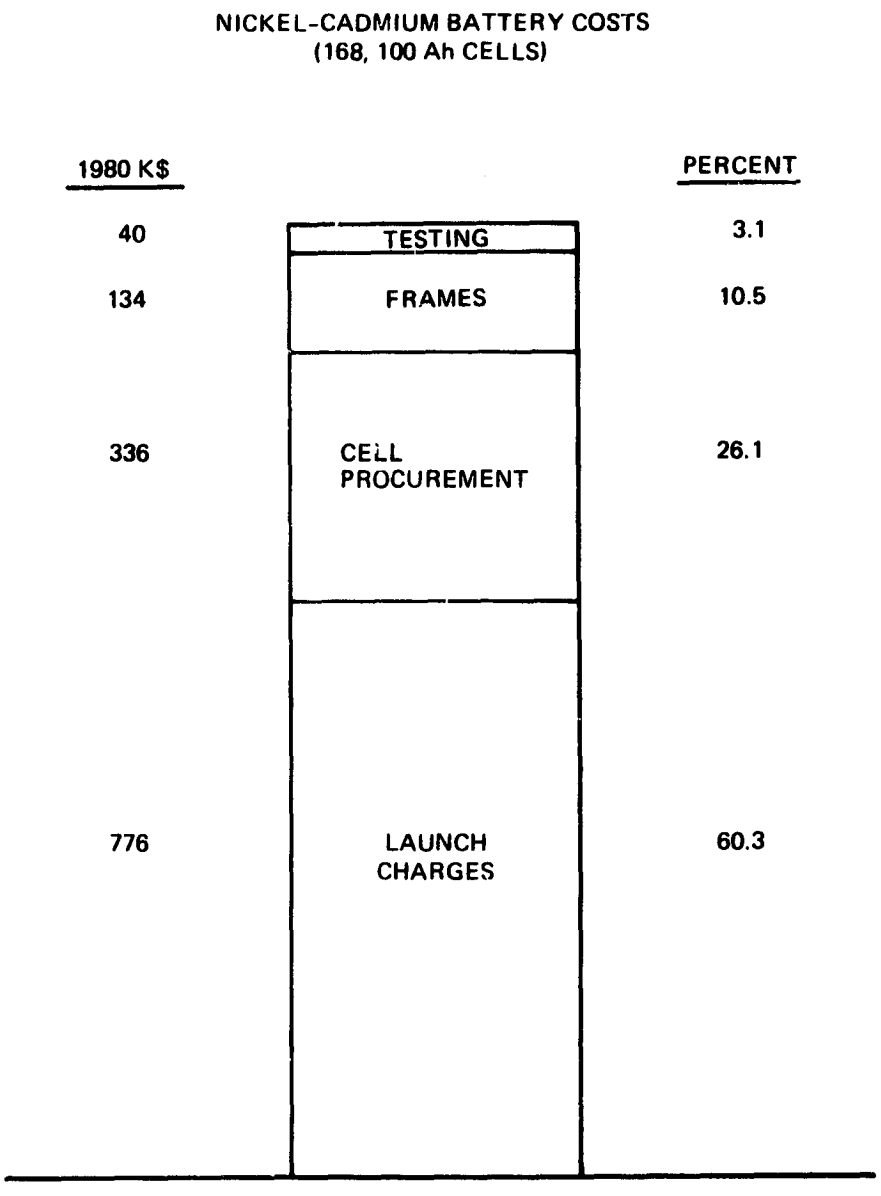

Figure 5-6. Transportation Dominates Ni-Cd Cost

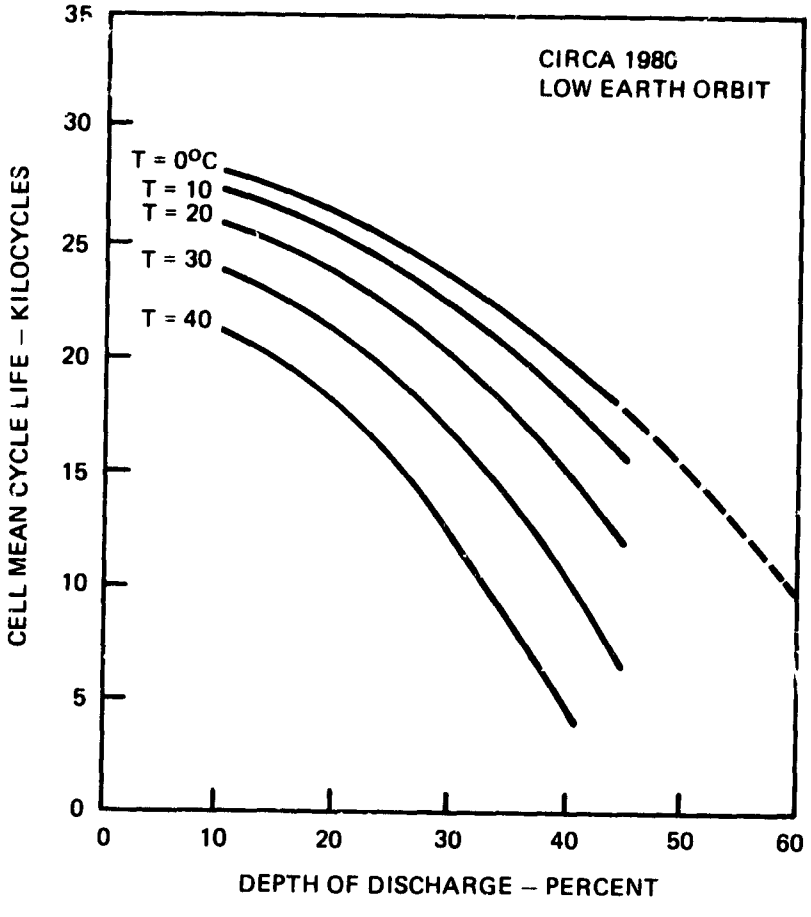

Figure 5-7. Nickel-Cadmium Battery Life Data Base

Table 5-3. Baseline Nickel-Cadmium Battery Costs

Operating Temperature	Depth of Discharge	Cell Quantity (1)	Cycle Life (2)	Calendar Life (4)	Initial Battery Weight	Annualized Resupply Weight	30-Year Orbital Weight	Initial Cost (5)	Annualized Resupply Cost (5)	30-Year Cost (5)
°C	%	Cells	Cycles	Years	Pounds	Pounds	Pounds	M$	M$	M$
0°	10	14,905	28,000	4.79	149,000	31,100	1,082,000	114.1	23.8	829
	15	9,936	27,500	4.71	99,400	21,100	732,400	76.1	16.2	561
	20	7,453	26,500	4.53	74,500	16,400	506,900	57.1	12.6	388
	25	5,961	25,000	4.28	59,600	13,900	476,600	45.6	10.6	365
	30	4,936	23,500	4.02	49,400	12,300	418,400	37.8	9.4	320
	35	4,258	22,000	3.76	42,600	11,300	381,600	32.6	8.7	292
	40	3,726	20,000	3.42	37,300	10,900	364,430	28.6	8.3	279
	45	3,312	18,000	3.08	33,100	10,700	354,100	25.3	8.2	271
	50	2,981	16,000(3)	2.74	29,800	10,900	356,800	22.8	8.3	273
	60	2,484	10,000(3)	1.71	24,800	14,500	459,800	19.0	11.1	352
20°	10	14,905	26,000	4.45	149,000	33,500	1,154,000	114.1	25.7	884
	15	9,936	25,000	4.28	99,400	23,200	795,400	76.1	17.8	609
	20	7,453	23,500	4.02	74,500	18,500	629,500	57.1	14.2	482
	25	5,961	22,000	3.76	59,600	15,900	536,600	45.6	12.2	411
	30	4,936	20,000	3.42	49,400	14,400	481,400	37.8	11.0	369
	35	4,258	17,500	3.00	42,600	14,200	468,600	32.6	10.9	359
	40	3,726	15,000	2.57	37,300	14,500	472,300	28.6	11.1	362
	45	3,312	12,000	2.05	33,100	16,100	516,100	25.3	12.3	395
	50	2,981	8,000(3)	1.37	29,800	21,800	683,800	22.8	16.7	524

Notes:

(1) 178,400 watt-hours utilized energy; 100-Ahr cells; 1.20-volt average discharge voltage.
(2) From Figure 5-7.
(3) Extrapolation from Figure 5-7 to verify cost trend reversal.
(4) Resupply scenario: replace failures, or degraded batteries, on next available resupply mission. Total battery complement replaced each calendar life period.
(5) Launch weight specific cost = 462 $/lb.

Table 5-5. Baseline Nickel-Cadmium Battery Costs (Continued)

Operating Temperature	Depth of Discharge	Cell Quantity (1)	Cycle Life (2)	Calendar Life (4)	Initial Battery Weight	Annualized Resupply Weight	30-Year Orbital Weight	Initial Cost (5)	Annualized Resupply Cost (5)	30-Year Cost (5)
°C	%	Cells	Cycles	Years	Pounds	Pounds	Pounds	M$	M$	M$
30°	10	14,905	23,500	4.02	149,000	37,100	1,262,000	114.1	28.4	966
	15	9,936	22,000	3.85	99,400	25,800	873,400	76.1	19.8	669
	20	7,453	21,000	3.59	74,500	20,800	698,500	57.1	15.9	535
	25	5,961	19,000	3.25	59,600	18,300	608,500	45.6	14.0	466
	30	4,936	17,000	2.91	49,400	17,000	559,400	37.8	13.0	428
	35	4,258	14,000	2.40	42,600	17,800	576,600	32.6	13.6	442
	40	3,726	10,500	1.80	37,300	20,700	658,300	28.6	15.9	504
	45	3,312	7,000	1.20	33,100	27,600	861,100	25.3	21.1	659
40°	10	14,905	21,500	3.68	149,000	40,500	1,364,000	114.1	31.0	1,045
	15	9,936	20,000	3.42	99,400	29,100	972,400	76.1	22.3	745
	20	7,453	18,000	3.08	74,500	24,200	800,500	57.1	18.5	613
	25	5,961	15,500	2.65	59,600	22,500	734,600	45.6	17.2	563
	30	4,936	12,000	2.05	49,400	24,100	772,400	37.8	18.5	592
	35	4,258	8,500	1.45	42,600	29,400	924,600	32.6	22.5	708
	40	3,726	5,000	.86	37,300	43,400	1,339,300	28.6	33.2	1,026

Notes:

(1) 178,400 watt-hours utilized energy; 100-Ahr cells; 1.20-volt average discharge voltage.
(2) From Figure 5-7.
(3) Extrapolation from Figure 5-7 to verify cost trend reversal.
(4) Resupply scenario: replace failures, or degraded batteries, on next available resupply mission. Total battery complement replaced each calendar life period.
(5) Launch weight specific cost = 462 $/lb.

depth of discharge, yet provides sufficient cycle life and reasonable resupply costs. The result is a somewhat more frequent replacement of a significantly smaller battery complement -- and cost optimization (Figure 5-8). Further, sufficient cost advantage is observed at the lower temperatures (88 M$ for a reduction of 0°C from 20°C) that the increased thermal radiator costs of operating the batteries at 0°C are more than offset.

The recurring battery costs for 40 to 50 percent depth of discharge at 0°C are essentially the same (8.2 to 8.3 M$/yr, Table 5-5). Thirty-year costs are 279, 271, and 273 M$, respectively, for 40, 45, and 50 percent depth of discharge at 0°C. This is an insignificant spread considering the uncertainty of the estimates. Hence, other considerations are needed to choose the most cost-effective depth of discharge. Initial battery costs for 50 percent depth of discharge are the least (fewer batteries in the energy storage complement), and the costs of auxiliary equipment (battery chargers, wiring, installation space, cold plates, and control functions) are also lowest for 50 percent depth of discharge (versus 40 or 45 percent depth of discharge). Hence, a 50 percent depth of discharge is considered the appropriate design point and is further pursued herein.

5.2.5 Operating Rates

At 50 percent depth of discharge, half of the nameplate capacity will be removed from each cell during the eclipse period. That is, 50 Ah will be removed in 36.8 minutes. The discharge current is thus 81.5 amperes:

$$\frac{50\ \text{Ah}}{36.8\ \text{min}} \times 60\ \text{min/h} = 81.5\ \text{amperes (average)}$$

This is a 0.815 discharge rate (0.815C or C/1.2). The resultant discharge plateau voltage is projected as 1.20 volts (average) per Figure 5-9 (1.00C rate).

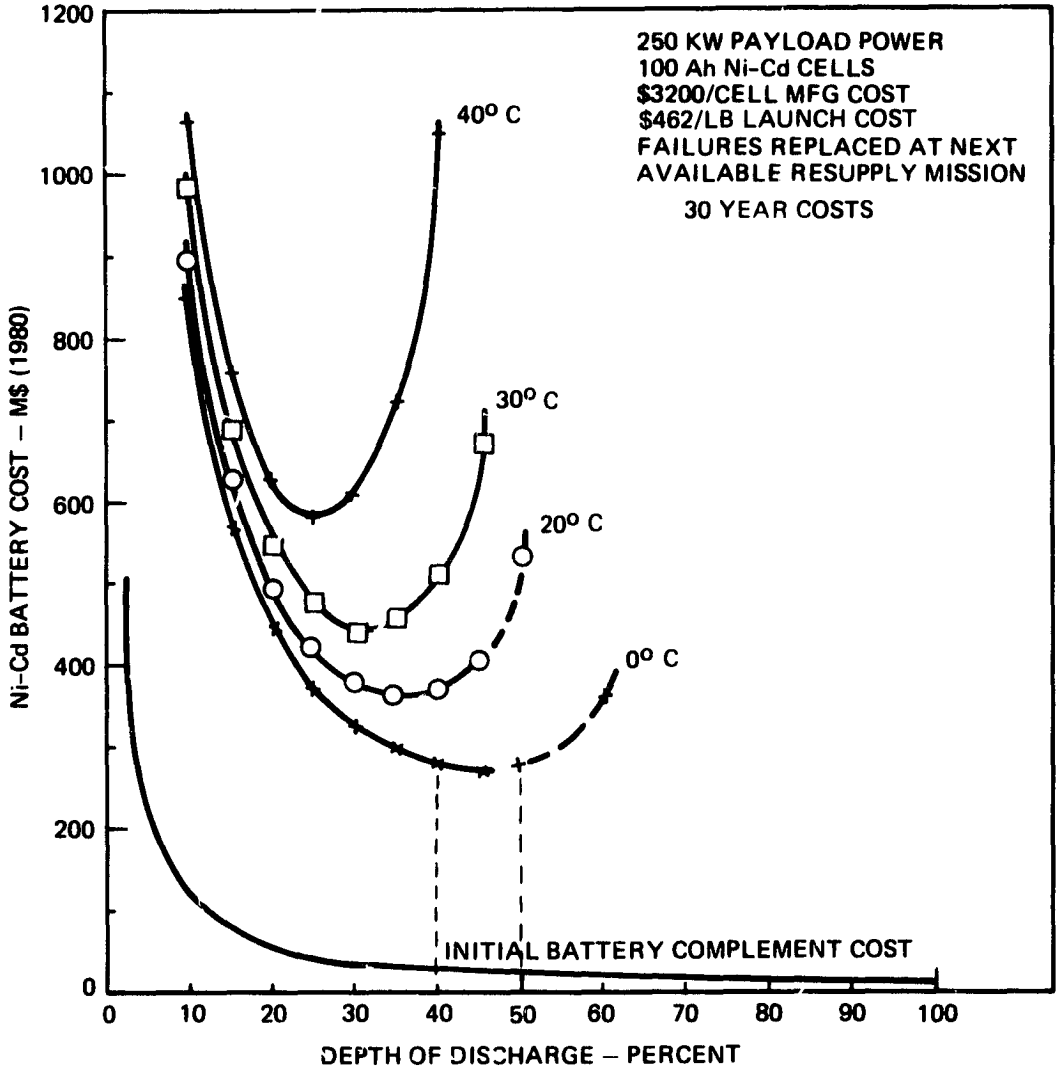

Figure 5-8. 40 to 50 Percent Depth of Discharge and 0°C Temperature Minimizes Cost for Nickel-Cadmium Batteries

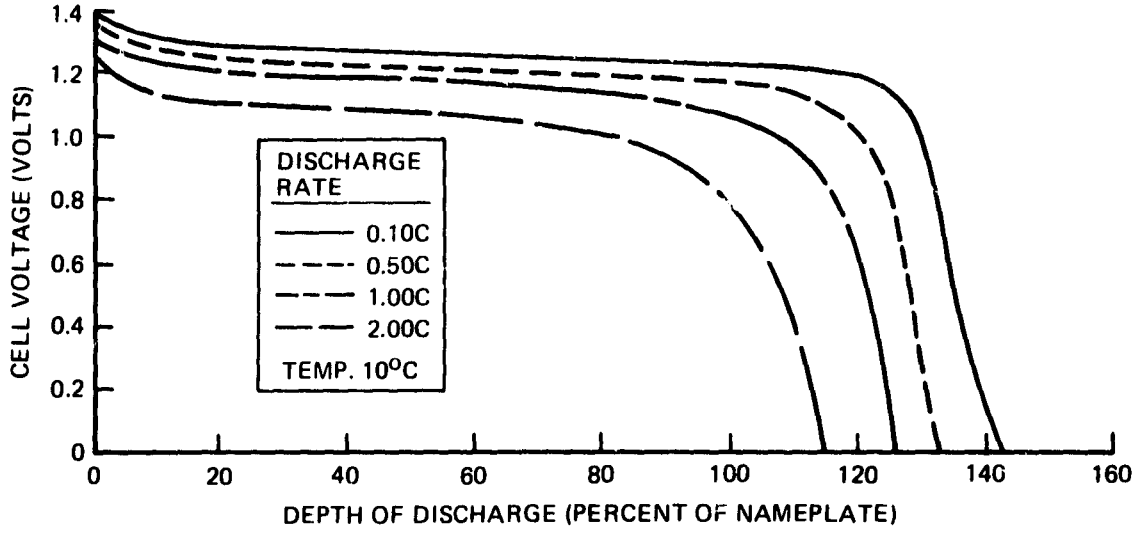

Figure 5-9. C/1.2 Results in 1.20-Volt Discharge Voltage Plateau

During charge, the eclipse energy is replaced over the sunlight period. In addition, an allowance of perhaps 10 percent (recharge ratio of 1.10) is needed to account for oxygen evolution during charge. Hence, the average charge current is 61.6 amperes:

$$\frac{50\ \text{Ah}}{53.6\ \text{min}} \times 60\ \text{min/h} \times 1.10 = 61.6\ \text{amperes (average)}$$

This is a C/1.6 charge rate and is relatively high. As such, it cannot be sustained in a constant current charging mode without excessive overvoltage after 80 percent or more of the charge return (battery state of charge). A taper charging mode is to be used with higher initial currents which reduce as the battery is recharged (typically at 80 percent state of charge). However, charge currents will still be high for the last 20 percent of recharge, and significant oxygen will be generated. Hence, the 10 percent overcharge allowance.

5.2.6 Thermal Dissipation

Considerable heat is generated in nickel-cadmium cells during discharge due to the exothermic electrochemical reaction of discharge and the recombination of oxygen (previously generated during overcharge). Electrical losses (I^2R) within the cell are considered negligible by comparison. During charge, heat is generated only due to recombination of oxygen. This oxygen recombination exponentially decreases as the oxygen partial pressure is reduced by recombination. Further, heating during charging is slightly moderated by the endothermic electrochemical reaction of charging. At the end of charge and during overcharge, oxygen is generated, cell pressure rises, and heating from oxygen recombination rapidly increases. However, the major heat generation period is during discharge due to the dominant heat generation mode of the exothermic discharge electrochemical reaction (Figure 5-10).

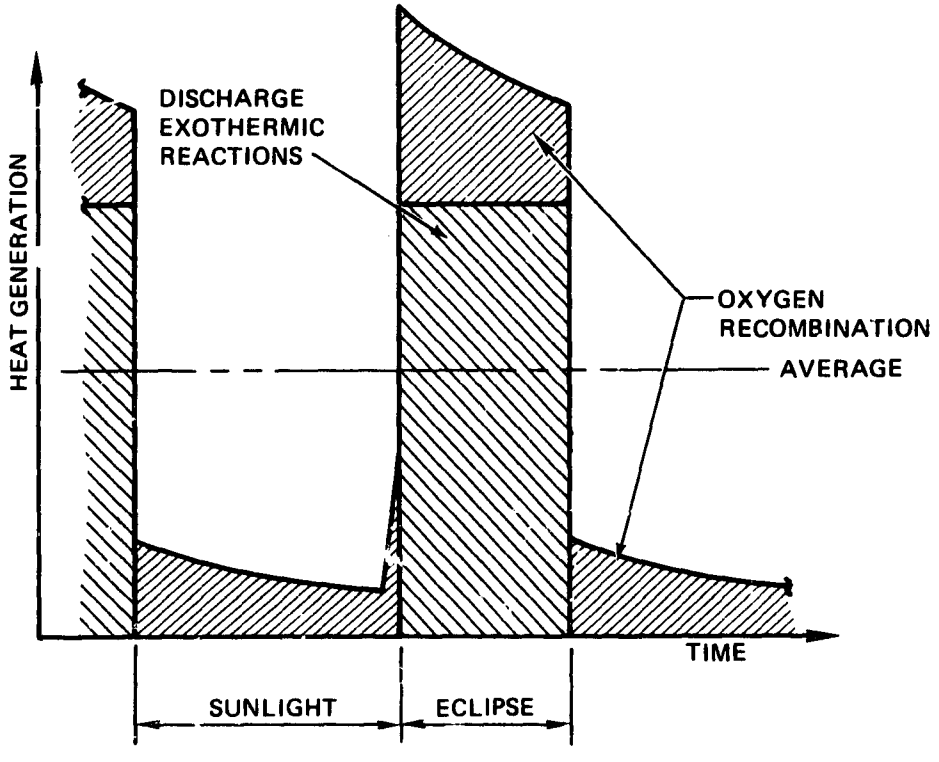

Figure 5-10. Major Heat Production Occurs on Discharge

The heat generation within the cell interior (plate pack) is much larger during eclipse (discharge) than the heat generated during sunlight (charge). However, the dominant mode of heat transfer to the battery exterior surfaces is by conduction. The thermal mass, cell internal thermal structure, and thermal paths from the cell surfaces to the battery thermal baseplate provide an integrating effect to produce a generally uniform heating rate at the thermal system interface (battery baseplate). Consequently, the battery baseplate and thermal system essentially service the average heating rate.

The difference between the charging energy (input) and the discharge energy (output) is dissipated as heat in the battery:

Charging energy (input) - discharge energy (output) = heat

$$\frac{1.45\ \text{V/cell} \times 61.6\ \text{A} \times 3000\ \text{cells} \times 53.6\ \text{min}}{60\ \text{min/h}}$$

$$- \frac{1.20\ \text{V} \times 81.5\ \text{A} \times 3000\ \text{cells} \times 36.8\ \text{min}}{60\ \text{min/h}}$$

= 239,378 - 179,952 = 59.4 kWh of battery heat per orbit.

Averaging this energy over the 90.4 minute orbit yields the thermal dissipation rate:

$$\frac{59.4\ \text{kWh/orbit} \times 60\ \text{min/h}}{90.4\ \text{min/orbit}} = 39.4\ \text{kW average heat rate}$$

This is the heat dissipation requirement for the thermal system radiator area. Typical radiator area will be approximately 1894 square feet (43.5 feet square) for 0°C battery baseplate operation and 39 kW average heat dissipation.

5.2.7 Technology Projection

Baseline nickel-cadmium battery costs, applying the price projection for the GE 100-Ah nickel-cadmium cell (Figure 5-5), are 3038 $/cell for manufacturing and test, 4620 $/cell for launch, and 8.3 M$/year for battery replacement (50 percent DOD). The resulting 30-year cost per satellite (250 kW power system) for nickel-cadmium batteries is 273 M$. Cost reduction is needed for a viable nickel-cadmium energy storage system.

The cost of nickel-cadmium batteries can be reduced by three means:

1) Reduce the recurring manufacturing cost of cells

2) Increase the effective battery energy density to reduce weight, and thereby, decrease the applicable Shuttle transportation costs

3) Increase the battery cycle life to reduce the incidence of battery replacement, and thereby, decrease replacement costs.

Each of these approaches is addressed herein to project a potential minimum cost for nickel-cadmium batteries.

The baseline manufacturing cost of $3038/cell for 100 Ah batteries is composed of cell procurement, battery framing, and battery testing:

Cost Term	Per Cell	Per Battery	Per Satellite
Cell procurement	$2,000	336 K$	6.4 M$
Battery frames	800	134	2.4
Battery tests	238	40	0.7
Total	3038	510 K$	9.1 M$

Two methods are available to reduce these costs: (1) greater manufacturing efficiency and (2) fewer cells and batteries, that is, bigger individual cells and batteries. Cell procurement costs were conservatively projected (Figure 5-5) for the baseline 100-Ah cell. An optimistic extrapolation yields $1510/cell for a 200-Ah cell (Figure 5-11). The 200-Ah cell is considered attainable but a reasonable limit to this cost extrapolation. Larger cells, up to 500 Ah rating are desirable, but common sense suggests their cost to be closer to the conservative projection of $10,000/cell than the optimistic extrapolation of $2,800/cell. Further a 200-Ah cell might be reasonably expected in a lightweight design with adequate thermal paths for the high rate of heat generation at the C/1.2 discharge rate.

Battery frame costs are also reduced. Battery framing is considered to be simplified to a thermal baseplate (including intercell thermal shims), a flat pressure-containment endplate, and tie rods. [Use mechanical support fixtures (aerospace ground equipment, AGE) for terrestrial handling.] Framing costs are, therefore, projected to reduce to $5,000 per module of 28 cells, $30K per battery.

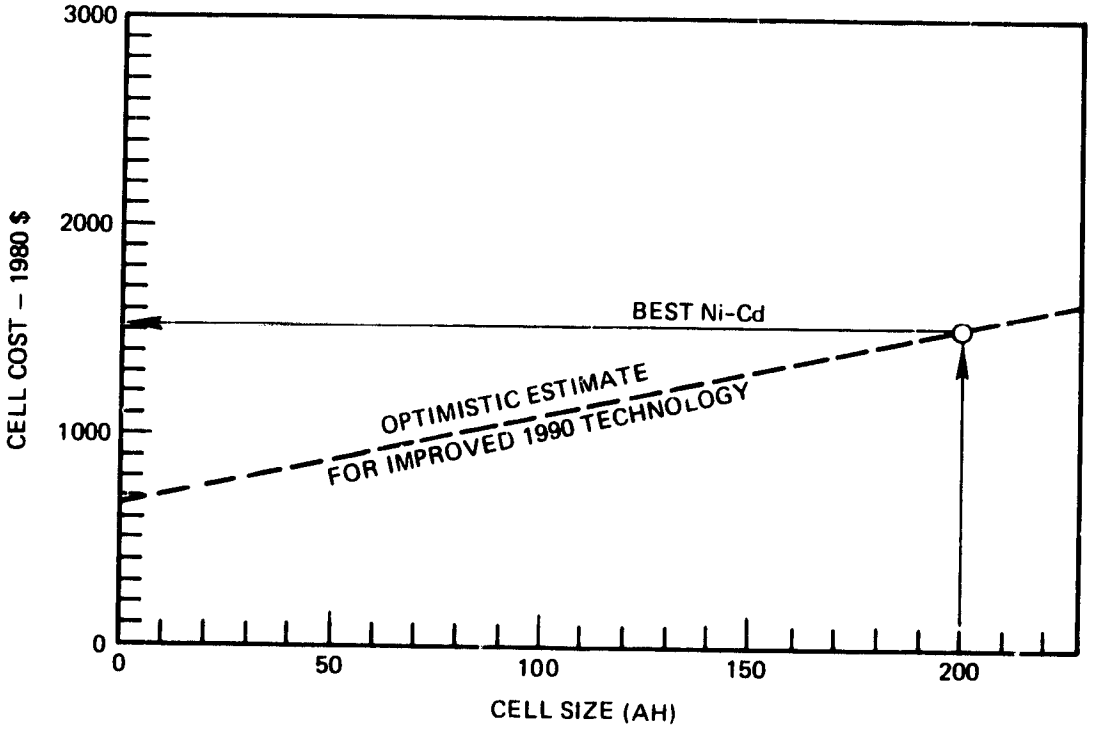

Figure 5-11. Optimistic Cost Projection for Ni-Cd Cells

These improvements reduce aggregate battery manufacturing costs to $1,926/cell.

Cost Term	Cell Cost	Rationale
Cell procurement	$1,510	Figure 5-11
Battery frames	178	$5000 ÷ 28 cells
Battery tests	238	$40,000 ÷ 168 cells
Total	$1,926	

Utilizing the 200-Ah capacity cell reduces the quantity of batteries to 9 (168, 200-Ah cells) from 18 (168, 100-Ahr cells) for the optimum 50 percent depth-of-discharge operation (Section 5.2.4). Thus, the quantity (and therefore, cost) of cells, battery frames, and battery tests is directly reduced:

Cost Term	9, 200-Ah Batteries	Rationale
Cell procurement	2.38 M$	$1,510 x 1512 cells
Battery frames	0.27	$5,000 x 6 modules x 9 batteries
Battery tests	0.36	$40,000 x 9 batteries
Total	2.91 M$	

Thus, nickel-cadmium battery manufacturing costs for the initial energy storage complement on a 250 kW power system are dramatically reduced to 2.9 M$ from the 9.1 M$ baseline.

Lightweight nickel-cadmium cells of 20-Ah nameplate capacity have been developed with energy densities of 23 Wh/lb yielding a battery energy density of 21 Wh/lb although of short life (Reference 5-3). Therefore, a goal of 24 Wh/lb for nickel-cadmium batteries can be projected to be achievable with further development in large cell sizes appropriate to a 250 kilowatt power system, even with the thermal design considerations of the higher power densities. This increased energy density of 24 Wh/lb doubles the baseline nickel-cadmium energy storage density of 12 Wh/lb.

Installed nickel-cadmium battery weight is, thereby, reduced to 15,120 pounds from 30,240 pounds for the baseline (3024, 100-Ah cells at 50 percent DOD). Allocated launch costs are, thereby, halved to 7.0 M$ from 14.0 M$ per 250 kilowatt system (or satellite):

$$1512 \text{ cells} \times \frac{1.2 \text{ V} \times 200 \text{ Ah}}{24 \text{ W/lb}} \times \$462/\text{lb} = 6.99 \text{ M\$}$$

$$3024 \text{ cells} \times \frac{1.2 \text{ V} \times 100 \text{ Ah}}{12 \text{ W/lb}} \times \$462/\text{lb} = 13.97 \text{ M\$}$$

Launch costs remain the dominant portion of the nickel-cadmium battery cost (Figure 5-12).

The projected reductions in manufacturing costs and allocatable launch cost (from reduced battery weight) inherently reduce the cost of each battery replacement event. Additional reduction in resupply cost is projected from a hypothesized increase in battery cycle life (Figure 5-13). This reduces the incidence of battery replacement and changes the depth of discharge for optimum cost (Figure 5-14). This is a significant reduction from the baseline costs (Figure 5-15) and provides a potential payback of 138 to 175 M$ in the 30 year life cycle cost for nickel-cadmium technology investment.

The technology improvements to realize these cost goals are reasonable individually, but would require a potentially expensive and dedicated technology development program. Furthermore, these improvements oppose one another and would represent a major improvement in nickel-cadmium technology. A lightweight design implies greater stresses and tighter tolerances. Increased stress potentially reduces life and tighter tolerances increase cost. Longer life implies reduced stresses and better fits (closer tolerances). This usually requires heavier and costlier designs. Further, thermal considerations for the heat generation and dissipation rates per unit weight implied in light-weight high-depth-of-discharge designs oppose cost reductions. Hence, these goals are considered a significant extrapolation of realizable nickel-cadmium technology and difficult to achieve simultaneously. Therefore, these cost projections for nickel-cadmium batteries in a 30-year, 250 kilowatt power system (Figure 5-15) are

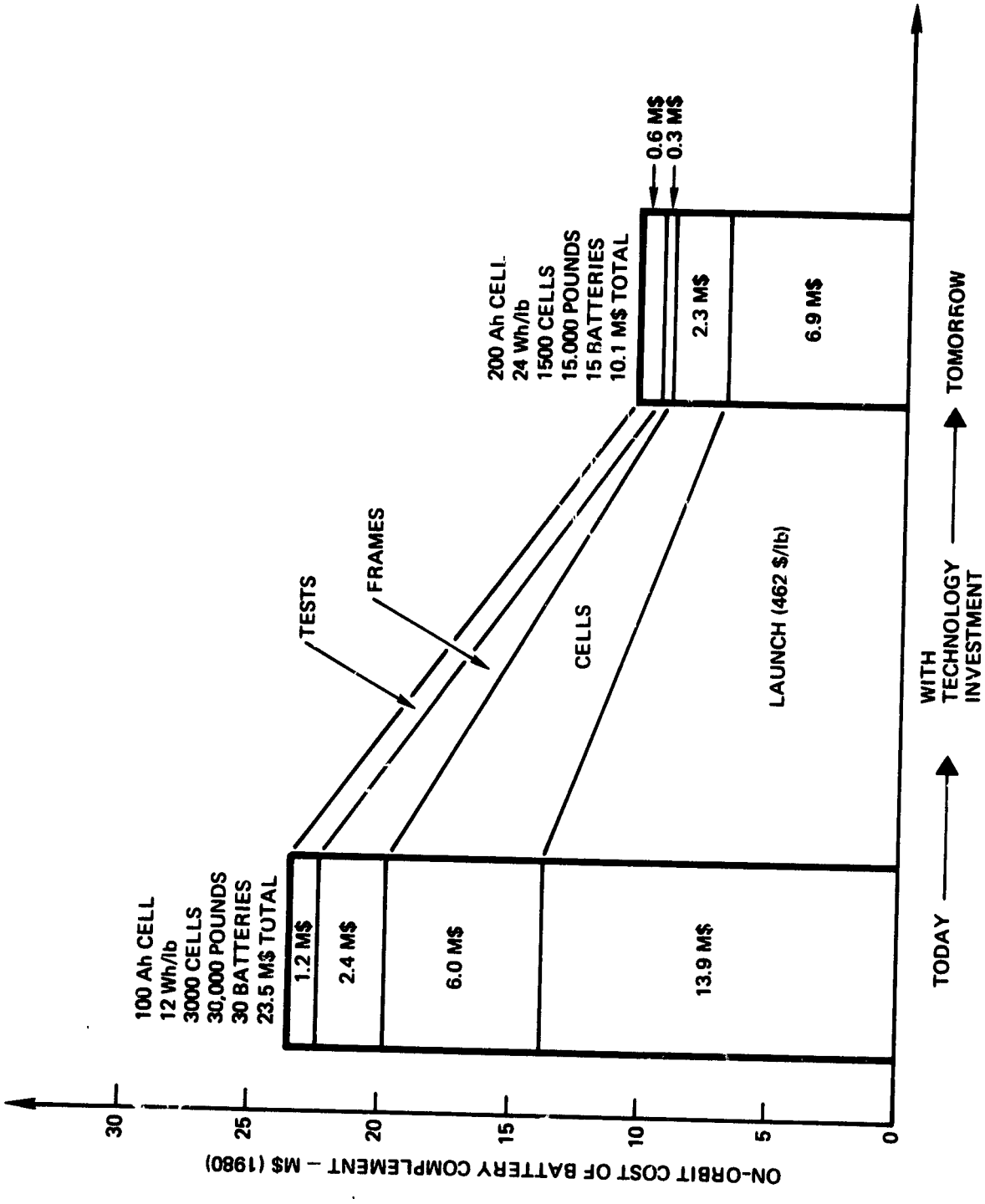

Figure 5-12. Launch Cost Keeps Ni-Cd Cost High

C-2

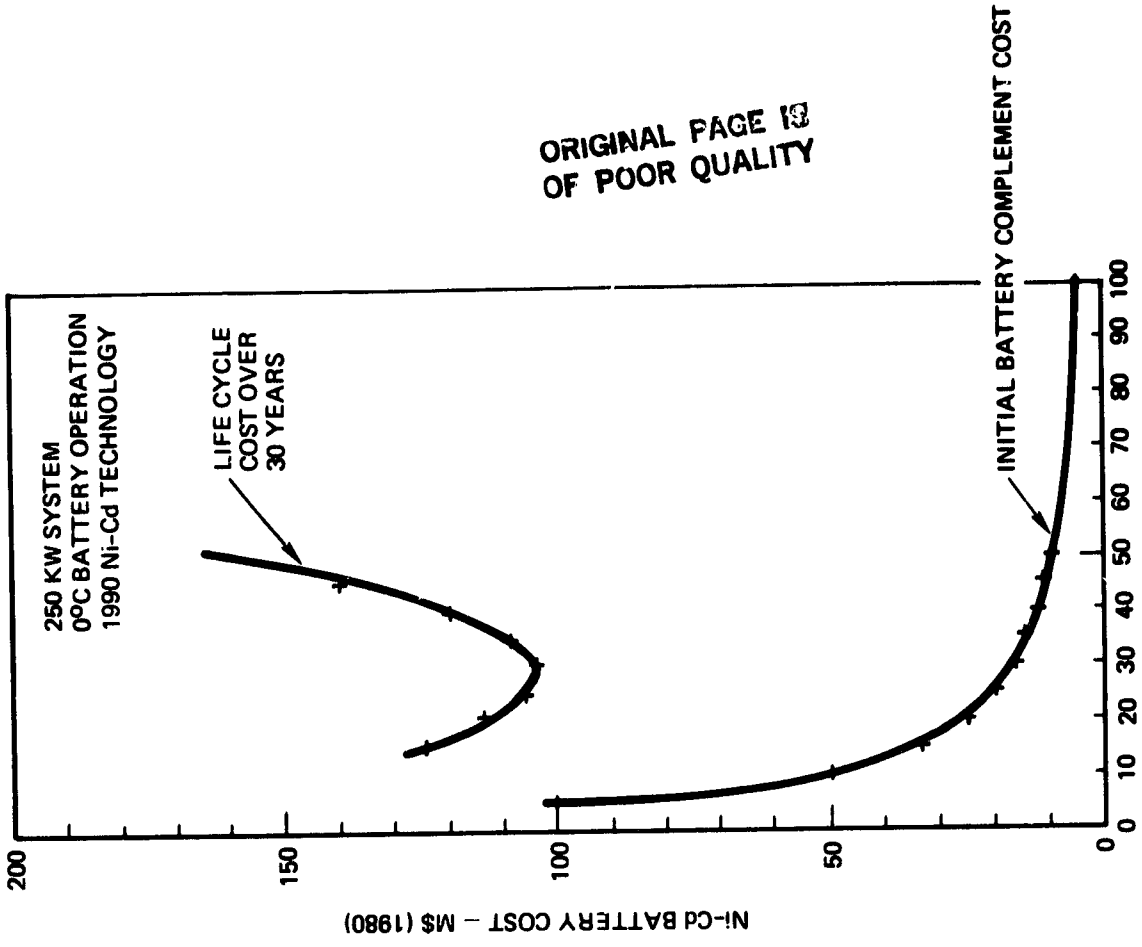

Figure 5-14. Technology Improvements Change Optimum Depth of Discharge

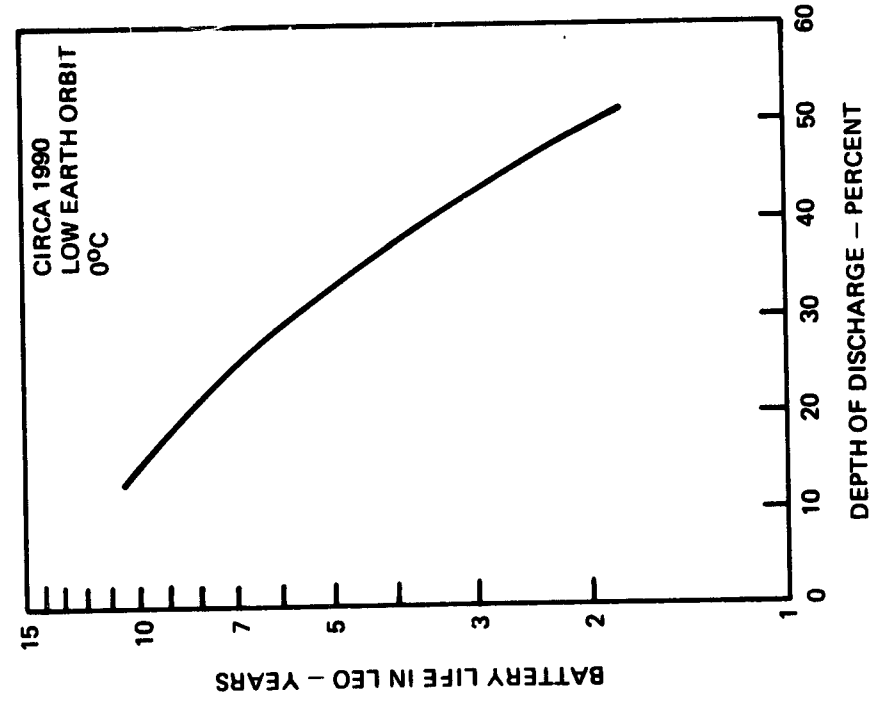

Figure 5-13. Hypothesized Ni-Cd Battery Life

best attainable with nickel-cadmium aerospace technology. To realize this cost goal, an expensive dedicated development program will be required. But this cost goal is not sufficient. Nickel-hydrogen ($Ni-H_2$) batteries, a young technology, projects similar costs and has the potential for further cost reductions as the nickel-hydrogen technology develops.

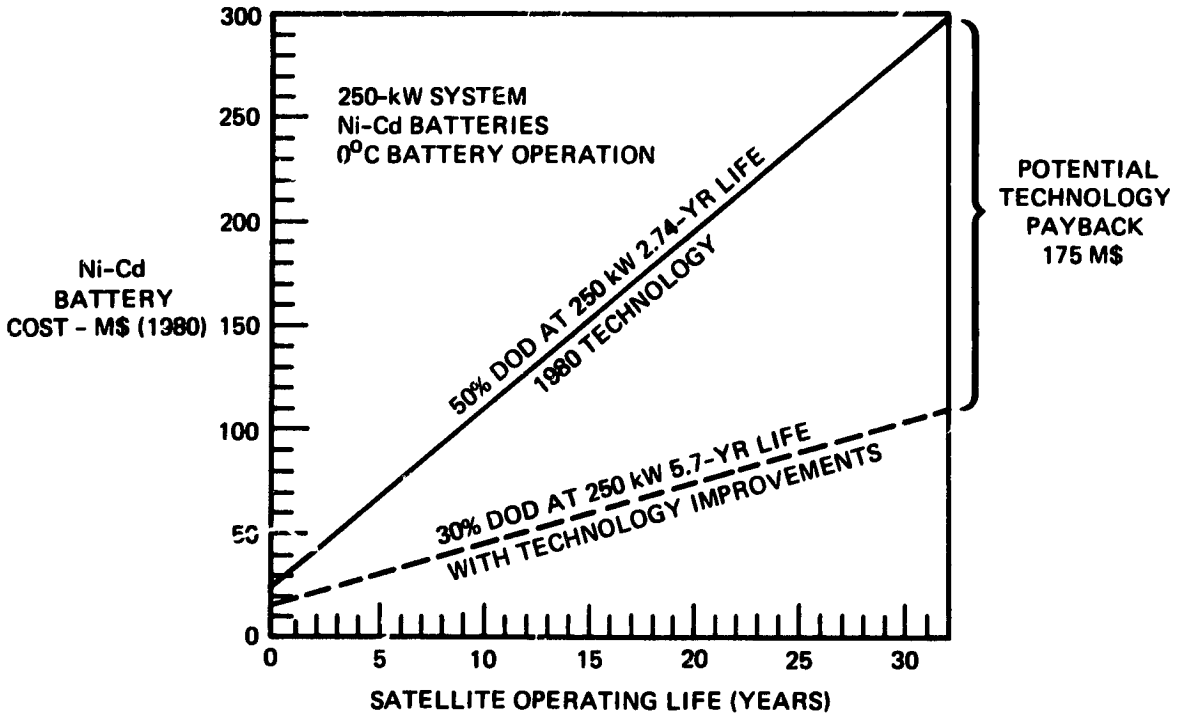

Figure 5-15. Technology Improvements Change Optimum Depth of Discharge

5.3 NICKEL-HYDROGEN BATTERY PARAMETERS

Serious nickel-hydrogen cell technology development commenced early in the 1970 decade with laboratory cell samples. Subsequent development has led to two viable concepts for nickel hydrogen cells (Comsat and AFAPL*) in less than a decade and with modest capital investment. This attests to the benign or forgiving nature of the basic electrochemistry in the nickel-hydrogen cell:

$$2NiO(OH) + H_2 \underset{\text{charge}}{\overset{\text{discharge}}{\rightleftharpoons}} 2Ni(OH)_2$$

Major development problems stem from electrolyte management, negative electrode flooding, oxygen recombination during overcharge, heat removal as cell sizes increase, and weight reductions.

The Comsat design includes 30- and 50-Ah cells that are intended for geosynchronous satellite applications. The AFAPL design (Figure 5-16) is a 50-Ah cell and is more suitable to low earth orbit operation than the Comsat design. The AFAPL cell is therefore selected as the reference technology base for nickel-hydrogen battery parameter development.

5.3.1 Capacity

A 250-kilowatt electrical power system, powered by a solar array, requires energy storage to provide power during solar eclipses. The eclipse energy to supply the 250-kilowatt payload in a typical low earth orbit is 153,333 Wh:

$$\text{Eclipse energy} = \frac{PT_1}{60} = \frac{250{,}000 \times 36.8}{60} = 153{,}333 \text{ Wh}$$

*AFAPL = Air Force Aero Propulsion Laboratory, Wright-Patterson Air Force Base, Dayton, Ohio.

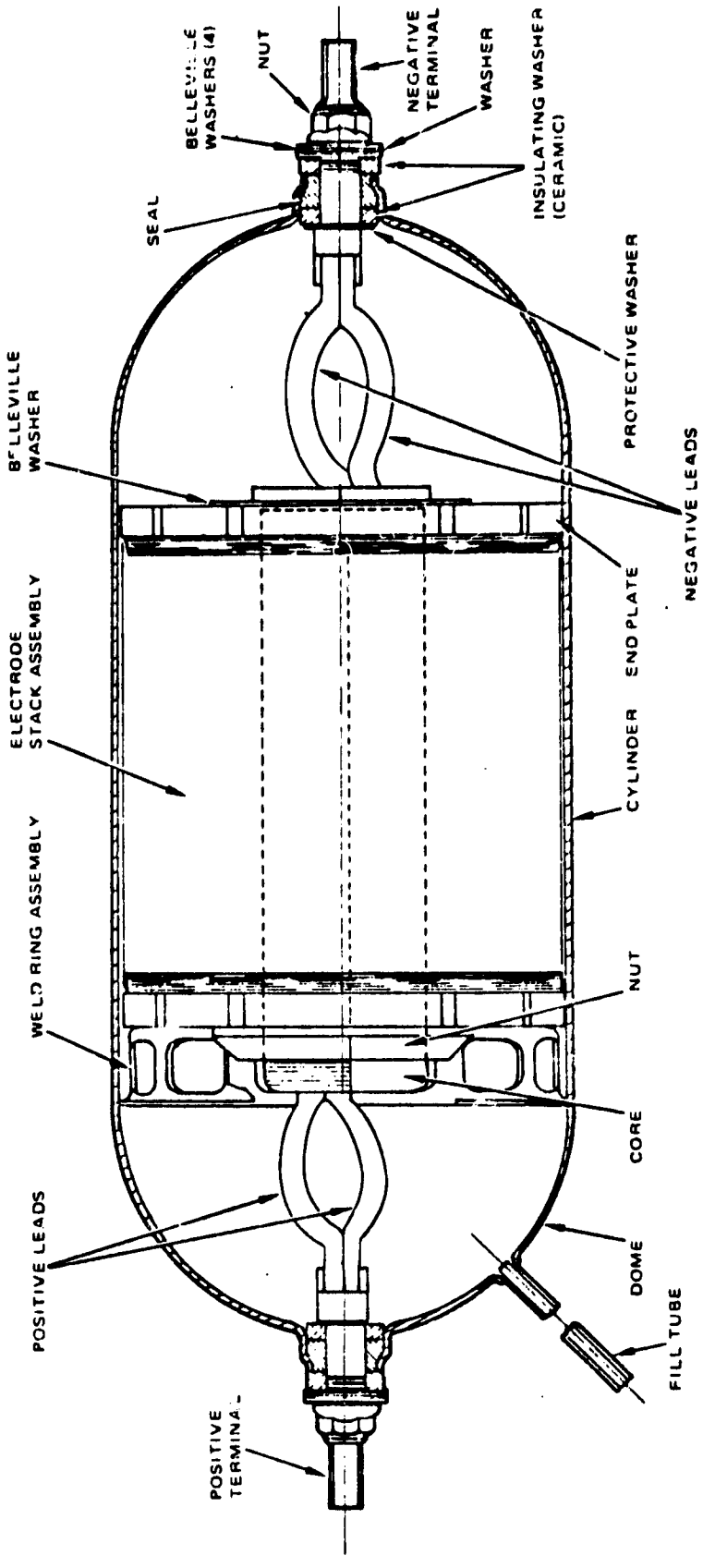

Figure 5-16. 50 Ah Nickel-Hydrogen Cell Construction

where P is the payload power demand and T_1 the eclipse time in minutes (36.8 minutes for 160 nmi orbit).*

This payload energy must be increased for battery sizing by the losses incurred in the transmission conductors and the intervening power conversion equipment. This energy requirement is increased by the reciprocals of the efficiencies for the transmission conductors (ϵ_T), for the battery to transmission line voltage power conversion equipment (ϵ_D), and for the transmission line to service voltage power conversion equipment (ϵ_2). Assuming a 0.95 efficiency factor for each of these losses, the required capacity is increased to 178,840 Wh:

$$\text{Utilized energy} = \frac{PT_1}{60} \times \frac{1}{\epsilon_D} \frac{1}{\epsilon_2} \frac{1}{\epsilon_T} = \frac{153{,}333}{0.95 \times 0.95 \times 0.95} = 178{,}840 \text{ Wh}$$

Installed battery capacity will be even greater due to the allowable depth of discharge (D) applied to the system to produce adequate cycle life:

$$\text{Battery energy} = \frac{\text{utilized energy}}{\text{depth of discharge}} = \frac{178{,}840}{D} \text{ Wh}$$

Typical depths of discharge for nickel-hydrogen cells presently approximate 80 percent of nameplate capacity for geosynchronous operation. Low earth orbit applications are suggested at 50 to 60 percent depth of discharge. The optimum depth of discharge (33 percent) that minimizes life cycle costs will be addressed to size the nickel-hydrogen battery capacity.

---

*A 160 nautical mile orbit is addressed herein as a worst case for eclipse duration and for the ratio of eclipse to sunlight durations. Eclipse duration varies little (34.8 to 36.8 minutes) between 160 and 2000 nmi. However, in a 160 nmi orbit, the drag on the large solar array area (two football fields) will require considerable propulsion fuel to maintain the orbit. Higher orbits reduce the drag and the fuel requirement but impose a reduced Shuttle cargo capability and an increased Shuttle transportation specific cost (dollars per pound of payload). Optimization of the orbit altitude for reduced fuel consumption but increased Shuttle transportation costs is indicated. This optimization is addressed in Appendix C.

5.3.2 Cell Manufacturers

Four companies recently have produced nickel-hydrogen cells under various development programs:

1) Eagle-Picher Industries, Joplin, Missouri

2) Energy Research Corporation, Bethel, Connecticut

3) Hughes Aircraft Company, El Segundo, California

4) Yardney Electric Corporation, Pawcatuck, Connecticut

In addition, SAFT, France, produces nickel-hydrogen cells for European programs.

Eagle-Picher has considerable experience with various cell designs (Comsat, AFAPL* back-to-back, AFAPL recirculating) and appears the most viable vendor. Consistently high price quotations from Hughes Aircraft indicate a reluctance to become a commercial supplier of nickel-hydrogen cells. Hughes Aircraft is presently considered a developer of nickel-hydrogen technology and a potential supplier of cells primarily for use in Hughes batteries. Energy Research presently is not involved in hardware development and assembly. Yardney Electric is engaged in a manufacturing technology development program sponsored by AFAPL* for cell cost reduction and is considered an alternate cell manufacturer.

The nickel-hydrogen parameters developed herein, including pricing, are derived from the Eagle-Picher experience on the AFAPL recirculating design with the Eagle-Picher pressure vessel.

5.3.3 Cell Parameters

Three cell sizes are evaluated herein for nickel-hydrogen batteries: 50, 150, and 250 Ah capacities. These cells represent present capability (50 Ah), near term development expectations (150 Ah), and a longer term possibilities (250 Ah). The data base derived for these cells is summarized in Table 5-6.

*Air Force Aero Propulsion Laboratory (AFAPL), Wright Aeronautical Laboratory (WAL), Wright-Patterson Air Force Base, Dayton, Ohio

Table 5-6. Ni-H_2 Cell Parameter Summary

Parameter \ Time	1980	1985 - 1986	1988 - 1990
Capacity	50 Ah	150 Ah	250 Ah
Weight	2.75 lb	6.6 lb	9.4 lb
Specific Energy, 1.25 V	22.7 Wh/lb	28.4 Wh/lb	33.2 Wh/lb
Manufacturing Cost	2300 $	4000 $	4000 $
Technology Improvement	-	Scale Up	Common Pressure Vessel

The 50-Ah cell is the AFAPL recirculating electrolyte management design presently produced by Eagle-Picher. This cell weighs 2.75 pounds (1250 grams) and has a specific energy of 22.7 Wh/lb based on nameplate capacity:

$$\frac{(1.25 \text{ volts}) \times (50 \text{ ampere hours})}{2.75 \text{ pounds}} = 22.7 \text{ Wh/lb } (10.3 \text{ Wh/kg})$$

The cost of this 50 Ah cell in large quantities is $2,300 (1980) based upon a recent (late 1979) purchase from Eagle-Picher.

Near term (by 1986) improvement is projected with the 150-Ah cell size. Initially, development of this cell is based upon computerized scaleup of the AFAPL 50-Ah cell maintaining similar computerized heat transfer characteristics. (A development program for this cell was projected for early 1982 but is presently deferred pending better definition of application(s) for this cell size.) The projection of the 150-Ah parameters include improvements for the increased ratio of active material to total weight, higher impregnation levels, and better utilization of the positive electrodes. The resultant cell weight is projected at 6.6 pounds (3000 grams) which produces a specific energy of 28.4 Wh/lb:

$$1.25 \text{ V} \times 150 \text{ Ah} \div 6.6 \text{ lb} = 28.4 \text{ Wh/lb } (12.9 \text{ Wh/kg})$$

A unit cost of $4,000 is projected for these 150-Ah cells. This cost is based upon the $2,300 price for the 50-Ah cell and the inherent scaleup factors: the increased size and quantity of plates contained in a single, but larger, pressure vessel.

The 250-Ah design represents additional scaleup from the 150-Ah cell and includes a common pressure vessel (CPV) for multiple cell stacks. This second level of scaleup and the packaging of multiple cell stacks into a single pressure vessel places readiness of this technology into the 1988-90 period. Common pressure vessel technology for nickel-hydrogen cells is in its infancy. Development programs at EIC Laboratory, Newton, Massachusetts, addressed three to five small cell stacks in a common laboratory container with promising results. However, these cell stacks are not compatible with the AFAPL cell design incorporating recirculating electrolyte management. Furthermore, large capacity cell stacks and common pressure vessel packaging with 20 or more cell stacks remain to be built and tested - a significant development effort.

The 250-Ah CPV design is estimated at 9.4 pounds (4250 kg) and $4,000 per cell equivalent. This estimate is based upon the AFAPL computerized scaleup from the 150-Ah cell to the 250-Ah as an individual pressure vessel design which indicates an 11-pound weight and $6,000 cost per cell. Packaging cells into a common pressure vessel (CPV) reduces the effective weight and cost per cell by 15 and 33 percent, respectively:

EP/AFAPL 50-Ah Cell		150-Ah Scaleup		250-Ah Scaleup		250-Ah CPV
2.75	→	6.6	→	11	→	9.4 pounds
2,300	→	4,000	→	6,000	→	4,000 dollars

Energy density is thereby increased to 33.2 Wh/lb for the 250-Ah design:

$$(1.25\ V) \times (250\ Ah) \div (9.4\ lb) = 33.24\ Wh/lb.$$

5.3.4 Battery Parameters

Nickel-hydrogen battery sizes are defined herein for the three cell sizes: 50, 150, and 250 Ah capacity (Table 5-7). Assuming a nominal battery discharge voltage of 200 volts and a 1.25-volt per cell average discharge voltage, 160 series-connected cells per battery is the reference

design point. Each battery is presumed to be assembled (electrically connected) from several smaller battery modules of 20 cells each to facilitate handling during replacement. AGE is required for terrestrial handling of the larger modules, but their size is small enough to handle in zero gravity.

Present nickel-hydrogen battery designs incur a packaging weight of approximately 15 percent of the 50-Ah cell weight. This packaging weight is estimated to reduce to 12 percent for the 150-Ah cells based upon a learning curve projection to 1986. A 10 percent packaging weight is projected for 1990 technology with multiple cells in a common pressure vessel. These packaging factors produce batteries weighing 506, 1183, and 1654 pounds and reduce the specific energy to 19.7, 25, and 30 Wh/lb, respectively (Table 5-7).

Battery manufacturing costs are composed of cell procurement, battery module assembly, and battery acceptance test costs. Cell costs are

Table 5-7. Nickel-Hydrogen Battery Parameter Summary

Parameter \ Time	1980	1985 - 1986	1988 - 1990
Cell Capacity	50 Ah	150 Ah	250 Ah
Cell Quantity	160	160	160
Cell Weight	440 lb	1056 lb	1504 lb
Battery Weight	506 lb	1183 lb	1654 lb
Packaging Weight	15%	12%	10%
Specific Energy	19.7 Wh/lb	25 Wh/lb	30 Wh/lb
Manufacturing Cost	536 K$	808 K$	808 K$
Shuttle Transportation Charge	234 K$	547 K$	764 K$
On-Orbit Cost	770 K$	1,355 K$	1,572 K$
Specific Manufacturing Cost	54 $/Wh	27 $/Wh	16 $/Wh
Specific Cost On Orbit	77 $/Wh	45 $/Wh	31 $/Wh

identified in Table 5-5 (Section 5.3.3). Assembly costs for 20-cell nickel-hydrogen battery modules are estimated at $16,000 per module: $128,000 per 160-cell battery; $800 per cell. This is based upon recent costs to build nickel-hydrogen cell modules adjusted for appropriate scaleups and learning allowances.

Manufacturing tests (acceptance tests) for present nickel-cadmium batteries (22, 15-Ah cells) cost approximately $40,000 per battery. This value is also the projected test cost for larger batteries because the tests are automated and are not dependent upon the quantity of cells in a battery. Hence, a 160-cell battery would have essentially the same $40,000 test cost. This yields a cost increment of $250/cell for battery testing. (Cell testing is included in the cell procurement cost.)

Shuttle transportation charges are derived from battery weight and the specific charge of 462 $/lb. For the present-day 50-Ah batteries, Shuttle charges are only 30 percent of total on-orbit cost, and manufacturing costs are 70 percent of the total on-orbit battery cost. Potential cost reductions are available through technology advancements. These potential reductions are included in the projections of 1986 and 1990 technology (150 Ah and 250 Ah cell designs). The result is a 20 M$ cost reduction in each battery complement installed in a 250-kW power system (Figure 5-17). This 20 M$ cost reduction recurs for each resupply of a spacecraft battery complement.

5.3.5 Depth of Discharge

Data for extended cycling of nickel-hydrogen cells in support of a low earth orbit is extremely limited. The plot of cycle life versus depth of discharge (Figure 5-18) suggested by Don Warnoch of AFAPL is utilized for this study. Low earth cycling data from continuing Hughes Aircraft and TRW tests tend to confirm this projection at this time (early 1980). The continuing tests at Hughes and TRW also suggest improvements will be attained in cycle life for 1986 and 1990 nickel-hydrogen technology. These improvement are projected as essentially increasing the cycle life uniformly from the 1980 baseline. Hence, the 1986 and 1990 projections are parallel lines to the Warnoch estimate (Figure 5-19).

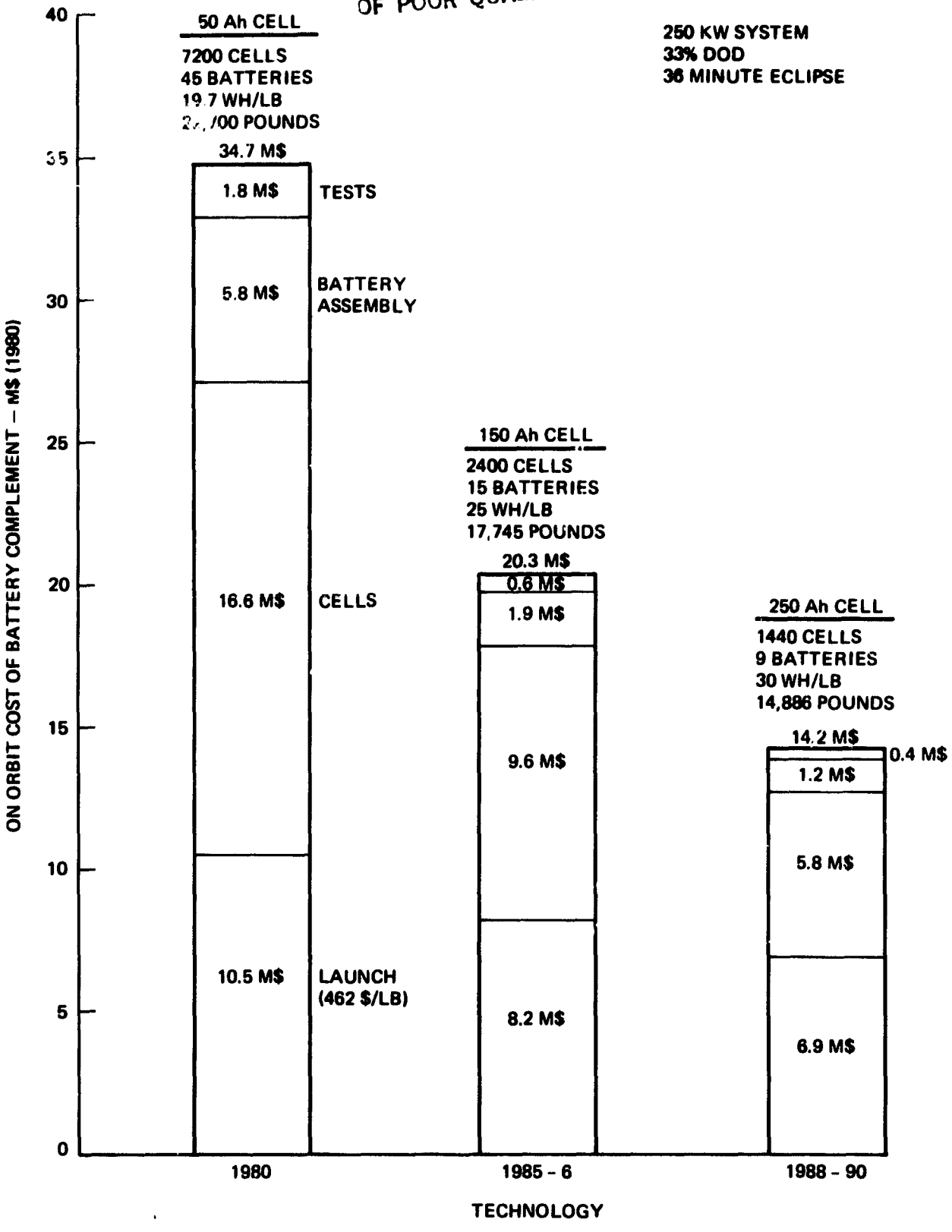

Figure 5-17. Technology Improvement Reduces Nickel-Hydrogen Costs by 20 M$

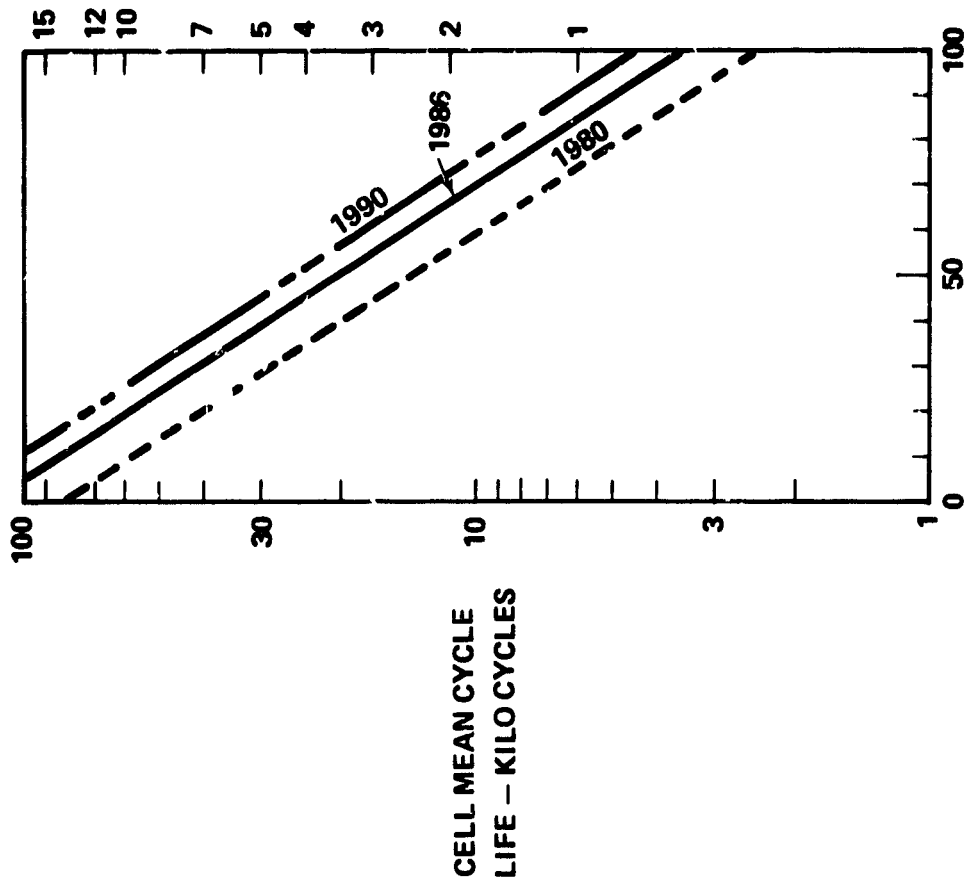

Figure 5-19. Nickel-Hydrogen Cycle Life Projections

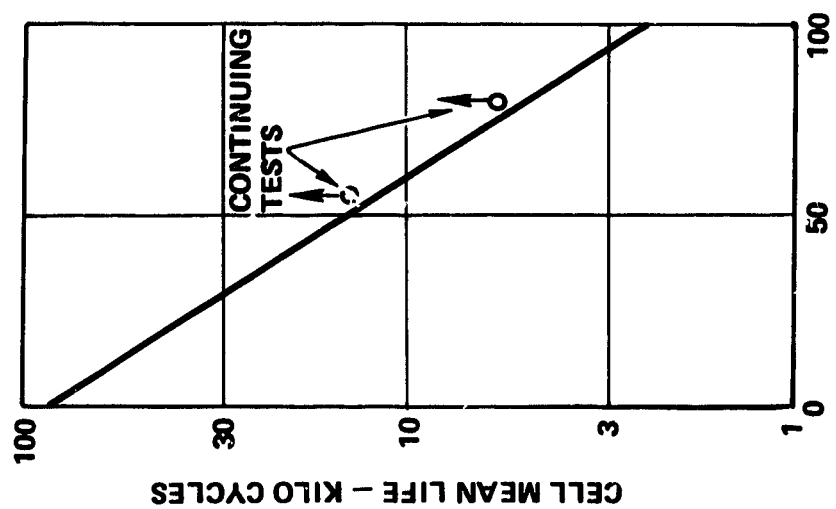

Figure 5-18. Nickel-Hydrogen Cycle Life Baseline

Translation of these semi-logrithmic plots of cycle life versus depth of discharge into a log-log plot (Figure 5-20) indicates the depth of discharge to minimize battery replacements over an extended mission life. (See Section 5.5.) The projections of nickel-hydrogen cycle life versus depth of discharge (Figure 5-18) produce a 30 percent depth of discharge (Figure 5-20) for weight and cost optimization of battery replacements. Optimum depth of discharge becomes 33 percent when the cost and weight effects of the initial battery complement is included.

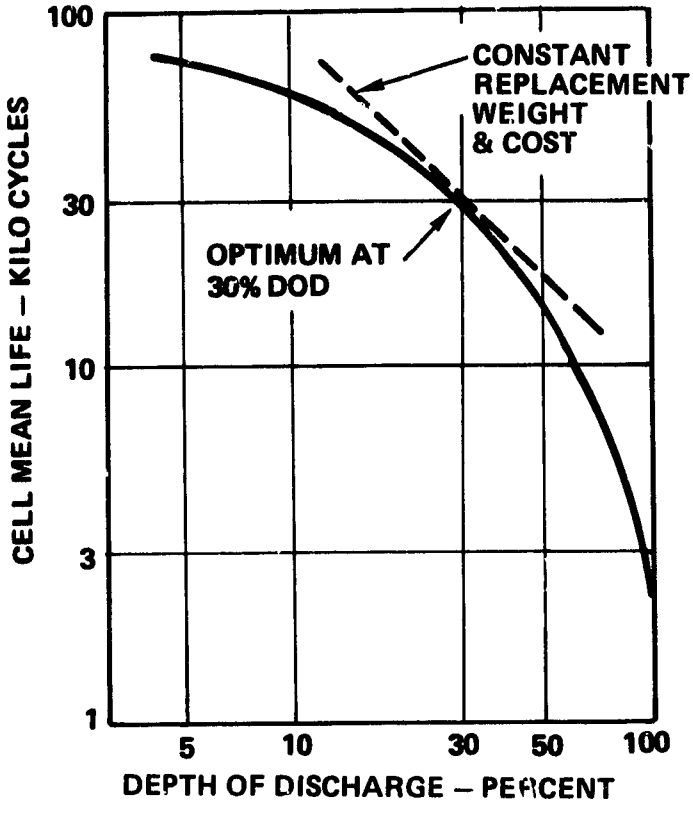

Figure 5-20. Replacement Costs and Weight are Minimized at 30 Percent Depth of Discharge for Nickel-Hydrogen Batteries

This optimum depth of discharge (33 percent) is unexpectedly low. Normally, nickel-hydrogen batteries are expected to be operated at high depths of discharge, 50 to 80 percent. To attain these higher values, a significant change is required in the slope of the projection of cycle life versus depth of discharge (Figures 5-18 and 5-19). Hence, a critical need in nickel-hydrogen technology is a data base to substantiate the relationship of cycle life versus depth of discharge.

5.3.6 Weight

The weight of the initial battery complement for a 250-kilowatt system is an inverse function of the allowable depth of discharge.

$$\text{Battery complement weight} = \frac{\text{eclipse energy}}{\text{depth of discharge}} \times \frac{\text{battery weight}}{\text{battery energy}}$$

A high depth of discharge consistent with life requirements is desirable to minimize total battery weight on nonserviceable missions (Figure 5-21). However, extended life requirements and replacement capability (Shuttle transportation and servicing) dictates a new design approach based on minimum life cycle cost and weight.

The total weight of batteries delivered to orbit increases as satellite life is significantly extended and battery wearout occurs requiring replacements. The weight of the battery replacements becomes dominant, and optimization of life cycle weight is needed. Initial weight is reduced by using a greater depth of discharge, but this reduces potential battery life and increases the resupply incidence. Hence, an optimization exists for selecting the optimum depth of discharge. The weight of battery replacements is a function of the satellite life, battery life, and the initial battery complement weight:

$$\text{Battery replacement weight} = \frac{\text{eclipse energy}}{\text{depth of discharge}} \times \frac{\text{battery weight}}{\text{battery energy}} \times \frac{\text{satellite life}}{\text{battery life}}$$

The weight of the battery replacements is minimized by maximizing the product of depth of discharge and battery (cycle) life. The projections of the depth of discharge and cycle life relationship (Figure 5-19) define the depth of discharge for minimum replacement weight as 30 percent. Adding the inverse depth of discharge effect of the initial battery complement (Figure 5-21) produces a 33 percent depth of discharge (the optimum) to minimize the total battery weight (initial complement plus replacements) delivered to orbit over the 30-year period of interest. The optimized life cycle weights of batteries are significant (Figure 5-22) and represent the dominant weight (and cost) component in the power system.

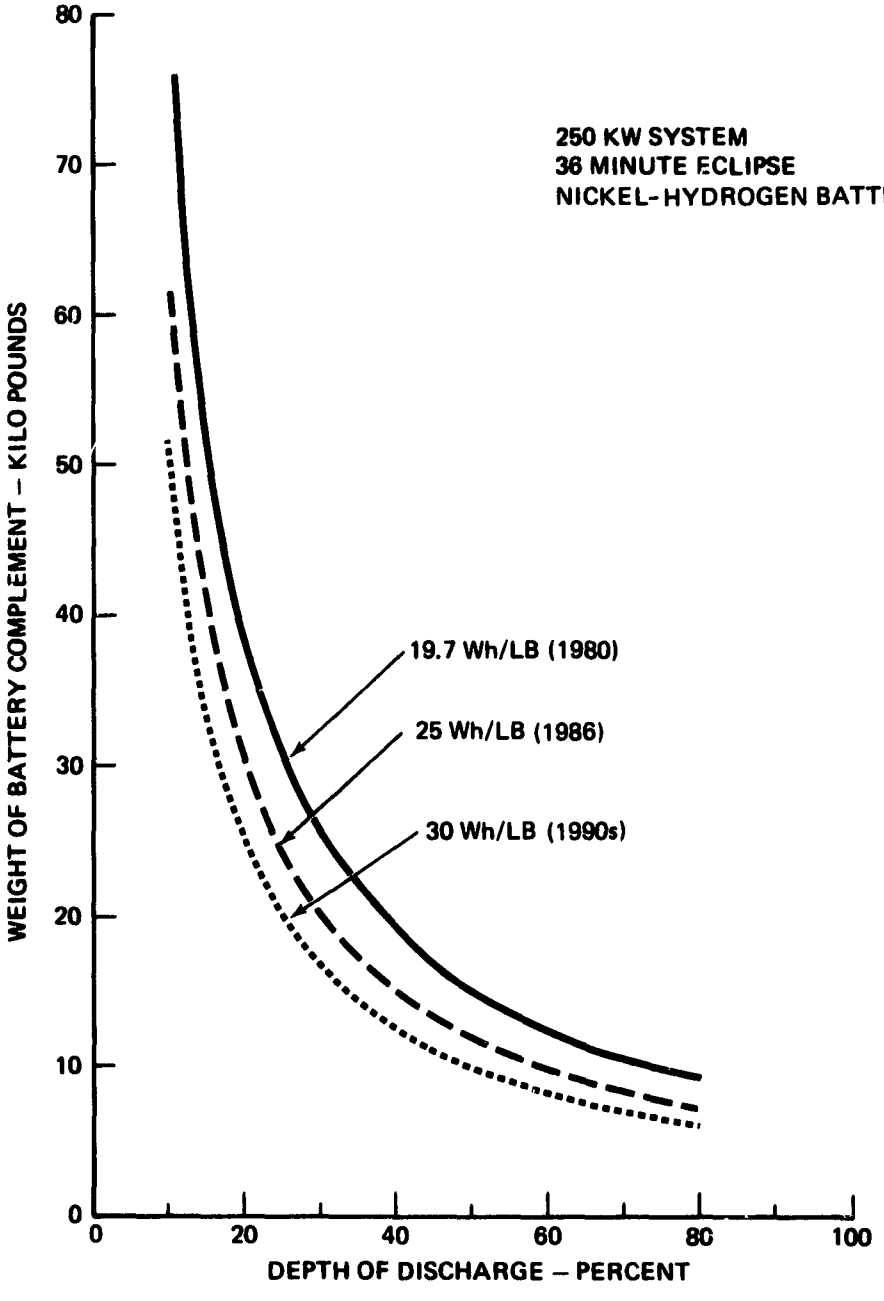

Figure 5-21. Initial Batt[illegible]eight Inversely Related to Dep[illegible]of Discharge

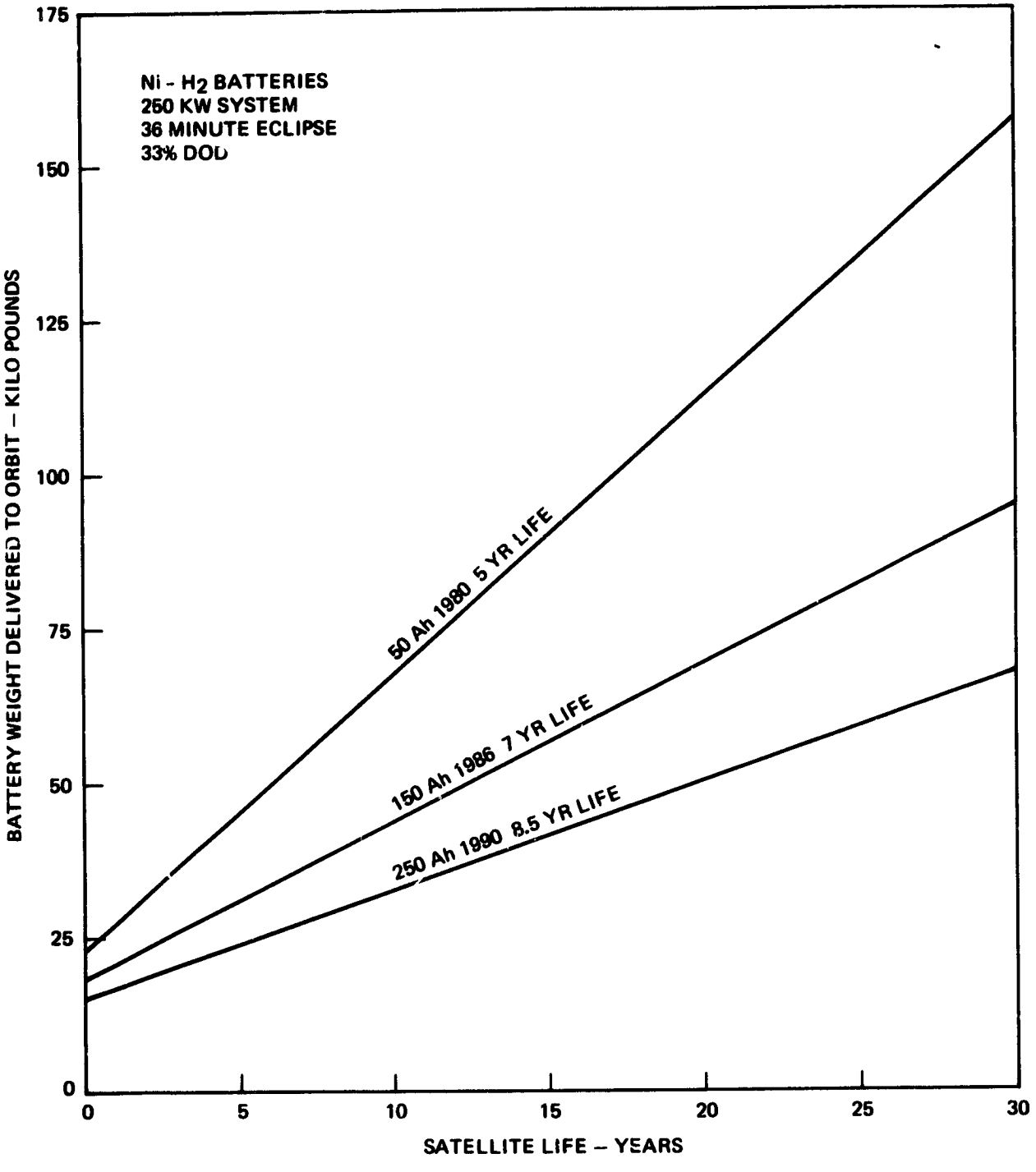

Figure 5-22. Technology Improvement Reduces Life-Cycle Weight of Ni-H_2 Batteries

5.3.7 Life Cycle Cost

Life cycle costs are the sum of the costs for the initial battery complement and the replacement batteries over the satellite operational life. The cost of the initial battery complement is reduced by using a greater depth of discharge to reduce the installed nameplate capacity. However, this reduces potential battery cycle life and increases the incidence of battery replacement and the associated cost. Hence, an optimization exists for selecting the cost effective (the optimum) depth of discharge.

The cost of the initial battery complement is an inverse function of the allowable depth of discharge (Figure 5-23):

$$\text{Initial battery cost} = \text{battery nameplate energy (Wh)} \times \text{battery specific cost (\$/Wh)}$$

$$= \frac{\text{eclipse energy}}{\text{depth of discharge}} \times \frac{\text{battery cost}}{\text{battery energy}}$$

The cost of battery resupply is a function of the satellite life, battery life, and the cost of the initial battery complement (Figure 5-24):

$$\text{Battery resupply cost} = \frac{\text{eclipse energy}}{\text{depth of discharge}} \times \frac{\text{battery cost}}{\text{battery energy}} \times \frac{\text{satellite life}}{\text{battery life}}$$

Battery resupply cost is minimized when the product of depth of discharge and battery (cycle) life is maximized. This product is solely a function of the cycle life versus depth of discharge relationship assumed for the technology. Based upon present projections of this relationship (Figure 5-19) the resupply cost is minimized with a 30 percent depth of discharge. This is verified in the plots of calculated replacement costs (Figure 5-24).

Life cycle costs (Figure 5-25) are the sum of the costs for the initial battery complement (Figure 5-23) and the cost of resupply batteries (Figure 5-24). These costs include Shuttle charges for delivery to low earth orbit (160 nautical miles). Optimum depth of discharge for minimum cost occurs at approximately 33 percent. Higher depths of discharge were

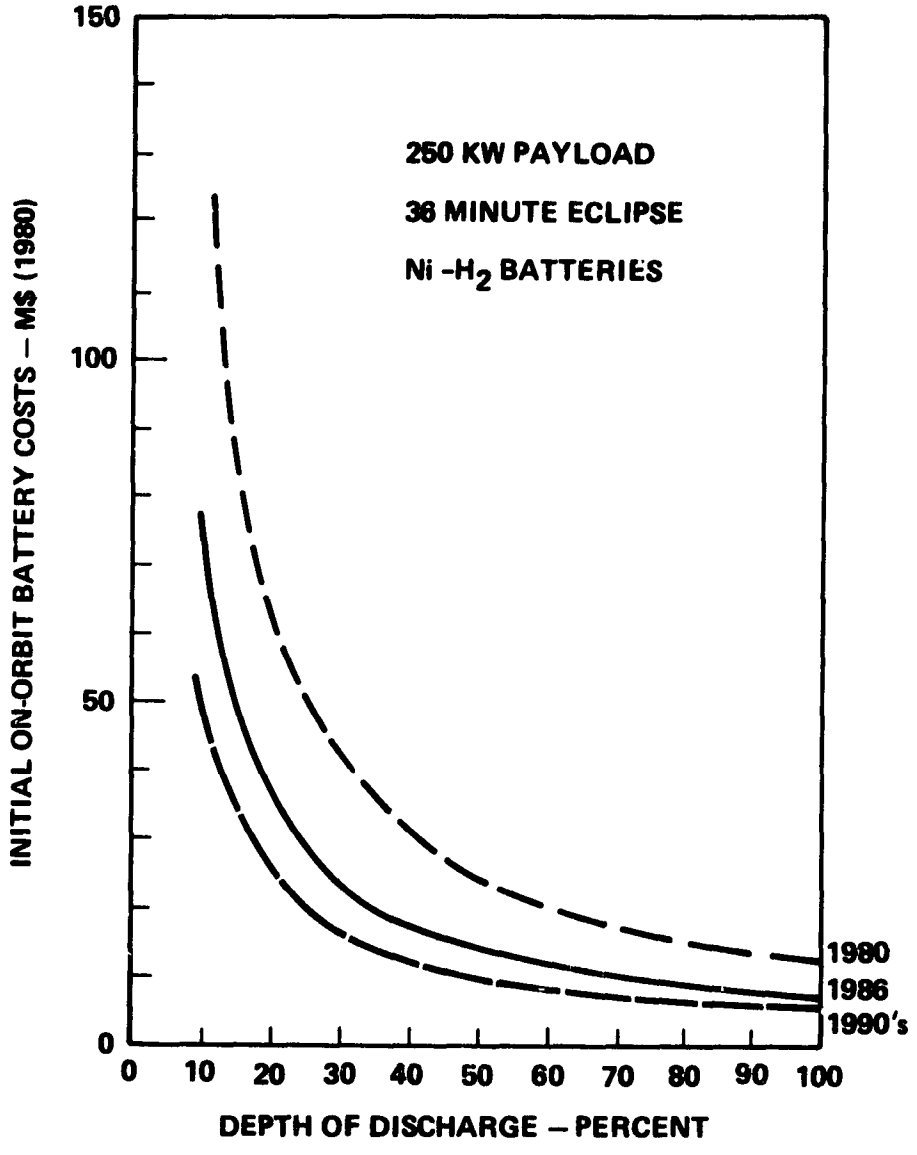

Figure 5-23. Initial Cost Is Inversely Related to Depth of Discharge

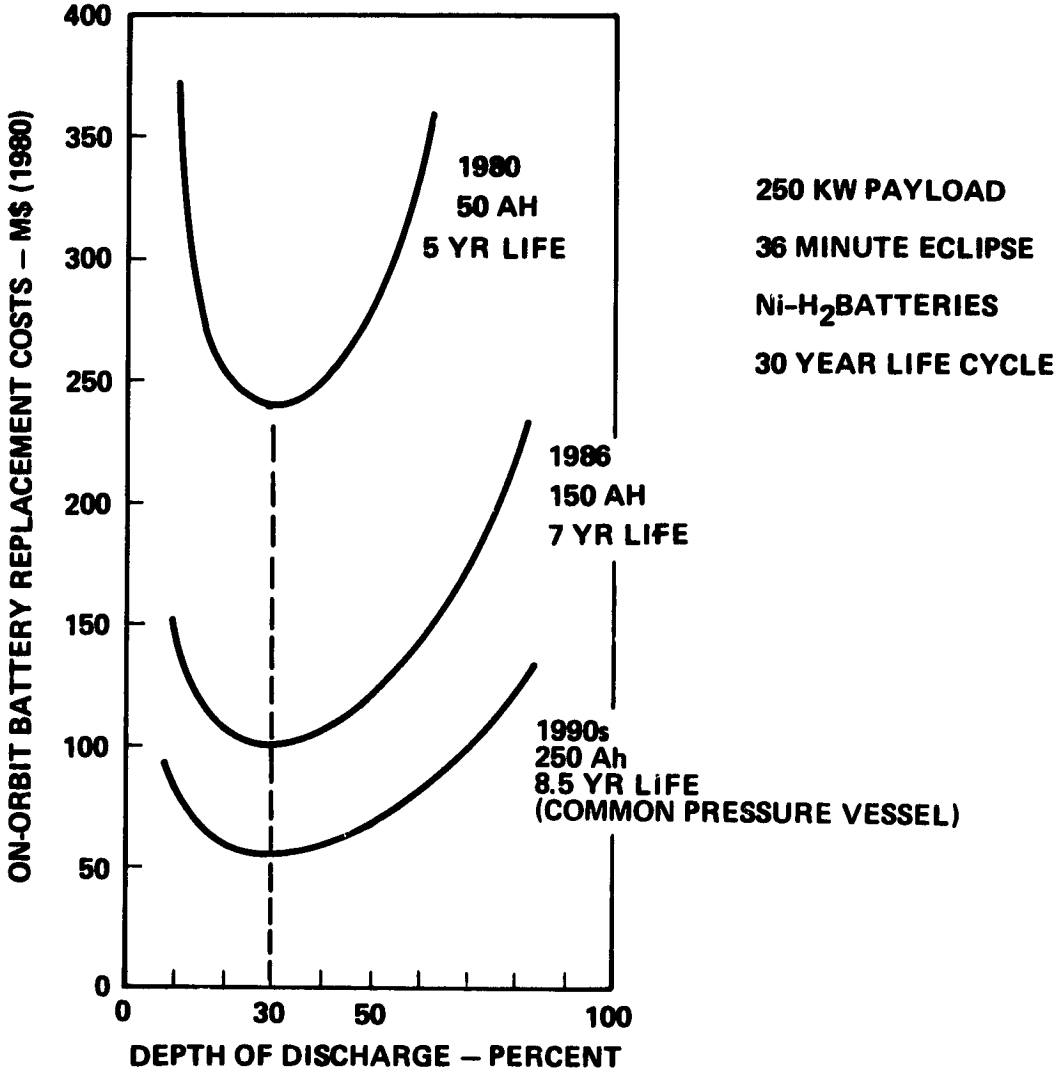

Figure 5-24. Resupply Costs Minimized at 30 Percent Depth of Discharge for Nickel-Hydrogen Batteries

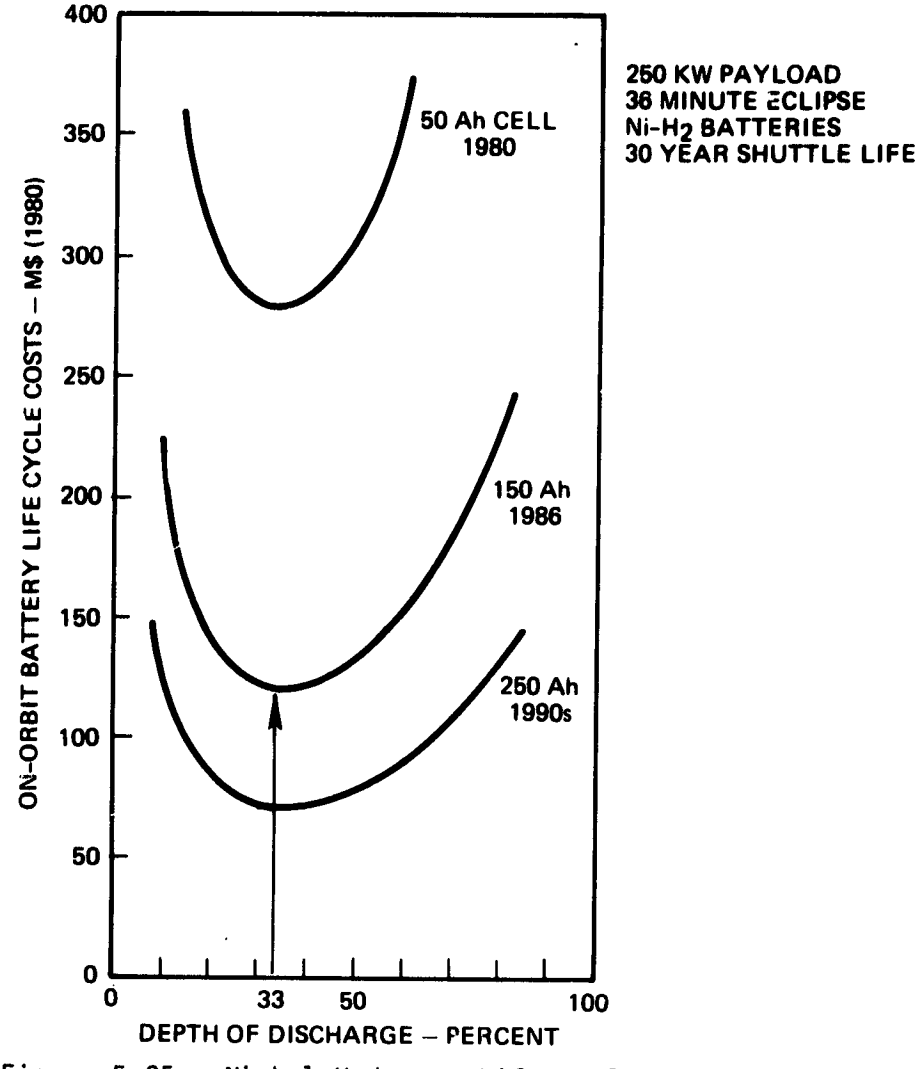

Figure 5-25. Nickel-Hydrogen Life Cycle Cost Minima Occur at Approximately 33 Percent DOD

expected for optimum cost, but a shallower slope of the cycle life versus depth of discharge relationship, Figure 5-19, would be required. Hence, the 33 percent depth of discharge is applied to nickel-hydrogen batteries.

Initial battery costs are modest for the 250-kilowatt system, but battery costs escalate as replacements occur (Figure 5-26) and represent the dominant component of the electrical power system cost. Technology investment in the 150- and 250-Ah cells can reduce these costs dramatically (Figure 5-27). Improvements in specific weight (e.g., scale-up to larger sizes) project greater payback/investment ratio than improvements in battery life (Figure 5-27). However, better definition of the relationship of cycle life to depth of discharge, hopefully leading to a greater optimum depth of discharge for nickel-hydrogen, is of paramount need.

5.3.8 Operating Rates

At 33 percent depth of discharge, one third of the nameplate battery capacity will be removed from each cell during the eclipse period. These discharge currents are approximately a C/1.8 rate (Table 5-8). The resultant discharge plateau voltage is projected as 1.25 volts (average) per cell.

During charge, the eclipse discharge (coulombs) is replaced over the sunlight period plus a 10 percent allowance to account for oxygen evolution during recharging (1.10 recharge ratio). This is a C/2.5 rate for a 33 percent depth of discharge condition.

Table 5-8. Nickel-Hydrogen Operating Currents

Operation \ Cell Size	50 Ah	150 Ah	250 Ah
Discharge:			
Current (amperes)	27.8	83.3	139
Rate	C/1.8	C/1.8	C/1.8
Charge:			
Current (amperes)	20.4	61.1	102
Rate	C/2.5	C/2.5	C/2.5

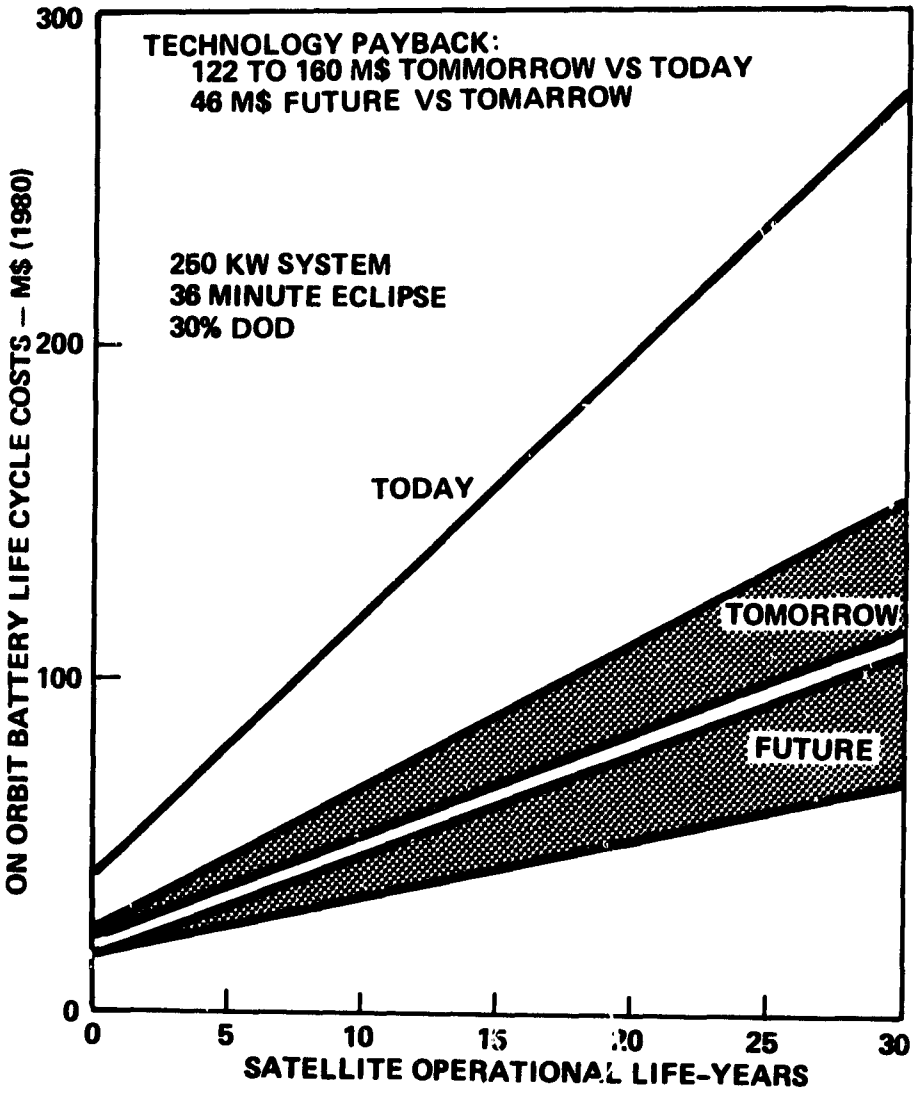

Figure 5-26. Technology Improvement Can Dramatically Reduce Costs of Nickel-Hydrogen Batteries

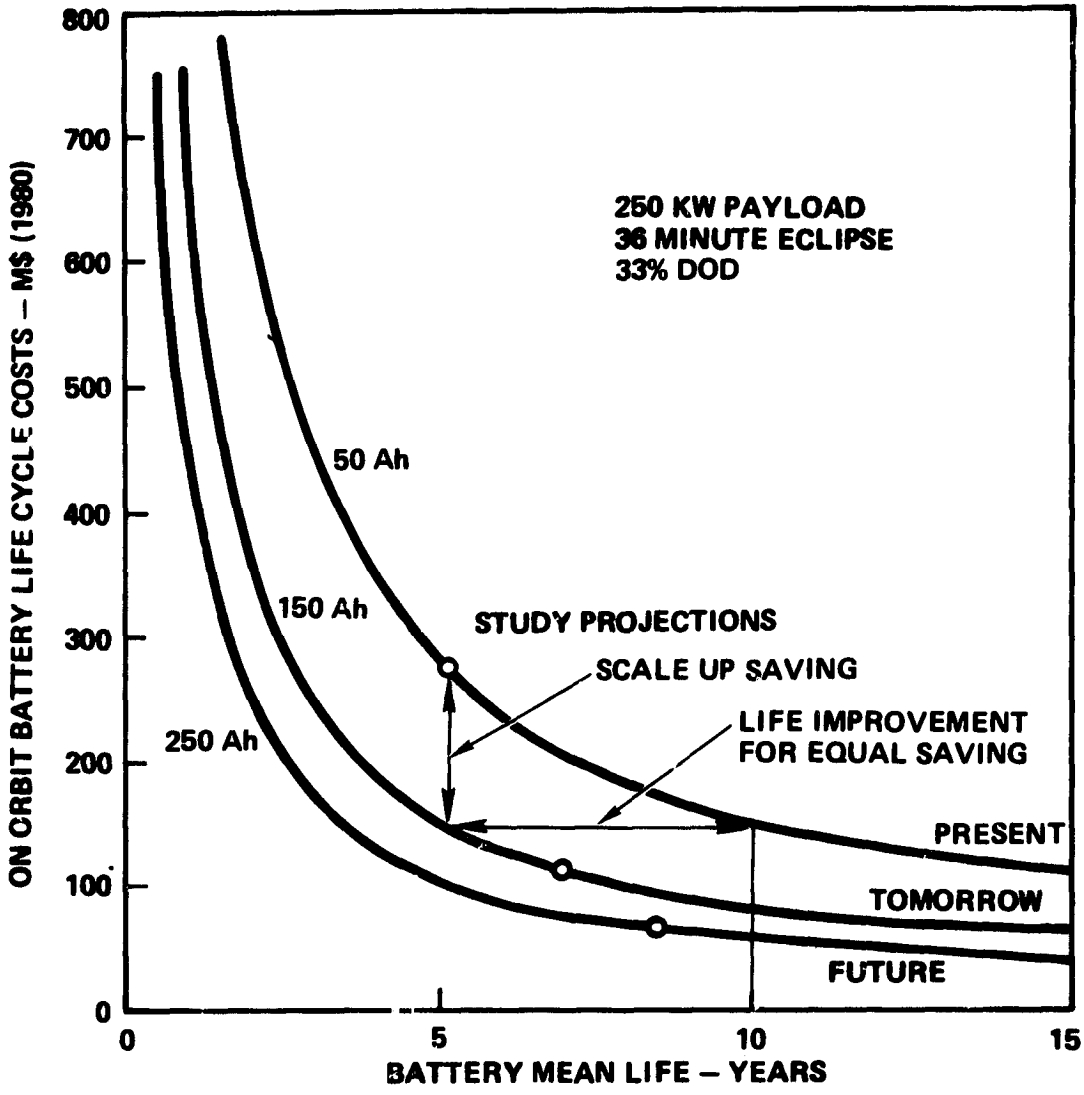

Figure 5-27. Improvement of Present Nickel-Hydrogen Battery Life Has Major Cost Impact

5.3.9 Development Cost

A development cost of 4.5 to 5 M$ is estimated for the 150-Ah nickel-hydrogen battery. This cost is projected from the recent Air Force experience in developing a 50 Ah nickel-hydrogen cell. The Air Force development program aggregated approximately 2 M$ and produced the 50-Ah recirculating cell design. The 150 Ah cell is proposed as a computerized scale-up of the 50-Ah cell based upon similar thermal transfer parameters. A modest cell diameter increase to 4-1/2 inches from 3-1/2 inches is required. An initial Air Force contract (estimated at approximately 500 K$) for a scale-up demonstration of the 150-Ah cell was expected in early 1981. [This was deferred pending better identification of an Air Force program need for this technology.] Further cell development of 2-3 M$ was expected for detail development and technology readiness verification; 2 M$ was estimated for cell integration into a viable battery design and for concept demonstration. Hence, the 150 Ah nickel-hydrogen development program for technology readiness is estimated at less than 5 M$. This program and projection is consistent with the risks and confidence level inherent in the fuel cell plus electrolysis unit development cost of 50 M$ (Section 5.4).

5.4 FUEL CELL + ELECTROLYSIS UNIT (FC+EU)

There are two viable fuel cell suppliers for space applications: General Electric with solid polymer electrolyte technology, and United Technologies with asbestos matrix technology from earlier Allis-Chalmers development. The asbestos matrix fuel cell from United Technologies was selected for the Shuttle vehicles. United Technologies has no electrolysis experience with this cell, but has considerable commercial fuel cell experience with phosphoric acid electrolyte systems.

The General Electric solid polymer electrolyte technology was employed in fuel cells for the Gemini and Biosatellite programs. Advancement of this technology continued with the hardware development program for the Shuttle fuel cell selection. General Electric also has developed the polymer membrane technology as an electrolysis unit, disassociating water into hydrogen and oxygen for submarine environmental applications.

A potential multiyear program was initiated by NASA/JSC in May 1979 to bring to maturity the solid polymer electrolyte electrochemical cell technology for application to energy storage on low-earth-orbit, high-power satellites. The first phase, consisting of a 1-year contract to General Electric, included an initial task for a comprehensive state-of-the-art assessment. The resulting summary report, Reference 5-4, contains the analyses and results of that task and forms the basis for the fuel cell data used herein.

5.4.1 Concept

The fuel cell plus electrolysis unit concept for energy storage (Figure 5-28) utilizes a fuel cell module to catalytically combine the gaseous reactants of hydrogen and oxygen to produce electrical current. Operation is similar to typical battery chemistry except that the gaseous hydrogen and oxygen reactants are the chemically converted material rather than the metallic compounds of battery plates. Water and heat are by-products of the fuel cell chemistry. Individual cells are assembled into a stack for common manifolding of reactants and coolant, but the cells are electrically connected in series to produce the desired higher voltages. One or more cell stacks plus the ancillary plumbing, valves, regulators, pumps, separators, compressors, and controls comprise a fuel cell module.

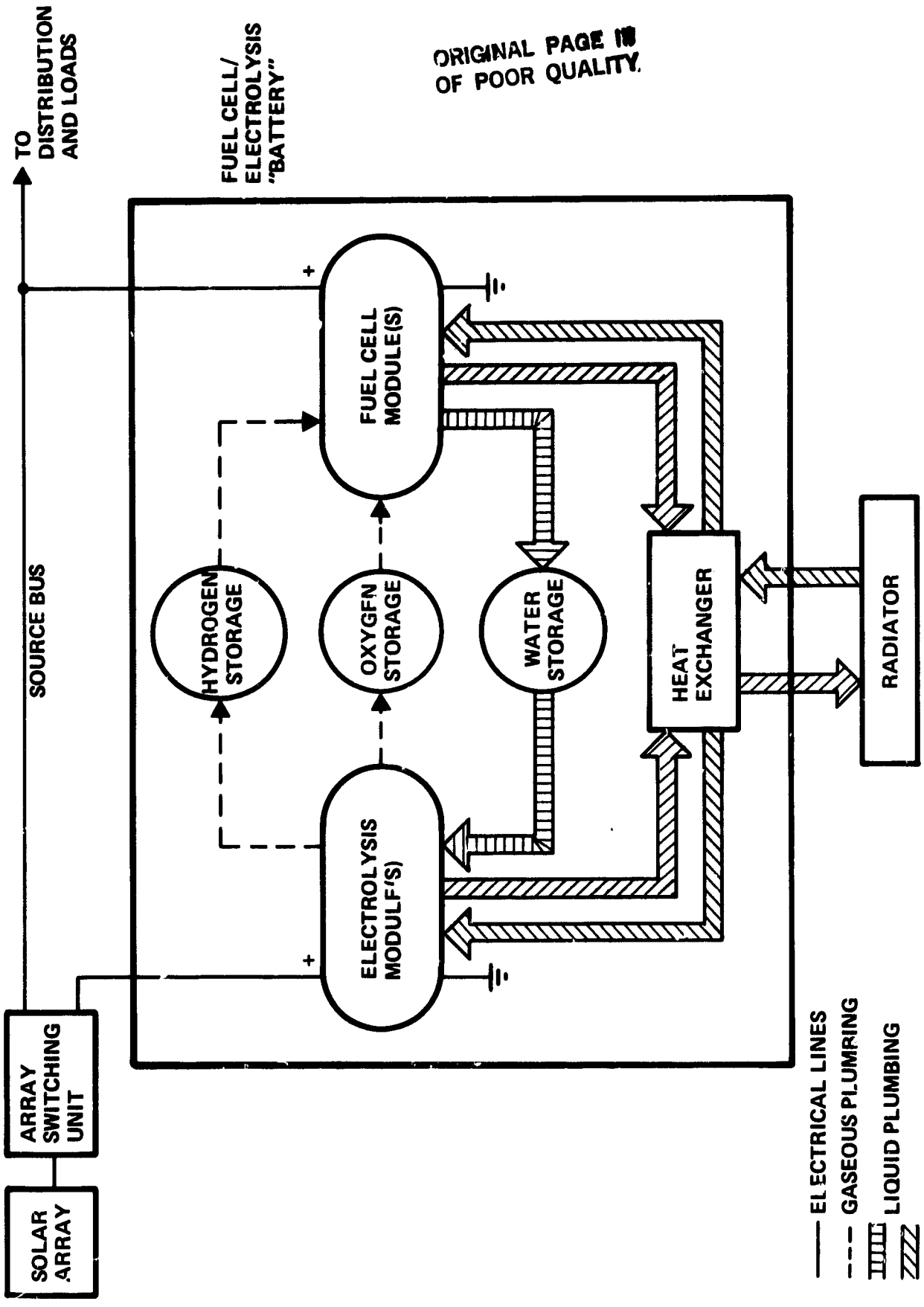

Figure 5-28. Fuel Cell/Electrolysis Concept

The electrolysis cell is very similar to a fuel cell and catalytically disassociates water into hydrogen and oxygen gases with electrical power and energy input. Electrolysis cells are also assembled into stacks and, with ancillary equipment, become an electrolysis module. Combining a set of fuel cell modules and the corresponding electrolysis modules produces a powerplant. Adding the appropriate reactant storage tanks, water tanks, and heat exchangers, produces a viable energy storage concept (Figure 5-28) for long eclipse periods with a high-power photovoltaic electrical power system.

The General Electric study (Reference 5-4) translates this energy storage concept into theoretical hardware based upon the acid polymer membrane technology and addresses powerplant sizing and parameter optimization issues. Translation of the conceptual schematic (Figure 5-28) into operational hardware entails considerable complexity (Figure 5-29) to accommodate water separation and transport and the concurrent heat rejection.

The fuel cell stack in Figure 5-29 represents a unit with individual cell coolant cartridges for heat removal. Removal of waste heat from the electrolysis stack is accomplished by operating the oxygen side of each cell with process water in excess of that required for electrolysis. Heat exchangers remove waste heat from the water coolant loops in the electrolysis and fuel cell stacks. Each loop has independent temperature regulating valves which modulate the flow in each loop to maintain essentially constant stack outlet temperatures during the entire orbital cycle. Heat is transferred to Radiator 1 loop (Figure 5-29) through the primary heat exchanger.

A condenser removes heat from the oxygen and hydrogen gases generated from the electrolysis stack in order to keep the outlet saturation temperature (dew point) below that of the reactant storage tanks. Similarly, the product water heat exchanger reduces the discharge water temperature from the fuel cell stack to the desired storage value. The process water outlet temperatures from these heat exchangers are independently controlled by temperature regulating valves. The waste heat is rejected to a second

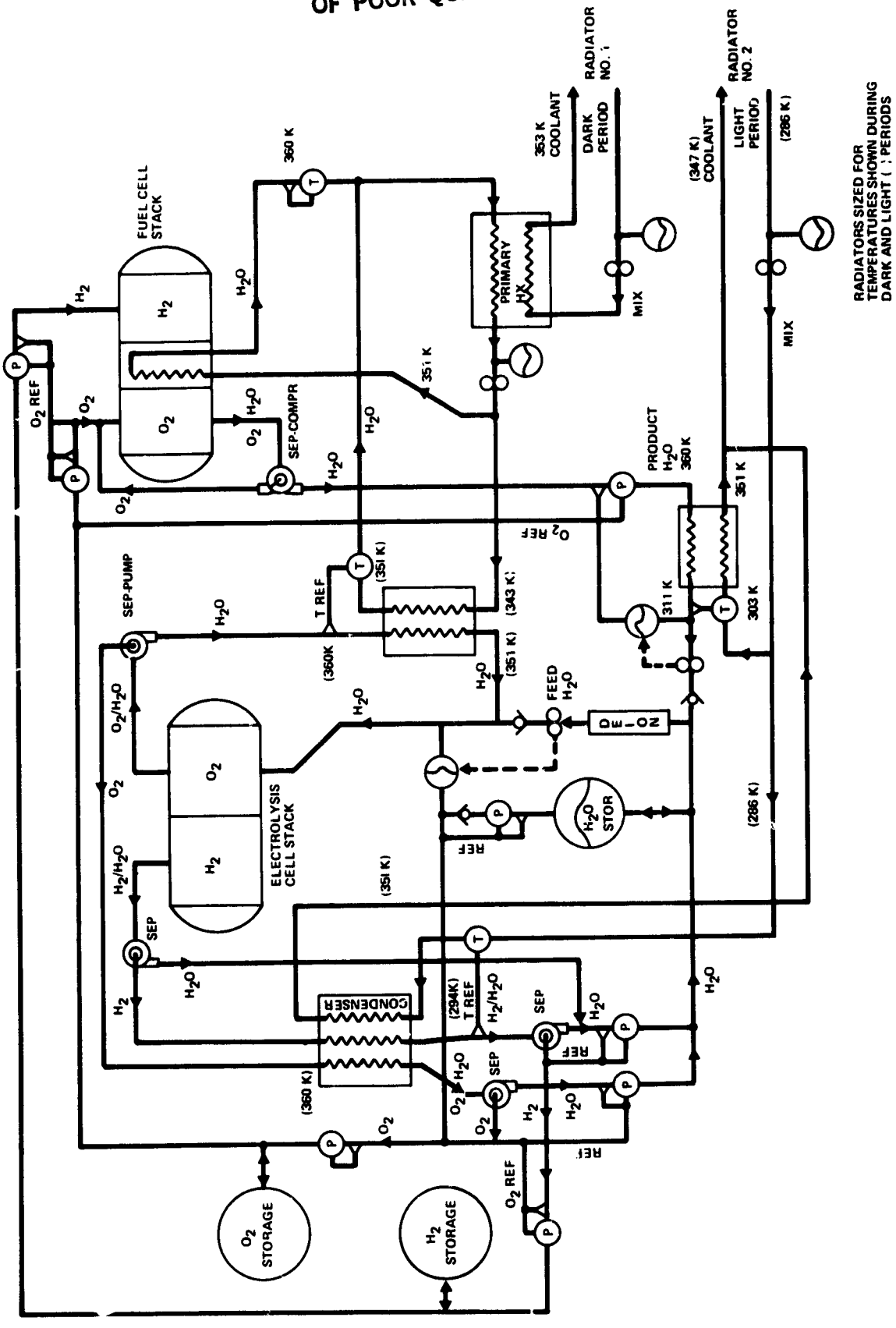

Figure 5-29. Fuel Cell and Electrolysis Power Plant Hardware

radiator - Radiator 2 loop (Figure 5-29). The quantity of heat to Radiator 2 loop is relatively small, but requires an outlet temperature under 70°F (294 K). It is therefore separated from the main radiator (Radiator 1 loop) to lower total system weight.

The hardware concept (Figure 5-29) includes centrifugal separators to handle two-phase fluid flow and pumping for water management in a zero gravity environment. Reference-type back pressure regulators are provided in the electrolysis modules, whereas reducing regulators control pressure to the fuel cell stacks.

5.4.2 FC+EU Parameters

The parameters of the fuel cell plus electrolysis unit concept for energy storage (Figure 5-30) for the reference 250-kilowatt electrical power subsystem are developed herein from the parameters of Case 365 of the General Electric study (Reference 5-4). Case 365 is a performance and weight summary from the computerized math model of dedicated fuel cell modules and electrolysis modules for a 250-kilowatt electrical power subsystem operating at 243 volts. Parameters in Figure 5-30 include modifications from Table 5-9 data for module quantity, reactant tankage capacity, and ancillary equipment weight.

The fuel cell and electrolysis unit requirements taken directly from Case 365 data are 4 and 5 units, respectively. However, loss of one unit increases the load on the remaining units by 33 or 25 percent, respectively. This increases the current density accordingly, and voltage regulation and temperature control deteriorate. Hence, to assure "fail operational" redundancy at full power rating (250 kilowatts), one additional fuel cell module and one additional electrolysis module are included in the powerplant complement of Figure 5-30. Normal operation with this increased powerplant complement reduces the current density, reduces the current per module, and improves regulation slightly. Operation reverts to Table 5-9 parameters upon failure of one module.

The tankage for reactants in Case 365 is sized for 500 kWh of energy storage. Eclipse duration in low earth orbit is only 36 minutes and requires 150 kWh of energy. The reactant tankage of 200 kWh of energy storage (Figure 5-30) for the reference 250 kW electrical power subsystem

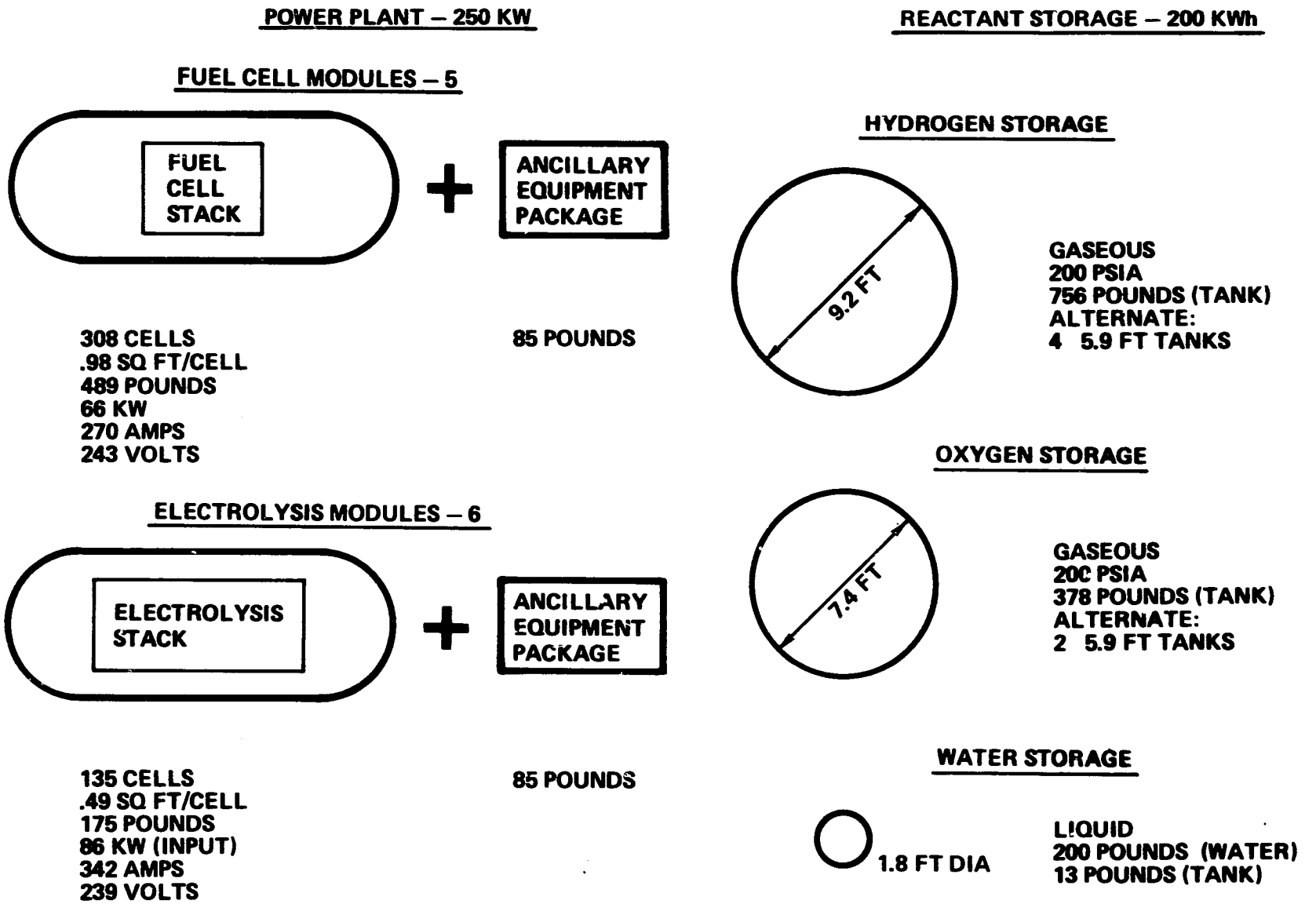

Figure 5-30. Fuel Cell and Electrolysis Components for Reference 250 kW EPS

Table 5-9. Fuel Cell and Electrolysis Summary
Case 365: 250 kW, 243 Vdc System
(From Reference 5-4)

BUS POWER	250.0	kW
BUS VOLTAGE	243.0	VOLTS
FUEL CELL OPERATING CONDITIONS		
MEAN CELL PRESSURE	30.0	PSIA
MEAN CELL TEMPERATURE	180.0	DEG F
CELL CURRENT DENSITY	275.0	AMP/SQ FT
CELL VOLTAGE	0.7896	VOLTS
NO. OF CELLS PER MODULE	308.0	
NUMBER OF MODULES	4.0	
INDIVIDUAL CELL AREA	0.98	SQ FT
TOTAL AREA OF CELLS	1211.94	SQ FT
MODULE SPECIFIC WEIGHT	1.61	SQ FT
CELL CURRENT, PARALLEL MODULES	270.52	AMP
MODULES OUTPUT POWER	263.158	kW
CELL CURRENT EFFICIENCY	0.9921	
PERMEABILITY LOSS (EQUIV)	2.182	AMP/SQ FT
MODULES HEAT GEN. RATE (DARK)	231.200	kW
MODULES HEAT GEN. RATE (LIGHT)	4.605	kW
ELECTROLYSIS UNIT OPERATING CONDITIONS		
MEAN CELL PRESSURE	200.0	PSIA
MEAN CELL TEMPERATURE	180.0	DEG F
CELL CURRENT DENSITY	700.0	AMP/SQ FT
CELL VOLTAGE	1.7705	VOLTS
NO. OF CELLS PER MODULE	135.0	
NUMBER OF MODULES	5.0	
INDIVIDUAL CELL AREA	0.49	SQ FT
TOTAL AREA OF CELLS	330.02	SQ FT
MODULE SPECIFIC WEIGHT	2.65	LB/SQ FT
CELL CURRENT, PARALLEL MODULES	342.24	AMP
MODULES INPUT POWER (LIGHT)	429.453	kW
POWER CONDITIONER INPUT POWER	456.865	kW
STANDBY INPUT POWER (DARK)	0.0004	kW
STANDBY INPUT CURRENT (DARK)	.0006	AMP
CELL CURRENT EFFICIENCY	0.9842	
PERMEABILITY LOSS (EQUIV.)	11.051	AMP/SQ FT
MODULES HEAT GEN. RATE (LIGHT)	74.408	kW
MODULES HEAT GEN. RATE (DARK)	0.627	kW
SYSTEM OPERATING CONDITIONS		
SOLAR ARRAY OUTPUT POWER	720.023	kW
IDEAL REGEN FUEL CELL EFF.	0.4355	
SYSTEM ENERGY STORAGE EFF.	0.3648	
WATER PRODUCED (2 HR.)	497.834	LB
MINIMUM BOTTLE PRESSURE (2 HR.)	40.000	PSIA
H2 STORAGE BOTTLE VOLUME	1047.165	CU FT
H2 BOTTLE DIAMETER	151.19	IN.

includes 50 kWh of energy contingency based upon an engineering judgment of a suitable reserve. Reactant storage for 500 kWh would increase the orbital weight, increase the tankage volume, and potentially increase Shuttle transportation costs by 6 to 10 M$ (based upon Shuttle cargo bay length utilization charges).

The computer model of the General Electric study does not fully address ancillary equipment. Only the heat exchangers which vary with power rating and operating parameters are included in the model. Plumbing, pumps, valves, regulators, separators, compressors, and controls are not included in this model. Discussion with General Electric estimated the ancillary equipment at 765 pounds for Case 365 (approximately 85 pounds per fuel cell or electrolysis module).

5.4.3 Life

A mean life of 40,000 to 50,000 hours for fuel cell and electrolysis stacks and a mean life of 10,000 for the ancillary packages is indicated by General Electric (Reference 5-5). The 40,000-hour value is used herein for life cycle cost projections on stacks (Section 5.4.5). Pumps are identified as the potential life-limiting component of the ancillary group. Consequently, equipment replacement is needed and becomes significant for a 30-year mission.

The replacement scenario envisioned for the fuel cell plus electrolysis unit concept considers each fuel cell stack or electrolysis cell stack as a replaceable canister and the ancillary equipment (pumps, separators, valves, regulators, sensors, and associated plumbing) for each canister a separate, replaceable entity. This approach is chosen to allow simplified EVA replacement of ancillary equipment without replacing the associated heavy and costly fuel cell or electrolysis cell stack. Individual replacement of the various pumps and separators (eight are shown in Figure 5-29) is considered inappropriate for EVA. Replacement of seals and bearings in pumps or separators requires depot facilities. Such facilities in orbit intuitively appear inappropriate; they would be both heavy and costly. Replacement of an ancillary package therefore occurs at bearing or seal wearout (pump life), and this life determines the ancillary package life for replacement incidence and influences costs accordingly.

Hence the weight and cost of an ancillary package is used for replacement calculations, while the projected pump life (10,000 hours) is used to determine the frequency of replacement.

Pump life longer than 10,000 hours is possible, even probable. However, significantly longer pump life approximating the indicated fuel cell stack life of 40,000 hours requires demonstration and/or development. Pumps and separators are typically rotating machinery; bearings and seals are involved, and these have limited lifetimes as wearout ultimately occurs. Extrapolation of random failure rates to indicate potential life must be carefully evaluated. Wear becomes the dominant factor if random failure rates are low. Projections of long equipment life based upon random failure rates need validation. Other ancillary components may become life limiting as pump life is extended significantly.

Pump life under fuel cell and electrolysis applications is not expected to be equivalent to pump life in typical thermal control applications. The operational conditions are distinctly different. Thermal control pumps typically have demonstrated 25,000 hours of life, or more, and wear indications project 40,000 to 50,000 hours of useful life. These pumps operate in a liquid media, typically a fluorocarbon (Freon 21, 114, etc.). Carbon bearings have been developed which are compatible with the meager lubrication quality of this media. Water content in the fluorocarbon is typically less than 10 parts per million to preclude any freezing or corrosion problems.

The pumps and separators of the fuel cell and electrolysis unit accessory packages typically operate in a gaseous media (hydrogen or oxygen) with significant water vapor, or in water with dissolved gases (hydrogen or oxygen). None of these fluid mixtures are conducive to long life. Hydrogen promotes embrittlement; water and oxygen are corrosive. Further, the lubrication quality of these fluids is relatively poor, and lubrication additives appear incompatible with the fuel cell and electrolysis process. Hence, this more inhospitable operational media suggests a reason for a shorter life of fuel cell and electrolysis unit pumps and centrifugal separators compared to the life realized for thermal system pumps.

5.4.4 Weight

The initial complement of energy storage equipment for the fuel cell plus electrolysis concept weighs 5776 pounds (Table 5-10). This weight includes one fuel cell module and one electrolysis module on standby for "fail operational" redundancy and reactant storage tankage for 200 kWh. The equipment weight delivered to orbit over a 30-year period becomes 44,500 pounds (Table 5-10) based upon the life projections of Section 5.4.3. This weight excludes any additional reactants (water) needed to replenish any gas leakage, extended reactant purging, or extraneous chemical combinations consuming the reactants.

Table 5-10. Fuel Cell Plus Electrolysis Weight Summary (200 kWh Storage; 250-Kilowatt, 243-Volt System)

Equipment \ Period	Initial Complement		Replacements (30 Years)	30-Year Life Cycle Total
	Operational	Redundant		
Fuel Cell Stacks	1,955	489	12,853	15,297
Electrolysis Stacks	875	175	5,752	6,802
Ancillary Packages	765	170	20,118	21,053
Reactant Storage:	1,347	-	-	1,347
Hydrogen Tanks	756			
Oxygen Tanks	378			
Water Tank	13			
Water	200			
Totals	4,942	834	38,723	44,499
	5,776			

Weights in pounds.

The weight of the replacement equipment is calculated based upon the life cycle of 30 years (262,980 hours), the projected equipment life, (10,000 hours for pumps, 40,000 hours for stacks), and the weight for the respective equipment:

Fuel cell stacks: $\frac{1954.92 \text{ lb} \times 262{,}980 \text{ hr}}{40{,}000 \text{ hr}} = 12{,}853$ pounds

Electrolysis stacks: $\frac{874.91 \text{ lb} \times 262{,}980 \text{ hr}}{40{,}000 \text{ hr}} = 5{,}752$ pounds

Ancillary packages: $\frac{765 \text{ lb} \times 262{,}980 \text{ hr}}{10{,}000 \text{ hr}} = 20{,}118$ pounds

Ancillary equipment dominates the life cycle weight (Figure 5-31) principally due to the shorter life projection.

The weight of the fuel cell and electrolysis equipment is derived from the weight summary (Table 5-10) for Case 365 of the General Electric Study (Reference 5-4). The ancillary equipment is projected by General Electric to weigh 765 pounds for Case 365 (four fuel cell modules plus five electrolysis modules). This ancillary weight includes the heat exchangers and condensers itemized separately in Table 5-11. The weight of the equipment in the supporting subsystems (solar array area, radiators, and power conditioners) is addressed in the energy storage comparison (Section 5.1).

5.4.5 Cost

The life cycle costs for the fuel cell plus electrolysis concept for energy storage are developed from manufacturer cost estimates, projected equipment mean life, the life cycle period (30 years), and Shuttle transporation charges for orbital delivery. Costs, Table 5-12, are developed by equipment type (fuel cell electrolysis stacks, ancillary packages, and reactant supply) and from manufacturing cost estimates and equipment size (weight or volume). Recurring costs (manufacturing plus transportation) aggregate 102 M$ over the 30-year life cycle.

Manufacturing costs are based upon the General Electric estimate of 5 to 6 M$ (Reference 5-5) for the 250-kilowatt, 243-volt powerplant of Case 365 (Table 5-9). This 250 kilowatt powerplant includes four fuel cell modules and five electrolysis modules each rated at 66 and 86 kilowatts respectively.

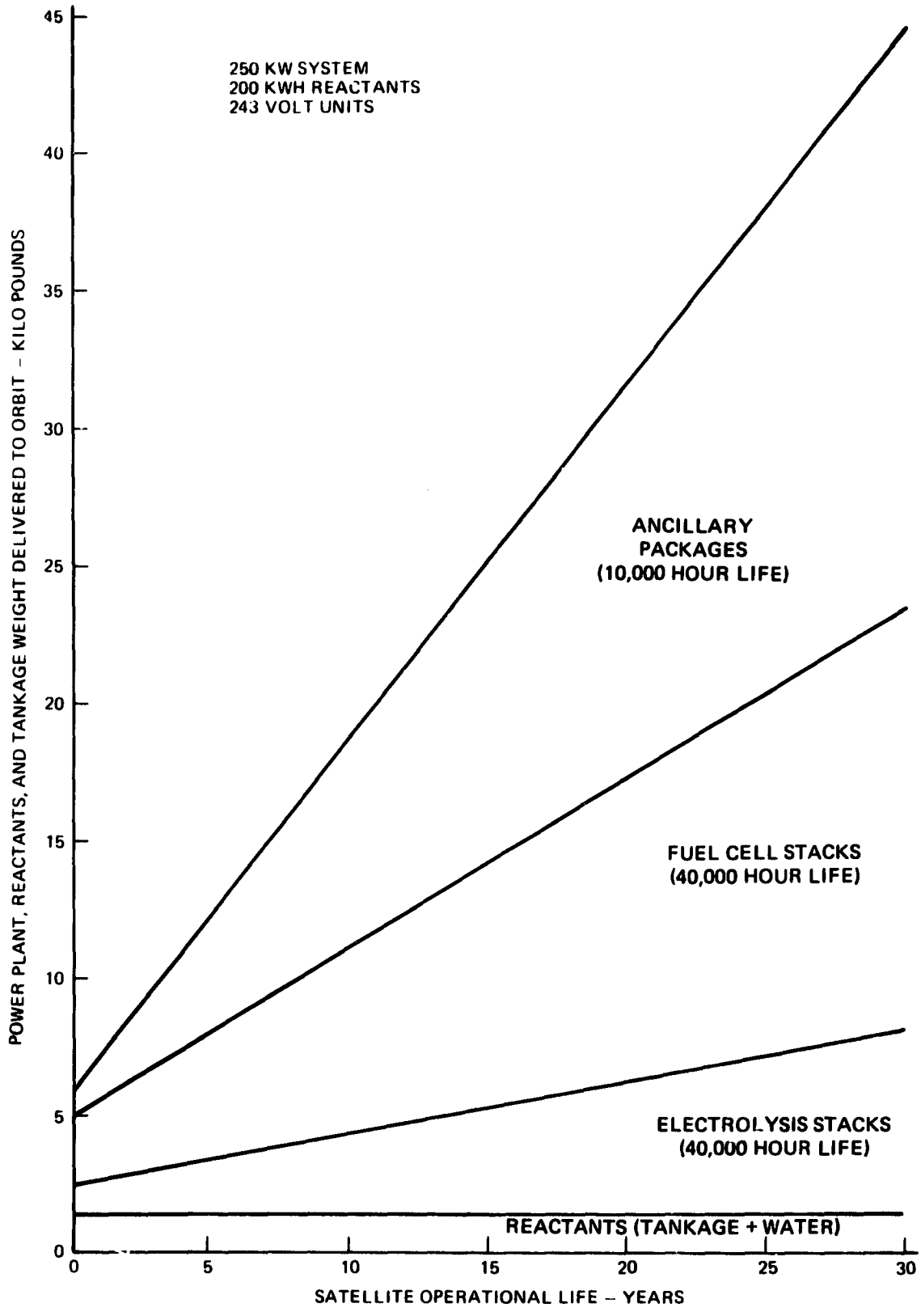

Figure 5-31. Ancillary Equipment Dominates 30-Year Weignt

Table 5-11. GE Electrolysis/Fuel Cell Weight Summary
Case 365, 250 kW, 243 Vdc System

Solar Array Weight	32,546.82	lb
Radiator No. 1 Weight	4,471.22	lb
Radiator No. 2 Weight	175.23	lb
H_2, O_2, & H_2O Bottle Weights	3,366.55	lb
Primary Heat Exchanger Weight	295.81	lb
Regenerative Heat Exchange Weight	80.80	lb
Condenser Weight	38.35	lb
Product H_2O Heat Exchange Weight	7.26	lb
Fuel Cell Modules Weight	1,954.92	lb
Electrolysis Modules Weight	874.91	lb
Power Conditioner Weight	2,284.32	lb
System Variable Launch Weight	46,096.19	lb
System Variable 10-yr Orbit Weight	51,210.35	lb

(From Reference 5-4; excludes plumbing and values of ancillary equipment.)

Table 5-12. Fuel Cell and Electrolysis Cost Synopsis
(200 kWh 250-Kilowatt, 243-Volt System)

Equipment	Initial Costs (M$)		Replacement Costs (M$)		30-Year Costs (M$)	
	Mfg	Launch	Mfg	Launch	Mfg	Launch
Stacks	5.5	1.6	29.6	8.6	35.1	10.2
Ancillaries	1.83	0.43	39.4	9.3	41.2	9.7
Tankage	0.3	5.5*	-	-	0.3	5.5
Totals	7.63	7.53	69.0	17.9	76.6	25.4
	15.2		86.9		102	
Development	50		-		-	

*Based on Shuttle cargo bay length utilization.

Present fuel cell modules for the Shuttle vehicles are only 12-kilowatt units but are costing nearly 1 M$ each. The General Electric cost estimates of 6 M$ for the 250-kilowatt powerplant, while apparently optimistic, is used herein.

The 6 M$ manufacturing costs are allocated as 4.5 M$ to the nine fuel cell and electrolysis stacks and 1.5 M$ to the nine ancillary packages. The initial powerplant costs are increased by the ratio 11/9 for the additional fuel cell module and electrolysis module included for "fail operational" redundancy.

Costs are relatively low initially (15.2 M$), but grow to 102 M$ over 30 years (Figure 5-32). Initially, Shuttle transportation charges are 50 percent of the costs. This is due to the 4.9 M$ penalty incurred for reactant tankage volume in the Shuttle cargo bay:

Length charges - weight charges = penalty charge

(11 ft/60 ft) x 30 M$ - 1347 lb x 462 $/lb = 4.9 M$

Replacement costs, however, quickly dominate the life cycle cost trend. The major factors contributing to this trend are the manufacturing costs and equipment life. Shuttle transportation charges (launch costs) are only 21 percent of the replacement costs.

The life of the fuel cell and electrolysis stacks and ancillary components are indeterminate and potentially controversial without the benefit of extensive and rigorous long-term testing. The longest flight application of a powerplant is 2 weeks (~336 hours) on Gemini and does not verify 10,000 or 40,000 hours of life. Consequently, a graphical representation of replacement costs (manufacturing costs and Shuttle transportation charges) versus equipment mean life for stacks (fuel cells and electrolysis cells) and for the ancillary package (including pumps) is furnished as Figure 5-33. This graph illustrates vividly:

a) The relationship of ancillary cost and stack cost

b) The sensitivity of cost to equipment life

c) The leverage and need for ancillary life improvement

d) The potential payoff on development investment for improvement of ancillary life and stack life.

e) The data points for this study.

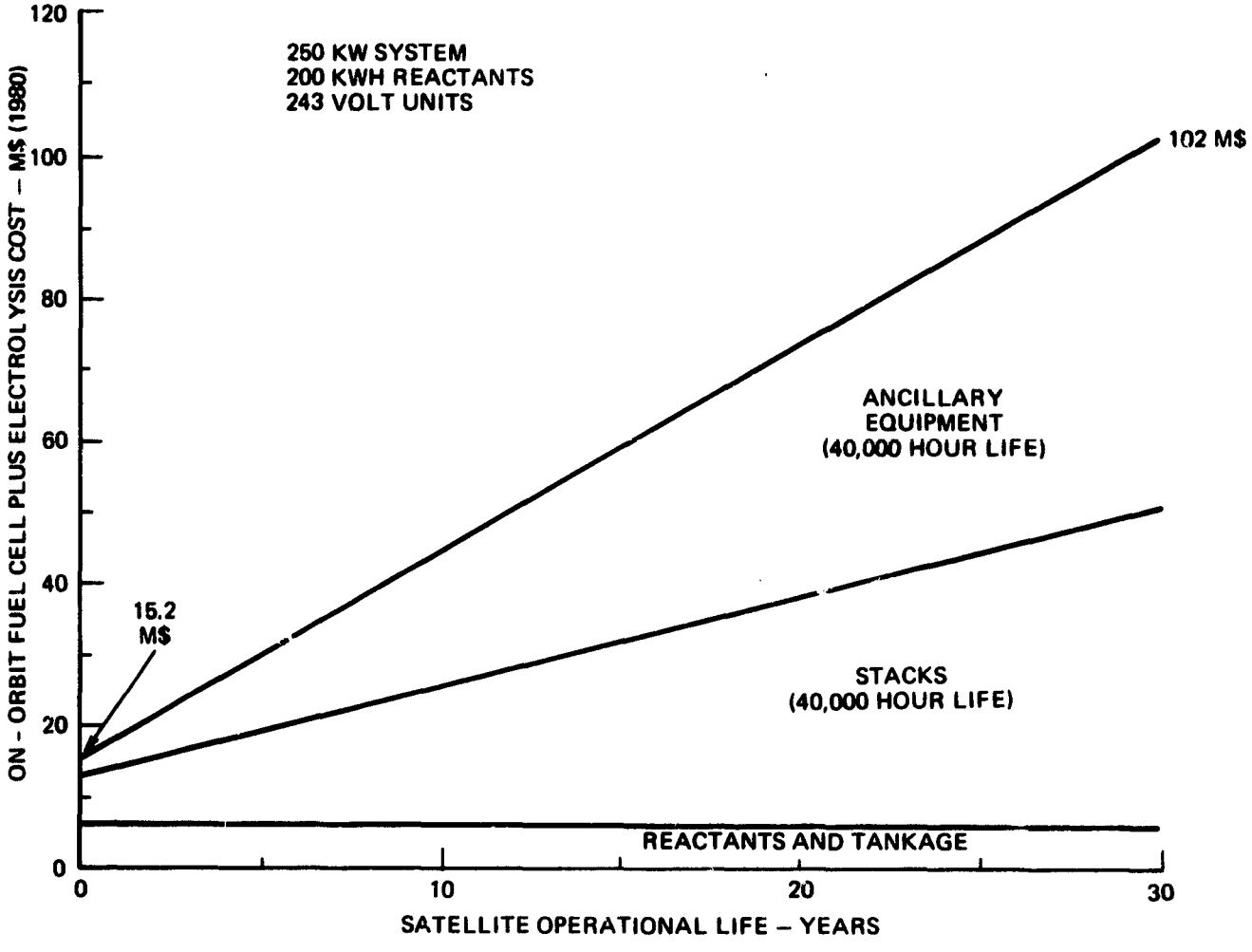

Figure 5-32. Ancillary Equipment Dominates 30-Year Cost

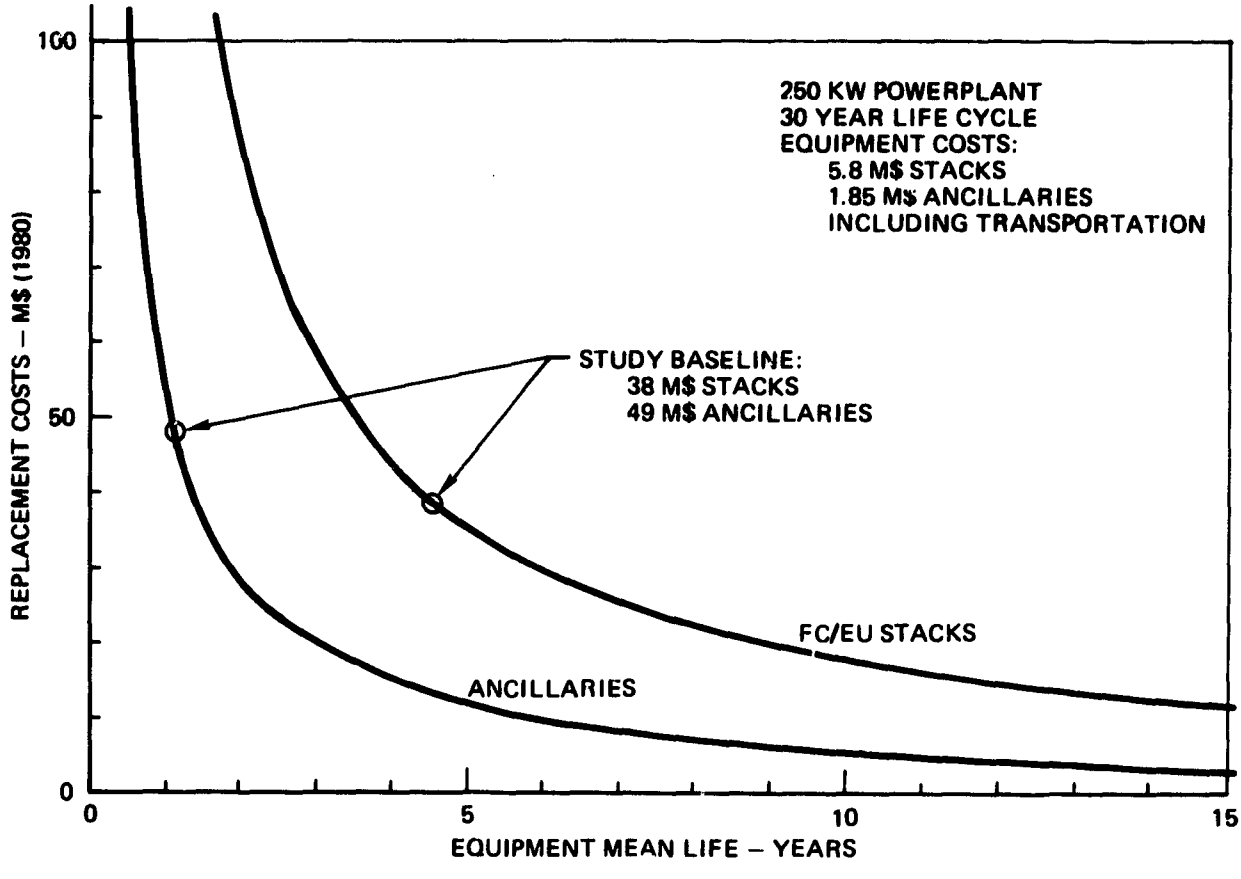

Figure 5-33. Present Life Projections Produce High Replacement Cost

The reactants and tankage aggregate 1347 pounds and incur a Shuttle transportation charge of 622 K$ based upon weight alone. However, the gaseous reactant tanks are large if manufactured as a single hydrogen tank and single oxygen tank (Figure 5-30). These tanks require approximately 17 feet of the 60-foot Shuttle cargo bay and are assessed 8.5 M$ in transportation charges based on cargo bay length utilization:

(17 feet/60 feet) x 30 M$ = 8.5 M$.

An alternate approach to the gaseous reactant tanks reduces this charge by 3 M$. The alternate approach uses six 70-inch diameter tanks to provide the same volume: four tanks for hydrogen, two tanks for oxygen. These tanks are assembled into sets of three tanks (two hydrogen, one oxygen) each, and the two sets are nested in the Shuttle cargo bay (Figure 5-34). This configuration reduces the requirement for Shuttle cargo bay length to approximately 11 feet, and the transportation charge becomes 5.5 M$:

(11 feet/60 feet) x 30 M$ = 5.5 M$.

The gaseous reactant tanks contain only modest pressure levels. The maximum tank pressure is 200 psi at full system charge with present fuel cell and electrolysis unit design; perhaps 300 psi for advanced designs. The manufacture of 6-foot diameter tanks for these pressures is estimated at $50,000 per tank based upon a 1980 price quote for another application of similar size tanks. Total manufacturing cost for six tanks is only 300 K$.

The tanks are expected to have extended life at these low pressures, even though subjected to 175,320 pressure cycles in a 30-year period. Hence, no replacement costs are incurred over the 30-year life cycle.

The small size of the water tank (Figure 5-30) allows it to be packaged as one or two tanks within the envelop of the gaseous reactant tank sets. The life of the water tanks is also considered to be indefinite; no replacements. The cost of the water tank is considered negligible compared to fuel cell and electrolysis stacks or ancillary packages.

Development costs were estimated by General Electric at 40 to 50 million dollars (Reference 5-5). The 50 M$ figure is used in this study.

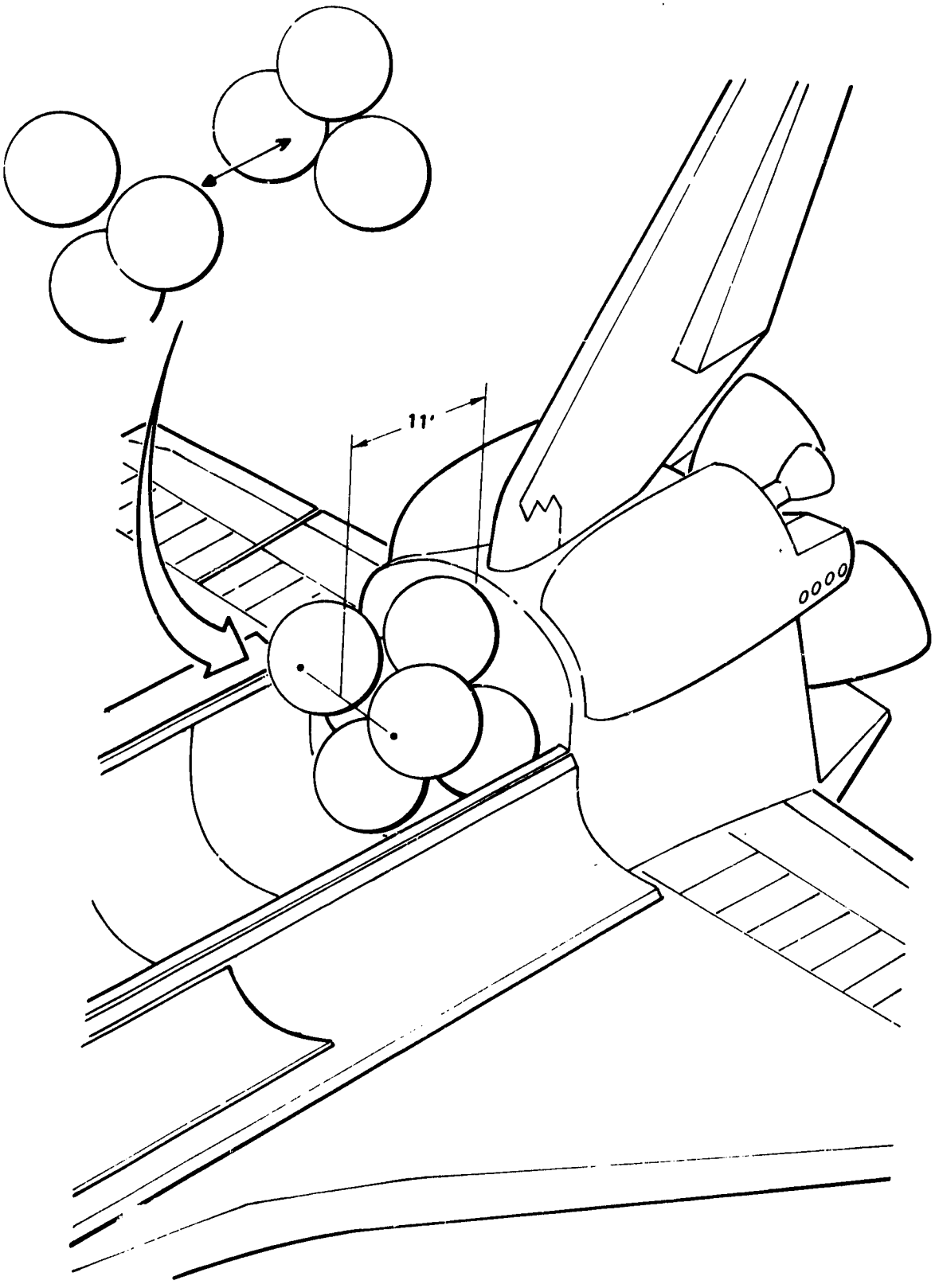

Figure 5-34. Nested Tanks Require Less Cargo Bay Volume

5.4.6 Solar Array Support

The fuel cell plus electrolysis concept of energy storage for a 250 kilowatt powerplant requires 430 kilowatts of input power from the solar array (Table 5-7). The beginning of life power requirement of the solar array becomes 566 kilowatts based upon a 20 percent solar array degradation over 30 years (Section 4.6) and a 5 percent loss for power transmission, solar array output regulation (switch losses), and off peak-power operation:

$$\frac{430 \text{ kW}}{(1 - 0.2) \times (1 - 0.05)} = 566 \text{ kilowatts}$$

GR.

A system efficiency of 38.8 percent is indicated based upon the 36.48 percent efficiency from the General Electric study (Reference 15) and removing the power conditioner efficiency (94 percent) in this value:

36.48 percent/0.94 = 38.8 percent efficiency.

The efficiency of the fuel cell plus electrolysis concept is low compared to the 65 to 70 percent efficiency of nickel-cadmium or nickel-hydrogen batteries.

5.4.7 Radiators

Waste heat from the fuel cell and electrolysis modules aggregates 210 kWh at full load: 232 kilowatts during eclipse and 79 kilowatts during sunlight (Table 5-9). Two radiators for this heat load total 4647 pounds (Table 5-11). This radiator weight is developed in the General Electric study (Reference 5-4) based upon the desired coolant temperatures and these radiator parameters:

Emissivity	0.92
Thermal view factor, sunlight	0.50
Thermal view factor eclipse	1.00
Sink temperature	-127°F
Specific weight	1.3 lb/sq ft

5.5 OPTIMUM DEPTH OF DISCHARGE

The life of nickel-cadmium and nickel-hydrogen cells is considered to be inversely dependent upon the depth of discharge incurred in the repetitive discharge and recharge cycling required for low earth orbit applications. This inverse relationship affects long term energy storage costs dramatically (Figure 5-35), and an optimization exists to select a valid depth of discharge that minimizes total energy storage costs.

The life cycle cost for energy storage is composed of the cost of the initial equipment complement plus the cost of subsequent replacement units as wearout occurs from cycling:

Life cycle cost = Initial equipment cost + replacement equipment cost

wherein equipment cost includes manufacturing and Shuttle transportation costs.

Equipment cost = Manufacturing cost + transportation cost.

The aggregate capacity of replacement batteries is dependent upon the amount of energy storage required, the wearout rate for this storage, and the satellite life of interest:

$$\text{Replacement battery capacity} = \frac{(\text{load power})(\text{eclipse duration})}{\text{depth of discharge}} \times \frac{\text{satellite life}}{\text{battery life}}$$

Battery replacement costs are defined by including specific costs:

$$\text{Battery replacement cost} = (\text{specific cost}) \times \frac{(\text{load power})(\text{eclipse duration})}{(\text{depth of discharge})} \times \frac{(\text{satellite life})}{(\text{battery life})}$$

The battery variables in this equation are battery type (electrochemistry) which defines the specific cost, depth of discharge, and battery life. Maximizing the product of depth of discharge and battery life minimizes replacement costs.

Battery cycle life as a function of depth of discharge is often projected as a straight line estimate on a semi-logarithmic graph (Figure 5-36). Analysis of such a straight-line semi-log relationship indicates the slope of this line defines an analytically optimum depth of discharge for minimum replacement costs. Further, the optimum cycle life concurrent with the optimum depth of discharge is a function of the cycle life projection at zero depth of discharge.

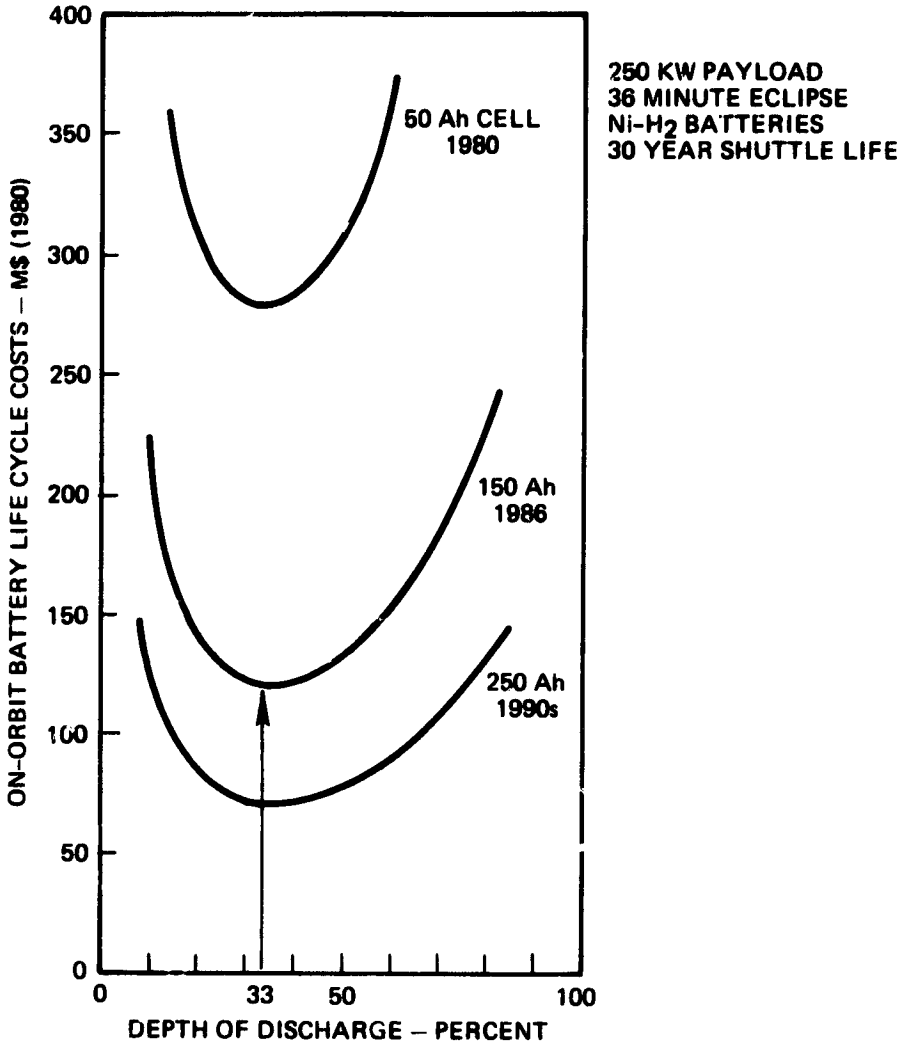

Figure 5-35. Life Cycle Cost Depends Upon Depth of Discharge

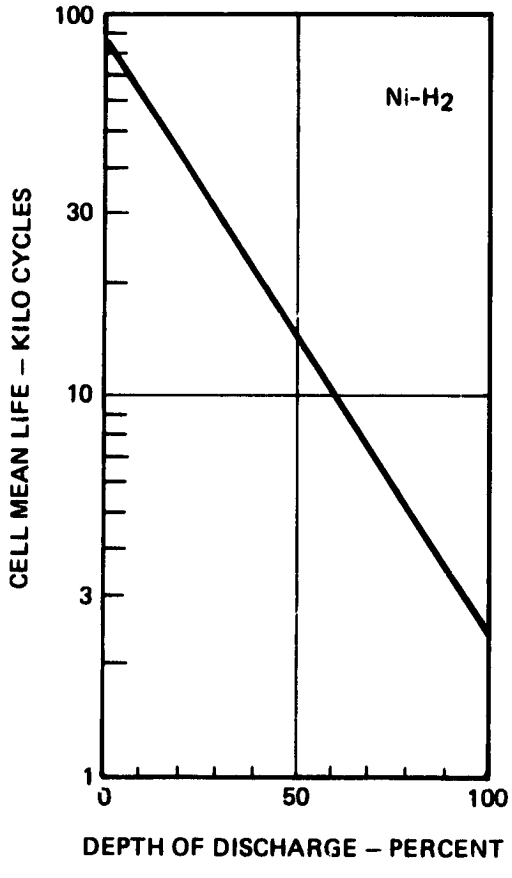

Figure 5-36. Typical Estimate of Cycle Life Versus Depth of Discharge

The generalized equation of a straight line relationship of life versus depth of discharge on a semi-log graph is:

$$y = 10^{(b - ax)}$$

where y = battery life, x = depth of discharge, 10^b is the y intercept at x = 0, and a is the slope of the line:

$$a = \frac{\Delta \log y}{\Delta x} = \frac{\log y|_{x=0} - \log y|_{x=1}}{1} = \text{Constant}$$

Maximizing the product x•y (depth of discharge and life) minimizes replacement costs. Differentiating x•y with respect to x (depth of discharge), setting the result equal to zero, and solving for x_o (optimum depth of discharge), yields 1/(a ln 10):

$$x \cdot y = x \cdot 10^{(b-ax)}$$

$$\frac{d(x \cdot y)}{dx} = \frac{d\left(x \cdot 10^{(b-ax)}\right)}{dx}$$

$$= \frac{10^b}{10^{ax}} - \frac{a\ 10^b \times \ln 10}{10^{ax}} = 0$$

$$1 - ax \ln 10 = 0$$

$$x = \frac{1}{a \ln 10} \triangleq x_o$$

Hence, the slope (a) determines the optimum depth of discharge (x_o) to minimize replacement battery costs.

The battery life at this analytically optimum depth of discharge ($y|_{x_o}$) is a function of 10^b, the y intercept at x = 0:

$$y = 10^{(b-ax)}$$

$$y|_{x_o} = 10^{(b-ax_o)} = 10^{(b-a/a \ln 10)} = \frac{10^b}{10^{1/\ln 10}}$$

$$y|_{x_o} = \frac{10^b}{e}$$

where the constant e is the base of natural logrithms. Hence, the $y|_{x=0}$ intercept (10^b) determines the battery life at optimum depth of discharge. This life value for the optimum depth of discharge is analytically independent of the slope estimated for the life versus depth of discharge projections and provides a means to estimate optimum depth of discharge on semilogrithmic plots (Figure 5-37). Optimum depth of discharge, to minimize replacement costs, occurs at the intersection of the life cycle curve and 37 percent of the zero-cycle life (Figure 5-37).

An alternate method, employing a simple graphical technique, exists to select the analytical optimum depth of discharge and the resultant battery life that minimizes battery replacement costs. The projected estimate of battery life versus depth of discharge is plotted on a log-log graphical format. The product of life and depth of discharge on a log-log graph is a constant represented by a -45 degree line from upper left to lower right (Figure 5-38). Successive -45 degree lines have higher numerical values for the life and depth of discharge product toward the upper right on the log-log format. Optimum depth of discharge is therefore defined by the -45 degree slope (tangent point) on the life versus depth of discharge curve, provided the relationship is plotted on log-log format. For example, replotting the nickel-cadmium projection of life versus depth of discharge (Figure 5-39a) as a log-log presentation (Figure 5-39b) verifies the selection of a high depth of discharge derived by the laborious tabulation of costs (Table 5-5).

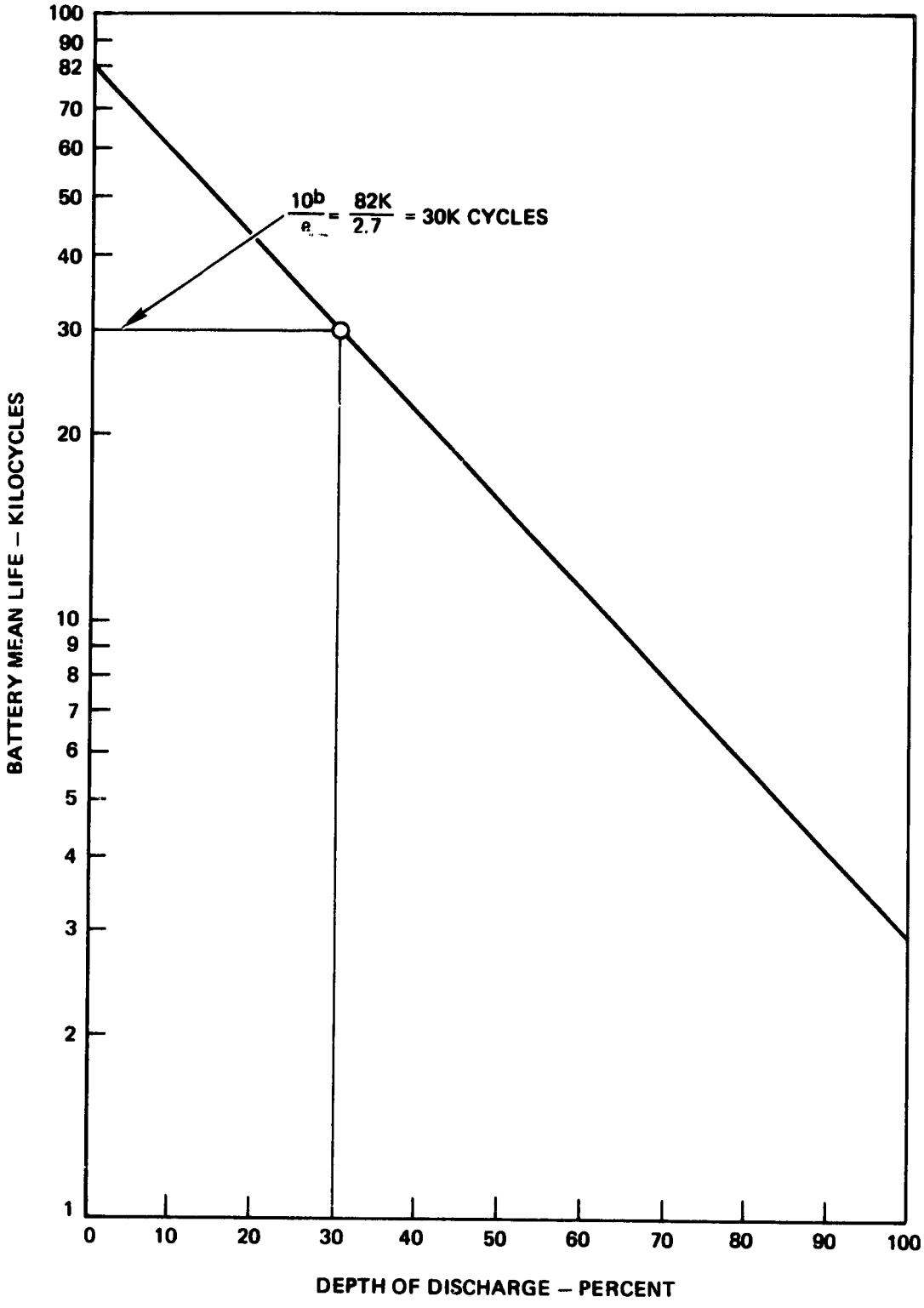

Figure 5-37. Cycle Life/DOD Semilog Plot Defines DOD and Cycle Life for Optimum Battery Utilization

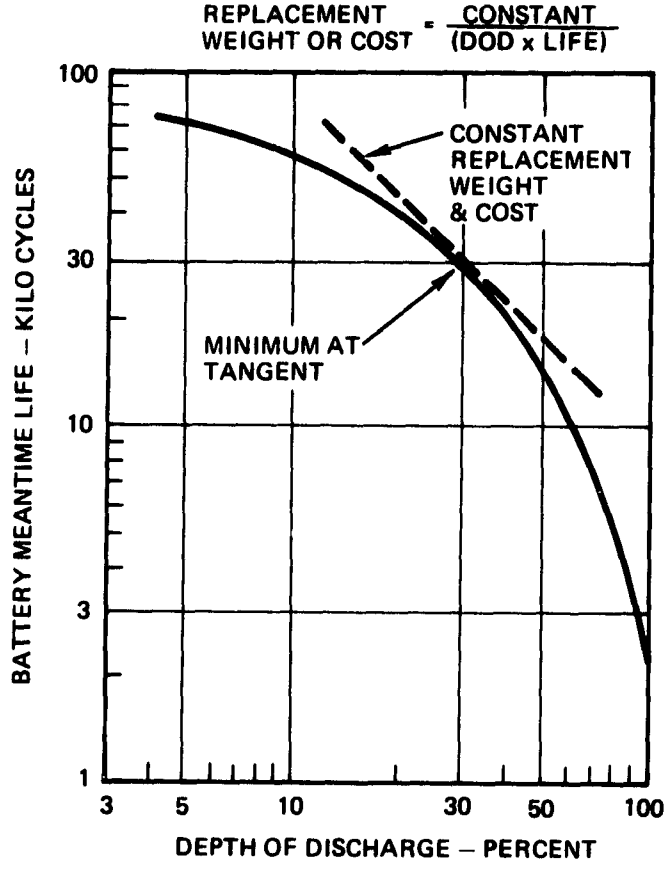

Figure 5-38. Log-Log Plot Shows Optimum Depth of Discharge and Cycle Life

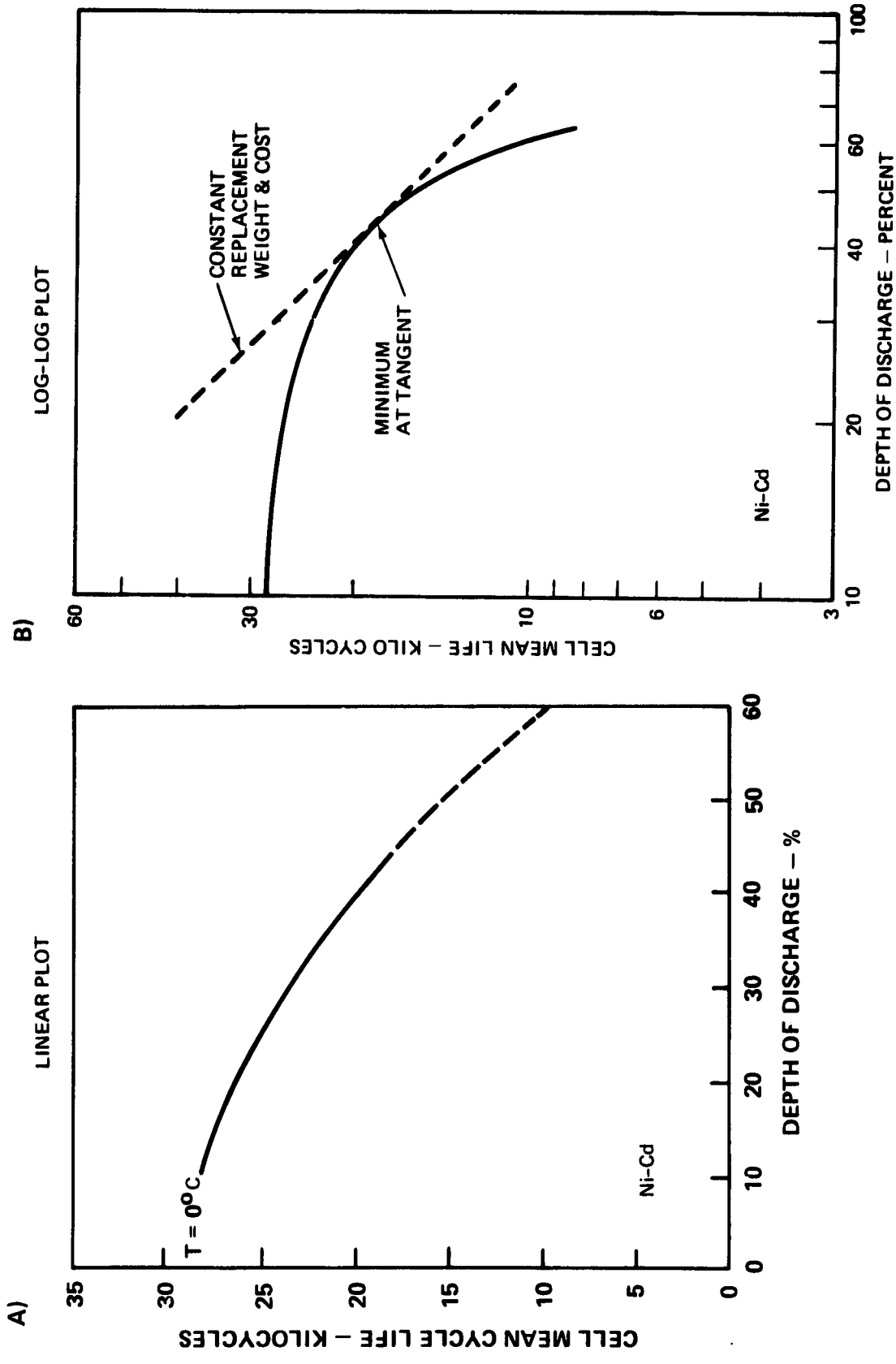

Figure 5-39. Log-Log Plot for Ni-Cd Verifies Optimization at High Depth of Discharge

5.6 RELIABILITY

The mean time to failure of a multi-cell, high-voltage battery (nickel-hydrogen or nickel-cadmium) is essentially the same as for present 28-volt 20-cell batteries (Figure 5-40) and is primarily dependent upon the inherent cell reliability. This result is based upon a Weibull distribution analysis of cell failures and an allowance of 5 percent in loss of battery voltage, i.e., the loss of 1 cell in 20, 5 cells in 100, 10 cells in 200, etc. Consequently, energy storage reliability is maintained even though increasing numbers of cells are series connected to attain higher system voltage (Figure 5-40).

Experience indicates the failure mechanism of nickel-cadmium cells to be dominated by wearout. The constant-failure-rate, exponential approach to a reliability model is therefore inappropriate and yields misleading life projections. The two-parameter Weibull probability density function appears a more appropriate model. Analytically, the function is of the form:

$$f(t) = \frac{\beta}{\delta}\left(\frac{t}{\delta}\right)^{\beta-1} \exp\left[-\left(\frac{t}{\delta}\right)^{\beta}\right]$$

where t = time, β = shape factor, and δ = scale factor. The Weibull function is bell-shaped (Figure 5-41). The β factor defines the skewness and the density distribution about the mean, and the δ factor determines the time location of the mean. This function corresponds to observations that cells operating under similar conditions (as in a battery) tend to fail at a common time period - not randomly or uniformly over the entire operational period.

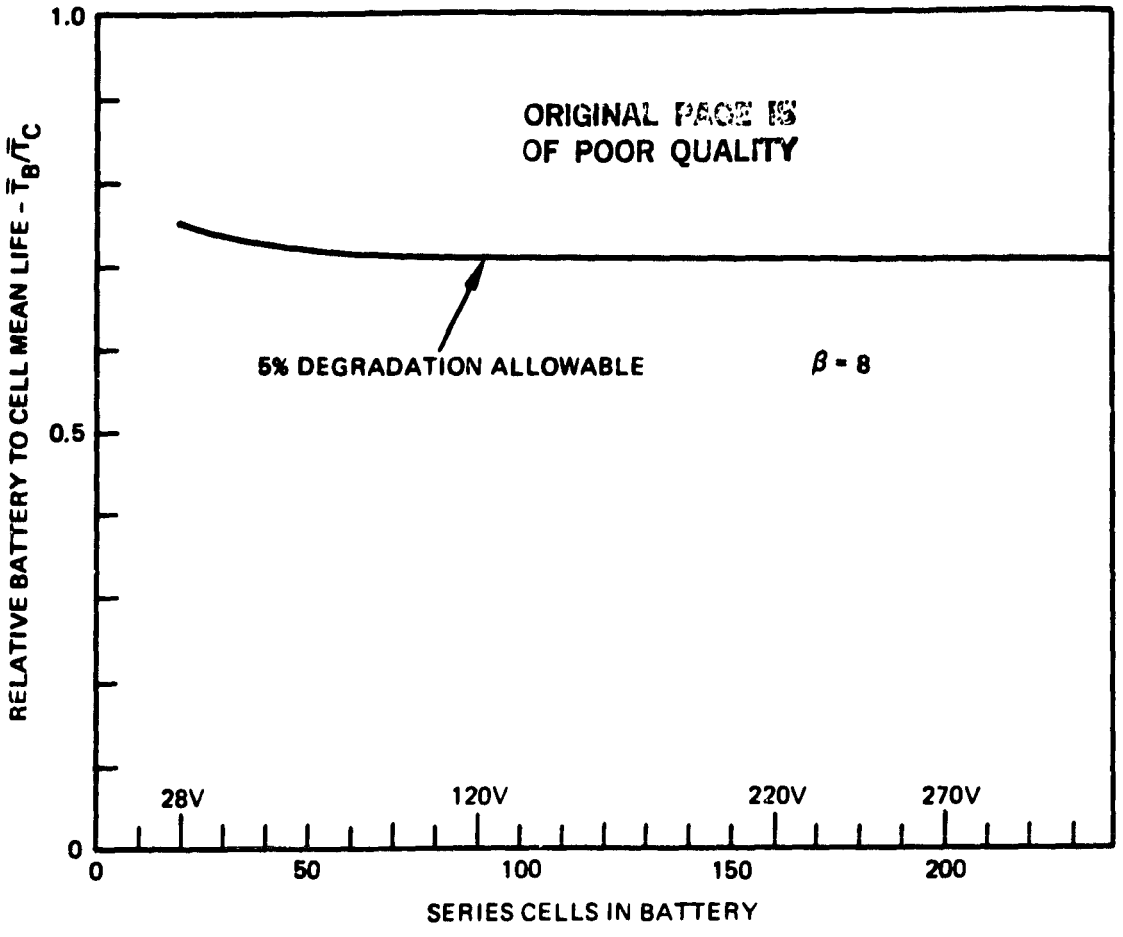

Figure 5-40. High Voltage Batteries Are Reliable

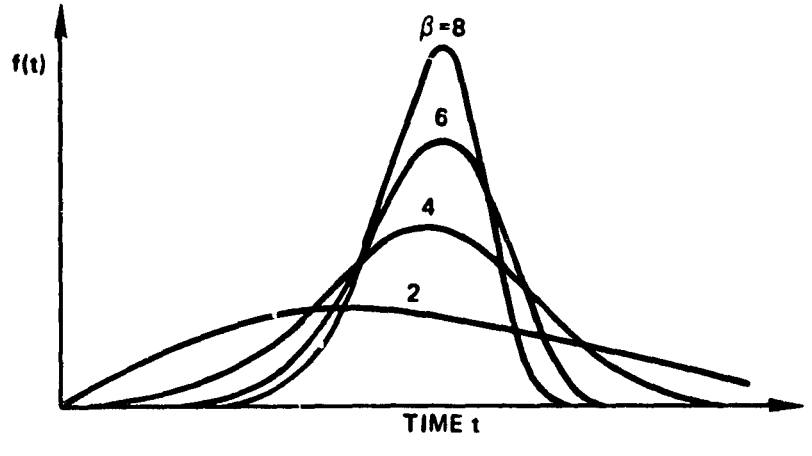

Figure 5.41. Weibull Probability Density Functions

Integration of the Weibull function and its moments provides the reliability (R), expected cell life ($\bar{T}$), and standard deviation (σ) for a cell:

$$R_1(t) = \exp\left[-\left(\frac{t}{\delta_1}\right)^{\beta}\right]$$

$$\bar{T}_1 = \delta_1 \Gamma(1 + 1/\beta)$$

$$\sigma_1 = \delta \sqrt{\Gamma(1 + 2/\beta) - \Gamma^2(1 + 1/\beta)}$$

where Γ is the gamma function and the subscript refers to a single cell. Furthermore, in a battery of i cells, where the first cell failure constitutes battery failure, the above equations remain valid with the subscript changed to i and where:

$$\delta_i = \delta_1/(i)^{1/\beta}$$

A battery of i cells therefore has an expected life ($\bar{T}_B$) of:

$$\bar{T}_B = \frac{\delta_1}{(i)^{1/\beta}} \Gamma(1 + 1/\beta)$$

Normalizing the expected battery life ($\bar{T}_B$) to the expected cell life ($\bar{T}_1$) shows the expected life of multiple cells in series is independant of the scale factor δ and is dependent primarily on β:

$$\frac{\bar{T}_B}{\bar{T}_1} = \frac{\delta/(i)^{1/\beta}\ \Gamma(1 + 1/\beta)}{\delta\ \Gamma(1 + 1/\beta)} = \frac{1}{(i)^{1/\beta}}$$

An analysis of selected Crane data (Reference 5-6) shows a β of 7.6 as representative of nickel-cadmium cell testing failures. Experience indicates better life performance for actual spacecraft and satellite batteries. A β of 8 is therefore applied for this analysis (Figure 5-42). There is little loss in the expected life with increases in cell quantity for a spacecraft quality battery with battery voltages above 28 volts (20 cells).

The preceding analysis is appropriate for fuel cells and electrolysis units wherein a single cell failure (hydrogen to oxygen crossover) requires the shutdown of the entire stack of cells. For batteries, where an open circuit is extremely remote or not credible, only a modest voltage loss results from a failed cell (shorted cell), and the battery remains functional. Typically, in 28-volt batteries, a single cell failure (5 percent voltage loss) may be sustained by a battery, and the battery still be functional. This 5 percent allowance, also applied to high voltage batteries, produces essentially uniform mean time to failure regardless of the number of cells in series (Figure 5-40). Hence, high voltage batteries do not entail any reduced life, increased servicing or replacement, or adverse reliability penalty.

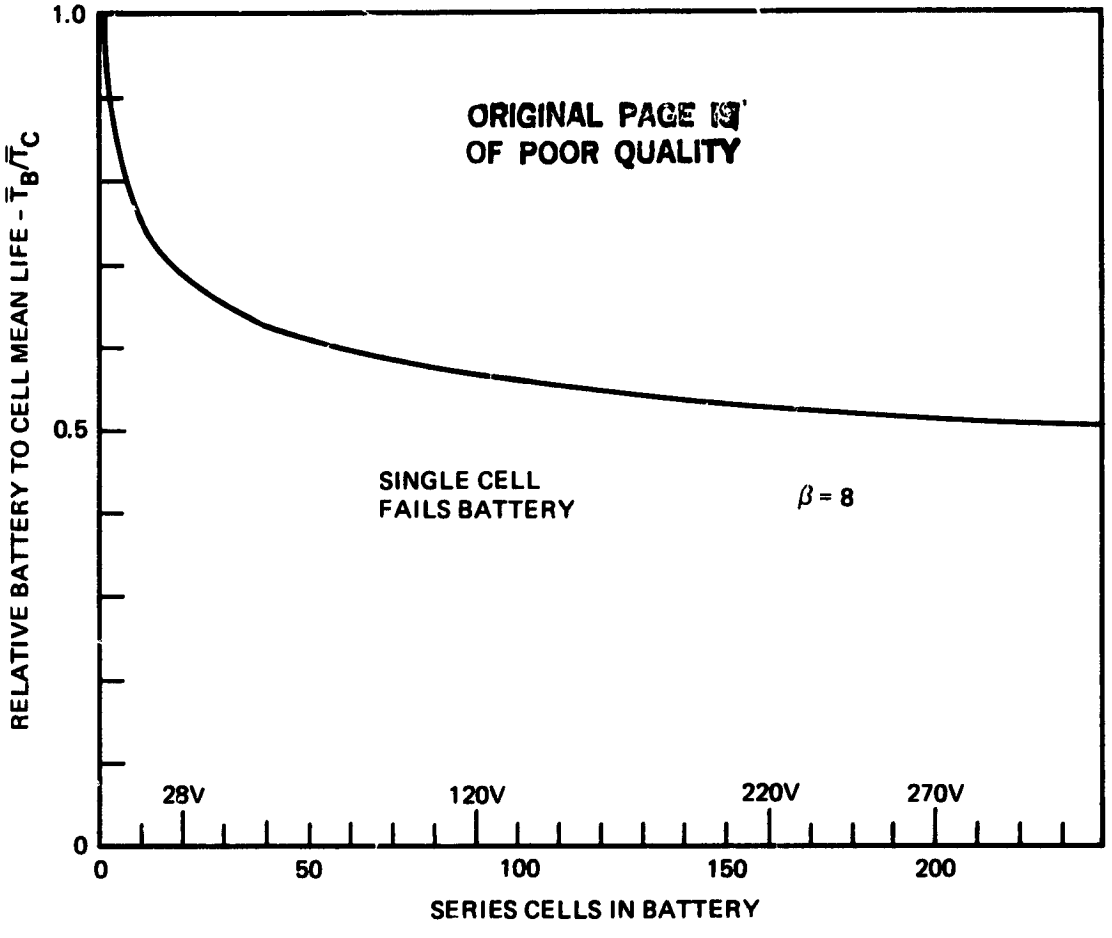

Figure 5-42. High-Voltage Battery Life Independent of Cell Quantity

5.7 LOAD PROFILE

Small, unmanned, nonrepairable satellites in the range of 500 watts to 2 kilowatts are typically designed for a sustained peak power level. Battery depth of discharge and the resulting projected battery life are based upon this operational scenario -- continuous full power operation. The 250-kilowatt system, considered herein, approaches an electric utility concept. Individual payloads are small (500 watts to 5 kilowatts) compared to the system capacity (250 kilowatts). The connected payload demand is not expected to aggregate 250 kilowatts at all times. Hence, actual battery depth of discharge is reduced from the design point (e.g., 33 percent for nickel-hydrogen) and battery life is extended beyond the life projection for full load operation (7 years for nickel-hydrogen at 33 percent depth of discharge). Estimation of battery life is critical to replacement costs, and replacement costs dominate battery costs (Figure 5-43) over any extended time period (e.g., 30 years). Therefore, a careful examination is needed of actual system load, the relationship to installed capacity, and the resultant battery cost projections.

Three simplified operational scenarios of payload power demand (Figure 5-44) are evaluated to identify their effect on battery depth of discharge, life, and cost:

1) Case 1, satellite power system operated at full power every eclipse cycle (worst case).

2) Case 2, a well managed but heavily loaded system (mature system usage).

3) Case 3, a typical utility load profile exhibiting 20 percent power margin and reflecting a terrestrial diurnal cycle (an early and perhaps typical utilization of the power system capacity).

Case 1 represents the typical design approach as defined in Section 5.3.

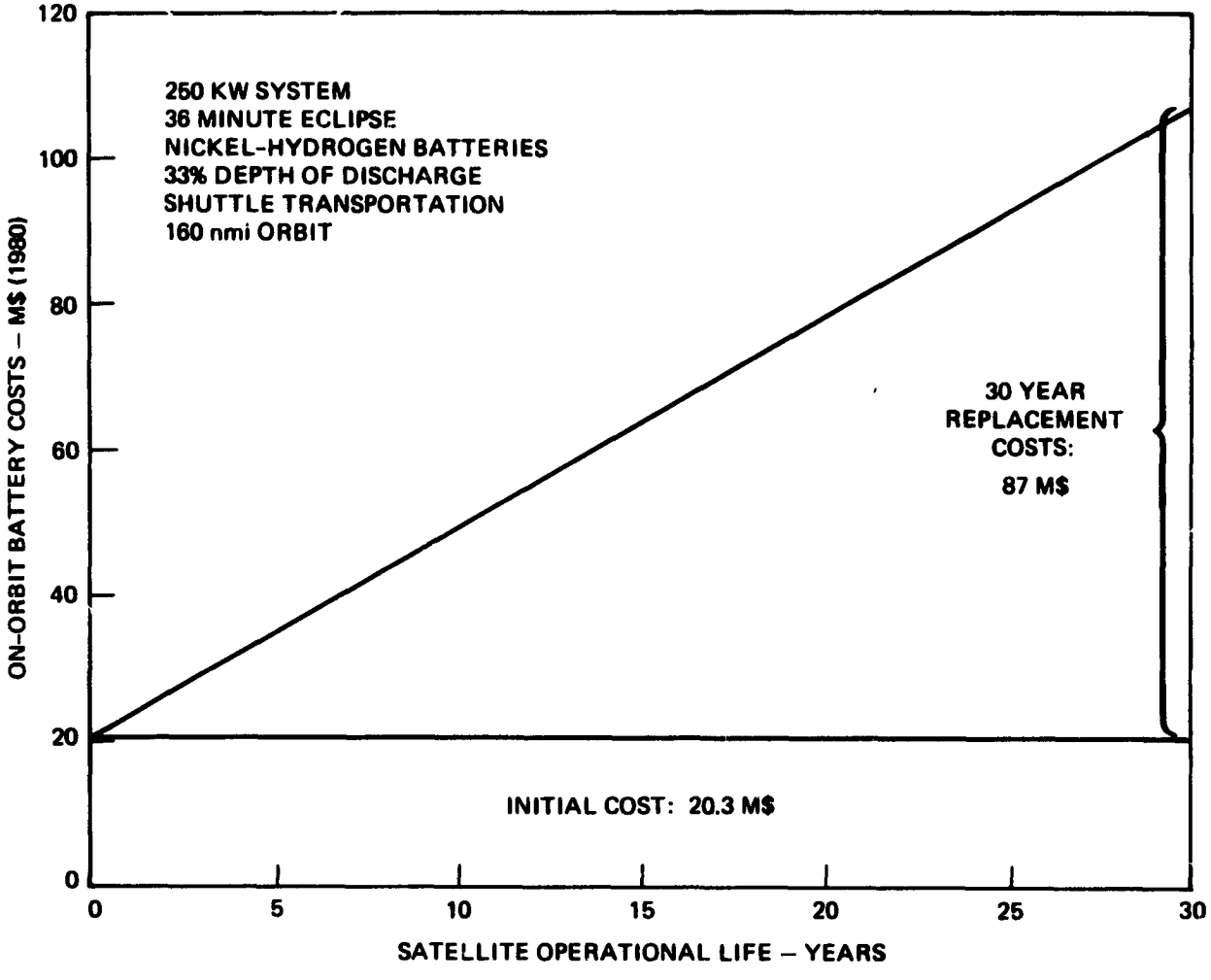

Figure 5-43. Replacement Costs Dominate Battery Costs

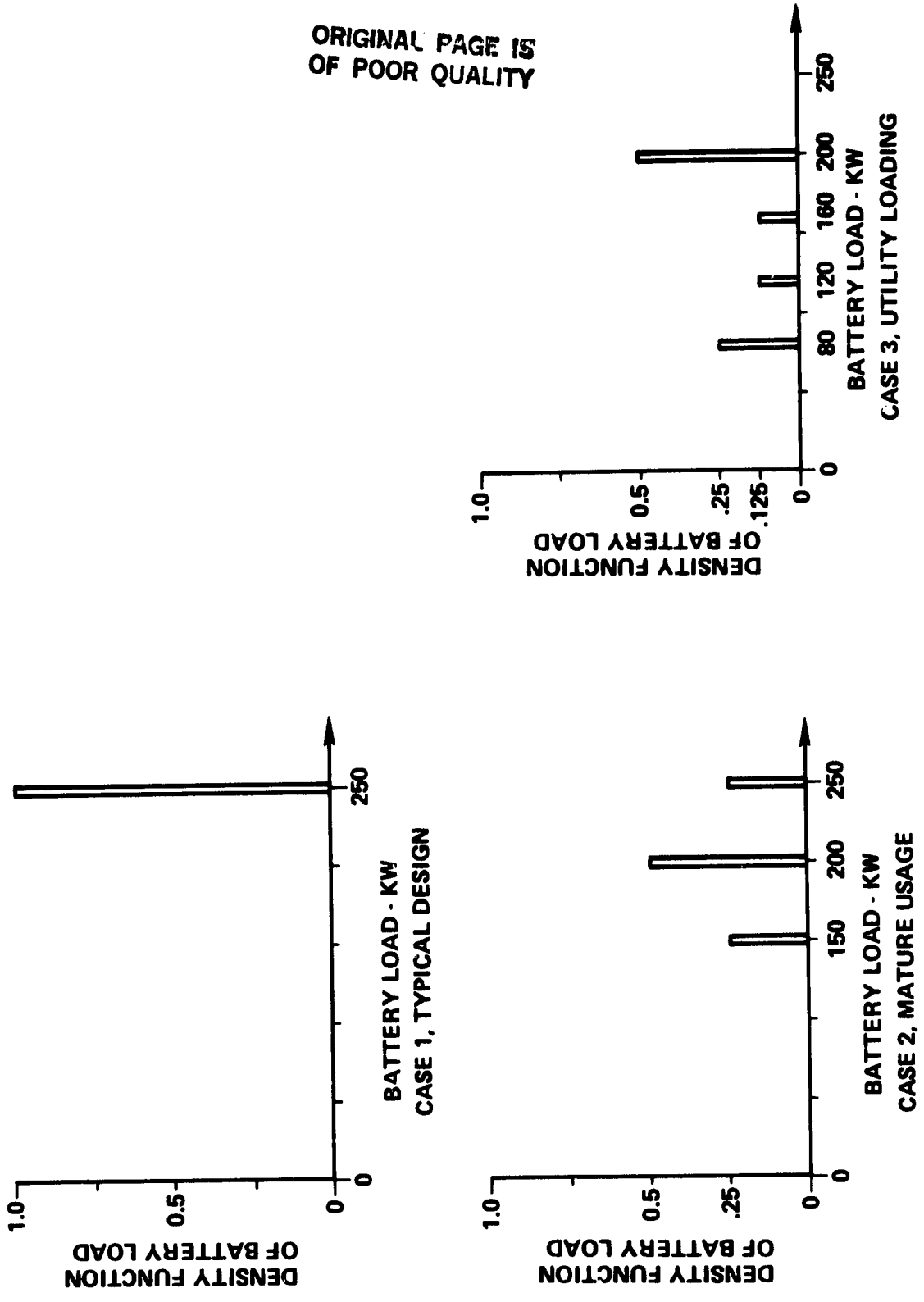

Figure 5-44. Payload Power Demand Scenarios

The power density distribution of Case 2 is structured arbitrarily to include significant full power loading (25 percent at 250 kilowatts), heavy usage near full power (50 percent at 200 kilowatts), and a modest amount of lower power use (25 percent at 150 kilowatts). This utilization density distribution is an arbitrary selection to provide an example of a well managed and heavily loaded system. Such an example may become representative of mature usage of a satellite and its electrical power system.

The power density distribution of Case 3 is derived from typical terrestrial utility profiles. Such power density distributions exhibit a large power density peak near 80 percent of capacity caused by the early afternoon to early evening utility loads. A smaller power density peak occurs at the lowest power level and represents the post midnight to dawn load. The two intermediate power density bands represent the transition periods between these two load extremes.

Case 3 loading essentially incorporates a terrestrial diurnal cycle of operation and may be representative of early and perhaps typical utilization of a satellite and its power system. Such a cycle is representative of the diurnal cycle for ground control and interrogation rather than the satellite local eclipse and sunlight cycle.

Caution must be exercised in formulating the equivalent depth of discharge and the effective life of a battery operated at several depth-of-discharge levels. The effective battery life is dependent upon <u>both</u> the depth of discharge level attained and the proportioned life duration at each load level. Hence, the distribution functions for battery loading (payload power) are translated into battery life using the depth of discharge to life relationship of Figure 5-19 and the sum of the proportioned life ratios:

$$\sum \frac{D_i}{L_i} = \frac{1}{L}$$

where L is the projected battery life, D_i = the density function (Figure 5-44) for load P_i, and L_i = the battery life if continuously cycled at load P_i.

Operation of a power system at any reduced power level from the design criteria extends the battery life due to the reduced depth of discharge. For example, a 250-kilowatt power system designed for Case 1 loads, but operated with Case 2 or Case 3 load scenarios, produces longer battery life and reduced replacement costs (Table 5-11). Battery cost reductions can be significant over a 30-year mission (Figure 5-45) depending upon the extent and duration of the reduced system loading. However, initial costs remain unchanged applying the design criteria of Case 1.

An electrical power system designed for the load scenario Case 2 or Case 3 shows cost reductions are possible in the initial battery complement by increasing the depth of discharge at the maximum power point (250 kilowatts). This design approach to minimize life-cycle costs for each load scenario reduces both initial costs and replacement costs by judicious calculation of the optimum depth of discharge for each load scenario:

33 percent for Case 1 at 250 kilowatts

40 percent for Case 2 at 250 kilowatts

50 percent for Case 3 at 250 kilowatts

The effective operational depth of discharge at the equivalent load of each load scenario is 33 percent and provides a 7-year mean battery life (Table 5-14). This design approach reduces both initial and replacement costs (Figure 5-46) yet provides support of a 250-kilowatt load though at a deeper depth of discharge than the Case 1 design approach.

A significant cost reduction over the typical approach of Case 1 design criteria is attained by considering the actual utilization scenario of the power system. A greater battery depth of discharge can be recommended, consistent with the load scenario, to reduce the installed battery capacity. Battery weight, the quantity of power channels (number of batteries), and the energy storage cost are consequently reduced. The potential for cost reduction is substantial (Figure 5-47) 6.8 M$ initially and 35.8 M$ over 30 years for Case 3 versus Case 1 design criteria with Case 3 operation, a 33 percent reduction. Further, if Case 3 design is implemented, and Case 1 loading actually occurs but is deferred beyond year 6, life-cycle costs are less than or equal to Case 1, but initial costs remain lower. Replacement costs increase should loads become greater than the design optimization.

Table 5-13. Calculations of Battery Life and Costs for Each Load Scenario

Load Scenario	Load Power P_i	Distribution Density D_i	Depth of Discharge DOD_i	Relative Life L_i	Projected Battery Life	Initial Battery Cost	Annualized Replacement Cost	30-Year Battery Cost
Case	KW	%	%	Years	Years	M$	M$	M$
1	250	100	33	7.0	7.0	20.3	2.9	107.3
2	150 200 250	25 50 25	20 27 33	10.8 8.6 7.0	8.5	20.3	2.4	92.0
3	80 120 160 200	25 12.5 12.5 50	11 16 21 27	14.7 12.3 10.3 8.6	10.3	20.3	2.0	79.4

Table 5-14. Calculation of Battery Costs Optimized for Each Load Scenario

Load Scenario	Load Power P_i	Distribution Density D_i	Depth of Discharge DOD_i	Relative Life L_i	Projected Battery Life	Initial Battery Cost	Annualized Replacement Cost	30-Year Battery Cost
Case	KW	%	%	Years	Years	M$	M$	M$
1	250	100	33	7.0	7.0	20.3	2.9	107.3
2	150 200 250	25 50 25	24 32 40	9.5 7.2 5.5	7.0	16.5	2.4	87.3
3	80 120 160 200	25 12.5 12.5 50	16 24 32 40	12.3 9.5 7.2 5.5	7.0	13.5	2.0	71.5

ORIGINAL PAGE IS
OF POOR QUALITY

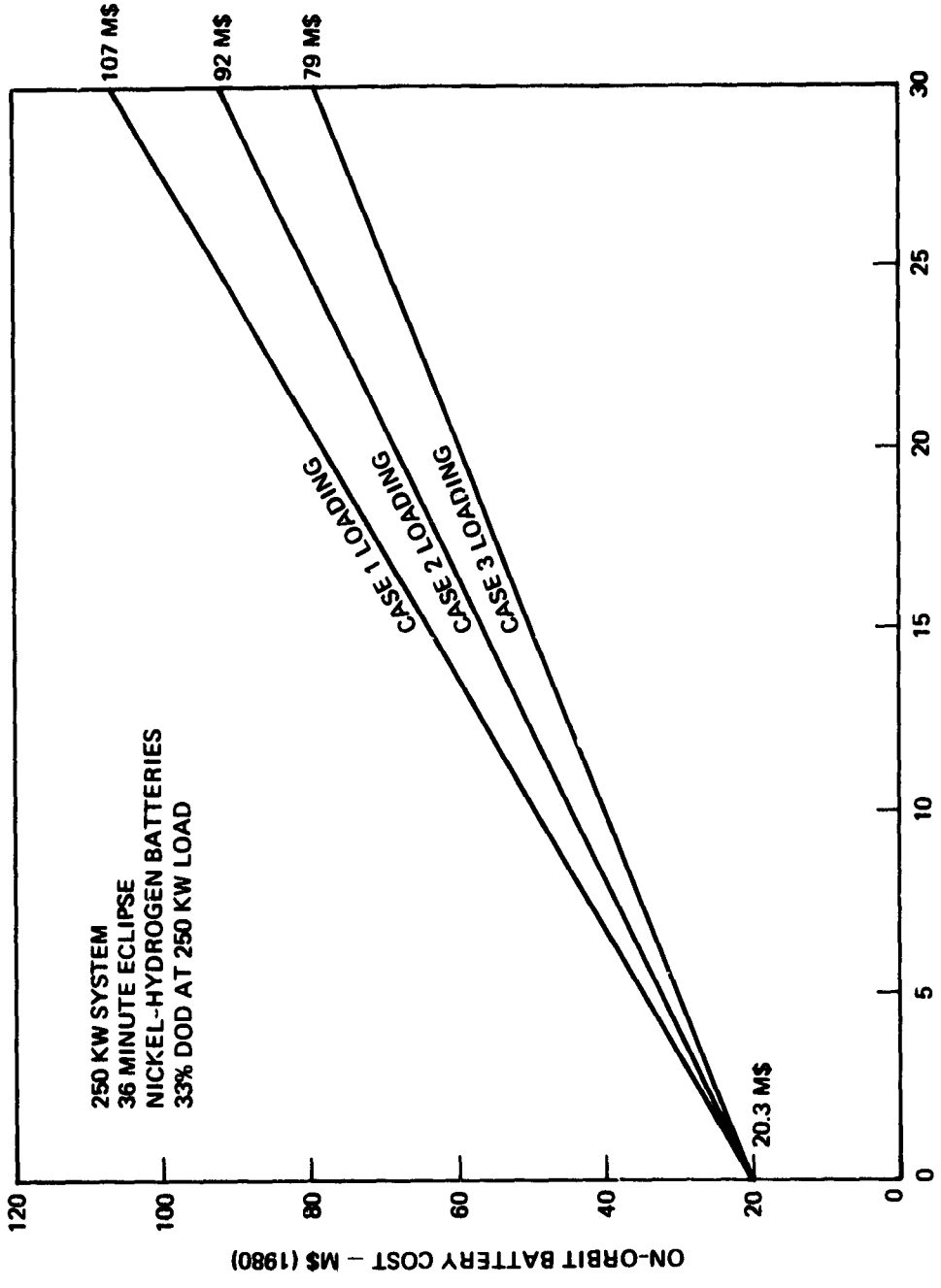

Figure 5-45. Load Scenario May Reduce Life-Cycle Costs

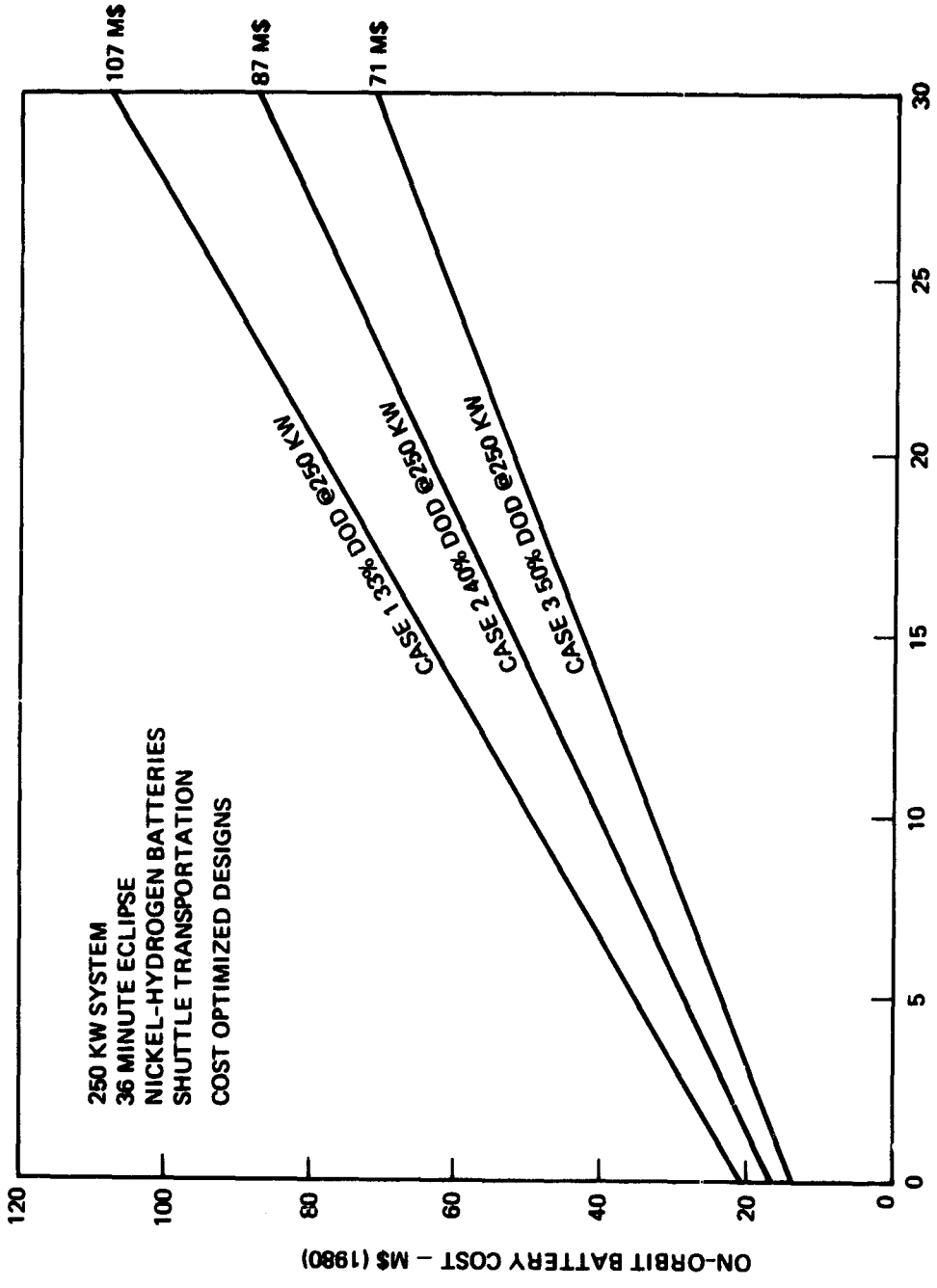

Figure 5-46. Design Optimized for Load Scenario Reduces Costs

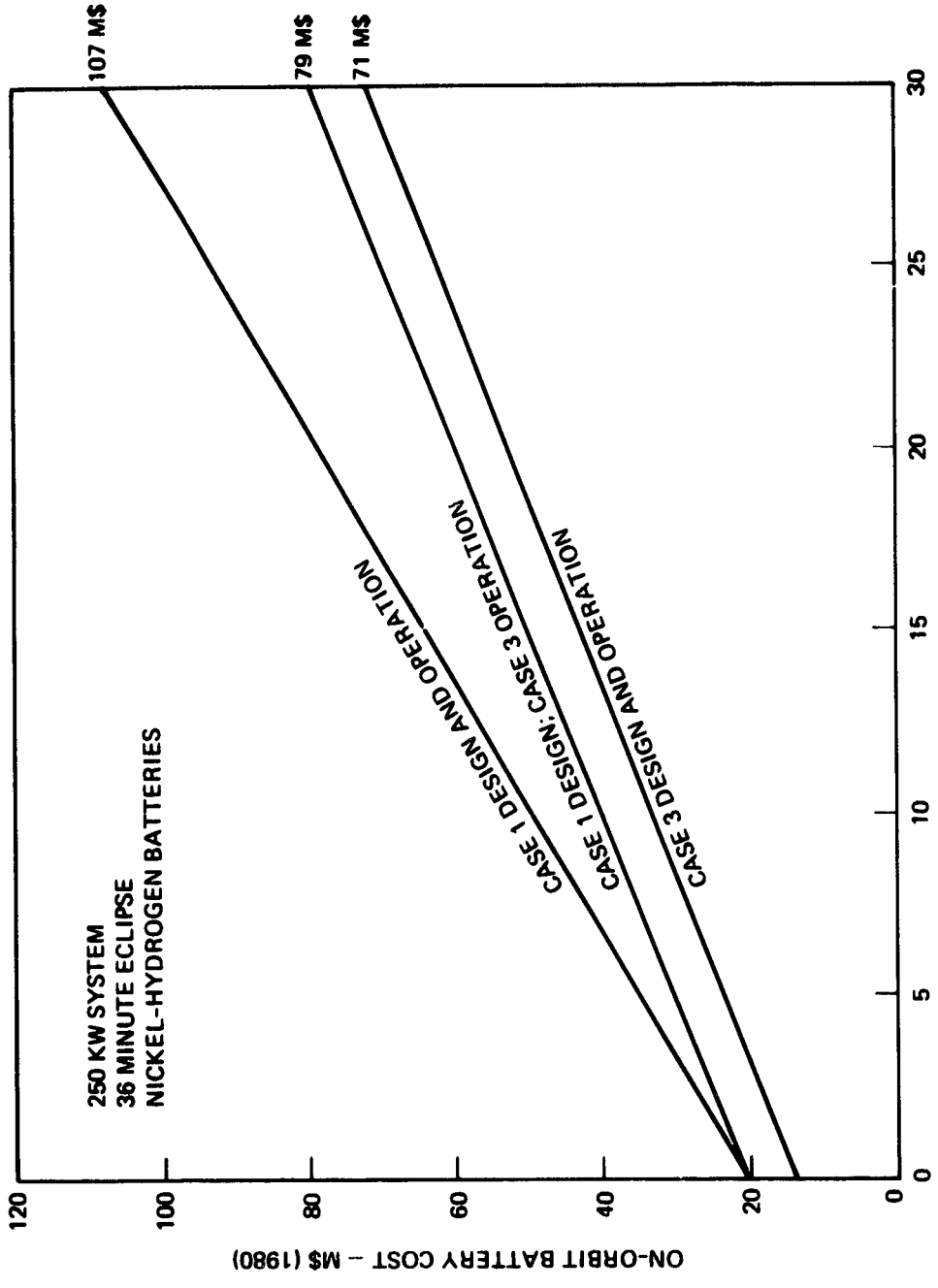

Figure 5-47. Design Optimized for Load Scenario Saves Initial Costs

The consideration of load scenarios for cost reduction is appropriate and significant for the shallow depth of discharge ($\leq$33 percent) considered herein for nickel-hydrogen. Should new data show depth of discharge optimization at deep depths of discharge ($\geq$60 percent), load scenario considerations yield little additional benefits.

6. DISTRIBUTION

The design of a distribution system for the 250 kW electrical power system entails selection of a suitable network topology, optimization of conductor cross section and material, identification of appropriate switch gear and protection devices, and selection of the distribution voltage (level and form). Analyses and comparisons of various options in each of these areas were made to develop the selected cost-effective distribution concept.

The system power level and the inherent satellite distribution distances of the 250 kW power system lead to direct energy transfer at a source voltage as high as practical (220 $\pm$20 Vdc, per Section 7). Channelized power distribution with radial topology provides a practical growth scenario and reduces the current handling requirements for switch gear. Active switchgear is limited to the lower power levels of individual loads (or load buses). Regulation of the source voltage and/or conversion to higher distribution voltages incur significant costs without a clearly projectable payback and are therefore avoided.

6.1 DISTRIBUTION DISTANCE

The 250-kW power system implies a considerably larger satellite than previously launched into orbit. To address the electrical distribution issues for 250-kW power, a hypothetical satellite was conceptualized which identifies the distribution distances and employs the load center approach.

The satellite concept utilizes incremental buildup from Shuttle cargo bay modules (Figure 6-1). The initial module contains the energy storage (batteries) and other basic housekeeping subsystems. The solar array is delivered on a subsequent (or concurrent) launch and attached to the energy storage module. Additional modules accommodate payload functions (internally or externally).

The interior of a payload module is suitable for habitation, a laboratory for manned experiments, or merely pressurizable to provide a shirt-sleeve environment for equipment repair or replacement. The exterior of each module is capable of supporting attachable payloads. Eight payload ports are hypothesized on each module arranged in sets of four with 30-foot

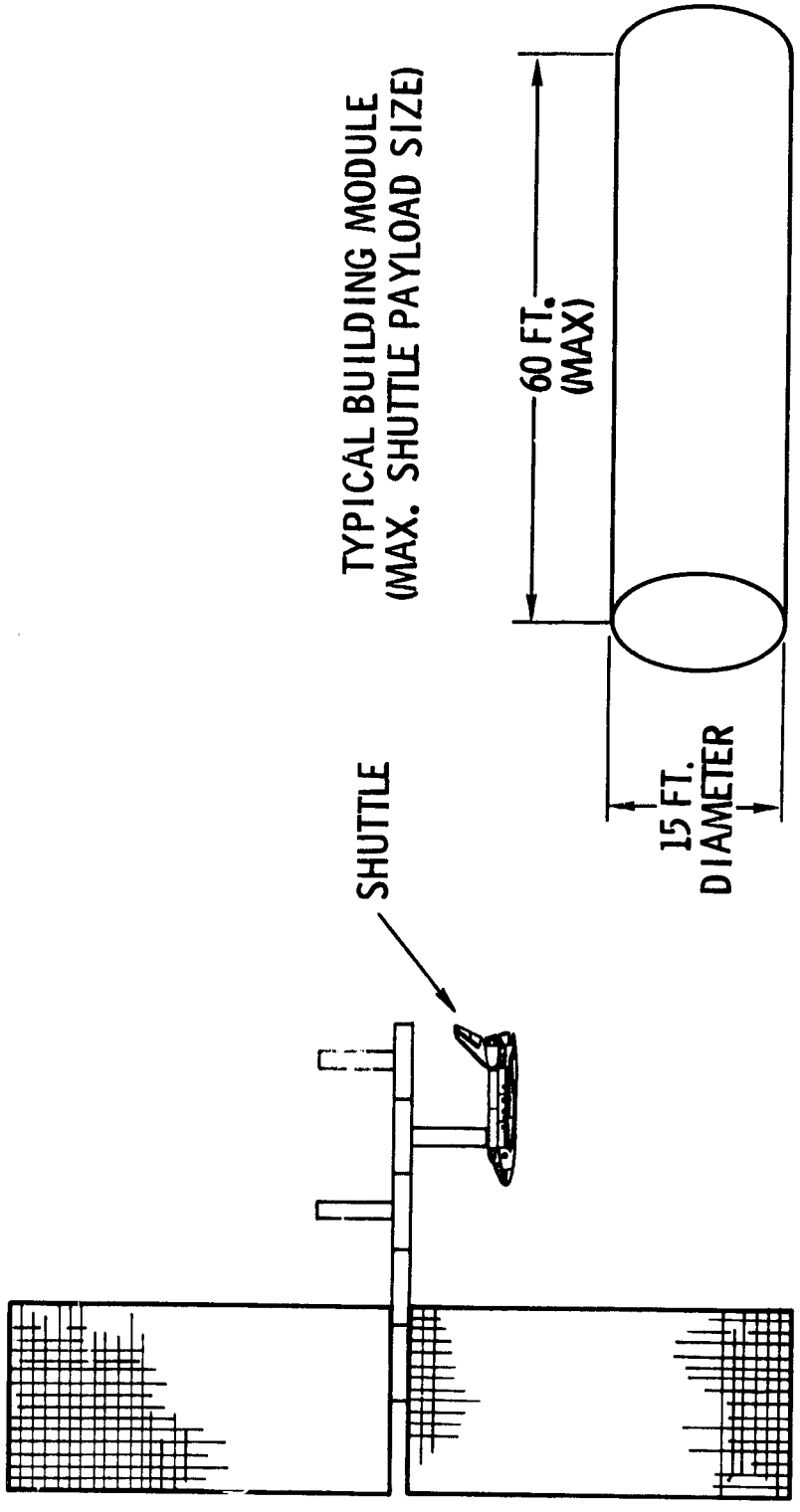

Figure 6-1. Space Platform Concept

spacing between sets (Figure 6-2). This provides 40 exterior attachment points for Payload pallets. Any special positioning or gimbal requirements are presummed provided by the payload. Some payload constraints may dictate a specific location on a satellite module or preclude full utilization of cell payload ports simulaneously.

The size of the satellite modules is constrained by the Shuttle cargo bay to essentially cylindrical modules 15 feet in diameter by 60 feet long. The cylindrical shape is particularly appropriate for internal pressurization as a manned environment for a habitat or for equipment repair. Each module end face provides the structural, electrical, and fluid interface connections for assembly to adjacent modules. For 1986 technology each module is fully assembled and tested prior to launch.

A growth scenario to five modules is considered herein over a 30-year life cycle. This produces a maximum distribution distance of 300 feet axially along the modules. Load centers are placed every 30 feet (two per module) to concentrate the switchgear and controls into localized load control centers for efficient equipment fabrication and effective control coordination.

6.2 DISTRIBUTION NETWORK

The distribution networks of terrestrial electric utilities employ various multiple feeder schemes to circumvent transmission and distribution line failures. This enables high power switchgear and additional (redundant) transmission and distribution conductors. Typically, utility distribution failures are from transmission line exposure to adverse weather. Satellite distribution lines are not so exposed. Electrical power failures are usually from generation, storage, conversion, and switch gear components rather than distribution conductors. Hence, the utility approaches to distribution, while adding transmission redundancy, add negligible improvement to the reliability of power availability at a spacecraft payload terminal. For spacecraft applications, network approaches that provide redundancy in the source, conversion, and switchgear components are more desirable.

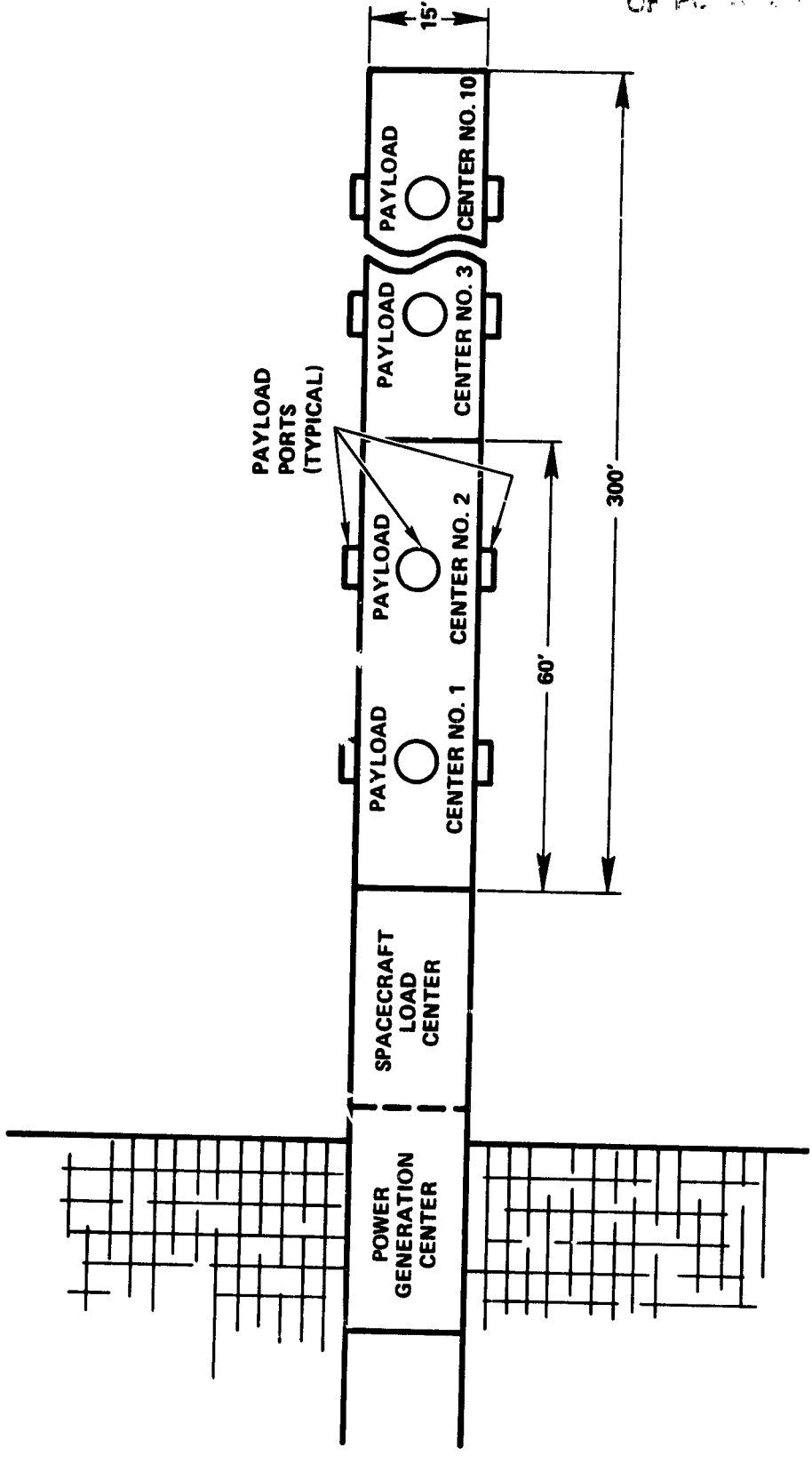

Figure 6-2. Load Center Concept

6.2.1 Network Topology

Three candidate approaches to network topology are evaluated for application to the 250 kW electrical power system: radial, loop, and grid topologies (Figure 6-3). Evaluation criteria are ease of expansion for modular assembly and growth, source interactions, switching and protection hierarchy, and redundancy. Comparison of these distribution topologies (Table 6-1) shows the loop and grid networks to require bi-directional current flow and hence bi-directional switchgear and to incur greater conductor weight - greater cost. Increased redundancy and power management flexibility are the chief benefits. The radial network is the lightest and least expensive topology (shortest conductors and simple switchgear) and hence desirable. The efficiencies in redundancy and power management flexibility can be overcome by several variations of the radial topology. Typically small satellites employ a single main bus and essentially radial distribution (Figure 6-4). Energy storage and critical equipment may be redundant but integrated with the single bus. Equipment redundancy, rather than distribution redundancy, is provided.

Manned vehicles (aircraft and satellites) typically employ two or more major electrical sources and distribution networks (Figure 6-5). The philosophy is to operate the system with isolated buses but provide a bus tie arrangement in order to support both buses in the event one source fails. The bus tie concept requires high capacity switchgear and is subject to abuse. Both sources may be interconnected (with the accompanying concerns of voltage matching and power/energy sharing) such that a single failure propagates the failure of the entire electrical power system.

A third approach provides isolated radial distribution from each source but includes dual switchgear at major or critical loads to allow transfer of the load to either of two source distribution networks (Figure 6-6). Improved redundancy and power management are attained without increased conductor weight or high-power switchgear. The conductors are sized by the source capacity as in all networks under consideration herein, but the switchgear is sized for the individual load powers. This approach is selected for the 250-kW distribution system.

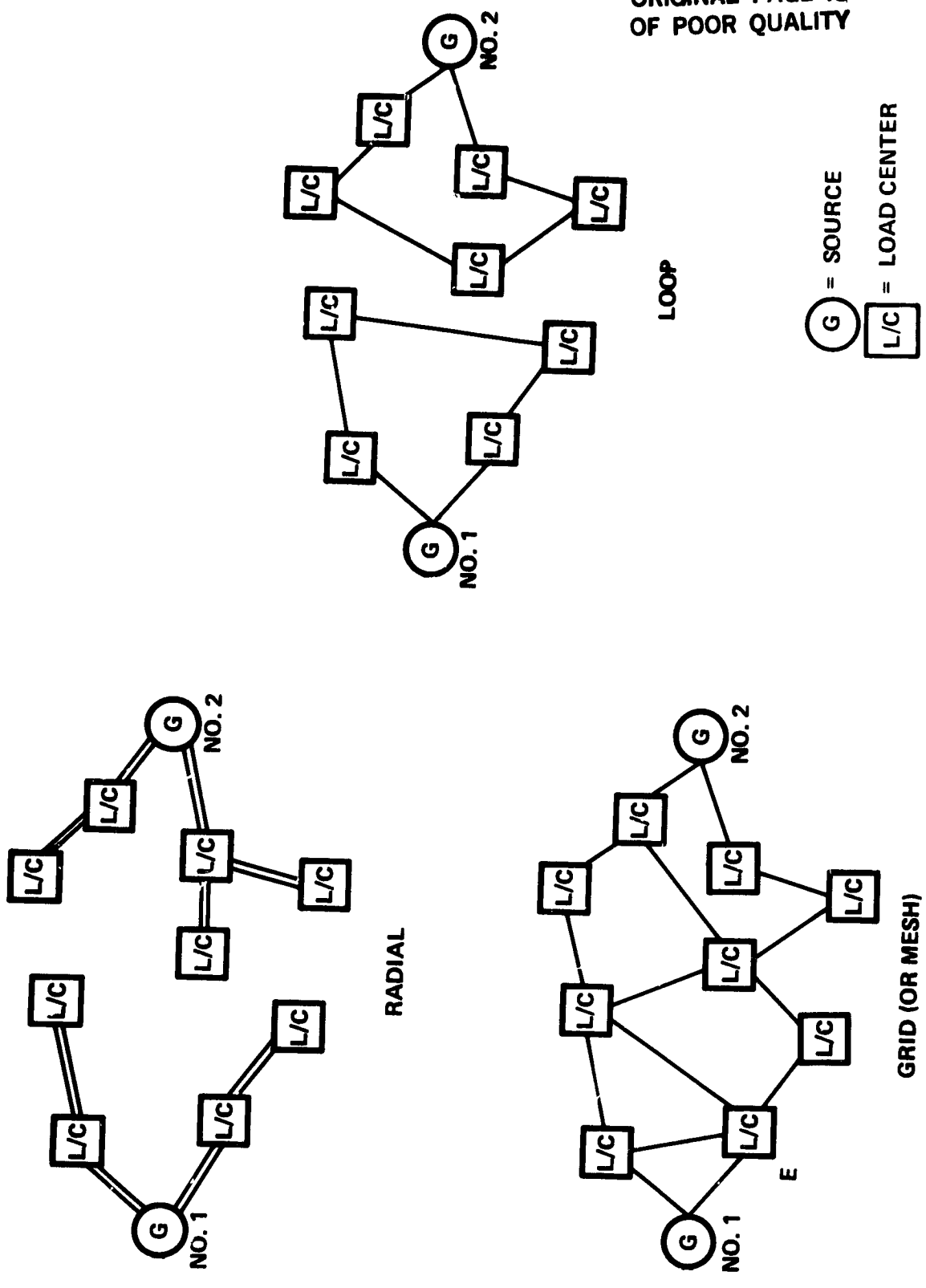

Figure 6-3. Distribution Network Approaches

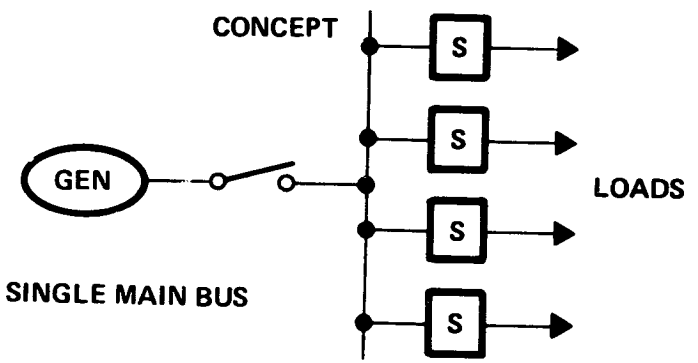

DISADVANTAGES

1) NONREDUNDANT MAIN BUS
2) NOT EASILY EXPANDABLE

ADVANTAGES

1) LOAD SWITCHING ONLY
2) SIMPLICITY
3) RELATIVELY LOW COST

Figure 6-4. Radial Distribution Network Concepts (Single Main Bus)

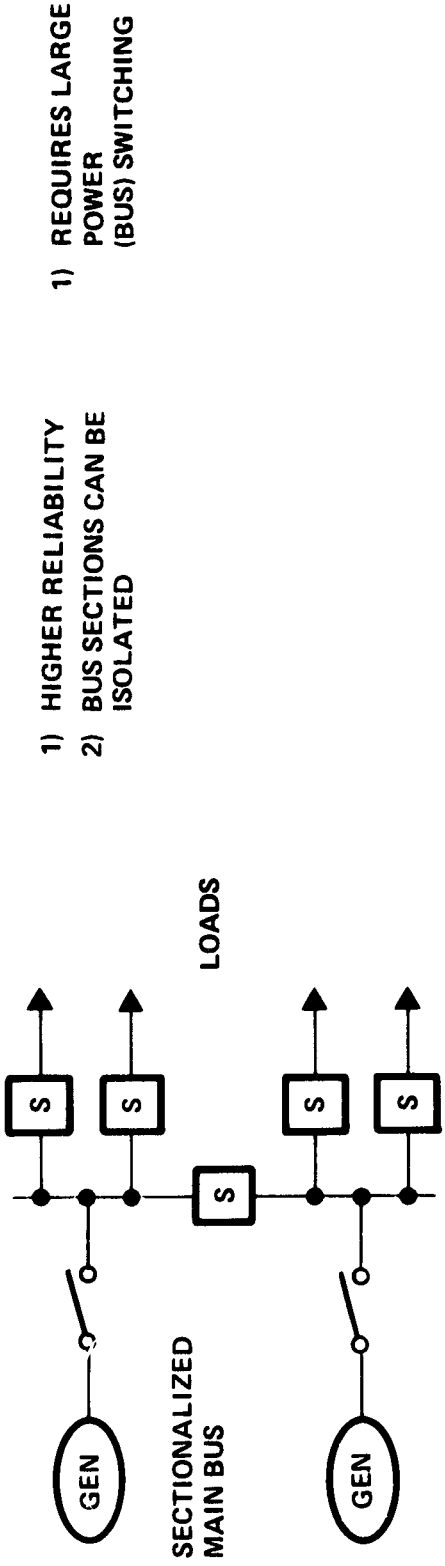

Figure 6-5. Radial Distribution Network Concepts (Sectionalized Main Bus)

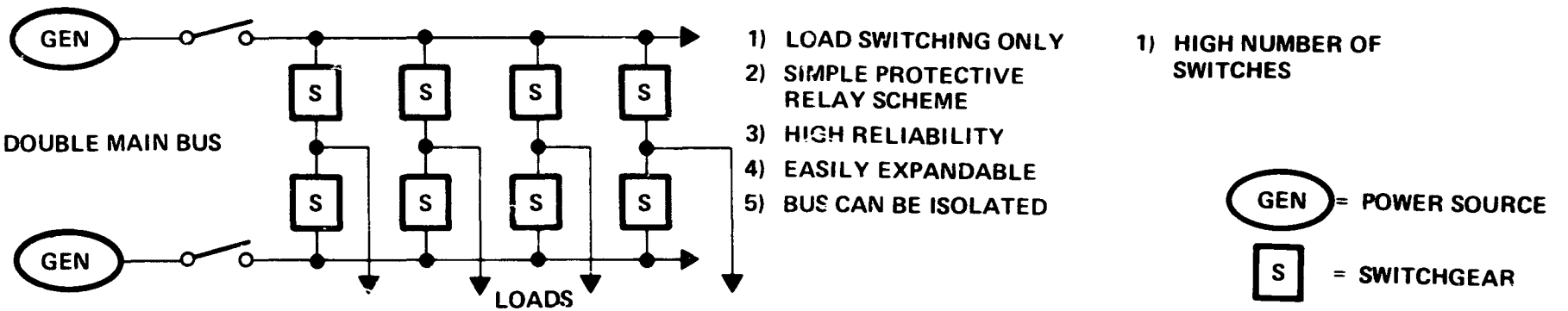

Figure 6-6. Radial Distribution Network Concepts (Double Main Bus)

Table 6-1. Comparison of Distribution Topologies (Figure 5-3)

Parameter \ Topology	Radial	Loop	Grid
Growth	Simple additions	Break loop	Affect several load centers
Current Flow	Unidirectional	Potentially bidirectional	Multipath, bidirectional
Conductor Size	Shortest, lightest	Double length	Potentially heaviest
Switchgear	Load switches	Bus isolation, bidirectional	Bus tie capacity, bidirectional
Source isolation	Isolated sources	Isolated sources	Source tie possible
Network Fault Isolation	None	One fault	Multiple faults
Power Management Flexibility	None	None	Many options
Cost	Lowest	Modest	Greatest

6.2.2 Conductor Configuration

Three generic distribution conductor configurations were evaluated to identify their relative merits:

1) Two-conductor distribution

2) Dual-voltage, 3-conductor distribution

3) Three-phase, 4-conductor distribution

The two-conductor configuration is selected for the distribution network of the baseline 250-kW power system for low overall distribution cost and compatibility with the radial distribution concept of Section 6.2.1 the dual-voltage configuration is awkward, costly, and ill-suited to

polarized electronic loads. The three-phase configuration requires expensive, heavy, and inefficient inversion equipment (see Section 6.4).

The two-conductor distribution configuration (Figure 6-7) is typically employed for direct current transmission in spacecraft and satellites. Control, switching, and protection are normally applied to the positive lead. The negative lead is usually grounded. Two wires are typically used. An alternate approach, typical of aircraft direct current distribution, utilizes the metallic structural elements (aluminum) for the return conductor as a weight reduction technique.

The dual voltage approach (110/220 volts) is often suggested in order to retain the lower voltage level for existing or near-term equipment yet provide a higher voltage for future high-power equipment. The dual voltage approach (Figure 6-8) employes a three-wire two-voltage transmission and distribution bus network similar to conventional house wiring. For direct current applications the buses are polarized: a positive bus of rated voltage (+V), a common, neutral, or return bus (the grounded bus), and a negative bus of rated voltage (-V). Between the two power buses (+V and -V) is the higher voltage, 2V.

The dual voltage approach requires protective switchgear in both the positive and negative equipment feed lines to assure fault clearing and to preclude sneak circuits. Hence, both polarites of semiconductor switchgear must be developed. This potentially doubles the development effort, cost, and losses associated with protective switchgear.

In practice, this dual voltage approach is not appropriate for spacecraft applications. Electronic/semiconductor equipment is polarized. Typically, the positive lead is fault protected, and the negative lead is the power return and referenced to ground. This equipment must be supplied from the +V bus. Only nonpolarized loads (such as resistive heater elements, incandescent lights, relays, solenoids, etc.) can readily utilized the -V bus. Electronic equipment must include an input bridge rectifier circuit (Figure 6-9) or input switching contacts must be included to allow universal operation with either polarity bus. Such input accommodations increase losses, weight, and cost and make EMI grounding and signal referencing more complex.

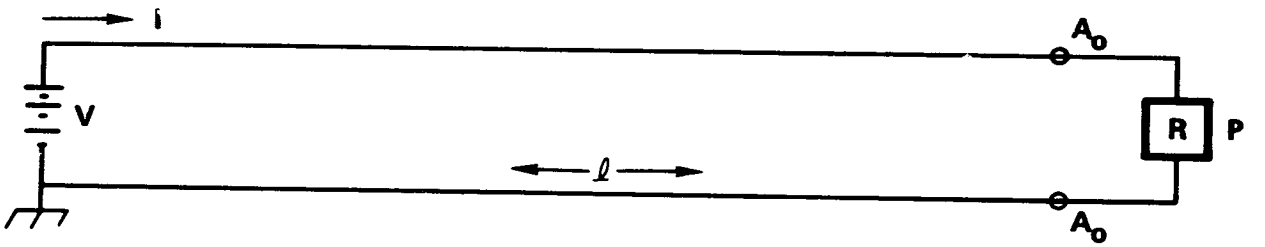

DC: $V = V_p$

$I = P/V = P/V_p$

$A_o = P/V \cdot K_1 = P/V_p \cdot K_1$

COST (2 WIRES) = $2\ell A_o \cdot K_2 = 2\ell PK_3/V_p$; $C_R = 2.0$

COST (1 WIRE)* = $\ell A_o \cdot K_2 = \ell PK_3/V_p$; $C_R = 1.0$

AC: $V = V_p/\sqrt{2}$

$I = P/V = \sqrt{2}P/V_p$

$A_o = P/V \cdot K_1 = \sqrt{2}P/V_p \cdot K_1$

COST (2 WIRES) = $2\ell A_o \cdot K_2 = 2\sqrt{2}\ell PK_3/V_p$; $C_R = 2.8$

COST (1 WIRE)* = $\ell A_o : K_2 = \sqrt{2}\ell PK_3/V_p$; $C_R = 1.4$

I = CURRENT (rms)
P = POWER
V = VOLTAGE (rms)
A_o = OPTIMUM CONDUCTOR AREA
V_p = PEAK VOLTAGE
K = CONSTANTS
ℓ = TRANSMISSION LENGTH

*SINGLE WIRE CASE UTILIZES CONDUCTIVE STRUCTURE FOR RETURN CONDUCTOR

Figure 6-7. Single Voltage Configurations

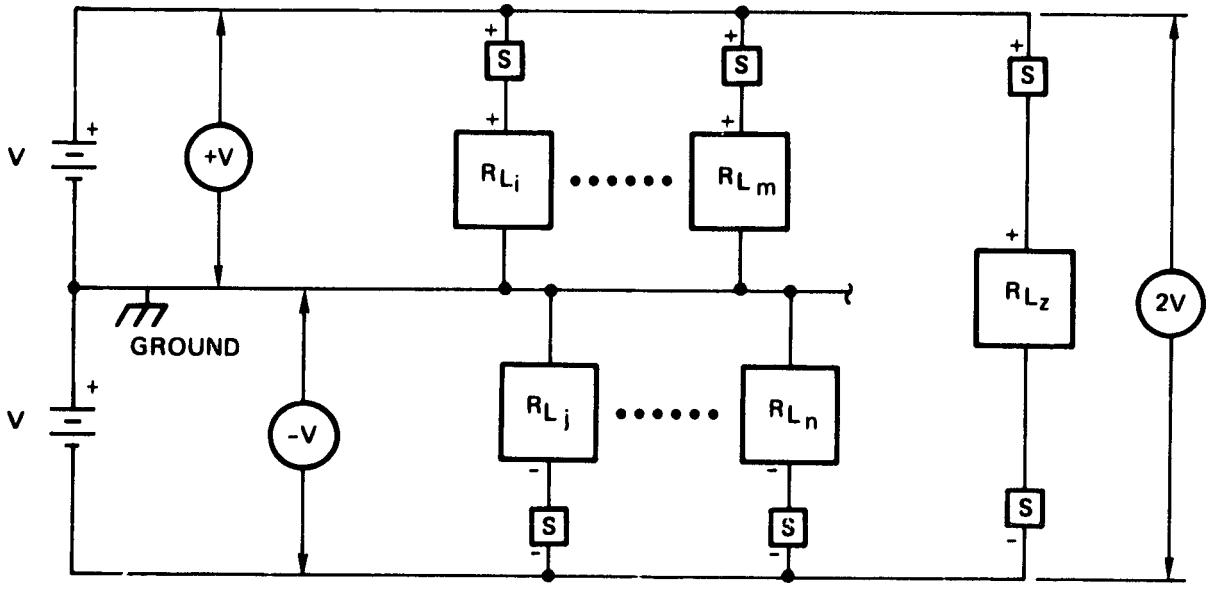

Figure 6-8. Dual Voltage System Requires Dual Polarity Equipment

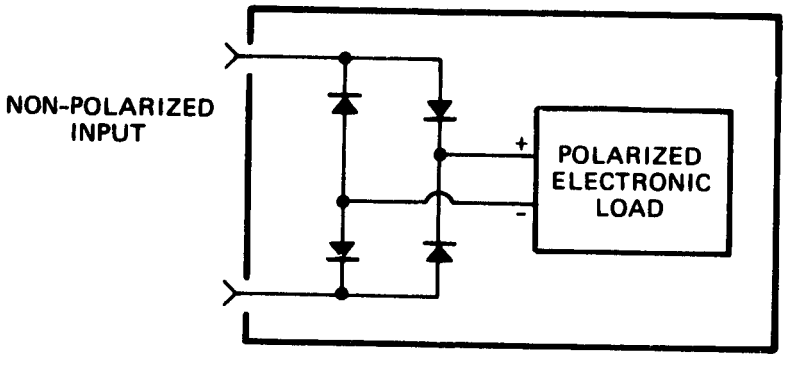

Figure 6-9. Bridge Rectifier Depolarizes Input

New equipment designed for the 2V input has neither power input line at ground reference. The power system neutral must be included for command and signal references and for EMI filtering. This is a 50 percent increase in distribution conductor weight over a two-wire system. Also both input feed lines must be protected - a 100 percent increase in protection equipment over a two-wire system. Hence, the designs for the 2V input of a dual voltage system are more complex, have greater system losses, and require additional wire and switchgear compared to an equivalent design for a two-wire, 2V, grounded-negative power system. Therefore, the dual voltage approach is not appropriate for general satellite and spacecraft applications.

The three-phase, four-wire, Y-connected conductor configuration (Figure 6-10) is typical of local utility distribution for small industries. This conductor configuration (120/208-volt, three-phase, four-wire) seeks to provide single-phase, double-voltage (almost), and three-phase service from a single distribution network. This configuration is also typical of modern 400-cycle alternating-current aircraft power distribution networks. Three power conductors (Phases A, B, and C) and a neutral conductor are employed. The neutral conductor is normally grounded. Hence, an adequately conductive structure may be utilized for the neutral conductor.

One-third of the aggregate power is provided by each of the three phase conductors. They are sized accordingly. The neutral conductor carries no current for balanced loads. Maximum unbalance (only one phase loaded) produces maximum neutral line current equal to that phase conductor current. The neutral conductor is, therefore, the same size as the phase conductors, assuming frequency synchronization and phase relationship of the three conductors (A, B, and C) are maintained. This synchronization and phase relationship is inherently assured with rotating alternators wound for three-phase output. Digital control of three single-phase electronic inverters is required to provide similar inherent assurance of frequency synchronization and phase relationship. Loss of either increases the current in the neutral conductor. In the worst case, the current in the neutral conductor is three times the current of any phase conductor.

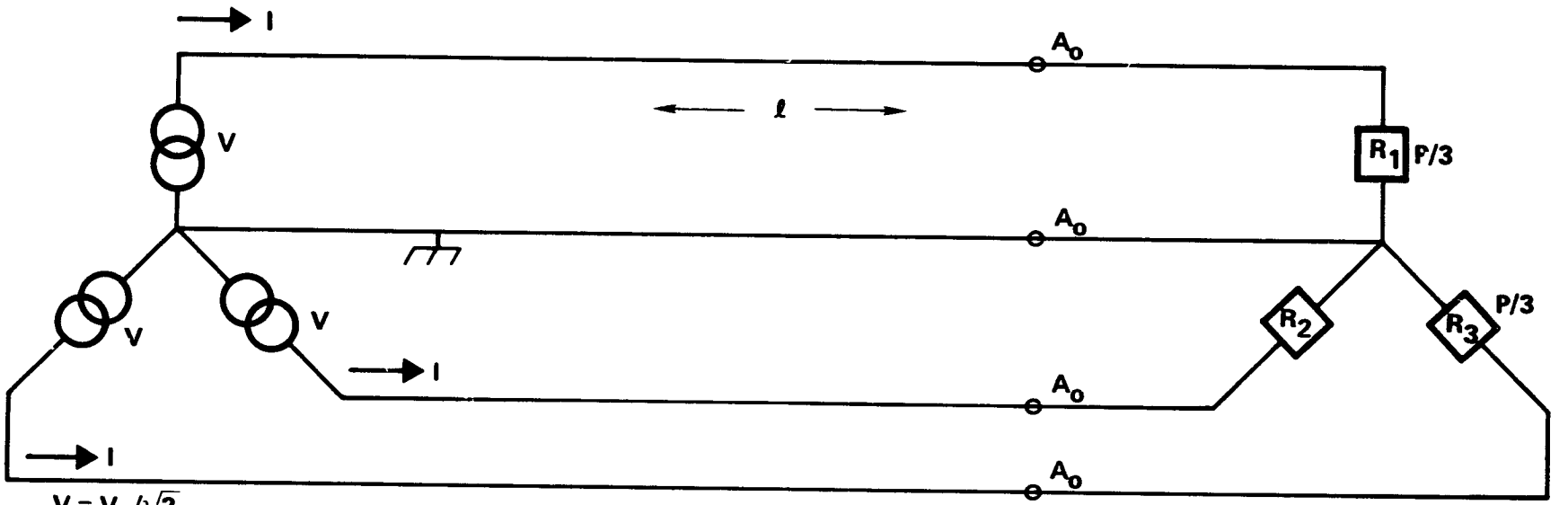

$V = V_p/\sqrt{2}$

$I = P/3V = \sqrt{2}\,P/3V_p$

$A_o^2 = P/3V \cdot K_1 = \sqrt{2}\,P/3V_p \cdot K_1$

COST (4 WIRE) = $4\ell A_o \cdot K_2 = 4\sqrt{2}\,\ell PK_3/3V_p$; $C_R = 1.9$

COST (3 WIRE) = $3\ell A_o \cdot K_2 = \sqrt{2}\,\ell PK_3/V_p$; $C_R = 1.4$

WHERE C_R = 1.0 FOR SINGLE WIRE DIRECT CURRENT

*STRUCTURE NEUTRAL

I = CURRENT (rms)
P = POWER
V = VOLTAGE (rms)
A_o = OPTIMUM CONDUCTOR AREA
Vp = PEAK VOLTAGE
K = PEAK VOLTAGE
ℓ = TRANSMISSION LENGTH

Figure 6-10. Three-Phase Wye Configuration

Three-phase transmission conductors with balanced loading have essentially no electromagnetic signature. The instantaneous product of current and voltage is a constant - a constant power flow similar to direct-current conductors. However, load imbalance among the three phases produces a net current flow in the return conductor, a pulsating power flow, and a significant electromagnetic signature. Balanced loads are not considered realistic for a 250-kW power system. Hence, a significant electromagnetic signature is expected with three-phase distribution.

6.3 CONDUCTORS

The cost for electrical power transmission is composed of the conductor cost plus the incremental cost of power generation and energy storage to supply the transmission losses and thermal control to dissipate these losses. In addition, the power conversion equipment must be increased to handle the increase in converted power due to these losses. As conductor size is increased, transmission losses decrease, transmission regulation improves, and an optimization exists. Surprisingly, the optimum conductor cross-sectional area is not dependent upon the distance of transmission nor upon regulation. Optimum conductor area is normally considerably larger than the conductors would be if sized for voltage regulation requirements, conductor current capacity, or minimum wire weight.

6.3.1 Conductor Sizing

The cross-sectional area of conductors for typical aerospace applications is selected to minimize the weight of the conductors consistent with voltage regulation requirements, conductor current ratings (capacity), and installation constraints (minimum practical wire gage for handling without breakage). For this study, cost is the minimized parameter, and conductor weight is translated to cost by the Shuttle transportation charge (462 $/lb). Hence, an optimum conductor size is developed that minimizes the cost impact to the entire electrical power system.

The cost for electrical power transmission is the sum of five relatable terms:

$$C_{trans} = C_{wire} + C_{power\Delta} + C_{energy\Delta} + C_{thermal\Delta} + C_{conversion\Delta}$$

where C_{wire} = the cost of electrical power conductors,

C_{power_Δ} = the cost of the incremental increase in power generation (solar array) to supply the transmission losses,

C_{energy_Δ} = the cost of the incremental increase in energy storage capacity (battery) to supply the transmission energy losses during eclipse

$C_{thermal_\Delta}$ - the cost of the incremental increase in thermal control equipment (radiators, plumbing, pumps) to dissipate the electrical transmission losses and the associated increase in energy storage thermal losses and conversion equipment losses.

$C_{conversion_\Delta}$ = the cost of the incremental increase in power conversion/regulation equipment due to the increased load attributable to transmission losses.

Each of these terms is complex but is related to the parameters of the transmission conductor under consideration (Figure 6-11) and is derived in Appendix D:

$$C_{trans} = C_W \sigma A \ell \qquad \text{[Wire]}$$

$$+ C_{ps}\left(\frac{P}{V\epsilon_2}\right)^2 \frac{\rho\ell}{A}\frac{1}{\epsilon_1 d}\left(1 + \frac{T_1}{T_2}\frac{1}{\epsilon_C\epsilon_B\epsilon_D}\right) \qquad \text{[Power]}$$

$$+ C_E\left(\frac{P}{V\epsilon_2}\right)^2 \frac{\rho\ell}{A}\frac{T_1}{60}\frac{1}{\epsilon_D\epsilon_B D}\left(1 + \frac{Ls}{L_i}\right) \qquad \text{[Energy]}$$

$$+ \left(\frac{P}{V\epsilon_2}\right)^2 \frac{\rho\ell}{A}\left[C_{TSW} + C_{TSB}\frac{1-\epsilon_B}{\epsilon_B\epsilon_D} + ZC_{TSE}\right] \qquad \text{[Thermal]}$$

$$+ \left(\frac{P}{V\epsilon_2}\right)^2 \frac{\rho\ell}{A}\left[C_{CSD} + \frac{T_1 C_{CSC}}{T_2\epsilon_B\epsilon_D} + C_{CS1} + \frac{T_1 C_{CS1}}{T_2\epsilon_C\epsilon_B\epsilon_D}\right] \qquad \text{[Conversion]}$$

where

$$Z = \left(\frac{1-\epsilon_C}{\epsilon_C}\right)\left(\frac{T_1}{T_2}\cdot\frac{1}{\epsilon_B\epsilon_D}\right) + \left(\frac{1-\epsilon_1}{\epsilon_1}\right)\left(1 + \frac{T_1}{T_2}\cdot\frac{1}{\epsilon_C\epsilon_B\epsilon_D}\right)$$

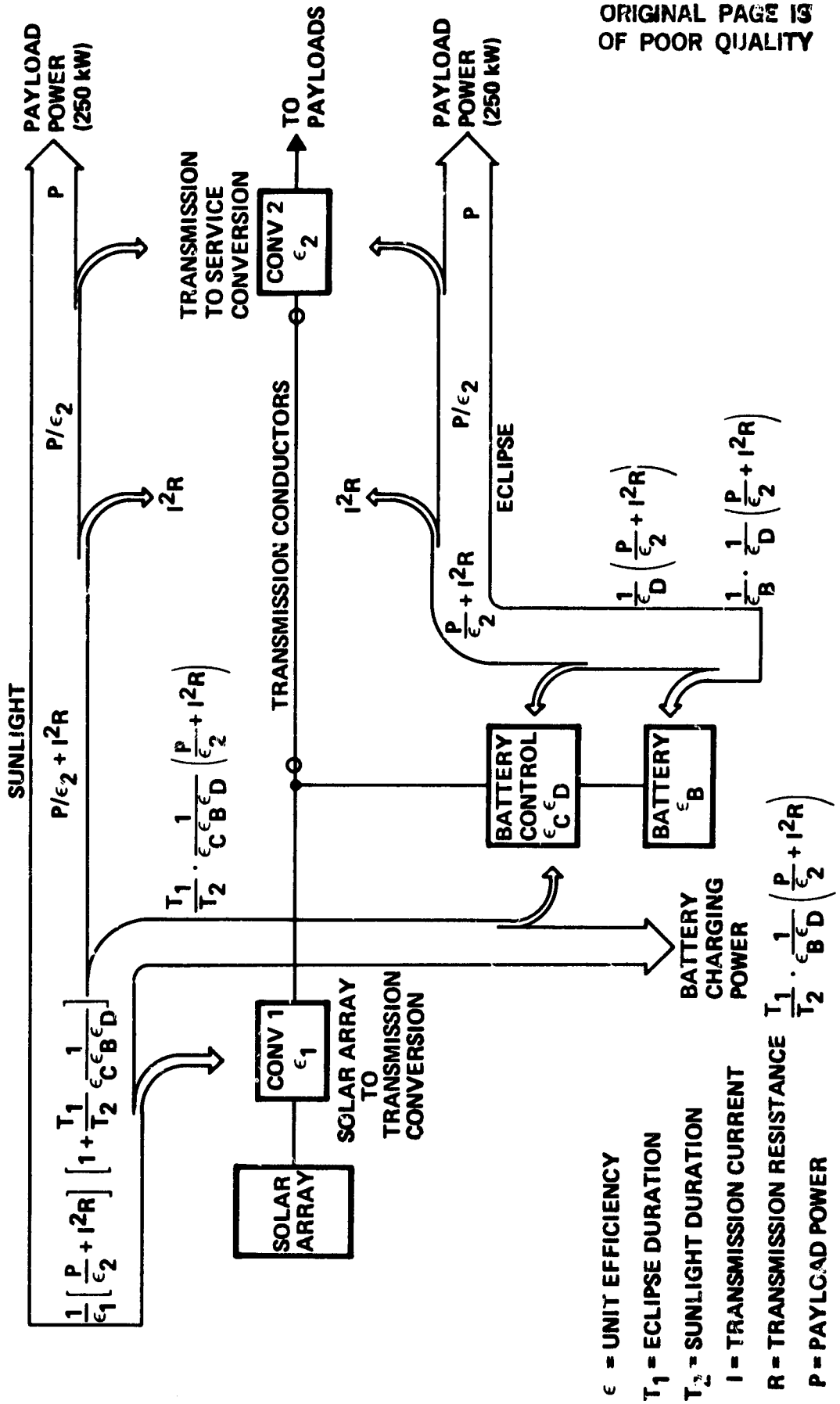

Figure 6-11. Power Flow in Transmission Subsystem

and C_W, C_P, and C_E are the specific costs for wire, solar array power, and battery energy, respectively. C_{TSI}, C_{TSB}, and C_{TSE} and C_{CSB}, C_{CSC}, and C_{CS1} are specific costs for thermal control and power conversion, respectively. [See Appendix D for definition of these terms.]

Simplifying the algebra:

$$C_{trans} = C_W \sigma A \ell + \left(\frac{P}{V\epsilon_2}\right)^2 \frac{\rho \ell}{A}[\text{factor}].$$

Note that "factor" is not a function of ℓ, P, A, ρ, σ, or V. Differentiating with respect to A, setting the result equal to zero, and solving for A yields the optimum-cost cross-sectional area (A_o) for transmission conductors:

$$\frac{d(C_{trans})}{dA} = C_W \sigma \ell - \left(\frac{P}{V\epsilon_2}\right)^2 \frac{\rho \ell}{A^2}[\text{factor}] = 0$$

$$A_o = \frac{P}{V\epsilon_2}\sqrt{\frac{\rho[\text{factor}]}{\sigma C_W}}$$

The optimum-cost cross-sectional area (A_o) is independent of the transmission line distance because ℓ appears in each term to the first power. Further, A_o is directly related to the transmitted payload power (P) and inversely related to the transmission voltage (V) and transmission-to-service conversion efficiency (ϵ_2 of Figure 6-11). As power levels and distances increase, higher voltages become imperative.

6.3.2 Transmission Cost

Power transmission cost is the sum of the conductor cost and the incremental support costs of solar array, battery, thermal control, and power conversion for the transmission losses:

$$C_{trans} = C_{wire} + C_{support\Delta}$$

$$= C_W \sigma A \ell + \left(\frac{P}{V\epsilon_2}\right)^2 \frac{\rho \ell}{A}[\text{factor}]$$

Cost optimization of the transmission conductor cross-sectional area occurs where conductor costs equal the support costs:

$$C_{wire} = C_{support\Delta}$$

$$C_W \sigma \ell A_o = \left(\frac{P}{V\epsilon_2}\right)^2 \cdot \frac{\rho \ell}{A_o} \cdot [\text{factor}]$$

and total transmission cost is twice the conductor cost:

$$C_{trans} = 2 \; C_W \sigma \ell A_o$$

$$= 2 \; C_W \sigma \ell \cdot \frac{P}{V\epsilon_2} \sqrt{\frac{\rho [\text{factor}]}{\sigma C_W}}$$

$$= 2 \; \frac{P\ell}{V\epsilon_2} \sqrt{\rho\sigma(C_W) \cdot [\text{factor}]}$$

The resistivity (ρ), density (σ), and specific cost (C_W), parameters of the conductor material affect the transmission costs. This suggests material evaluation and selection to minimize transmission costs (Section 6.3.3).

Transmission costs are directly porportional to power (P) and distance (ℓ) but inversely proportional to the transmission voltage (V). As power levels and transmission distances increase, transmission costs increase directly unless a higher transmission voltage is employed. However, for a given power level and distance, diminishing returns occur for continually increasing voltages (Figure 6-12).

6.3.3 Conductor Material

The transmission cost for electrical power is directly related to the factor $\sqrt{\rho\sigma(C_W)}$, where:

ρ = resistivity of conductor material, ohm-ft

σ = density of conductor material, lb/cu ft

C_W = conductor specific cost, $/lb

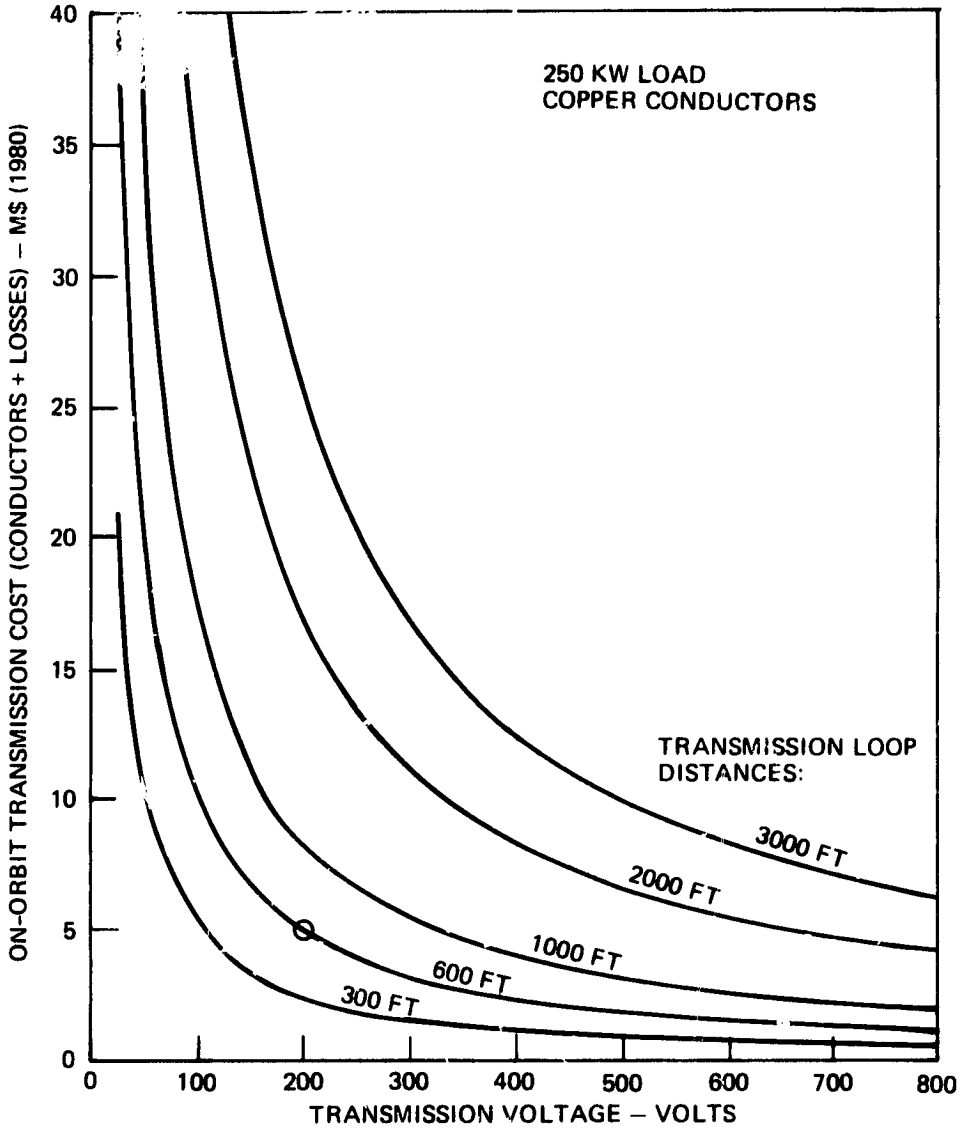

Figure 6-12. Expected Transmission Cost = 5 M$

These are parameters of the selected conductor material. Therefore, an evaluation and selection exists for conductor materials, such that the factor, $\sqrt{\rho\sigma(C_W)}$, is minimized (Table 6-2).

Copper is selected as the baseline conducor material. Pure aluminum conductors have a potential to reduce transmission costs by 15 percent. However, this reduction is not realizable due to the electrical termination considerations for pure aluminum and the short distance (30 feet) between load centers, distribution branching, and the consequent terminations.

Table 6-2. Baseline Transmission Conductors are Copper

Conductor Material	Resistivity ρ μ ohm ft	Density σ lb/ft^3	Mfg Cost C_{MW} \$/lb	Relative Cost $\sqrt{\rho\sigma(C_W)}$
Aluminum, pure	0.087	168	446	0.115
Aluminum, alloy	0.130	174	431	0.142
Copper	0.056	555	135	0.136
Magnesium	0.146	108	695	0.135
Silver	0.0522	651	165	0.146
Sodium	0.138	60.2	1250	0.119
Solder	0.492	551	136	0.402

$C_W = C_{MW} + C_L$, where:

C_L = 462 \$/lb, Shuttle transportation charge (Appendix B)

$$C_{MW} = \frac{\text{bus bar cost + installation costs}}{\text{bus bar weight}}$$

$$= \frac{\$60{,}000 + \$18{,}000}{(10 \text{ bars})(1/4" \times 1" \times 60' \text{ bar})(555 \text{ ft/ft}^3)(1/144 \text{ in}^2/\text{ft}^2)}$$

= 135 \$/lb for copper

For other materials, costs are expected to be relatively constant for the same size bus bar conductor. Therefore, C_{MW} for other materials are directly proportional to the inverse ratio of the material densities.

Sodium also projects a modest cost reduction over copper. However, sodium may have significantly increased manufacturing and installation costs over those stated in Table 6-2 in order to sheath the sodium from terrestrial humidity. Hence, sodium is considered inappropriate.

Aluminum alloy is slightly more costly than copper. However, if the aluminum alloy cross section is generous and the cost virtually free, it becomes attractive. Therefore, utilizing aluminum alloy structure for the power return conductor may save at least 25 percent and up to 50 percent of the transmission cost. Structure return reduces the cost of conductors by 50 percent as ℓ is reduced to zero for the power return conductor. The power, energy, thermal, and conversion cost terms (50 percent of the baseline total) are also reduced to the extent the structure cross section is significantly larger than the optimum conductor cross section (A_o) for aluminum alloy. The cost reduction target is 50 percent of these costs, but only 80 to 90 percent of this target is expected to be realized with normal aluminum structural design. Hence, a 40-45 percent transmission cost savings is realizable utilizing structure for the power return. Examination and demonstration of structure returns for large power transmission is warranted.

6.4 DISTRIBUTION REGULATION

The design of small satellites and their electrical power systems typically address wire sizing from a specification of a voltage regulation parameter. Conductors are sized for minimum weight consistent with this regulation requirement and manufacturing considerations for minimum size wire. Cost optimization is not performed, and the incremental costs for power, energy, thermal, and conversion equipment are not considered. This results in a small (but not readily visible) penalty of additional power, energy, thermal, and conversion equipment capacity to supply increased distribution losses.

The results of the cost optimization herein, show optimum conductor sizing (A_o) to be a function of power, voltage level, conductor material ($\sqrt{\rho\sigma}$), and the relationship of the various specific costs and equipment efficiencies. This approach to conductor size optimization normally results in a significantly large conductor cross-sectional area than the minimum wire size derived from typical regulation requirements. Hence, regulation requirements will be satisfied for reasonable transmission

lengths (Figure 6-13), and the installed capacity for power, energy, thermal, and conversion equipment optimized. This optimization of equipment and conductors becomes more pertinent as larger power levels are transmitted.

Regulation at a load interface is a function of the transmission regulation due to conductor losses plus the power source regulation. The voltage drop (ΔV) due to power transmission over conductors of an optimum cost cross section (A_o) is independent of the design power level and the transmission voltage:

$$\Delta V = I \cdot R = \frac{P}{V\epsilon_2} \cdot \frac{\rho \ell}{A_o} = \ell \sqrt{\frac{\rho \sigma C_W}{[factor]}}$$

The voltage loss (ΔV) is a function of conductor length, conductor material ($\sqrt{\rho \sigma C_W}$), and the source specific costs included in "factor." Transmission regulation ($\Delta V/V$) is consequently improved with higher transmission voltages. However, technology improvements which reduce the spacific costs of power generation and energy storage (solar array and battery) decrease the optimum-cost conductor area (A_o) and transmission costs (C_{trans}) but increase the transmission voltage drop (Figure 6-13) and impair regulations. However, the transmission regulation attained with optimum-cost conductors is more than adequate with present (1990) technology and foreseeable (1986-1990) technology improvements with the 600-foot transmission loop distances of interest for a space platform or space station (Figure 6-13).

Voltage variations at payloads (Table 6-3) are primarily due to energy storage regulation characteristics (with the direct energy transfer distribution configuration of Figure 6-14. A ± 9 percent regulation contribution is calculated for nickel-hydrogen batteries operating at 33 percent depth of discharge. The discharge plateau voltage is projected at 1.25 volts per cell; end-of-charge voltage is 1.50 volts per cell This produces a ± 0.125-volt variation from a midpoint voltage of 1.375 volts and ± 9 percent regulation. The additional transmission line voltage loss of 3 volts over 600 feet (Figure 6-13) produces a modest increase in the voltage variation at payload interfaces (Table 6-3).

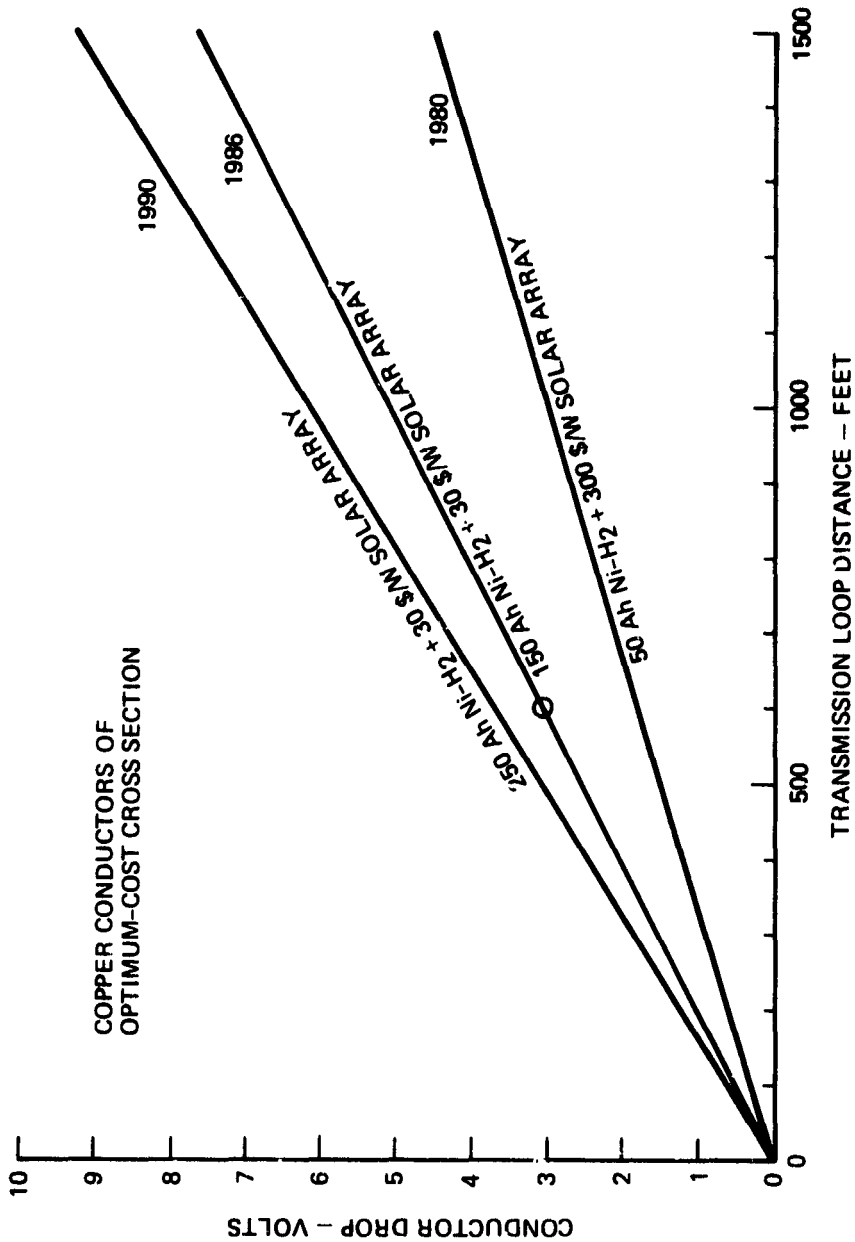

Figure 6-13. Cost Optimized Conductors Provide Good Regulation

GR.

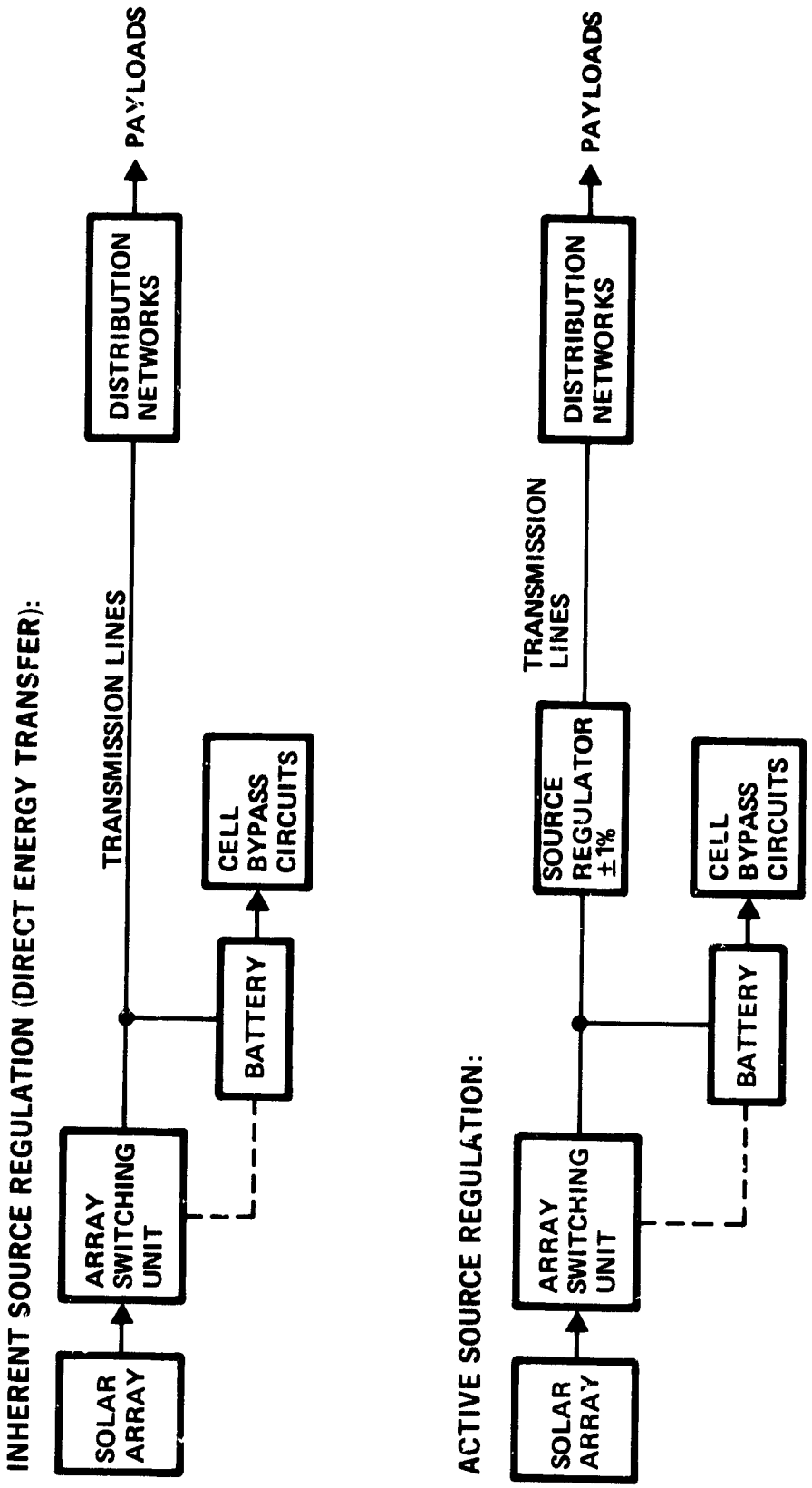

Figure 6-14. Source Regulation Concepts

Table 6-3. Distribution Regulation is Expensive

	Nominal Voltage		
	110 Volts	220 Volts	270 Volts
Direct Energy Transfer:			
Cells per Battery	80 cells	160 cells	200 cells
Source Voltage	110-120 volts	200-240 volts	250-300 volts
Source Regulation	20 volts	40 volts	50 volts
Line Regulation	3 volts	3 volts	3 volts
Total Regulation	23 volts	43 volts	53 volts
Regulation at Payload	±10.5%	±9.8%	±9.6%
Payload Voltage Range	97-120 volts	197-240 volts	247-300 volts
Regulated Source:			
Regulated Source	125-128 volts	250-255 volts	310-316 volts
Source Regulation (±1%)	3 volts	5 volts	6 volts
Line Regulation	3 volts	3 volts	3 volts
Total Regulation	6 volts	8 volts	9 volts
Regulation at Payload	±2.4%	±1.6%	±1.4%
Payload Voltage Range	122-128 volts	247-255 volts	307-316 volts
Regulator Costs (includes losses)	8 - 25 M$	6 - 17 M$	6 - 17 M$

Active regulation of the energy storage output voltage is required to reduce the voltage variation at the payloads. A 1 percent regulation of the energy storage output voltage is typically realizable with a boost regulator* (Figure 6-14). Regulation at the payload is thereby improved substantially (Table 6-4). Potentially, preregulation could be avoided in the payloads. However, practical considerations, such as on/off control, overload protection, and fault isolation within payloads, suggest that

*The boost regulator is chosen over a back regulator to provide essentially unlimited power transfer for overloads and fault clearing and to avoid adverse single point failure modes. In addition, boost regulation provides a somewhat higher tranmission voltage (more cost effective) and a better watt/hour utilization: low boost during 54 minutes of sunlight, high boost during 36 minutes of eclipse.

precluding payload regulation is impractical. Furthermore, the aggregate cost of source regulation at 230 volts is 6 M$ initially, rising to 17 M$ at 30 years (Figure 6-15). This amount must be saved in payload regulator hardware to break even - possible, but highly uncertain, and a poor return on the investment. In addition, a significant fraction of the 250-kW power level may be usable without regulation, for example in heaters, furnaces, and motors (pumps). Hence, direct energy transmission at the source voltage, with regulation at each payload as needed, is the economical and selected approach.

6.5 DISTRIBUTION VOLTAGE

Three distribution voltage approaches are considered in Figure 6-16:

1) Direct energy transfer

2) Central conversion to 600 volts

3) Source conversion to 600 volts

Comparison of the distribution parameters (Table 6-4) shows the direct energy transfer approach to be the most cost effective, particularly at voltages of 200 volts (or higher). The direct energy transmission cost is only 5 M$ at 200 volts for the 300-foot satellite distance. Longer distances (1000 feet or more) are required to make conversion to higher transmission voltages cost effective.

The 600-volt transmission options incorporating dc-to-dc conversion do not provide a clear economic payback nor technical advantage. Conductor weight and costs are reduced, but the converter equipment, and the incremental support from solar array, battery, and thermal overwhelm the conductor cost saving (Figures 6-17 and 6-18). Regulation is improved sufficiently that pre-regulators may be omitted in the power conversion equipment at the loads. However practical considerations, such as on/off control, overload protection, and fault isolation, suggest the essence of preregulation circuitry occurs within each load converter regardless of input voltage regulation. Little cost reduction is therefore projected as payback for regulation improvements, and a 30-year cost reduction of 10 M$ to 15 M$ is required to break even.

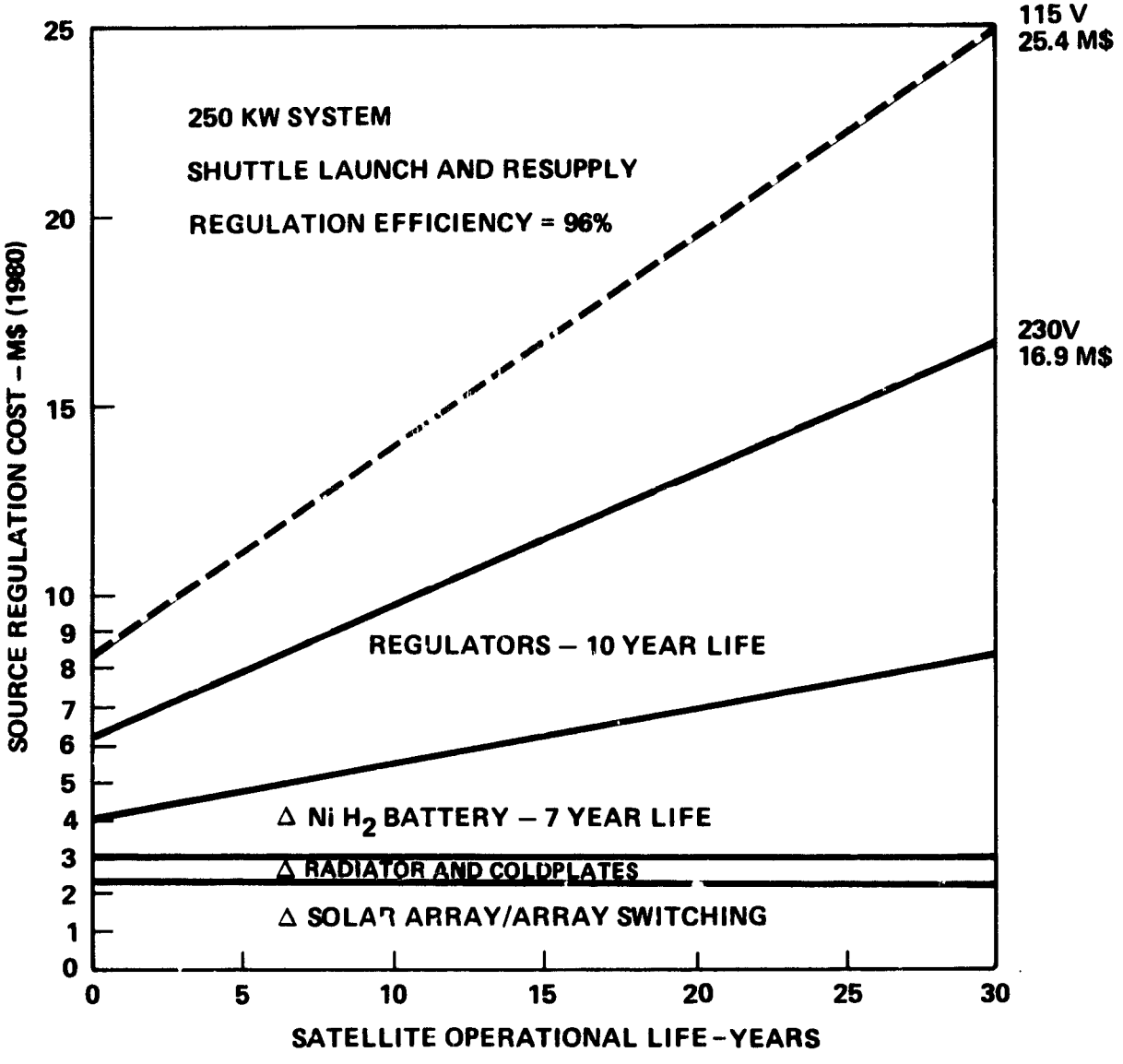

Figure 6-15. Source Regulation Costs

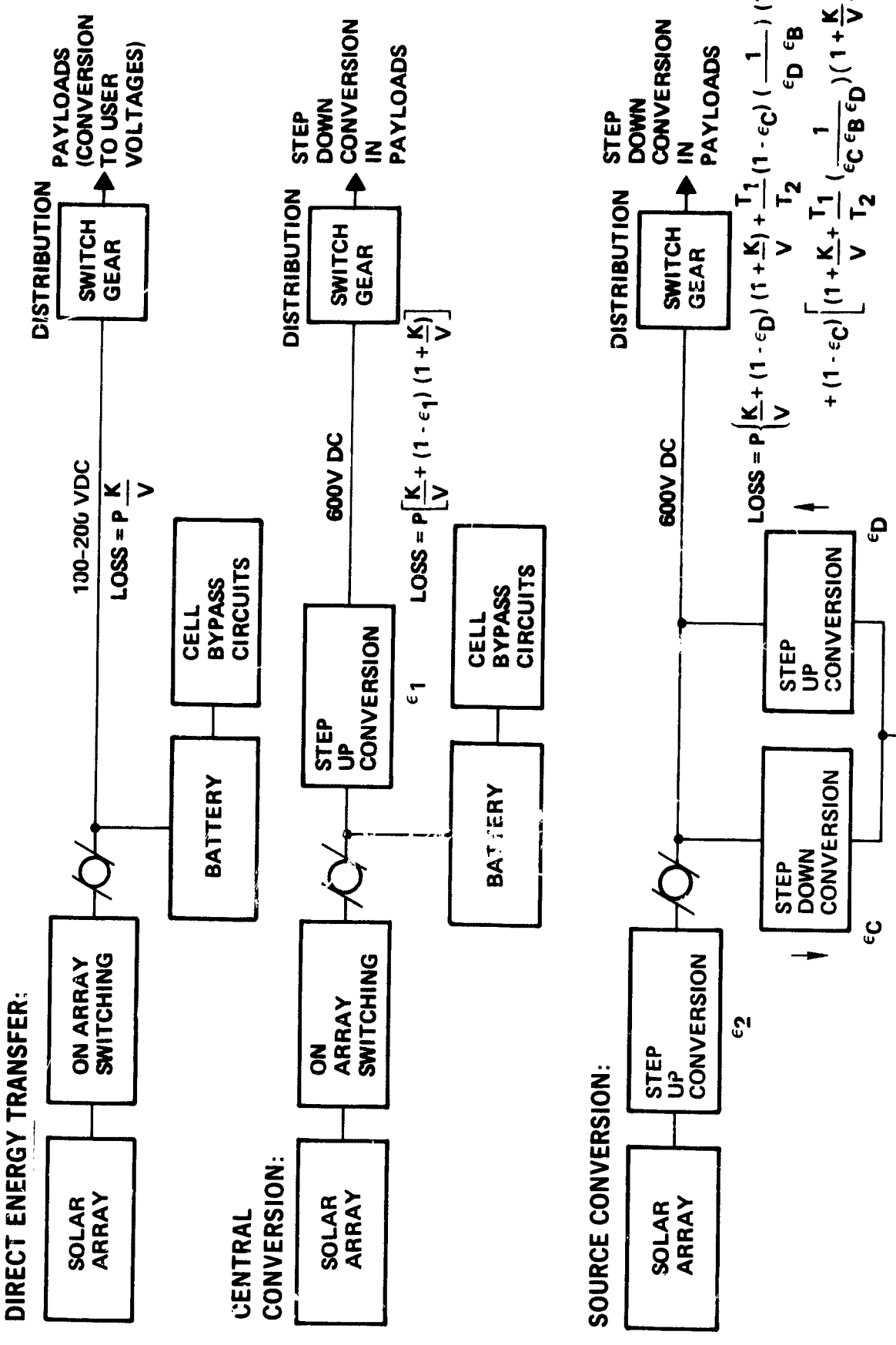

Figure 6-16. Transmission Concepts

Table 6-4. Source Voltage Transmission Is Cost Effective

Parameter	Direct Energy Transfer		Central Conversion	Source Conversion
Source Voltage	100 V	200 V	200 V	200 V
Transmission Voltage	100 V	200 V	600 V	600 V
Peak Power	Battery Limited		Converter Limited	Converter Limited
Reliability	Source		Source + Convertion	Source +3 Conversions
Switchgear	Medium Voltage		High Voltage	High Voltage
Losses	I^2R = L	L/2	L/6 + Converter loss	L/6 + 3 Conversion losses
Conductor: Area	3.6	1.8 sq in	0.6 sq in	0.6 sq in
Weight	8370	4160 pounds	1400 pounds	1400 pounds
On-orbit cost (with losses)	10 M$	5 M$	2 M$	2 M$
Conversion Costs:				
Initial	-	-	5 M$	8 M$
Life Cycle (with losses)	-	-	12 M$	17 M$
Total Transmission Cost	10 M$	5 M$	14 M$	19 M$
Regulation at Payloads	±11.6%	±10.3%	±1.4%	±1.4%
Payload Conversion	Includes pre-regulators		No preregulators required	No preregulators required

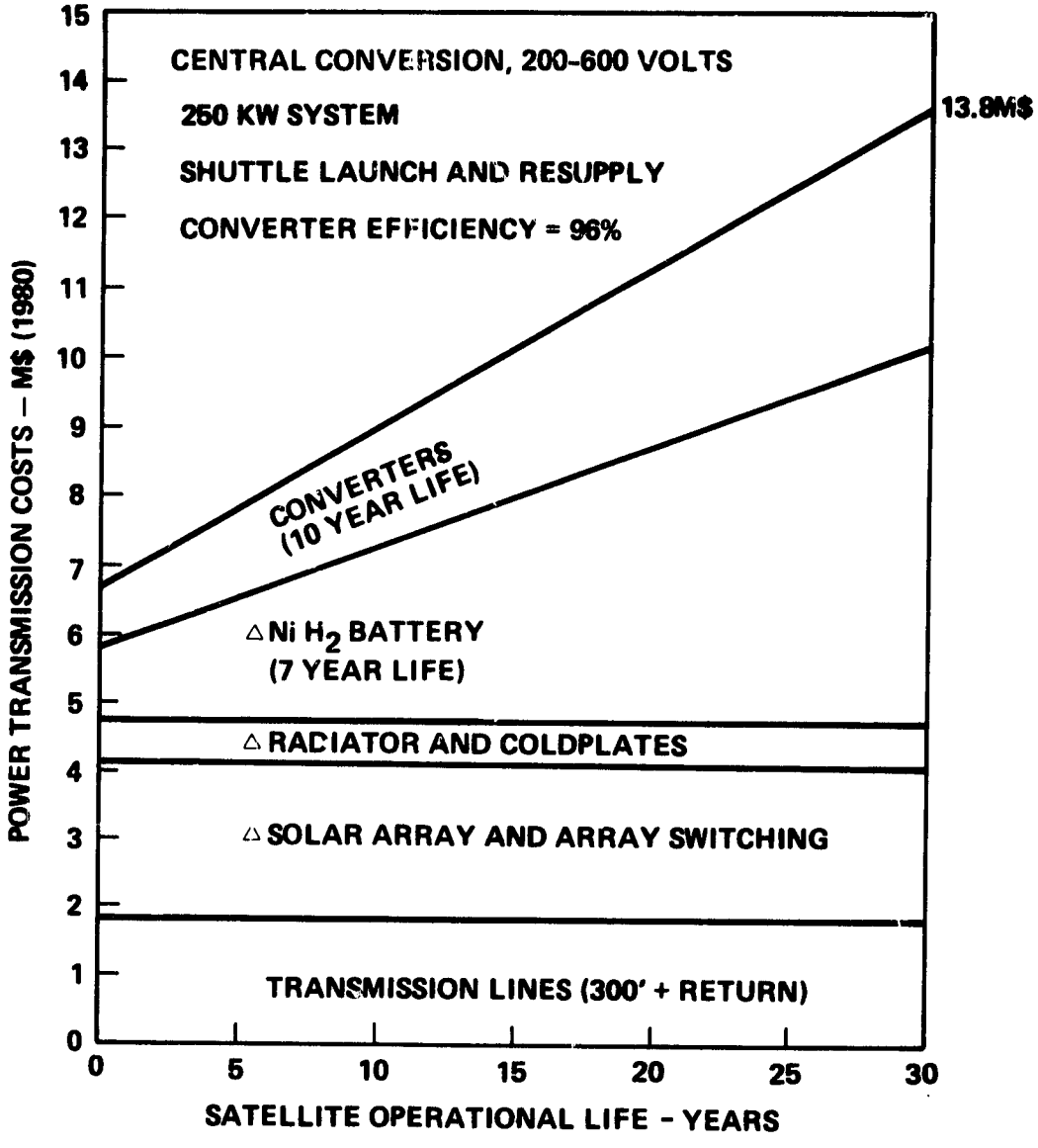

Figure 6-17. Conversion Costs Exceed Conductor Savings

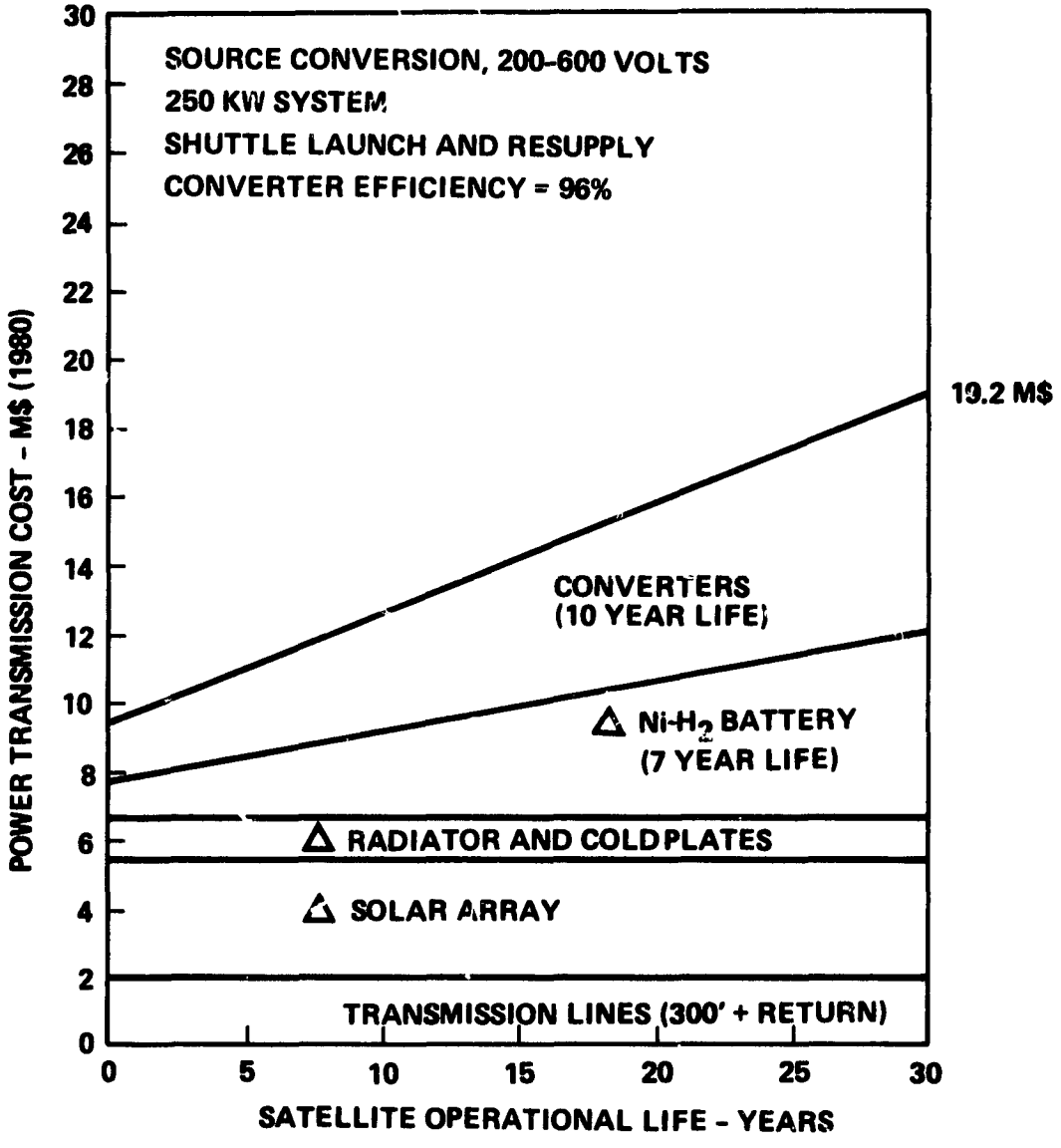

Figure 6-18. Conversion Costs Exceed Conductor Savings

Alternating current distribution at the common power frequencies of 60 and 400 cps and at the projected power frequencies of 1200, 1600, and 2400 cps, by inference to dc-to-dc conversion at 10 to 40 kilohertz, is also unattractive. Alternating current conversion equipment is heavier, typically less efficient with sinusoidal wave form, and requires greater attention to electromagnetic compatibility than the direct current counterpart. Hence, transmission and distribution with alternating current at power frequencies is costlier than the rejected source on central power conversion direct current conversion approaches. Alternating current transmission and distribution at typical power frequencies is, therefore, also rejected in favor of the baseline direct current transmission at the source generation voltage.

The alternating-current transmission approach at 20 to 30 kilohertz, produced by distributed resonant convertors with square wave voltage form and sinusoidal current flow and proposed for large space power systems (Reference 6-1) is inappropriate for the 250-kilowatt power system. The 20-kilohertz alternating-current approach is undeveloped, and a number of issues need resolution:

a) Synchronization method for parallel operation

b) Operation with widely variable load power

c) Development, manufacturing, and installation costs for tubular coaxial conductors and their connectors

d) Electromagnetic compatibility and power system signature.

In addition, any conversion to alternating current of primary power throttles the possible power flow and makes overload detection on the transmission lines more complex (compared to direct energy transfer). Therefore, conversion to higher voltages (ac or dc) is rejected in favor of direct energy transfer utilizing the highest practical source voltage.

6.6 SWITCHGEAR

The channelized distribution concept for the 250-kilowatt electrical power system requires two distinct types of switchgear. A source control switch is required at each battery in order to disconnect this source for distribution channel servicing, to allow battery reconditioning discharging, and to replace the battery. Distribution switches are required

for load (and load bus) management and to provide on/off control, power channel selection, and faulted load isolation. Switches for parallel operation of batteries or main buses are avoided with the selected distribution concept.

The battery disconnect switch requires high current-carrying capacity in both directions (charge and discharge currents). However, this switch is opened only upon controlled conditions of negligible or zero current flow. Hence, the hybrid switch approach with electromagnetic relay contacts and semiconductor arc supression is an appropriate device. The contacts provide the high current-carrying capacity. The semiconductor circuitry provides arc suppression for low currents (neither for rated nor fault currents). Fault protection of the battery output is provided by a fuse rated at three to five times nominal channel load in order to deliver the large peak power capability available from the batttery.

Westinghouse Electric Corporation has developed a hybrid power controller rated at 80 amperes, direct current, for 200 to 400 volt applications under contract to NASA/LeRC (Reference 6-1). This Westinghouse controller incorporates overload detection and trip and provides arc suppression for a 100-ampere current. Modification of this controller design to provide much larger contacts, to reduce the arc suppression to a more modest value (20 to 50 amperes), and to revise the overload detection circuits to preclude switch opening with currents above 50 percent of the arc suppression design value, provides the battery disconnect switch.

Fault protection of the battery output can be provided by a fuse (approximately 300-ampere rating) or be incorporated in the disconnect switch. Fault protection (fault current interruption) for the battery source must allow considerable sustained overload, perhaps 3 to 5 times the rated system capacity, to provide sustained peak power delivery from the battery. Fault protection at the battery is for a massive short of the main bus to the structure (electrical ground). Fault currents approximating 100 times the full load rating may flow from a nickel-hydrogen battery. Interruption of such currents (8000 amperes) is difficult, but a vacuum switch might provide this capability for a limited number of occurrences. Many such fault current interruptions are not indicated for any one switch. Such occurrences are an unusual event, and presumably entail extensive

mechanical repair to correct such a fault. Replacement of the switch concurrent with such repair is a reasonable scenario. A battery disconnect switch life of 5 to 10 fault current interrupt cycles and 5000 to 10,000 mechanical cycles is adequate and attainable. However, development is required.

Distribution switches are required within each load center to connect the respective loads (or load buses) to the selected power channel bus of the two (or more) options available. These switches require overload and fault protection to disconnect a faulted load and thereby maintain the main channel bus in operation for other loads. Switch power ratings of 5 or 10 kilowatts are adequate for most projected payloads. Larger switches are unnecessary until the channel capacity of 17 kilowatts (attainable with a 150 Ah, 220-volt battery) is significantly increased.

Westinghouse Electric Corporation has developed, under contract to NASA/LeRC (Reference 6-1), a semiconductor power controller rated at 50 amperes, direct current, for 200- to 400-volt applications. This Westinghouse controller incorporates both overload detection and current interruption capabilities that provide operation equivalent to a circuit breaker. At 200 volts and 50 amperes, this circuit breaker device controls 10 kilowatts which is adequate for the projected individual payloads on the 250 kilowatt distribution network. A family of controllers with lower current capacity is not necessary. However, reduced overload settings are desirable to avoid excessive oversizing of local distribution conductors. Incorporation within the power controller design of programmable over-current references in specific discrete steps coordinated with conductor current ratings is needed. Eight steps, commandable by a 3-bit word, provides a suitable overload range (Table 6-5). Commandable overload settings allow the capacity of each payload port to be revised as the payload complement on the satellite is changed. Alternatively, the overload setting may be wired into the controller to avoid commands for overload settings and may be appropriate for housekeeping equipment and associated distribution buses.

Semiconductor remote power controllers (RPC) for direct current application at 200 to 300 volts are estimated to cost approximately $3,400 each (Figure 6-19). This is based upon 1980 pricing for 28-volt remote

Table 6-5. Hypothetical Power Controller Overload Settings

Conductor Wire Size (AWG)	Current Rating* (amperes)	Load Power (watts)	Command (bits)
22	5	1000	0 0 0
20	7.5	1500	0 0 1
18	10	2000	0 1 0
16	13	2600	0 1 1
14	17	3400	1 0 0
12	23	4600	1 0 1
10	33	6600	1 1 0
8	46	9200	1 1 1

*Wires in bundles per MIL-W-5088

power controllers plus an allowance for the addition of D60T transistors and redundancy to bring 28-volt pricing in line with high-voltage component costs.

The distribution network for the 250-kilowatt electrical power system includes 10 load centers with four payload ports per load center. Four load buses are provided in each payload port and 10 controlled local loads (or load buses) are assumed in each load center area. Two remote power controllers are provided (as a minimum) for each load or load bus for main power channel selection and connection. A total of 520 distribution switches are required at $3400 each. Adding the cost of the 17 battery disconnect switches at 12 K$ each brings the distribution switch gear cost to approxiamtely 2 M$.

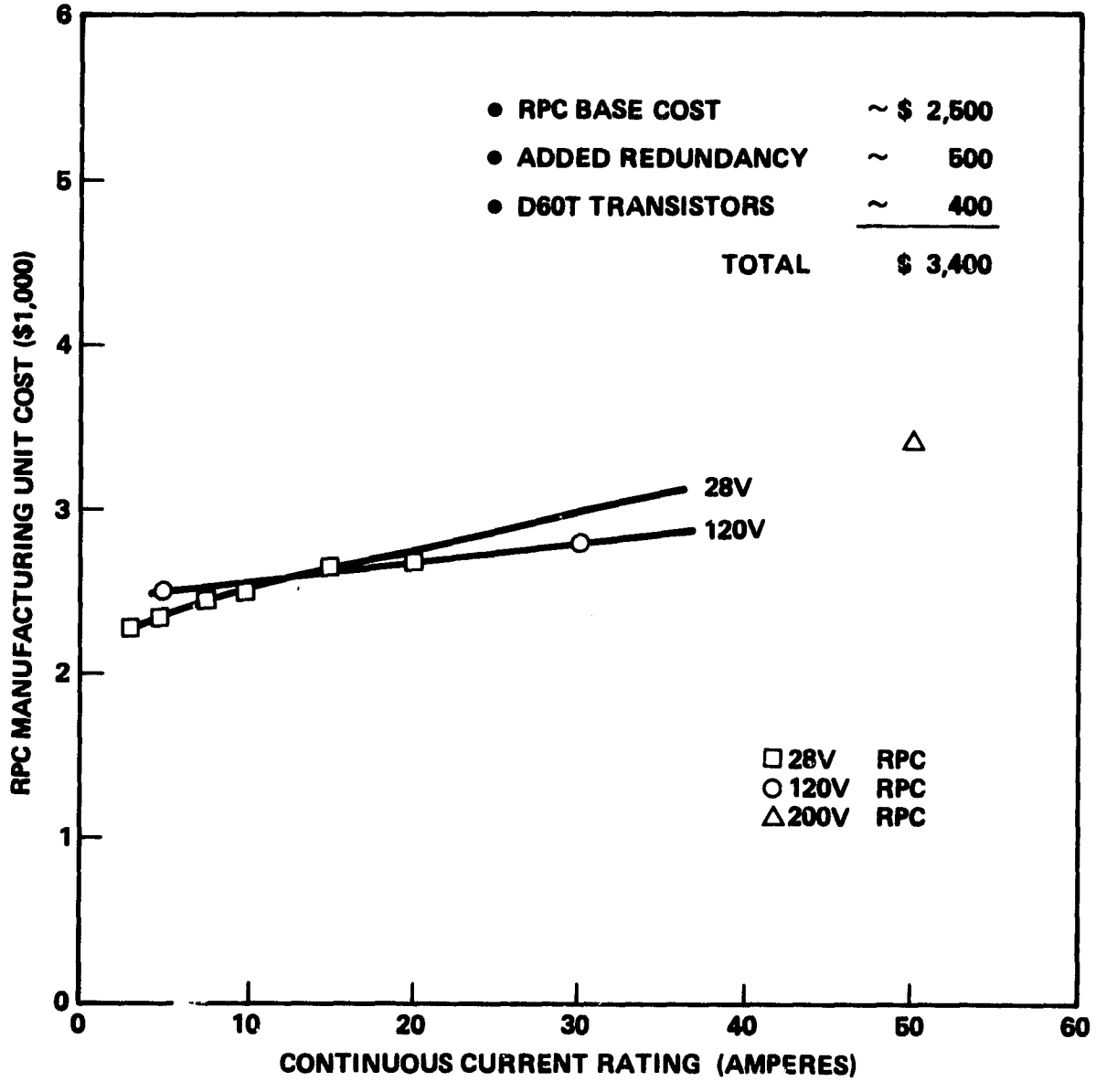

Figure 6-19. Remote Power Controller Cost Projection

7. VOLTAGE SELECTION

The selection of the power system voltage level defines the development of a new generation of high voltage power equipment. This power equipment becomes "off-the-shelf" for subsequent satellite and spacecraft programs and impairs any transition to another higher voltage even as power ratings grow well beyond 250 kilowatts and transmission distances extend beyond 300 feet. Hence, the voltage selection must balance the exigencies of near-term satellite requirements without an expanded development program, yet provide the maximum benefits for future higher-power satellite and spacecraft requirements. The recommendation of 220 volts as the power system voltage for generation and distribution meets these goals.

7.1 VOLTAGE BENEFITS

Analyses of the sensitivity of major electrical power system parameters show an inverse relationship to voltage. Higher transmission and distribution voltages improve the significant parameters of the electrical power system:

a) Conductor size is reduced, $A_o = K_1 P/V$

b) Conductor weight is reduced, $W = K_2 \ell P/V$

c) Voltage regulation is improved, $\Delta V/V = K_3 \ell/V$

d) Power loss is reduced, $P_\ell = K_4 \ell P/V$

e) Transmission costs are reduced, $C_t = K_5 \ell P/V$

where:

P = rated power (load)

ℓ = transmission or distribution loop distance

V = transmission or distribution voltage

Graphical display (Figure 7-1), illustrates this inverse voltage relationship of transmission costs.

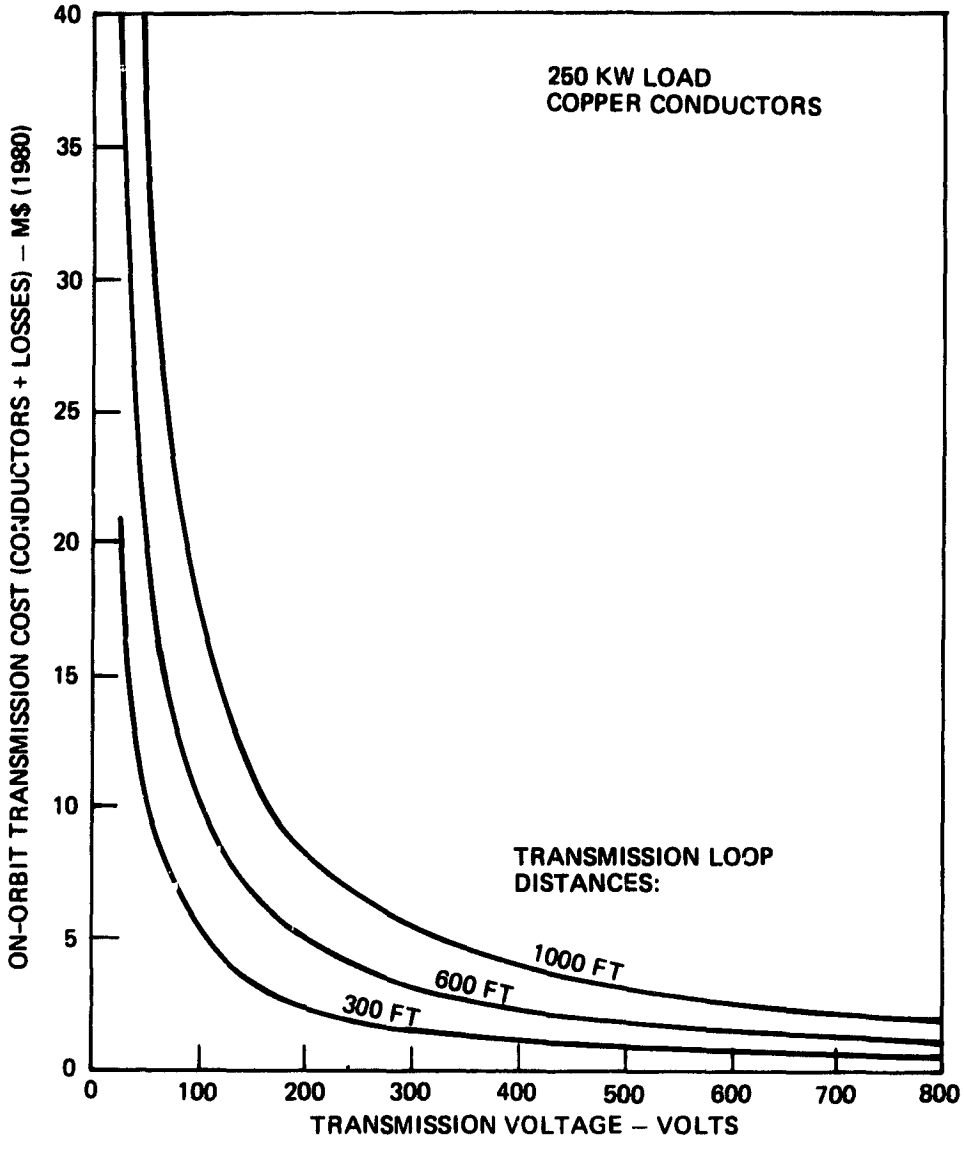

Figure 7-1. Transmission Costs Decrease Dramatically for Voltage Increases to 200 Volts

Energy storage also benefits from higher voltages:

a) Available energy per battery is increased, $E_a = C_r DV$

b) Individual battery power rating is increased, $P_b = C_r DV/t_e$ (Figure 7-2)

c) Battery (channel) quantity is reduced, $Q = \frac{Pt_e}{C_r DV}$

where:

C_r = rated capacity of a battery cell, ampere hours

D = depth of discharge

V = system voltage

t_e = eclipse duration, hours

P = rated power (load)

Increased power and energy from a single battery (more cells in series) reduces the quantity of batteries (but not cells). In turn, the power management task is simplified for battery load management (software) and battery charge/discharge control, and the quantity of the associated control hardware (battery charger, primary switch gear, power source controller) is reduced. These power management and equipment simplifications reduce electrical power system costs.

All of the performance parameters of the electrical power system respond favorably to increasing voltage. No mathematical trade optimum exists. Therefore, increasingly higher voltages are desirable, and the highest practical voltage, consistent with constraining influences, is appropriate. It should be noted, however, that cost (Figure 7-2) and weight reduction benefits are greatly diminished above 300 volts for a 250-kilowatt system with a loop transmission distance of 600 feet.

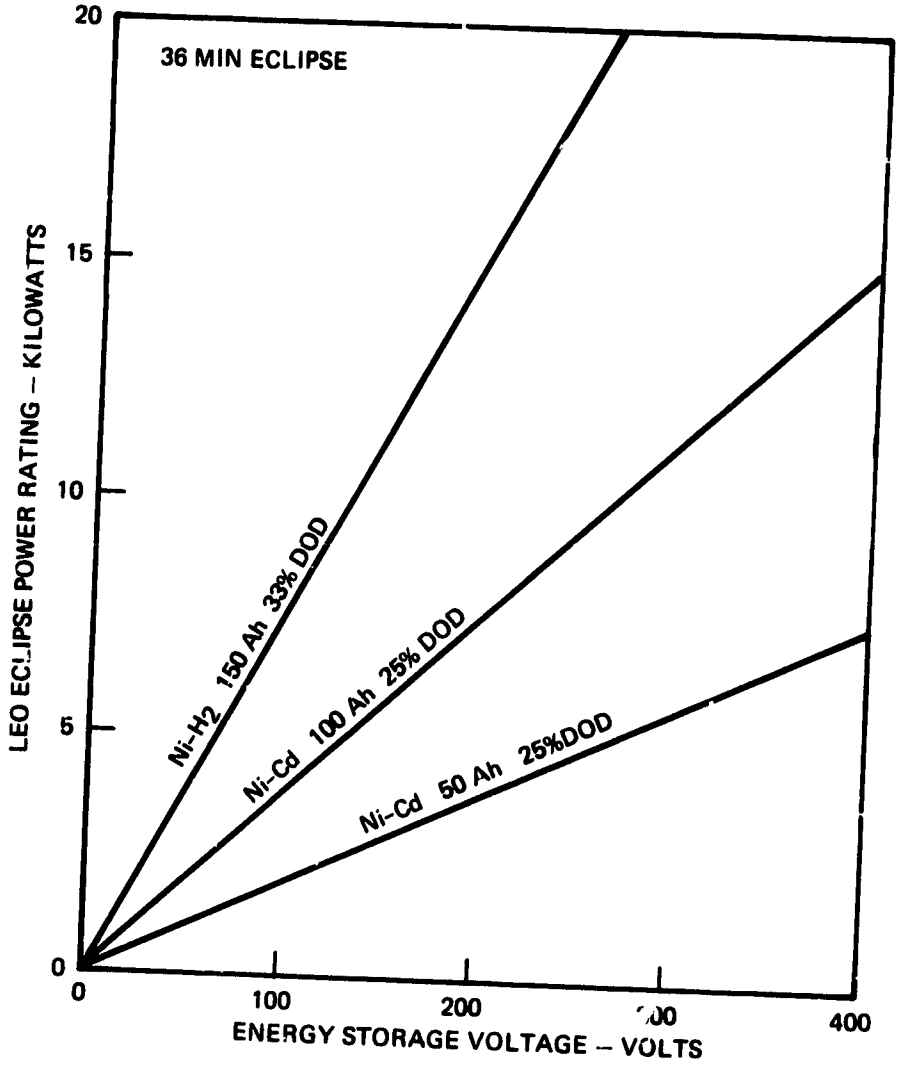

Figure 7-2. Higher Voltages Increase Battery Power Rating

7.2 CANDIDATE VOLTAGES

Viable candidate voltage levels considered for a new standard for application to satellite electrical power systems in the range of 10 to 1000 kilowatts are:

a) 110 volts

b) 220 volts

c) 270 volts

d) 440 volts

e) 600 volts

Four levels (110, 220, 440, and 600 volts) are commercial dc voltages for which design and operating experience and industrial equipment exists. The industrial equipment is typically large and heavy and is unsuited for the aerospace environment. For example, commercial direct current switch gear depends upon air mass one (AM1) and one g environment for arc extinction and current interruption. Naval ships (WWII submarine designs) have used these voltages and equipment.

The 270-volt level is an emerging approach for electrical power generation and distribution on Naval aircraft. Considerable aircraft related equipment is under development for this voltage.

7.3 CONSTRAINTS

Three major concerns limit the selection of increasingly higher voltages:

a) Plasma interactions at low earth orbit

b) Semiconductor technology status

c) Personnel shock hazard

In addition, the incremental cost (Figure 7-1) and weight benefits of higher voltages diminish rapidly above 300 volts for a 250-kilowatt space platform with a loop transmission distance of 600 to 1000 feet. Incremental benefits diminish at lower voltages for lower power levels and/or shorter transmission distances.

7.3.1 Plasma Interactions

Consideration of the solar array interaction with the plasma sheath surrounding any space platform in low earth orbit becomes pertinent as electrical power system voltages are increased. Leakage currents, corona, and ultimately arc discharges develop as the power system voltage levels are increased. However, the parameters which affect these interactions are ill-defined due to lack of space experience at the voltage levels of interest. The magnitude of the leakage currents are a function of the operational system voltage, orbital plasma density (assumed at 10^6 particles per cubic centimeter for LEO), and the ram and wake effects of the orbital trajectory. Various analyses and experiments (References 7-1 and 7-2) suggest leakage is minimal (less than 1 percent) below the 400-volt level (Figure 7-3). Cold array (post eclipse) open-circuit voltages are approximately twice operational voltages, but for system voltages below 400 volts, these leakage currents will be limited to one percent or less of the open circuited segment capacity. This is tolerable as these segments are not supporting loads. Arc discharges occur as voltage levels approach 1000 volts and may occur as low as 400 volts. Arc discharges are to be avoided as their cumulative effects may be destructive. Hence, system voltage levels in the range of 200 to 300 volts for low earth orbit application are "comfortable" pending better data.

At geosynchronous orbits, the particle density is sufficiently reduced (1 to 10 particles per cubic centimeter) that leakage currents are negligible until system voltages reach several kilovolts.

7.3.2 Semiconductor Technology

Semiconductors, transistors and/or MOSFETS, are employed in distribution switchgear, converters, inverters, regulators, and solar array segment switches. High-voltage, high-current transistor development is progressing at Westinghouse with the development of the D60T and D62T transistors rated at 40 to 60 amperes (with a gain of 10) and 400 to 500 volts, and the D7ST transistors with ratings to 150 amperes and 500 volts. In addition, 25-ampere, 1000-volt bipolar transistors and power MOSFETS have been built. Hence, power semiconductor technology exists to support 100- to 400-volt electrical power systems.

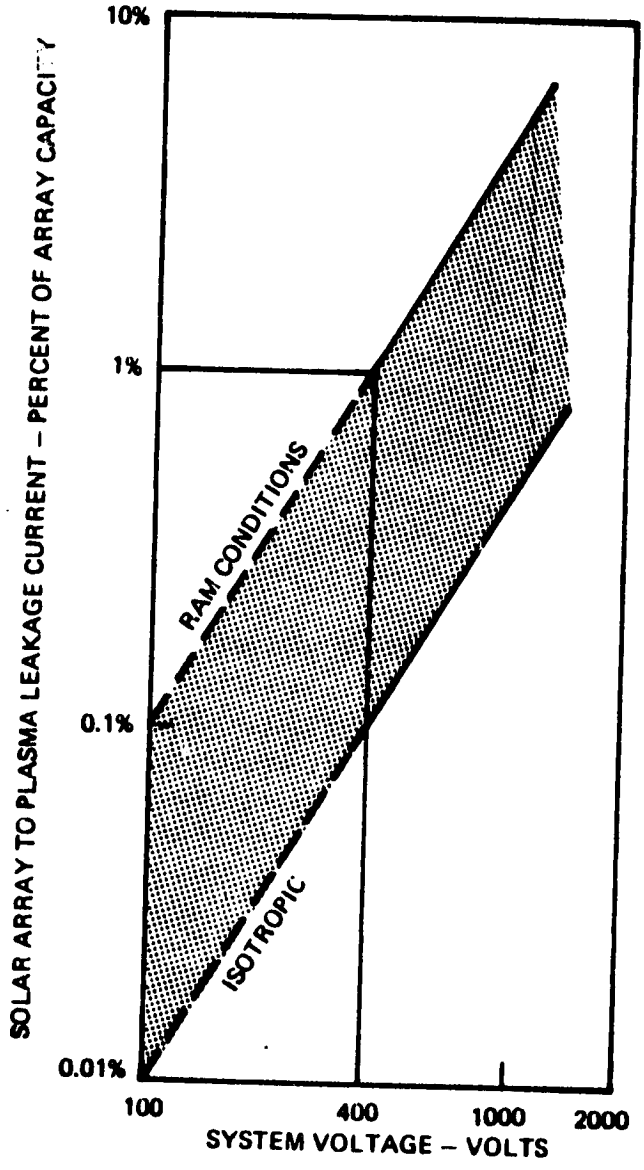

Figure 7-3. LEO Plasma Interactions Suggest Voltage Below 400 Vdc

Distribution switch gear for higher voltages (above 28 volts) has been under development for a considerable time by NASA/LeRC and the Naval Air Development Center. Remote power control equipment in the range of 200 to 400 volts is being developed by Westinghouse under contract to NASA/LeRC and has reached the breadboard phase with current ratings of 25 to 50 amperes using the D60T transistor family. Also, 1000-volt, 25 ampere switches are under development using MOSFET or bi-polar semiconductors. Other switch gear development efforts include hybrid designs with motor driven contacts in parallel with semiconductor components for current interruption. The electromechanical contacts provide a low-loss steady-state conductor path. Similar hybrid switch gear is being developed for the 270-volt Navy aircraft system application. Hence, distribution switch gear generic design development is well advanced for direct current system voltages of interest, 100 to 400 volts. However, the protection capability of these devices is limited, and semiconductor circuit breakers and space rated high-voltage fuses require development.

Converters, inverters, and pulsewidth regulators typically utilize semiconductor switching circuits operating from the power system bus voltage. These applications entail switching transients (spikes) typically to 150 percent of the applied voltage. In addition, component working voltages (including transient peaks) are normally limited to 80 percent of published manufacturer ratings. Hence, semiconductors for converter and inverter applications require published voltage ratings (V_{CEV}) of 2.5 times the nominal system voltage. This rating accommodates the twofold transformer voltage swing, switching transients to 50 percent above the applied voltage, and the 80 percent derating factor. Semiconductors for pulsewidth regulator applications require voltage ratings (V_{CEV}) essentially 2.16 times the nominal system voltage. This rating accommodates maximum system voltage, switching transients to 50 percent above the applied voltage, and the 80 percent derating factor. With 500-volt components, a nominal 220-volt system is supportable (Figure 7-4).

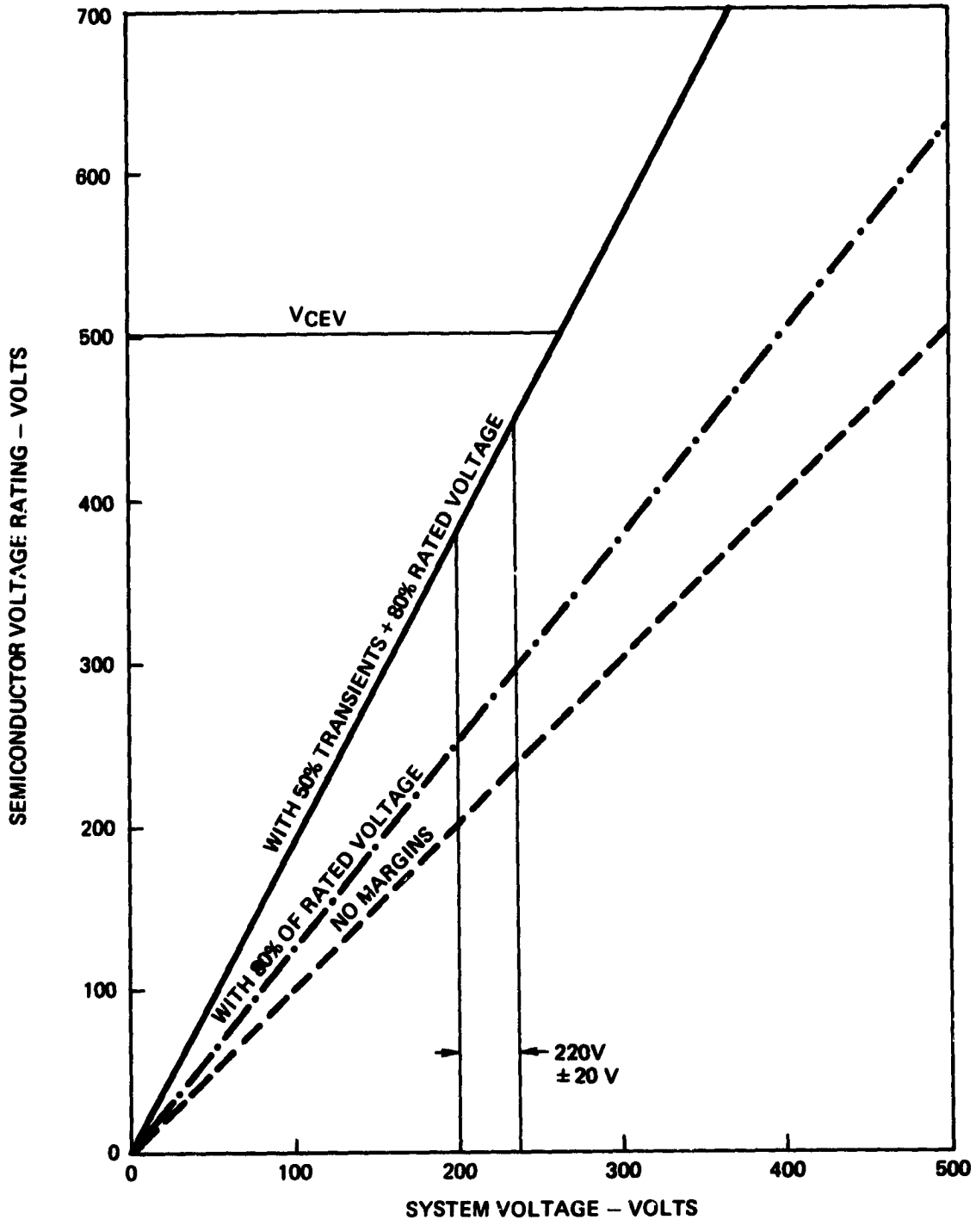

Figure 7-4. 500-Volt Devices Support 220-Volt System

7.3.3 Personnel Safety

Personnel safety for electric shock is adequate below 400 to 600 volts (woman, man) for direct current electrical systems (Figure 7-5). These voltages, in conjunction with the normal range of skin resistance, limit body currents to values (41 to 62 milliamperes) that still allow muscular control and virtually assure "let go" of the electrically energized device (Reference 7-3). However, the skin is the dominant resistive element in the body conduction path. The internal body resistance is only 100 to 600 ohms (Reference 7-3). Moist skin conditions, due to perspiration, wet clothing, water application, etc., dramatically reduce the electrical resistance of the skin and increase the shock current dangerously (Figure 7-5). However, for normal manufacturing, assembly, test, maintenance, launch, and retrieval scenarios for spacecraft and satellites, direct current voltages up to 400 volts are relatively safe for inadvertent personnel contact. [THIS IS NOT TRUE FOR 50 TO 60 HERTZ ALTERNATING CURRENT SYSTEMS; ONLY 6 TO 9 MILLIAMPERES (60 TO 90 VOLTS) ARE TOLERABLE.]

7.3.4 Battery Reliability

The reliability of a multicell high-voltage battery is essentially the same as present 28-volt 20-cell batteries (Section 5.6) and is primarily dependent upon the inherent cell reliability. This result is based upon a Weibull distribution of cell failures and an allowance of 5 percent in loss of voltage - 1 cell in 20, 5 cells in 100, 10 cells in 200, etc. Consequently, energy storage reliability is maintained even though increasing numbers of cells are series connected to attain higher voltage systems. Battery reliability does not constrain the voltage selection.

7.4 SELECTION

The various parameters of the electrical power system are improved with increasing system voltage level (Section 7.1). However, practical considerations of personnel safety, plasma interactions at low earth orbits, and the decreasing incremental benefits of increasing voltage levels bound the range of voltage interest at this time. The plasma interaction constraint is projected from chamber experiments and scientific hypotheses. Actual test experience in orbit is missing and not anticipated before late 1984. Hence, the selected voltage level must carefully

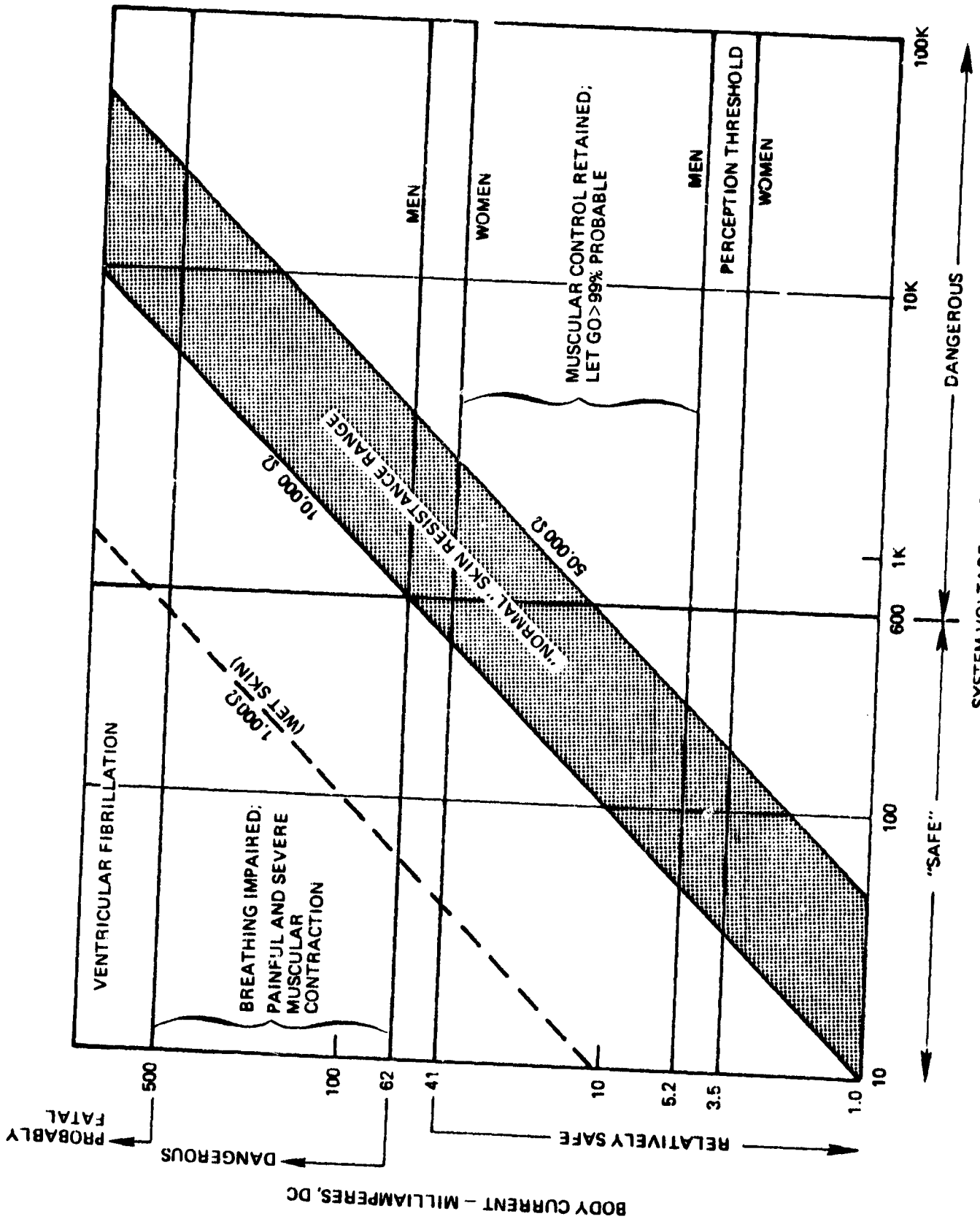

Figure 7-5. Shock Hazard Up to 600 Vdc is Acceptable

consider these constraints and provide a suitable margin for the present uncertainty of the plasma interactions. Therefore, the selection for a new system standard becomes a choice between 110, 220, and 270 volts.

The 220-volt level is selected (circa 1980) from these three to optimize, qualitatively, system benefits versus additional development costs. At the 220-volt level, the present D60T family of power transistors can provide adequate current and voltage ratings to provide the basic components for distribution switch gear, protective switch gear (circuit breaker equivalent using semiconductors), input power switching (10 to 40 kilohertz) for converters and inverters, and pulsewidth switching for regulators. The 220-volt level also allows utilization of the switch gear and equipment from the 200 to 400 volt NASA/LeRC and 270-volt Navy developmental efforts. Hence, duplication of significant basic component development is avoided at the 220-volt level. A few items, for example, fuses, power connectors, main circuit interrupters (battery fault-current interruption), etc., remain to be engineered, but these tasks are required at all three system voltages under consideration.

Tabular comparison of the benefits (Table 7-1) for the three voltage levels shows a major incremental cost reduction between the 110-volt and 220-volt levels at the 250-kilowatt power level. Smaller, but not inconsequential, incremental cost benefits would occur between 220 and 270 volts. Hence, the higher voltages are desirable for the 250 kilowatts electrical power system.

Table 7-1. Higher Voltages Reduce System Costs

Parameter \ Voltage Level	110 Volts	220 Volts	270 Volts
Cells per Battery	80	160	200
Channel Power Rating	8.3 kW	16.7 kW	20.8 kW
Channel Quantity (250 kW)	30	15	12
Distribution Conductor Cost	10 m$	5 m$	4 m$
Voltage Range (Battery)	100 to 120 V	200 to 240 V	250 to 300 V

Comparison of the constraining influences (Table 7-2) for the three voltage levels show the 110-volt and 220-volt levels to be similar. The

Table 7-2. Similar Constraints on Lower Voltages

Parameter \ Voltage Level	110 Volts	220 Volts	270 Volts
Personnel Safety	Acceptable	Acceptable	Acceptable
Power Conversion Semiconductors	Present D60T and D7ST Family	Present D60T and D7ST Family	Need 600-700 volt Extension of D60T and D7ST family
Switch Gear	Use Semiconductors Present D60T	Use Semiconductors Present D60T	Use Semiconductors Present D60T
Fuses (space rated)	None Available	None Available	None Available
Connection	AN/MS Class D series	None Available	None Available
Plasma Arcing	Probably OK	Need orbital tests	Need orbital tests
Solar Array Voltage (cold)	310-360	500-575	625-720

major difference is the potential plasma interaction with post-eclipse (cold) open-circuit solar array segments. These array segment voltages are initially in the range of 500 to 575 volts for a 220-volt system but quickly decline to the 300-volt level as the solar array temperature stabilizes. Some terrestrial plasma experiments suggest the onset of arcing may occur as low as 400 volts. If this becomes substantial, as indicated by orbital data, the control approach for the solar array can be revised to preclude the high voltage from occurring. One alternative is to substitute shunt control for series control (Figure 7-6). This shunt control alternative requires addressing partial shadowing of a solar array segment and the possibility of hot spots on the array elements if partial shadowing occurs. However, this shunt control is a suitable alternative if arcing is verified at below 575 volts and such arcing is shown to be deleterious to the open-circuited solar array segments. Hence, the 220-volt level has minimal risk and desirable cost benefits.

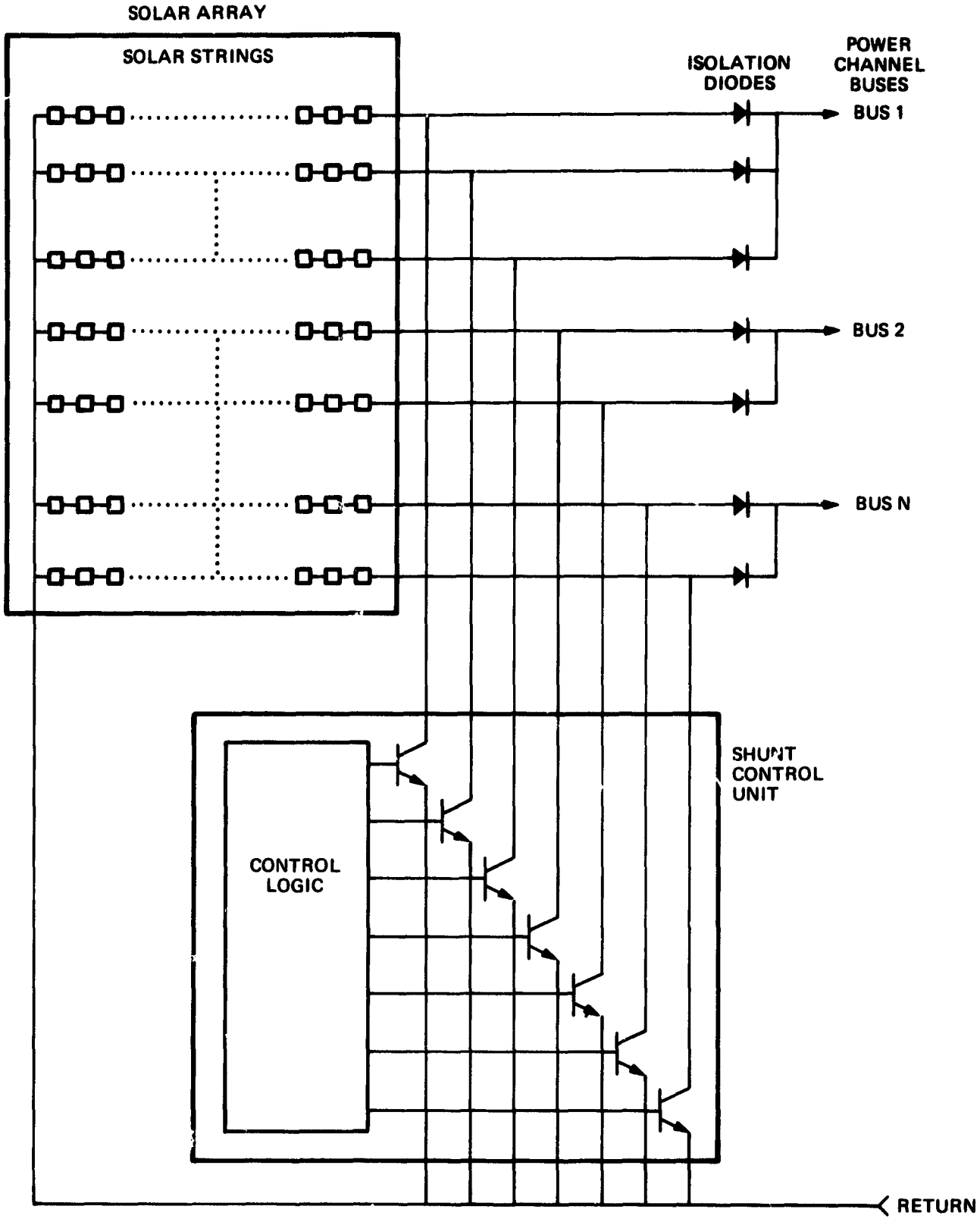

Figure 7-6. Shunt Control Limits Solar Array Voltages to Bus Voltages

The 270-volt option incurs greater risk of plasma arcing as the voltage level increases by 145 volts to 720 volts:

(200 cells) x (1.563 V/cell) x (2.3 cold array factor) = 719 volts.

Shunt control requirements for the solar array segments and shadow assessment become the expectation rather than the alternative. In addition, the 270-volt level requires semiconductor voltage ratings in excess of the present (circa 1980) voltage capability of the Westinghouse D60T and D7ST transistor family (500 volts and 40 to 60 amperes with a gain of 10). This should be remedied in later years, perhaps before the desired 1986 technology date. However, higher voltage components would be needed much earlier than 1986 (that is, be needed now) in order to develop and qualify the power conditioning technology by 1986 for the high-voltage, high-power levels of the 250-kilowatt system.

The 270-volt level introduces two areas of concern to be investigated and resolved:

1) Plasma arcing

2) High voltage, high-current semiconductors.

The benefits of 270 volts over 220 volts for a single satellite and the technology constraint schedule of 1986 do not warrant selection of 270 volts at this time. However, this is an attractive alternative to the 220-volt level. Development and equipment synergism is expected with the 270-volt program for naval aircraft, and benefits, when applied to many satellites, become significant.

The 120-volt level has been proposed in the initial studies for the 25-kilowatt Space Platform (25-kilowatt Power System). This level produces a fourfold reduction in the cost, weight, and losses of transmission and distribution conductors compared to the 28-volt level. Switch gear developments (NASA/LeRC and Navy) at 200 to 400 volts can easily be modified for 120-volt application, and power transistors are available with adequate voltage ratings. Plasma interactions are projected to be negligible at 120 volts, and electrical shock hazards are much less than at 220 or 270 volts.

For smaller electrical power systems, 10 to 50 kilowatts with transmission distances below 100 feet, a 110-volt system appears attractive. However, even these lower power platforms, when operated at higher altitudes (geosynchronous), can benefit by transmission conductor weight reduction from a higher voltage selection. Also, additional improvements in cost and efficiency by a factor of two are possible with a 220-volt selection without any corresponding increase in development costs or extension of development schedules. The same equipment needs to be developed at 110 or 220 volts: fuses, battery disconnects, circuit breakers, and high-current high-voltage connectors. Hence, for the same effort and investment, significantly greater transmission and distribution performance can be realized from the selection of 220 volts versus 110 volts.

At 110 volts, the energy storage capacity per battery is considerably reduced compared to a 220-volt system for a given maximum cell size. This reduces the power rating of a channel (assuming no battery paralleling):

150 Ah cell x 33% DOD x 100 V = 5000 watt-hours
150 Ah cell x 33% DOD x 100 V ÷ 0.6 hour = 8333 watts
250,000 watts ÷ 8333 watts = 30 channels
} at 110 volts

versus

150 Ah cell x 33% DOD x 200 V = 10,000 watt-hours
150 Ah cell x 33% DOD x 200 V ÷ 0.6 hour = 16,667 watts
250,000 watts ÷ 16,667 watts = 15 channels
} at 220 volts

Twice the number of power channels with batteries, primary switchgear, source protection and disconnect equipment, and the related power management equipment, are required at 110 volts as compared to 220 volts for the same system power level: as power levels increase, the historically inevitable trend, the higher power system voltage is the more attractive approach to maximize the energy storage per battery and thereby keep the channel quantity and power system complexity and cost to a minimum. Hence, the 220-volt level is selected over the 110-volt option.

8. REFERENCE DESIGN

Integration of the analyses, evaluations, comparisons, and selections of the various aspects of electrical power generation and distribution leads to the reference 250-Kilowatt Electrical Power System (Figure 8-1) This multichannel approach enables near-term realization of multi-hundred-kilowatt power levels. The advantages of this approach are many. Large system power ratings are attained with the modest power level components presently under development. Graceful degradation is inherent, and added capacity for power source redundancy (solar array and energy storage) is precluded. Further, the power levels for switchgear design are reduced, battery paralleling is avoided, and flexibility is inherently provided for isolation of otherwise interactive loads and to enhance equipment life through load balancing techniques. However 17 power channels with the corresponding switchgear are required for the 250-kilowatt system. Management becomes complex due to the large number of power system reconfiguration and load control options available. This is solved by incorporating autonomous (automated, on-board) control.

The electrical power subsystem is configured as seventeen 16.7-kilowatt channels (Figure 8-1) to support 250 kilowatts of payload power demand and 25 kilowatts of housekeeping equipment -- predominantly liquid coolant pumps in the thermal subsystem. Each channel includes one 160-cell, 150-Ah, nickel-hydrogen battery for energy storage in support of a 36-minute eclipse at full power (275 kilowatts). Each channel consists of one primary power bus and is electrically isolated from the other channels (no tie connections), but all channels utilize a common power return path. These isolated power channels are integrated into a cohesive operating utility by the electrical power management subsystem (PMS). (See Volume 2.) This power system concept fulfills the basic requirements for a 250-kilowatt electrical power system (Table 8-1).

Power is generated by a 690-kilowatt (BOL), miniature-faceted Cassegrain-concentrator, solar array (Table 8-2). This solar concept is selected for its projected cost advantage -- 30 $/W manufacturing cost. The generated power is allocated to the respective channels by a solar array switching unit (SASU) in accordance with the needs of the payloads

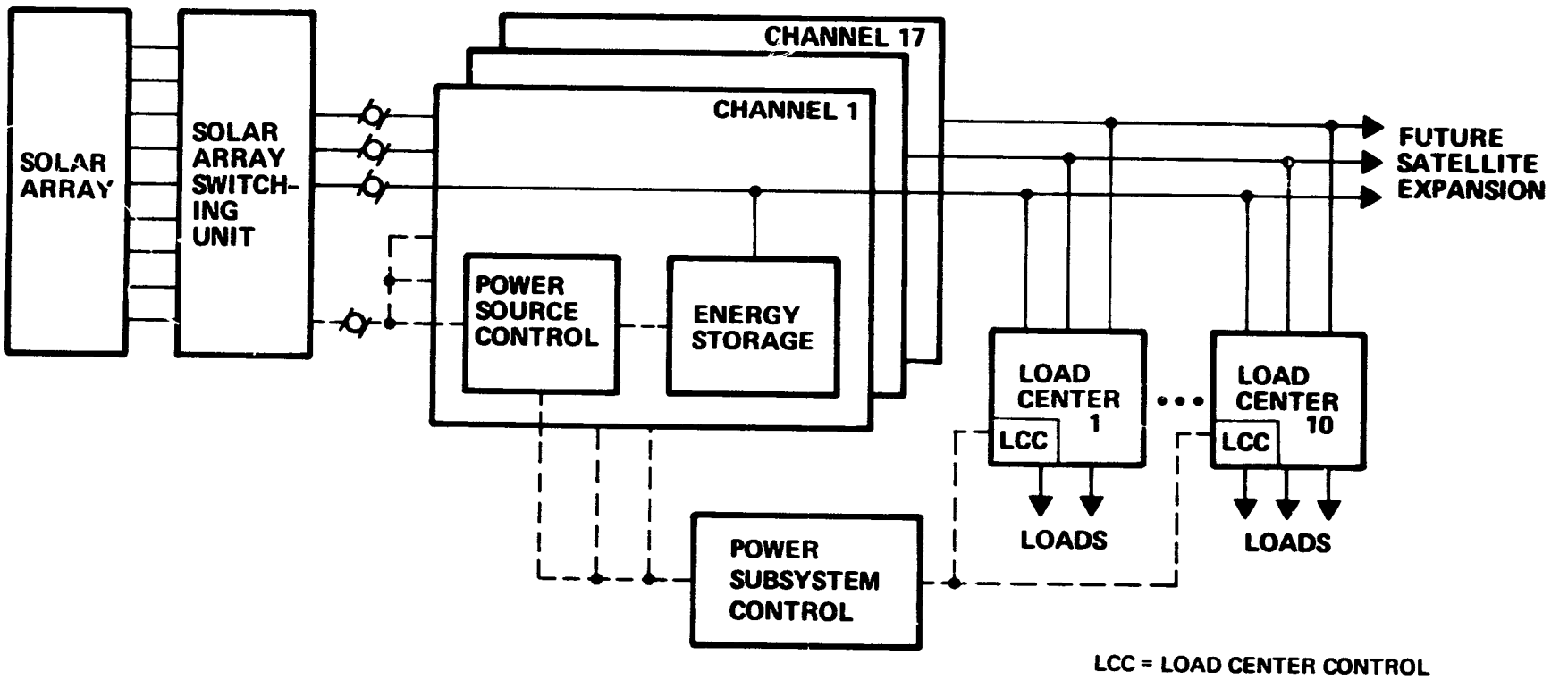

GENERATION – CASSEGRAIN CONCENTRATOR SOLAR ARRAY
ENERGY STORAGE – NICKEL-HYDROGEN BATTERY (160, 150-AH CELLS)
BATTERY CHARGER – SOLAR ARRAY SWITCHING UNIT
REGULATION – 220 ± 20 VOLTS (BATTERY CHARACTERISTICS)
POWER TRANSMISSION – DIRECT CURRENT AT SOURCE VOLTAGE
POWER DISTRIBUTION – DIRECT CURRENT AT SOURCE VOLTAGE
POWER PROCESSING – AS NEEDED WITHIN EACH PAYLOAD OR LOAD CENTER
CHANNEL QUANTITY – DEFINED BY BATTERY CAPACITY (17)
RELIABILITY – FAIL OPERATIONAL, FAIL SAFE
GRACEFUL CAPACITY DEGRADATION WITH FAILURES
LIFE – INDEFINITE; REPLACE FAILED UNIT AT NEXT SERVICE OPPORTUNITY

Figure 8-1. Reference Electrical Power System Design

Table 8-1. Study Guidelines

1) 250-Kilowatt Payload Power
2) Solar Array Power Generation
3) Low Earth Orbit Mission
4) 1985-86 Technology Readiness
5) 1988 Initial Operational Capability

Table 8-2. Cassegrain Concentrator Solar Array Parameters

Net Direct Load Power	275 kW
Battery Charging Power	270 kW
Net Power Required	545 kW
Solar Array Losses	7 kW
EOL Power	552 kW
BOL Power (EOL/.8)	690 kW
Area	49,500 sq ft
Weight	33,700 lb
Cost:	
Manufacturing	20.7 M$
Transportation	30.0 M$
Total	50.7 M$

and batteries. This switching unit connects sufficient solar array segments to each primary bus to provide load power demand and battery charging current. The power management subsystem (PMS) monitors the loads, battery, and solar array, and selects the switch closures of the solar array switching unit (SASU) to produce the desired solar array output current -- payload current plus desired battery charging current.

Table 8-3. Nickel-Hydrogen Battery Parameters

Eclipse Power	275,000 watts
Net Eclipse Energy	168,667 Wh
Installed Capacity (34 percent DOD)	2,550 Ah
Cell Size	150 Ah
Series Cells/Battery	160
Number of Batteries	17
Voltage Regulation	200-240 volts
Life	7 years
Weight (25 Wh/lb):	
Initial	20,400 pounds
30 Years	107,830 pounds
Cost (26 $/Wh + 18 $/Wh):	
Initial	22.5 M$
30 Years	118.6 M$

Energy storage is provided by 17, 160-cell, 150-Ah, nickel-hydrogen batteries (Table 8-3). The 150-Ah nickel-hydrogen battery is selected over the nickel-cadmium or fuel cell plus electrolysis options based upon reduced life cycle costs over a 30-year period. Each battery is essentially directly connected to its respective power channel bus. However a disconnect switch is incorporated to isolate the battery for power channel servicing or repairs, to perform battery reconditioning discharge yet utilize the power channel during sunlight, and to replace the battery. Battery fault current protection is also incorporated at 300-ampere levels in order to provide battery power for short term overloads.

The distribution approach continues the isolated channel concept at the source and employs direct energy transfer at the source voltage (220 ±20 volts). Source regulation is from the inherent battery voltage characteristics. The battery voltage fluctuates from the low extreme of 200 volts at the end of discharge to the upper extreme of 240 volts at the end of recharge. The distribution wiring incurs a 3-volt loss over 300 feet, and the semiconductor switchgear and isolation diodes introduce another 2-volt loss. A voltage range of 195-240 volts is expected at the payloads; a ±10.6 percent regulation (Table 8-4).

Table 8-4. Distribution Parameters

• Channels	17
• Regulation:	
Voltage at Payload	194 - 240 volts
Regulation at Payload	±10.6%
• Solar Array Conductors:	
Material	Copper
Distance	400 ft loop
Optimum-Cost Area	1.78 sq in 0.104 sq-in/channel (2/0 wire)
Weight	2744 pounds
Voltage Drop (at 240 volts)	4.2 volts
Power Loss (at 240 volts)	9586 watts
Conductor Cost	1.6 M$
• Transmission Conductors:	
Material	Copper
Distance	600 ft loop
Optimum-Cost Area	1.72 sq in 0.101 sq-in/channel (2/0 wire)
Weight	3976 pounds
Voltage Drop (at 200 volts)	3.86 volts
Power Loss (at 200 volts)	5318 watts
Conductor Cost	2.4 M$
• Distribution Switchgear:	
Unit Cost	3400$
• Load Switchgear Quantity	260
Redundant Units	260
Switchgear Cost	1.8 M$

The distribution conductors radiate from the respective sources (solar array and battery) to a series of load centers. The load center concept is employed to unitize locally the power distribution switchgear and the control logic hardware for practical packaging of components into an appropriate assembly for installation, heat removal, and equipment replacement (servicing). This load center concept supports continued expansion of the satellite structure, and allows removal and deletion or replacement of load centers wherein internal hardware is no longer appropriate or useful.

Growth and flexibility are thereby attained to accommodate a maximum variety of payloads, near term or future. Consequently, the distribution conductors are not tapered to smaller sizes as the distances from the source increases. The conductors are sized for full power delivery to whatever length the satellite grows. This provides full power at the satellite growth point and is consistent with typical power growth experience.

Copper is the conductor material (Table 8-4). Wire of 2/0 size, or a bus bar equivalent, is required (Table 8-4). Aluminum conductors do not exhibit significant cost reduction when the terminations that occur every 15 to 30 feet are considered.

The 2/0 copper distribution wire carries 83.5 amperes at full load. This size is rated at 175 amperes in a wire bundle for aircraft application (per MIL-W-5088).

The load centers contain the distribution switchgear. Three types of load distribution occur (Figure 8-2):

1) Secondary load bus for housekeeping or space station loads

2) Payload ports for external payload attachment

3) High power payload bus exceeding the capability of one channel.

A space station is expected to require control and protection of a number of small loads. This is accomplished with a local secondary load bus and low power switchgear. External payloads are attached to a service port. Electrical service is envisioned as four primary load buses to provide payload management flexibility. Some payloads may require a single bus of greater power capacity than one channel can supply. This power level is attainable by summing (not paralleling) through programmable power processors power from several main distribution channels. The programmable power processors provide channel-to-channel isolation and allow proportional selection of the power from the various channels.

At least two remote power controllers are required for each load or load bus to provide power redundancy. Each controller pair is arranged to connect power to each load from one or the other of two different power distribution channels (Figure 8-2). Critical loads may have three or four

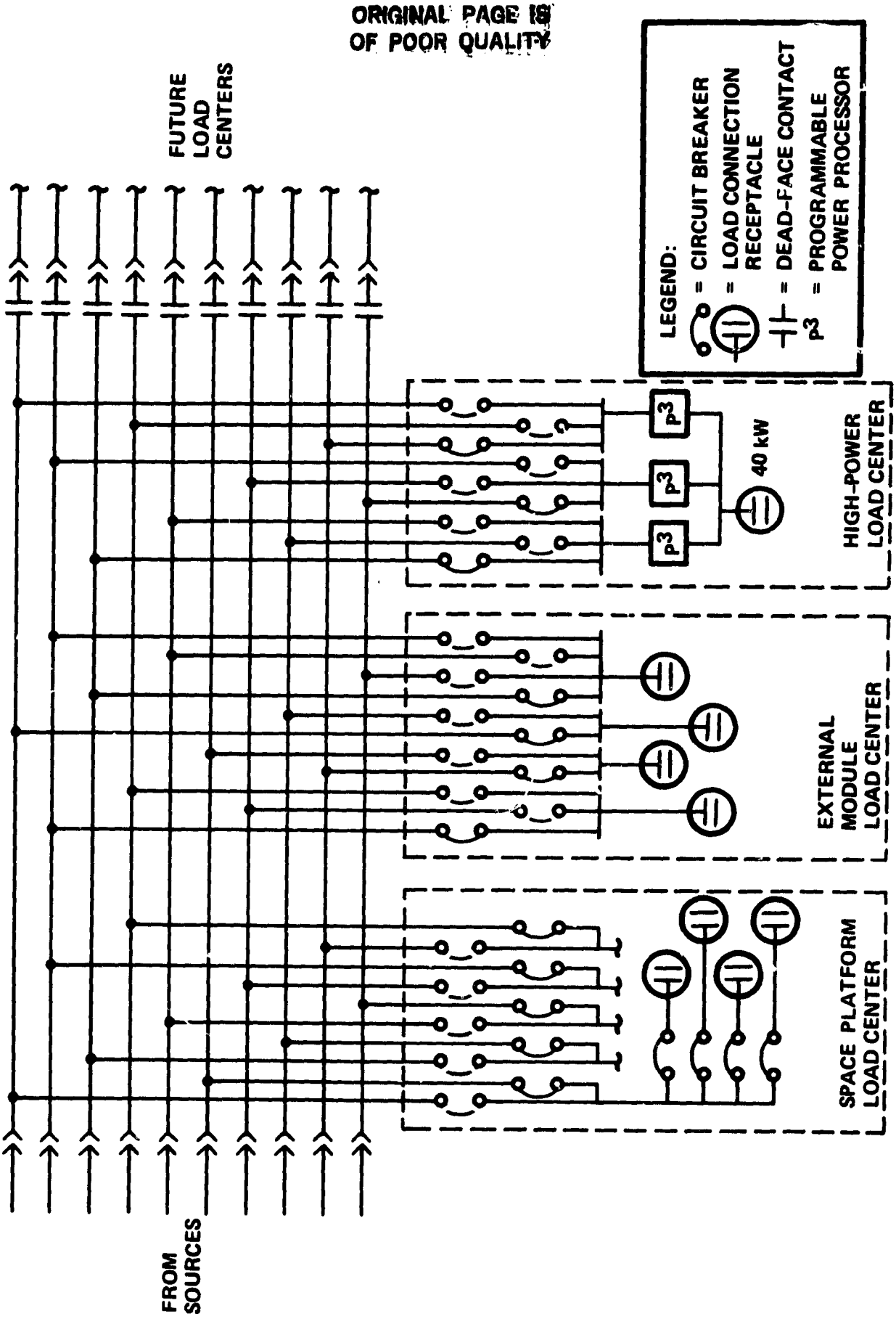

Figure 8-2. Recommended Power Distribution Network Concept

redundant power choices, and make-before-break switching between power channels can be provided for sensitive loads. The distribution switchgear is doubled by this approach, but the cost is small, excellent redundancy is attained, and flexibility to coordinate payloads with power channels is achieved.

Electrical energy is ultimately transformed into heat (except for minor radiated radio energy) and must be dissipated. On a satellite with a 275-kilowatt electrical power system, an active (pumped fluid loop) thermal system design is required to collect the heat from the distributed loads, batteries, and concentrated control equipment and transfer it to a radiator. The 275-kilowatt size of the electrical power load diminishes the significance of other active thermal loads such as human habitation control. Hence, the electrical power system incurs the cost and weight for active thermal support (Table 8-5).

The technology projections for 1986 capability provide dramatic reductions in the cost of solar arrays and in the weight and cost of energy storage. However, the solar array and battery remain the dominant components of weight and cost for the electrical power system (Figure 8-3 and 8-4). The solar array is approximately half of the initial weight and cost, while as operational life is extended and battery replacements are required, the battery becomes over half the weight and cost of the electrical power system at 30 years.

Table 8-5. Thermal Parameters

• Battery Cooling:	
Heat Flow	36 kW
Cold Plates:	
Weight	760 pounds
Cost (On Orbit)	3.1 M$
Radiators:	
Area	1240 ft^2
Weight	1400 pounds
Cost (On Orbit)	1.7 M$
Pumps:	
Power	1.7 kW
Weight - Initial	110 pounds
- Replacements*	1445 pounds
Cost (On Orbit) - Life Cycle	0.8 M$
• Payload Cooling:	
Heat Flow	275 kW
Radiators:	
Area	6,630 ft^2
Weight	7,500 pounds
Cost (On Orbit)	9.2 M$
Pumps:	
Power	11.4 kW
Weight - Initial	1450 pounds
- Replacement*	9,546 pounds
Cost (On Orbit) - Initial	4.7 M$
- 30 Years	34.7 M$

*20,000 hour mean life.

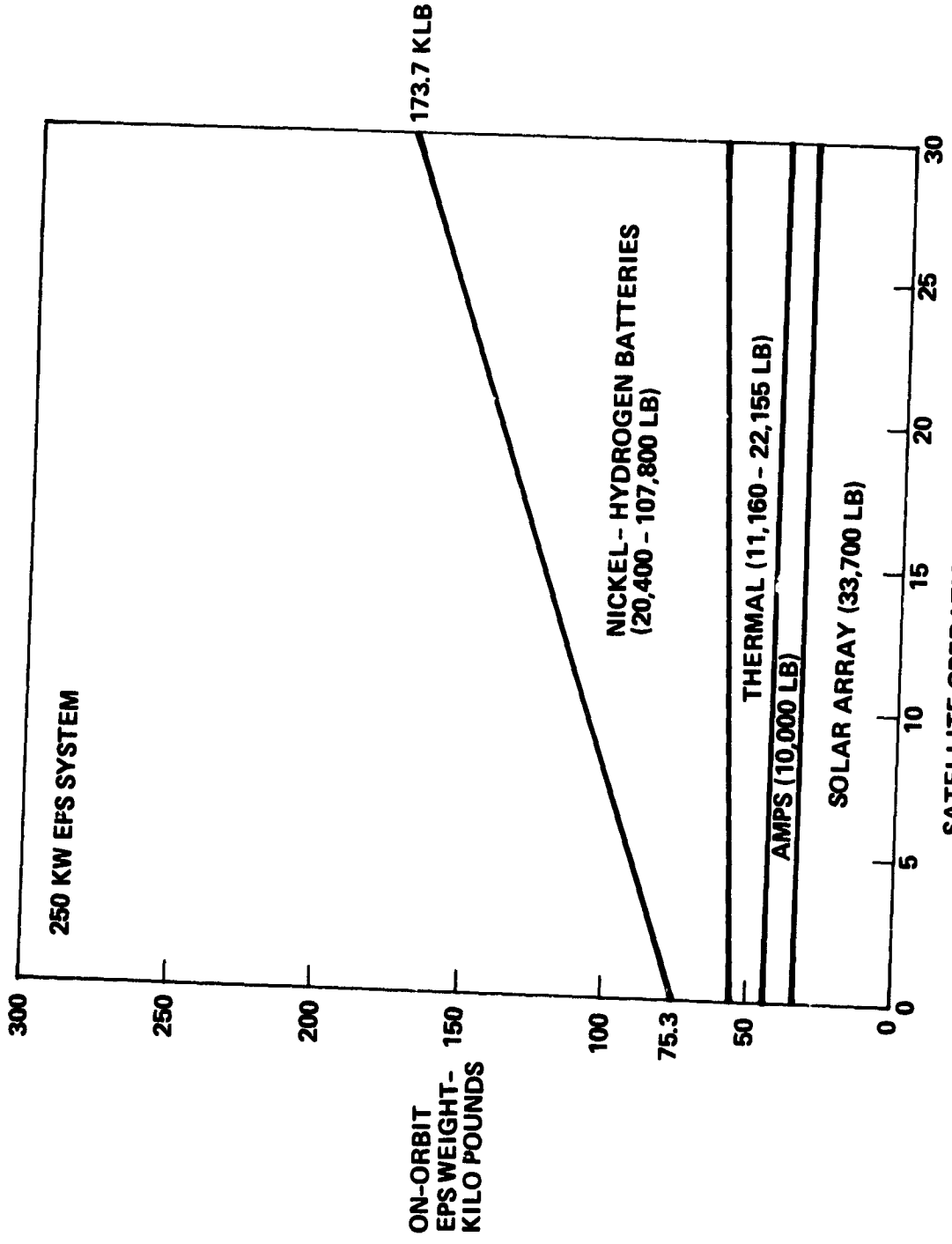

Figure 8-3. Batteries Dominate Life-Cycle Weight

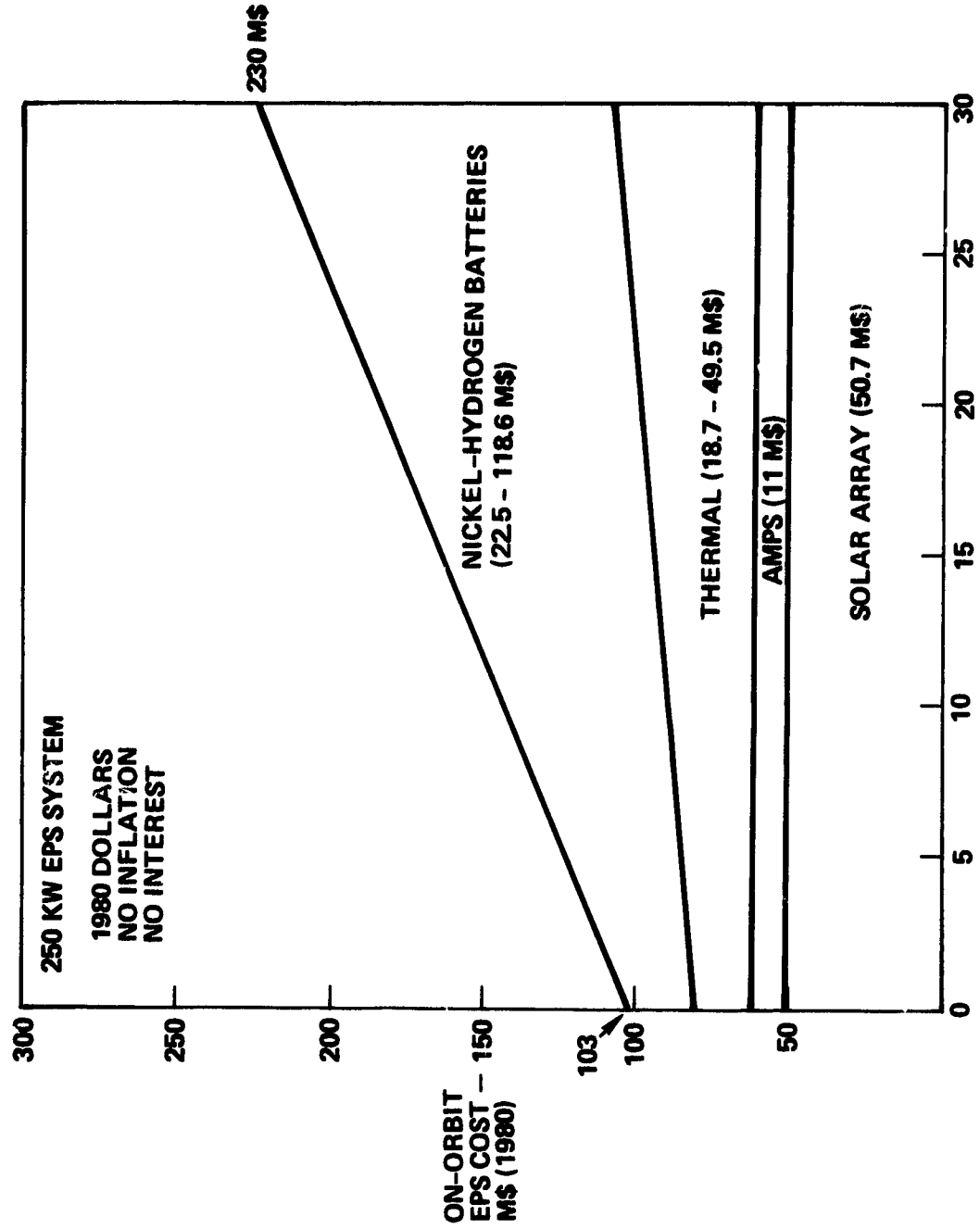

Figure 8-4. Batteries Dominate Life-Cycle Cost

9. TECHNOLOGY DEVELOPMENT NEEDS

The life cycle cost of spacecraft electrical power generation and distribution is high, 103 M$ initially, rising to 230 M$ over 30 years for a 250-kilowatt power subsystem (Figure 9-1). This translates to 400 $/W initially and 900 $/W at 30 years. However, these cost estimates are derived from 1980 projections of technology capability in 1986. To realize these cost estimates, three major technology areas must be pursued aggressively:

1) Miniature-element Cassegrain-concentrator solar array
2) 150-Ah nickel-hydrogen battery
3) Power system management.

Development programs have been formulated and initiated in each of these technology areas. However, a technology readiness of 1986 will require substantial acceleration of the present development pace and proportionally larger yearly funding allocations.

The major component of life cycle cost for the electrical power subsystem is energy storage. For 1986 technology readiness, the nickel-hydrogen battery is the cost optimized energy storage selection. However, a major weight and cost reduction, below the 1986 projections, is possible if the optimum depth of discharge* is higher than 33 percent. Improvement in the optimum depth of discharge potentially yields a greater and more immediate cost reduction than extended life. Even a modest increase in the optimum depth of discharge can reduce life cycle weight and cost dramatically (Figure 9-2). Such an improvement may entail no major technology development. Instead, a reasonable data base of life cycle testing is required (concurrent with good manufacturing quality control) to derive a better estimate of the cycle life versus depth of discharge relationship. As a minimum, the new data base would validate the present value selected for optimum depth of discharge - 33 percent. Hopefully, the data would indicate optimization at a higher depth of discharge and reduce energy storage costs accordingly.

*Cycle life, depth of discharge, and optimum depth of discharge are addressed in Section 5.5.

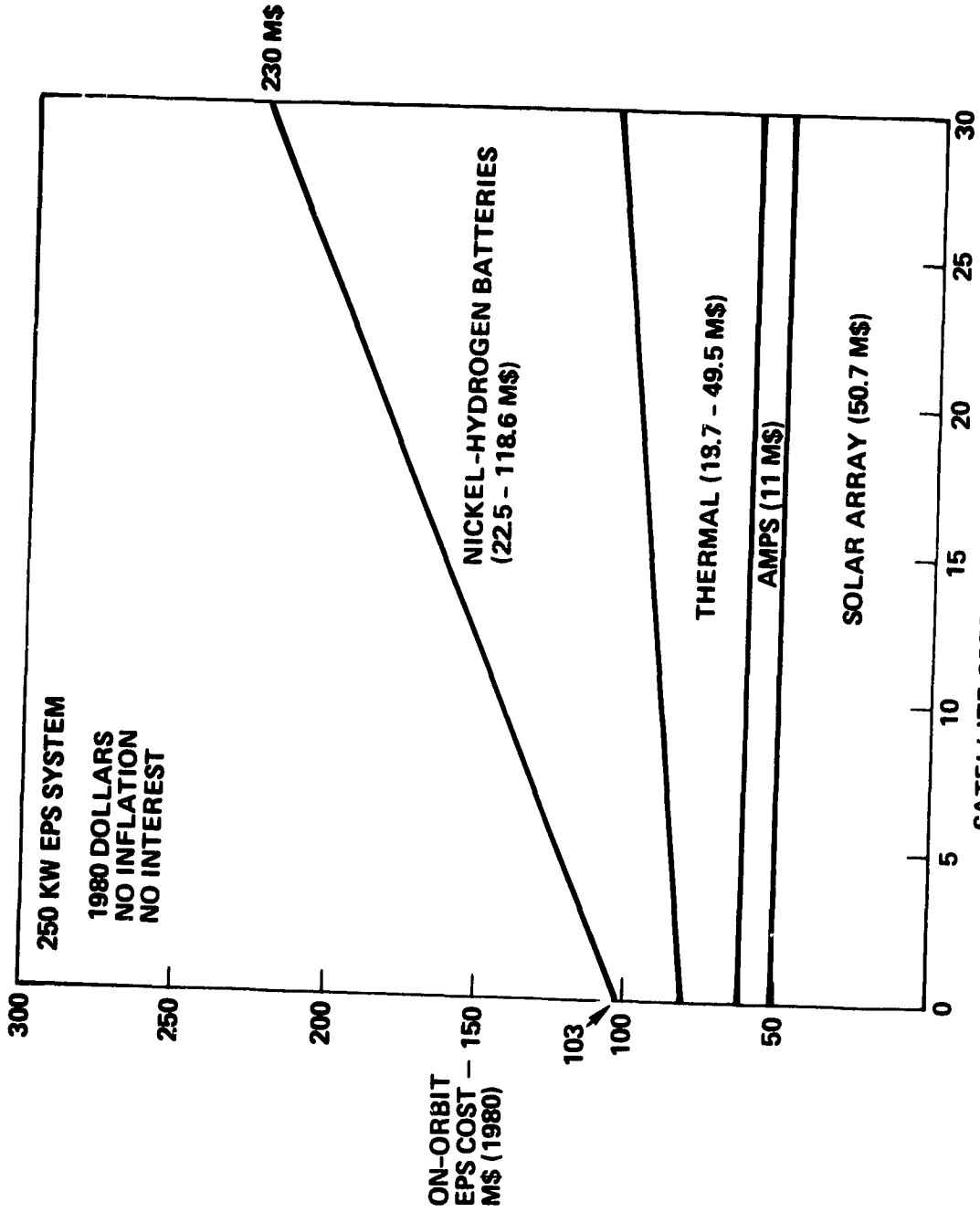

Figure 9-1. Batteries Dominate Life-Cycle Cost

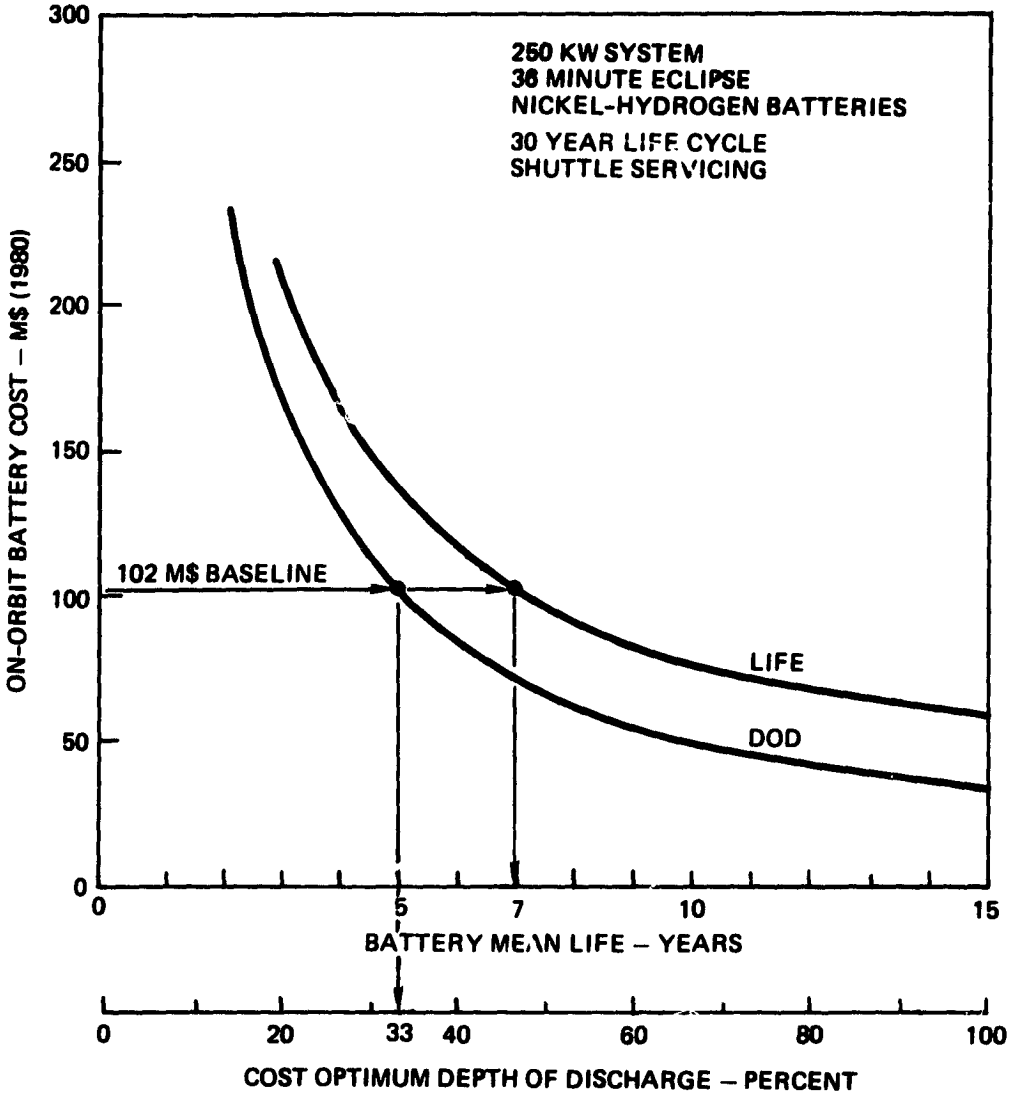

Figure 9-2. Improvement in Optimum DOD More Cost Effective Than Life Extension

The miniature-element Cassegrain-concentrator solar array concept selected for the 250-kilowatt system utilizes small 4 x 4 millimeter solar cells. With laboratory silicon cells, a 20-percent efficiency has been attained in small cells. This efficiency results in projected solar array specific costs in the range of 40 to 45 $/W. However, the small cell size makes it economically feasible to use higher efficiency, but more expensive, solar cells aiming for a solar array cost goal of 30 $/W. Hence, the development of higher efficiency solar cells should be actively pursued as this solar array concept can physically and economically apply these cells to reduce the recurring cost of present solar arrays by an order of magnitude.

Many electrical components require development to enable the control of a 250-kilowatt electrical power subystem and the power distribution at 220 +20 volts:

Solar array switching unit

Semiconductor relays

Semiconductor circuit breakers

Fuses

Connectors

Current monitors

Slip rings.

For a technology readiness of 1986, many of the items must have "off the shelf" availability as a family of sizes to enable the design of other power system equipment. For example, a power conditioner requires connectors and fuses to support the power conditioner design. Hence, these devices must be developed to a state of commercial availability in a range of sizes by the desired technology readiness date. The solar array switching unit is required to control the solar array output and to allocate the output appropriately to each power channel. Modest capacity semiconductor switches (transistors or power MOSFETs) are combined with control logic to maintain bus voltage and battery charging currents. An initial study (Reference 19) addressed this approach, but hardware validation of control interactions and an application demonstration is needed.

A coordinated family of switch gear and protective devices (current interruption using semiconductors) is required for direct current distribution at 220 ±20 volts. Application of the Westinghouse D60T, D62T, and D7ST transistor series to produce relay and circuit breaker equipment has started. Westinghouse Electric Corporation has demonstrated several designs for 200- to 400-volt application with 50-ampere ratings under contract with NASA/LeRC (Reference 20). Considerable additional development work remains to translate this initial accomplishment into a coordinated family of available switch gear.

Fuses may be employed as the ultimate backup for gross faults in semiconductor switch gear, filter capacitors of power conditioners, and as an ultimate battery disconnect for a main bus fault. Typical high-voltage, high-current terrestrial fuses depend upon an explosive effect to interrupt the current. This may not be practical in the space environment. A limited series of coordinated, space-rated fuses is needed for 220-volt, direct current applications.

A connector series is required for the high-voltage and high-currents of the 250-kilowatt electrical power system. Major power interfaces require connectors for up to 2/0 wire or equivalent bus bar conductors to accommodate satellite buildup and growth. Connectors with smaller contacts, but with contact spacing for a 250-volt continuous rating are also required for various equipment connections. Connectors for exterior payload or pallet attachment may require dead face provisions.

The accuracy of present current monitors is approximately ±3 percent. Reliance on these devices is required to control the multichannel electrical power system. Battery charge control requires current monitor accuracy of +1 percent or better to avoid excessive or inadvertent overcharge which reduces battery life expectations. Batteries are the most costly long term component of the electrical power system and warrant attention to extend their life.

Slip rings or roller rings are required for fully gimballed payloads requiring uninterrupted pointing. These payloads are anticipated to require relatively low power - several hundred to several thousand watts.

Low voltage slip rings have been successfully employed on spin stabilized satellites transmitting several kilowatts of power. Similar slip ring assemblies, redesigned for higher voltage insulation but lower current contacts, may be employed for gimballed payloads.

Slip rings may not be required for the solar array to main satellite body connection. Limiting the solar array angular travel with respect to the satellite allows a cable wrap approach to this flexible connection. Hence, large power slip rings are not required unless greater satellite pointing freedom is desired.

The 30-year life cycle cost of spacecraft electrical power production and distribution remains high, even with optimistic projections for the 1986 technology status. The major cost of the electrical power system remains in energy storage and substantial costs are in the solar array and thermal control elements (Figure 9-1). Long term goals to reduce these costs are lower manufacturing costs, lighter weight equipment to reduce shuttle transportation charges, and extended equipment life to reduce replacement frequency. In addition, larger battery capacity (250-Ah cell) would reduce the quantity of power channels (10 instead of 17), thereby simplifying the distribution system, reducing the power management complexity, reducing the system level testing, and lowering the associated costs. However, as each technology matures, performance improvements become more difficult to attain, and dramatically reduced specific costs ($/W, $/Wh) are elusive. The development of a new energy storage technology promising significant reductions in <u>both</u> cost and weight needs to be pursued.

10. TECHNOLOGY INVESTMENT CRITERIA

Technology improvements yield payback in the form of lower costs for future programs. Assessing this payback and comparing it to the development cost of the technology improvements provides an investment yardstick to judge the relative merits of otherwise confusing sets of performance data.

Potential technology payback from improvements in specific performance parameters is addressed with a series of graphs produced for the major electrical system components (solar array, battery, power processing) to identify the potential system value (cost savings) for these performance improvements. For example, battery costs are the sum of manufacturing costs, launch costs, and replacement costs. Launch costs are directly related to equipment weight and hence to specific weight. Replacement costs are affected by equipment life. Hence, manufacturing costs, specific weight, and life parameters were examined for their impact on system cost.

Nickel-hydrogen battery manufacturing specific costs are projected at 26 $/Wh (1980 $) for 1986 technology. Aggregate battery manufacturing costs over a 30-year satellite life are approximately 70 M$ for the reference 250-kilowatt system design:

$$\frac{\text{Payload power and housekeeping power}}{\text{Depth of discharge}} \times \text{eclipse time}$$

$$\times \text{ specific cost} \times \left(1 + \frac{\text{satellite life}}{\text{equipment life}}\right) = \text{life cycle manufacturing cost.}$$

$$\frac{(250\ \text{kW} + 25\ \text{kW})}{0.33\ \text{DOD}} \times \frac{36.8\ \text{min}}{60\ \text{min/h}} \times 26\ \$/\text{Wh} \times \left(1 + \frac{30\ \text{yr}}{7\ \text{yr}}\right) = 70\ \text{M\$}.$$

Hence, the technology specific payback is 280 $/system watt:

$$\frac{70\ \text{M\$}}{250\ \text{kW}} = 280\ \$/\text{system watt}.$$

Plotting technology specific payback related to manufacturing cost improvements as a function of specific manufacturing cost yields a linear relationship, Figure 10-1, and indicates the specific cost savings ($/system watt) as a function of reducing manufacturing specific costs.

Nickel-hydrogen battery specific weight is projected at 40 lb/kWh (25 Wh/lb) for the 1986 technology base. With a 30-year satellite, 7-year mean battery life, and a 462 $/pound launch cost, the resulting technology specific payback for weight reduction is projected at 200 $/system watt:

$$\frac{(250\ \text{kW} + 25\ \text{kW})}{0.33\ \text{DOD}} \times \frac{36.8\ \text{min}}{60\ \text{min/h}}$$

$$\times\ 40\ \text{lb/kWh} \times 462\ \$/\text{lb} \times \left(1 + \frac{30\ \text{yr}}{7\ \text{yr}}\right) = 200\ \$/\text{system watt}$$

Plotting technology specific payback related to the launch cost of equipment weight as a function of specific weight again yields a linear relationship (Figure 10-2) and indicates the specific cost savings as a function of reducing the battery specific weight.

Nickel-hydrogen battery average life is projected as 7 years for the 1986 technology base. Battery life enters the cost equations in the resupply term (1 + satellite life/equipment life) and produces a battery life related technology payback projection that is nonlinear (Figure 10-3).

These graphs do not purport to identify specific technology methods to achieve performance improvements, but instead are a tool to evaluate differing, and often confusing, proposals for performance improvement. For example, consider three hypothetical nickel-hydrogen battery proposals to reduce specific manufacturing costs:

	Proposal 1	Proposal 2	Proposal 3
Development cost (investment) (M$)	15	21	23
Resultant recurring cost ($/Wh)	12	10	9

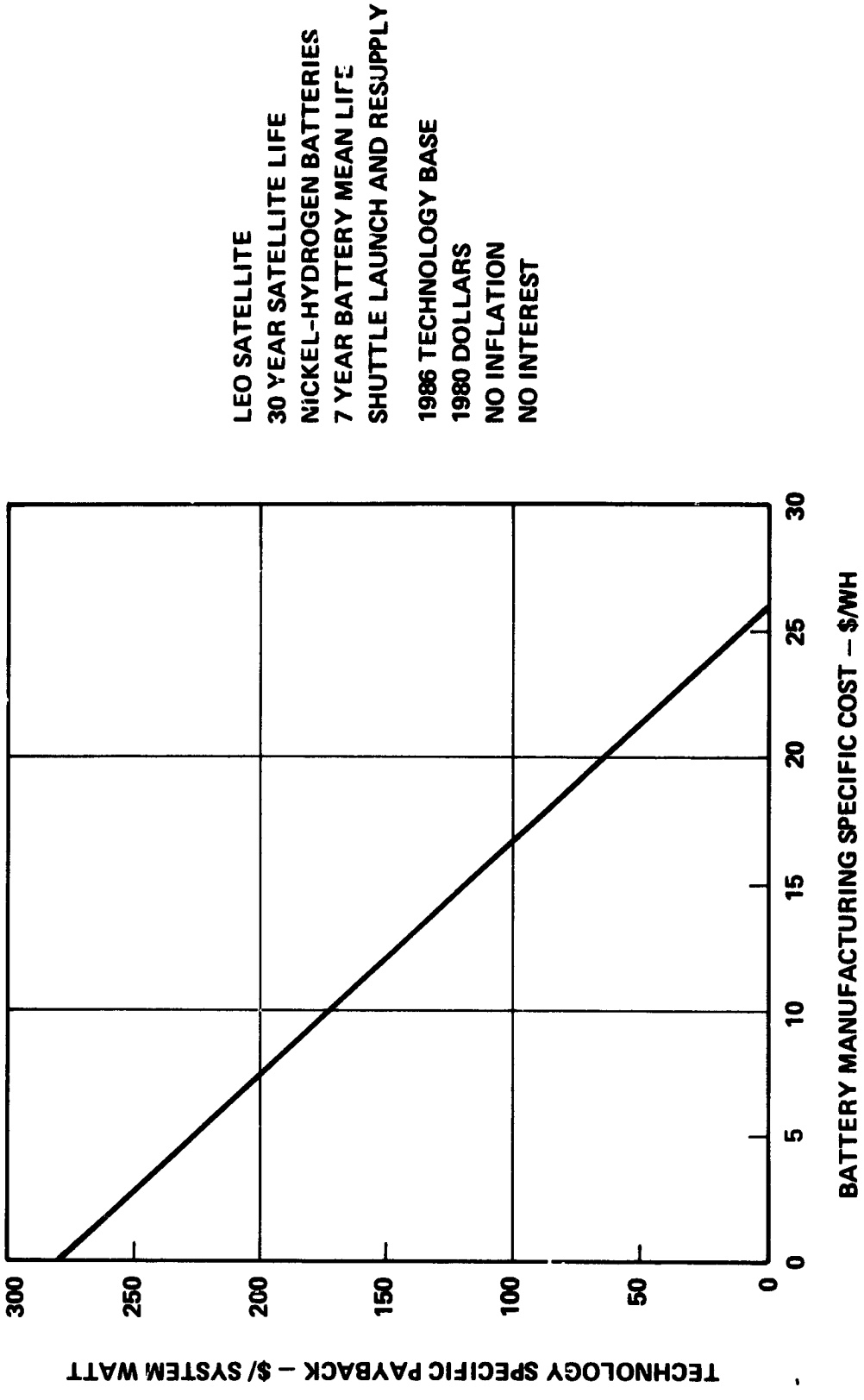

Figure 10-1. Investment Value of Manufacturing Cost Improvements

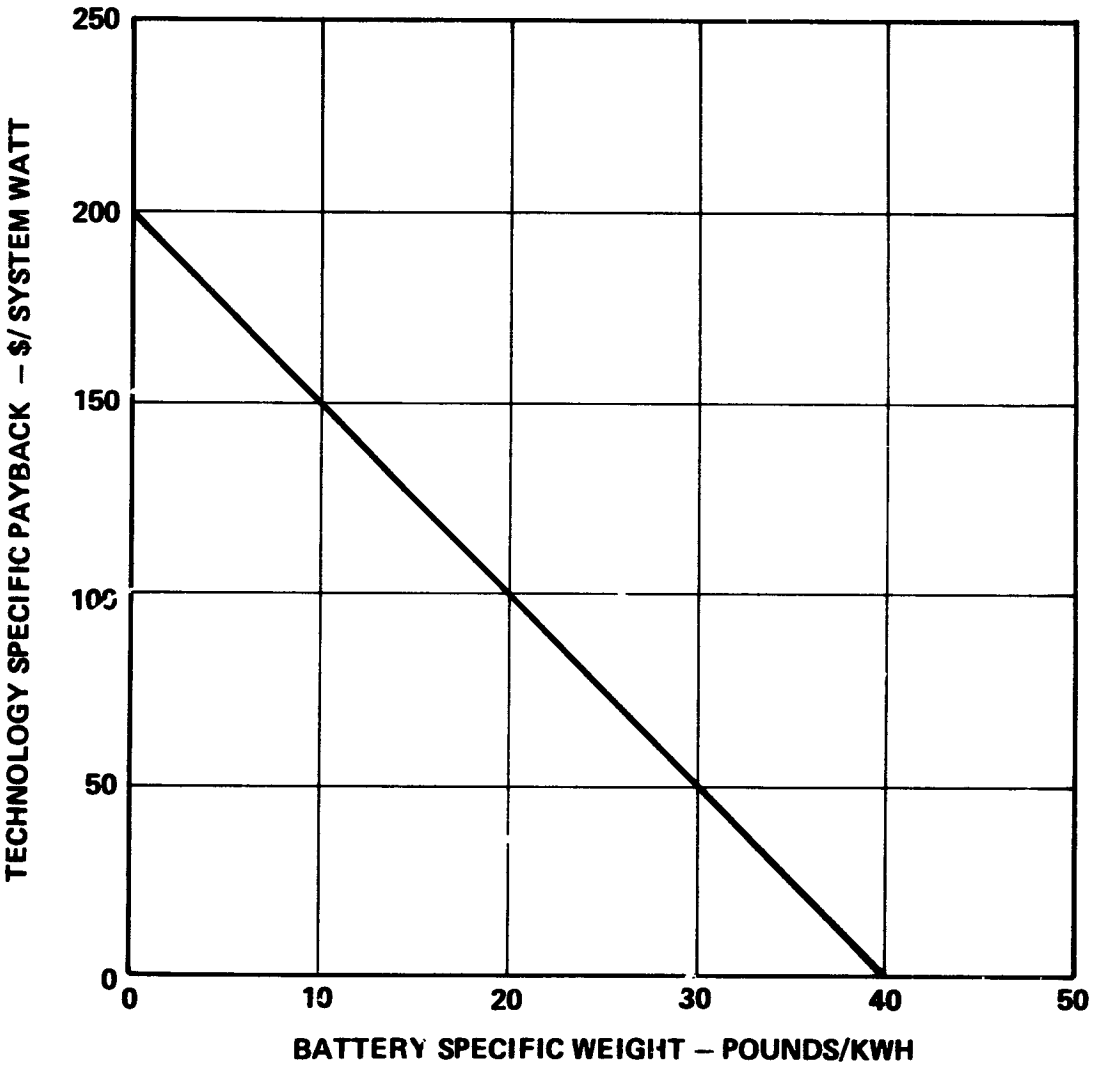

LEO SATELLITE
30 YEAR SATELLITE LIFE
NICKEL-HYDROGEN BATTERIES
7 YEAR BATTERY MEAN LIFE
SHUTTLE LAUNCH AND RESUPPLY

1986 TECHNOLOGY BASE
1980 DOLLARS
NO INTEREST
NO INFLATION

Figure 10-2. Investment Value of Battery Weight Reduction

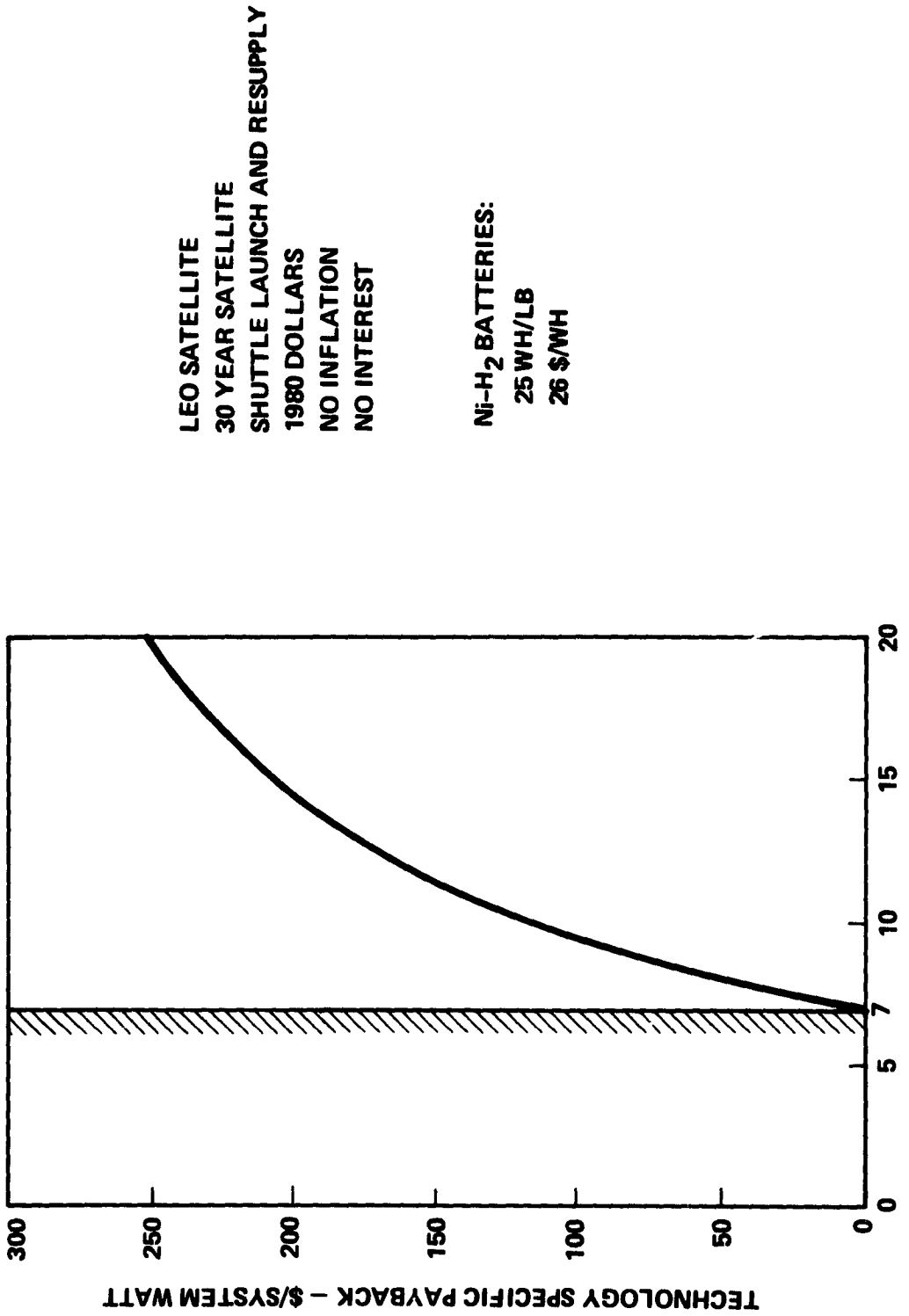

Figure 10-3. Investment Value of Battery Life Improvement

Applying the graph of technology payback (Figure 10-1) to the aggregate system power* (250 kilowatts for the example), yields the evaluation criteria, Figure 10-4. From this figure, gross payback is identified for each option, and net payback derived (gross payback minus investment):

	Proposal 1	Proposal 2	Proposal 3
Gross payback (M$)	37	43	46
Net payback (M$)	22	22	23

Now consider the total return (net payback/investment) and incremental return (difference in net payback/difference in investment between two options) of each proposal:

	Proposal 1	Proposal 2	Proposal 3
Total return (%)	147	105	100
Incremental return (%)	147	0	11

Each of the total returns looks attractive. However, comparing incremental returns shows Proposal 3 to be poor (11 percent return on the increased investment over Proposal 1). Hence, the economical choice is Proposal 1 rather than no investment, Proposal 2, or Proposal 3. However, Proposal 3 is acceptable if the additional investment capital is available and this money cannot be invested elsewhere (in other technologies) at a better return.

Similar graphs for technology specific payback of solar array manufacturing costs and specific weight, and power conversion specific cost were generated and are presented herein (Figures 10-5 through 10-11).

*Aggregate system power should be the sum of all satellite power systems to which the technology is applicable.

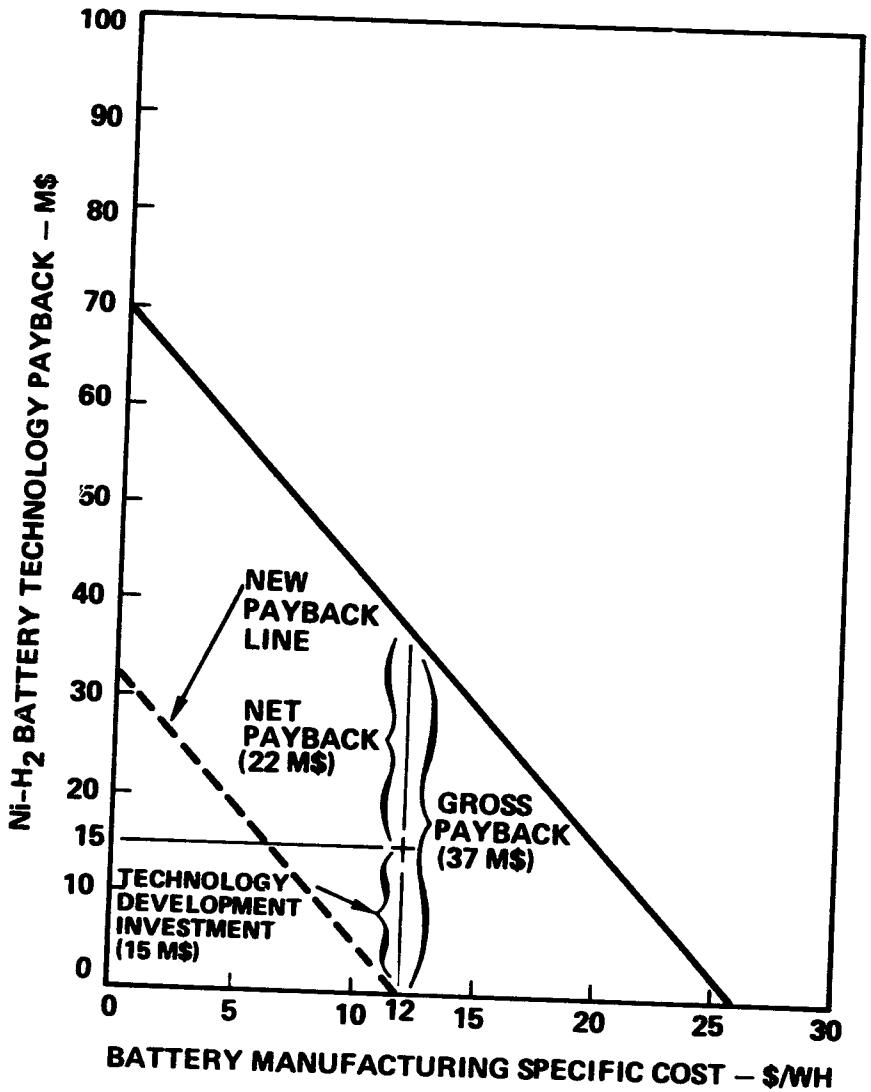

HYPOTHETICAL INVESTMENT = 15 M$

TECHNOLOGY IMPROVEMENT TO 12 $/WH

GROSS PAYBACK = 37 M$

NET PAYBACK = 22 M$

250 KW SYSTEM; LEO

Ni-H_2 BATTERIES

7 YEAR MEAN LIFE

1980 DOLLARS

NO INFLATION

NO INTEREST

Figure 10-4. Example of Technology Investment Evaluation (Nickel-Hydrogen Battery Manufacturing Cost Investment Value)

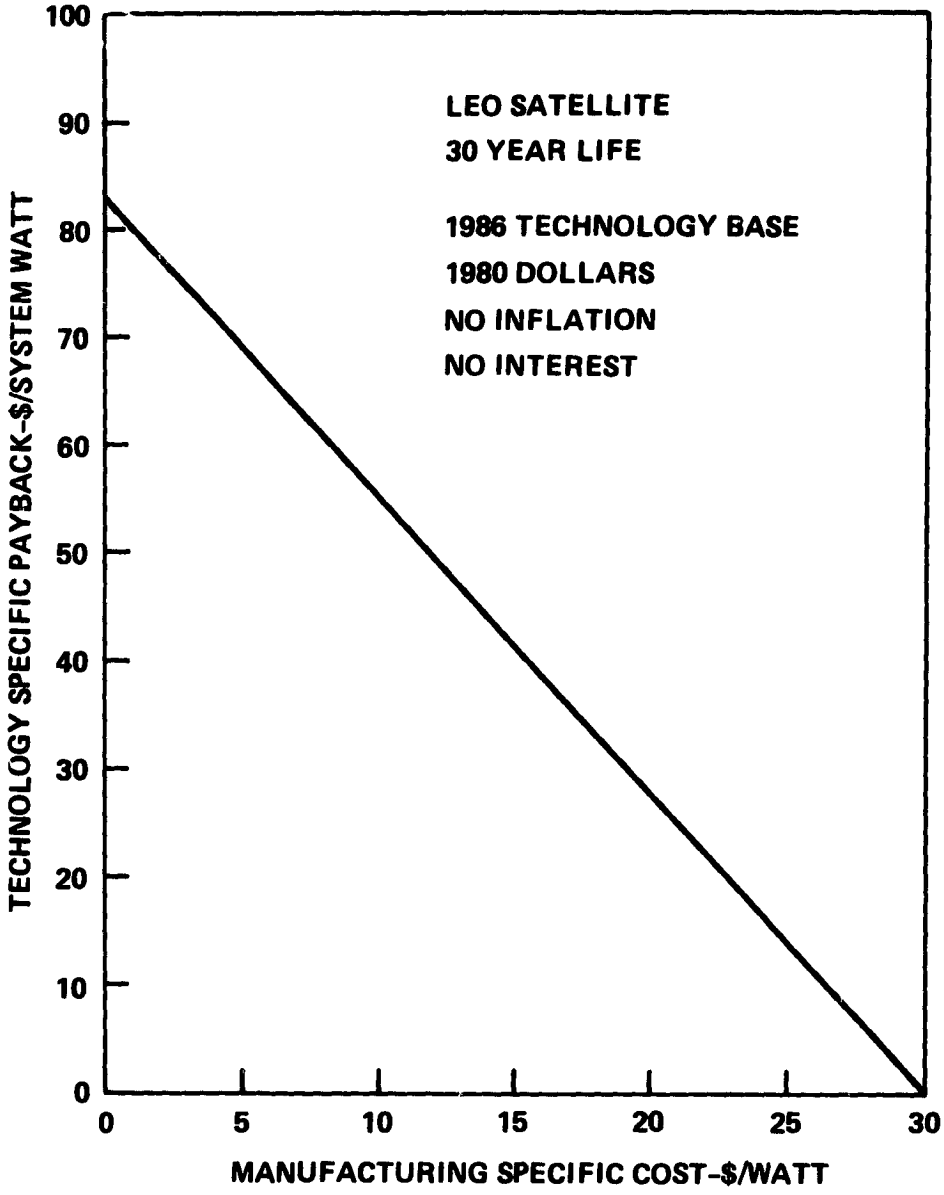

Figure 10-5. Solar Array Manufacturing Cost Investment Value

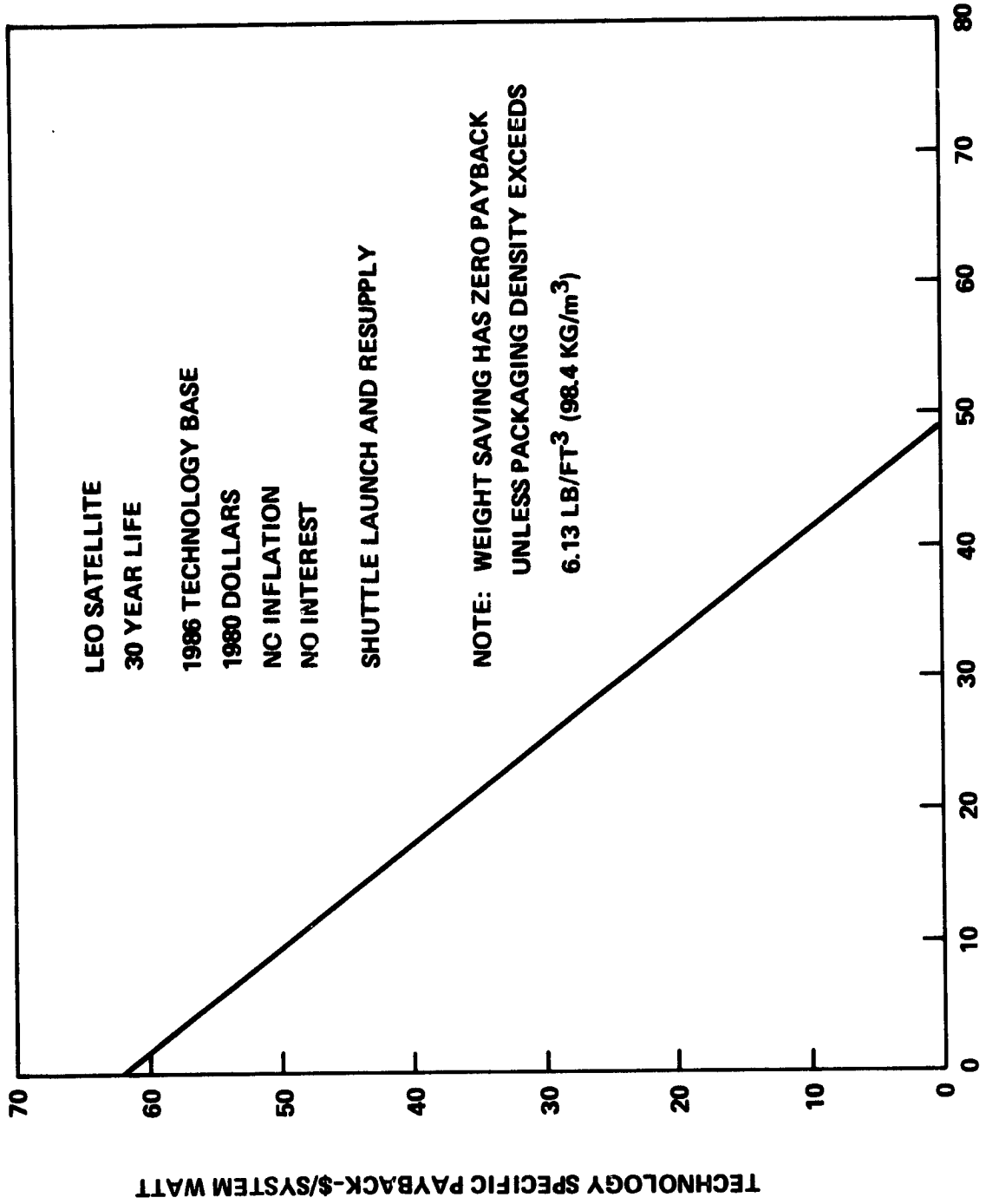

Figure 10-6. Solar Array Weight Investment Value

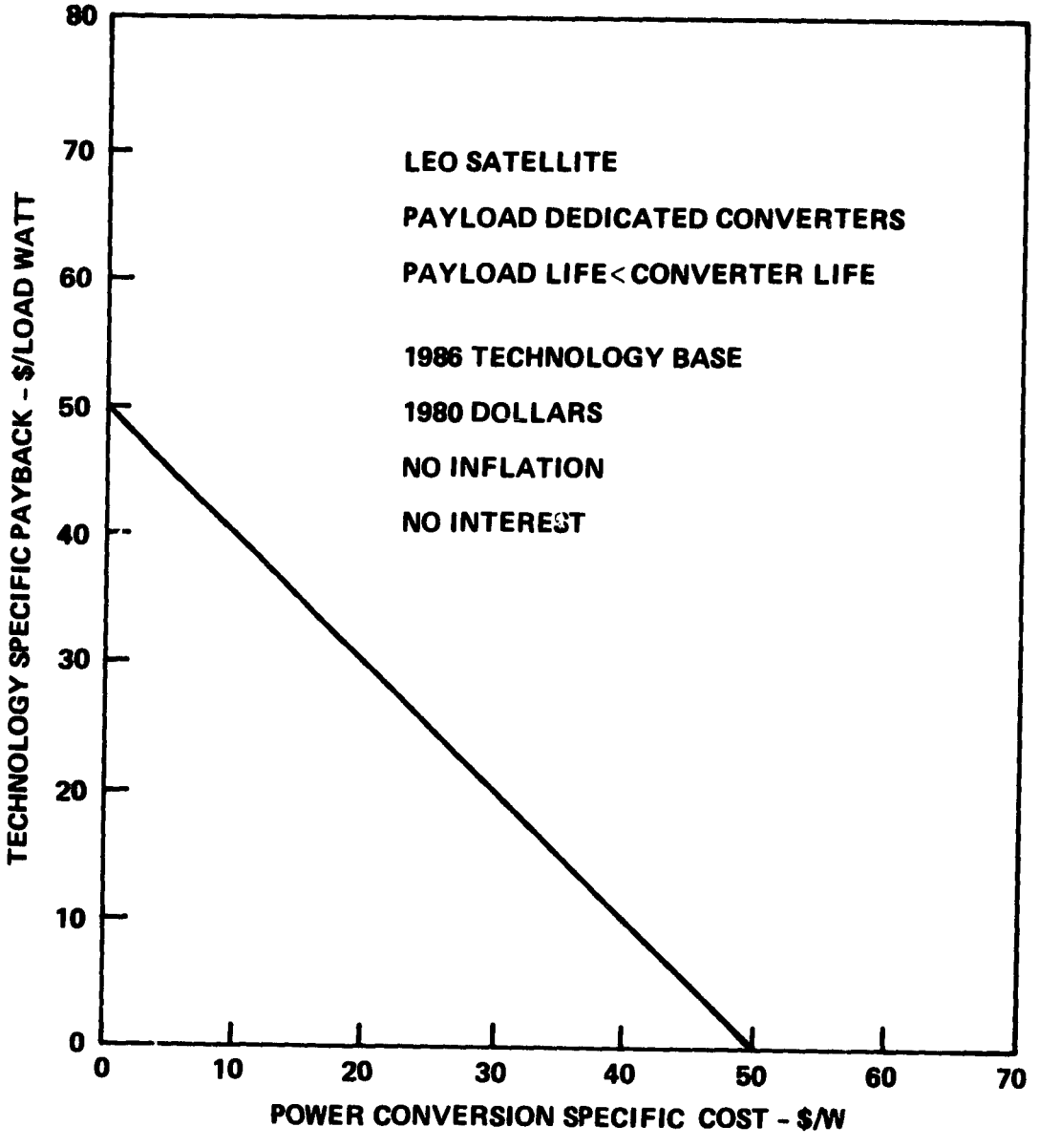

Figure 10-7. Power Conversion Manufacturing Cost Investment Value

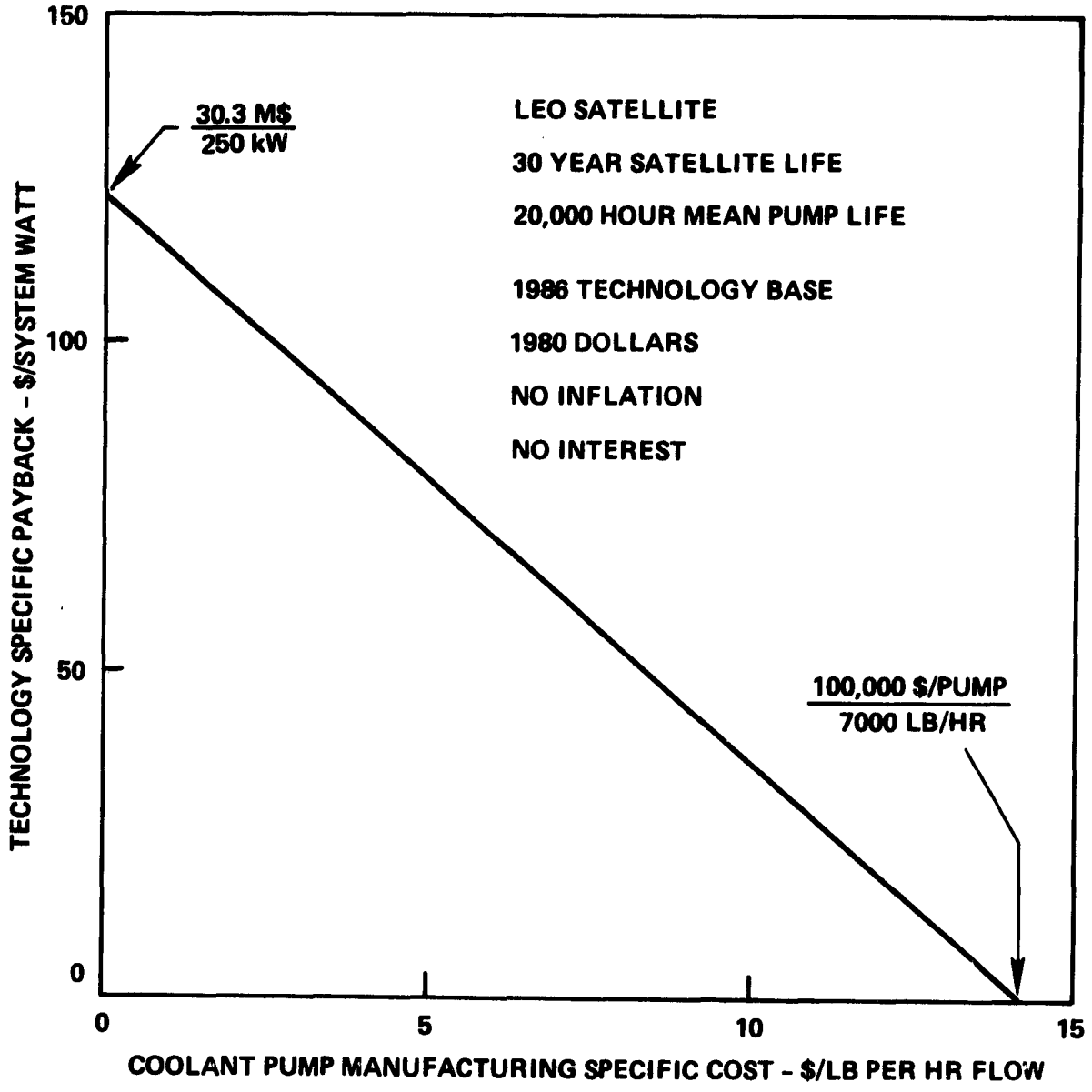

Figure 10-8. Coolant Pump Manufacturing Cost Investment Value

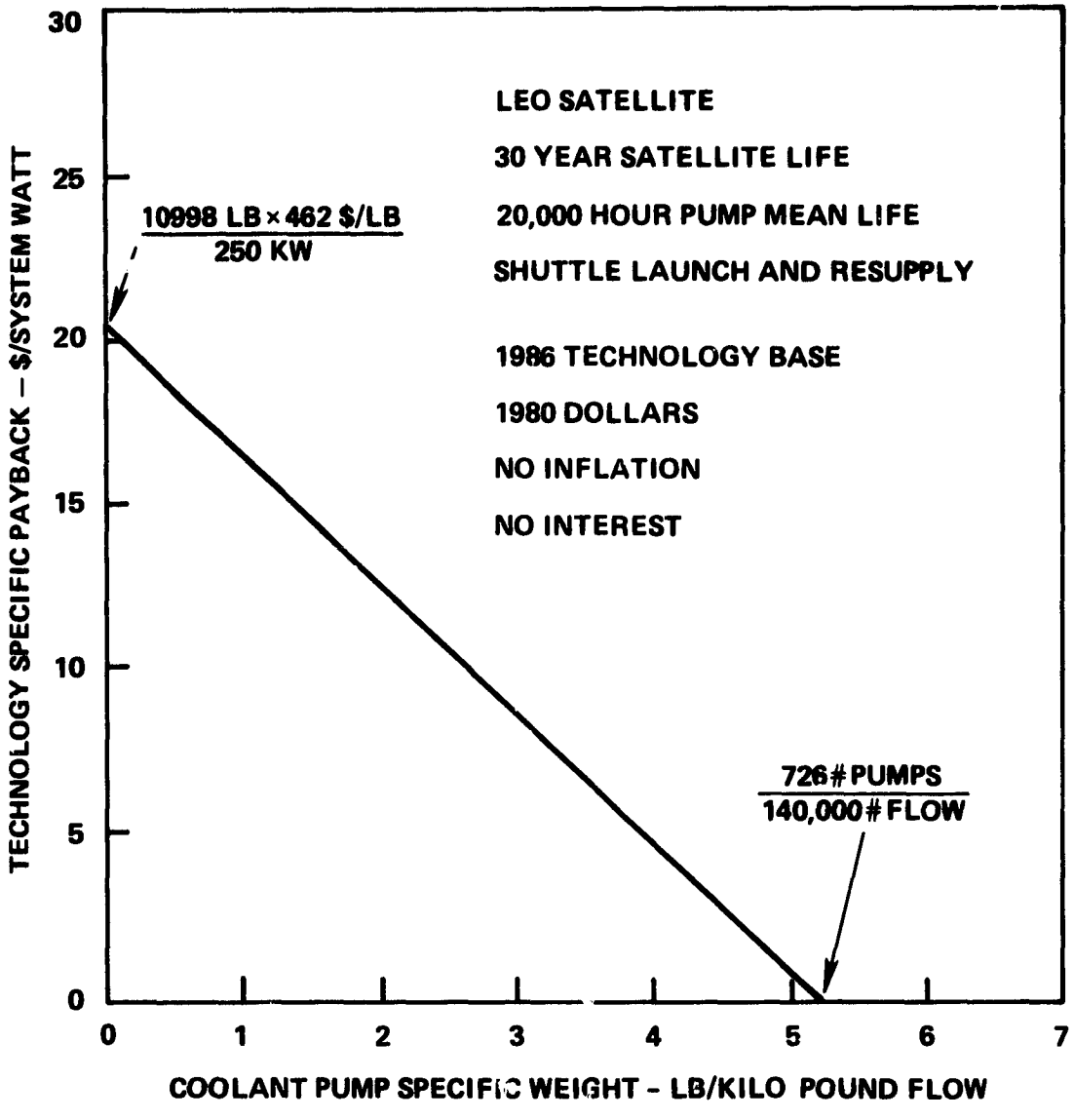

Figure 10-9. Coolant Pump Weight Investment Value

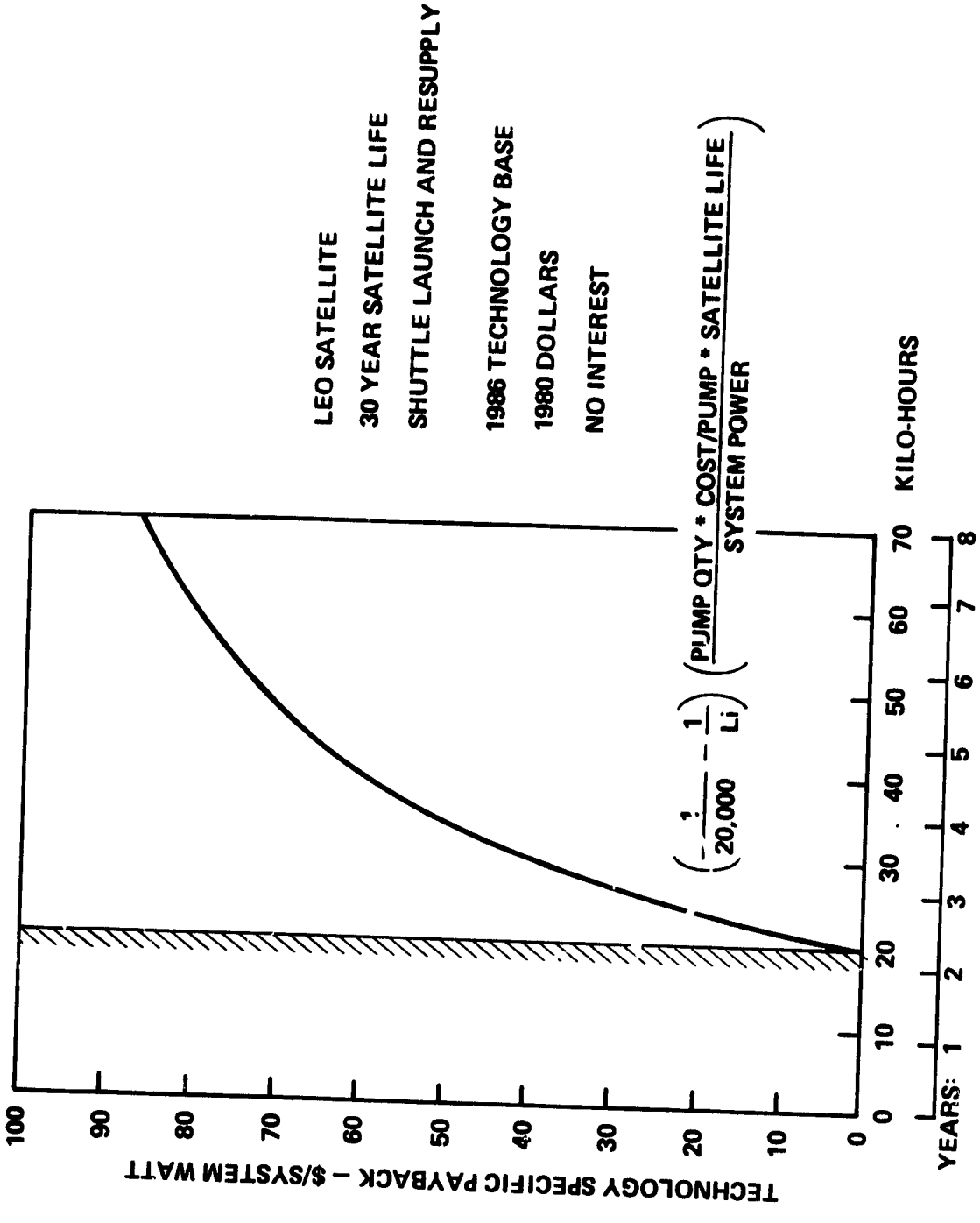

Figure 10-10. Coolant Pump Life Investment Value

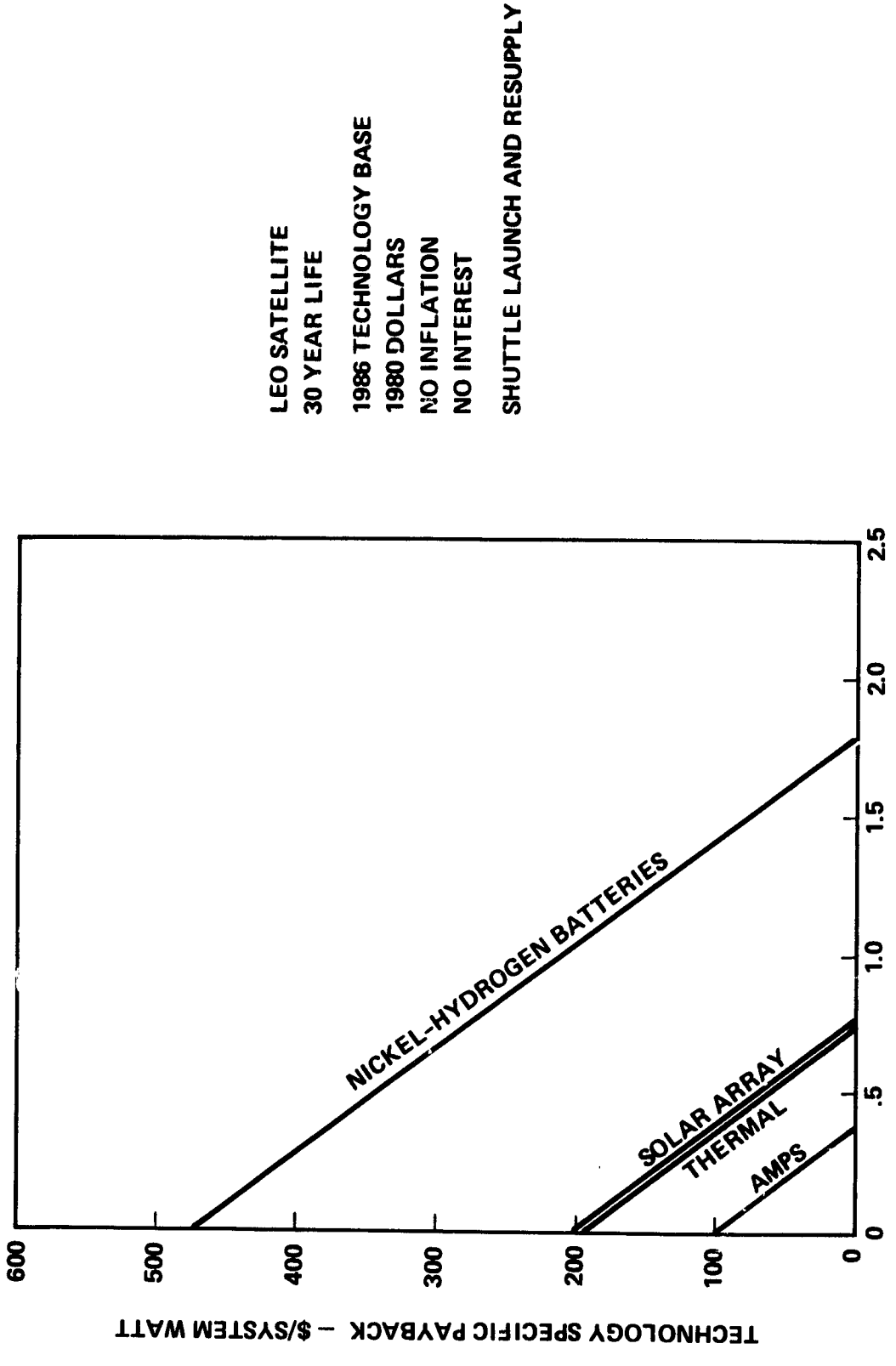

Figure 10-11. EPS Investment Payback

11. REFERENCES

4-1 33295-6001-UT-00, "Study of Multikilowatt Solar Arrays for Earth Orbit Applications," Final Technical Report, dated 19 September 1980, by TRW; Contract NAS8-32986.

4-2 SSD 80-0064, "Study of Multi-KW Solar Arrays for Earth Orbit Applications," Final Report, dated May 15, 1980, by Rockwell International; Contract NAS8-32988.

4-3 LMSC-D715841, "Study of Multi-kW Solar Arrays for Earth Orbit Application," Final Report, dated 30 April 1980, by Lockheed Missiles & Space; Contract NAS8-32981.

5-1 Willard R. Scott, AFAPL-TR-70-61, "Two Kilowatt Long Life Battery," dated September 1970.

5-2 W. R. Scott and D. W. Rusta, "Sealed-Cell Nickel-Battery Applications Manual," NAS5-23514, dated 5 May 1978.

5-3 P. F. Ritterman, Report 77-8725.6-132, "1977 IR&D Final Report, Lightweight Ni-Cd Battery Development Study," dated 31 December 1977.

5-4 ECOES-12, "Electrochemical Cell Technology for Orbital Energy Storage, State-of-Art Assessment", dated November 19, 1979, by General Electric; Contract NAS9-15831.

5-5 Letter from L. J. Nuttall of General Electric to Charles Sollo of TRW, dated April 22, 1980, on life and costs for 250 kW fuel cell and electrolysis system components of GE Report ECOES-12.

5-6 TRW 76-2286.56, "A Temperature and Depth-of-Discharge-Dependent Weibull Reliability Model for Satellite Batteries", by L. G. Robertson, dated July 23, 1976.

6-1 NASA CR-165413, High Voltage DC Switchgear Development for Multi-KW Space Power Systems", Final Report, dated November 1981, by Westinghouse Electric (WAED-81-05E); Contract NAS3-21755.

7-1 "Interaction of Large, High Power Systems with Operational Orbit Charged Particle Environments," by C. K. Purvis, J. J. Stevens, and F. D. Berkopec; NASA/LeRC TM-73867, dated October 1977.

7-2 "Sheath Effects Observed in a 10 Meter High Voltage Panel in Simulated Low Earth Orbit Plasma," by J. E. McCoy and A. Konradi; Spacecraft Charging Technology Conference - 1978 Proceedings NASA Conf. Pub. 2071, AFGL-TR-79-0082, November 1978.

7-3 "Accident Prevention Manual for Industrial Operations," National Safety Council, sixth edition, p. 976, Table 33-A.

APPENDIX A

STATEMENT OF WORK

I. BACKGROUND - SPACE POWER SYSTEMS

NASA has installed on orbit a cumulative total of about 100-kilowatts of solar power generating capability since its inception. Single missions are now being planned for initial operating capability (IOC) in the mid-1980's that greatly exceed that total. The high capacity technology for energy generation, storage and management that such systems require does not now exist, and must be provided if the cost and risk of major future orbital system developments are to be reduced to acceptable levels. The historical cost of space energy has been very high - in the range of $1000 per kilowatt-hour (kWh). For reference, this compares to energy costs on the ground of about 5 cents per kWh. Missions of the mid-1980's are expected to require 10^5 - 10^7 kWh per year implying unacceptable costs unless the historical cost trends can be dramatically reduced.

As a result of this critical need for low cost energy in orbit, NASA is actively seeking ways to increase its energy capacity in the immediate future to both extend the operating capability of the Shuttle and to power a broad range of space applications. It can be expected that the severity of this need will increase with Shuttle activity independent of the specific future that is chosen. Therefore, a 250 kilowatt, low earth orbit (LEO) photovoltaic power system with a technology readiness of 1985-86 and an IOC of 1988 has been selected as a technology focus. The objectives of this effort are to generate a reference design and an investment payback criteria for the technology focus and to assess the technology, identify the deficiencies and define the requirements and designs for the power management subsystem of the technology focus.

II. STUDY TASKS

The contractor will provide the personnel, facilities, materials, and equipment to perform the following tasks:

TASK 1 - SYSTEM DESIGN AND TECHNOLOGY DEVELOPMENT

a) Generate reference design(s) for a 250 kilowatt LEO photovoltaic electrical power system (EPS). Specific reference designs for the solar array, energy storage and power management sybsystems will be included. The reference design(s) will reflect 1985 - 86 technology readiness with an IOC of 1988.

b) Establish an EPS technology investment criteria and perform payback assessments for various investment options.

c) Assess geosynchronous earth orbit operations for commonality of interfaces and potential design options which can be selected to enhance investment payback.

d) Specific outputs from Task 1 will include:

   1) Candidate electrical power system and subsystem concepts and selection criteria.

   2) Technology assessment studies including analysis and definition of system and subsystem design parameters and preliminary specifications of component characteristics required to meet system criteria.

   3) A handbook of EPS technology investment criteria and payback assessments.

TASK 2 - POWER MANAGEMENT SUBSYSTEM DEVELOPMENT

a) Assess current technology and define the technology developments required for a 250 kilowatt Autonomously Managed Power System (AMPS). The assessment will include the selection of an AMPS concept and sufficient trade studies at the technology selection level, to justify the concept selected. Factors to be considered in the trade studies will include voltage levels, status monitoring and assessment, fault sensing, protection, load sequencing, and automatic load transfer.

b) Perform preliminary design of candidate AMPS approach based on 1985/86 technology readiness.

c) Define the component and process deficiencies and the technology drivers for the 250 kilowatt AMPS. Include software modeling and analysis requirements for AMPS system evaluation and integration and identify critical paths of technology development.

d) Perform final detailed design of the AMPS to meet the requirements of the technology focus. The detailed design shall include generation of final schematics, sketches, specifications, and parts lists for the AMPS and its associated hardware.

e) Fabricate and test a breadboard of the AMPS design generated in Task 2D. The breadboard shall include the power management, control and protection elements and shall be fabricated for integration into the high voltage test facility (AMPS Test Facility) at MSFC. The breadboard test results, operating instructions, and all required software shall be documented and included as a part of the final report for Task 2.

TASK 3 - AMPS TEST FACILITY

Support the expansion and upgrading of the NASA/MSFC 25 - 50 kW high voltage test breadboard into a test bed of the 250 kilowatt AMPS including power source, energy storage and load simulators. The test facility will include a minimum of three power channels to adequately simulate and assess the failure effects of one channel on the rest of the system and the interaction between the remaining on-line channels during fault isolation and load redistribution. Specific outputs for this task will include:

a) A preliminary design of the expanded test facility. The facility will support the evaluation of components considered for incorporation into the AMPS and the verification of the automated management, control and protection philosophy and hardware.

b) Schematic diagrams, installation sketches and component/unit interface wiring lists for the upgraded NASA/MSFC test facility.

c) A final detailed design of the expanded high voltage test facility. The facility shall support the evaluation of the AMPS and other advanced technology hardware proposed for use in multihundred kilowatt power systems. The detailed design shall include generation of final schematics, installation sketches, componenunit interface wiring lists, and parts lists for the upgraded NASA/MSFC test facility.

APPENDIX B

SHUTTLE TRANSPORTATION COST

1. SUMMARY

A typical Shuttle transportation cost is derived for 1980 from the "Space Transportation System Reimbursement Guide" (Reference 1). This cost is applied in the analyses of this study to optimize trade selections based upon life cycle cost and to assess payoff potential for technology development. Shuttle costs are both weight and volume computed, but weight is normally the applicable factor. Shuttle costs are 462 $/lb for a "dedicated user" wherein the entire Shuttle capability (10,600 cubic feet and/or 65,000 pounds) is applied to a single user (mission). This is typical for the initial deployment of a 250-kilowatt system as several launches are projected - one for the solar array; one for energy storage, conversion, and thermal control. Subsequent resupply/replacement/refurbishment missions may not require the entire Shuttle capability. Costs are then 615 $/lb for utilization of less than 75 percent of the Shuttle capability. Consequently, refurbishment scenarios utilizing less than the full Shuttle capability (implying user shared launches) should be avoided.

Table 1. Shuttle Transportation Costs

Specific Costs:
• 2,830 $/ft^3 (100,000 $/m^3)
• 462 $/lb (1016 $/kg)
Constraints:
• Shuttle launch dedicated to mission
• Shuttle capability fully utilized
• 160 nmi delivery (circular orbit)
• 28.5-degree orbit inclination
• 30 M$/launch (1980 $)

2. COST DERIVATION

The cost for a dedicated user of a Shuttle launch is defined as 18 million dollars in 1975 for a U. S. Government user (Reference 1). This is a base price and any optional services must be added to this price. [A nominal satellite mission can incur 12-15 M$ (1975) in options.] A minimum set of options is herein identified for the initial deployment of the 250-kilowatt system. These options aggragate 2.1 M$ (1975):

Option	Cost Rate	Estimate
Payload specialist	At $100,000/day	$300,000
Extravehicular activity	At $100,000/event	300,000
Additional time on orbit	At $300,000/day	900,000
JSC payload operations	(negotiated)	300,000
Launch site services	(negotiated)	300,000
		$2,100,000

A payload specialist is included in the crew to support the unique demands of initial deployment, solar array erection, and module assembly. Extravehicular activity is also included to support the buildup scenario. Several days are expected to remove the payload from the Shuttle cargo bay, to deploy, assemble, and erect the Shuttle payload, and to validate initial performance (checkout). (A faulty module would be retrieved and returned.) Hence, an allowance for three days on station is provided. During this period, special communications and/or control of the payload will be required. An allowance is included for JSC payload operation/coordination during this period. An allowance is also included for prelaunch payload installation and checkout. This allowance is small and primarily for mechanical installation and communication validation. Full scale payload checkout at the 250-kilowatt level is not considered practical in the Shuttle cargo bay.

Summing the base cost and option cost yields a 1975 cost of 20.1 M$ for a dedicated Shuttle launch. A similar scenario of options is expected for any resupply mission (dedicated or shared). Hence, this cost will be applied for both initial deployment and resupply missions. However, this value must be appropriately escalated to 1980 dollars.

3. INFLATION

The Shuttle transportation costs are stated in 1975 dollars (Reference 1). This study addresses cost in 1980 dollars. The Shuttle transportation costs must be escalated accordingly. Inflation escalation is accomplished by utilizing the Bureau of Labor Statistics index for total private, nonagricultural compensation per hour (per Reference 1) and an inflation estimate of 8-1/2 percent for 1980 labor rates:

$$\frac{\text{May 1979 labor rate}}{\text{January 1975 labor rate}} \times \text{projected 1980 labor inflation} = \frac{6.07}{4.41} \times 1.085 = 1.49$$

Applying this factor to the 1975 cost of 20.1 M$ yields 30 M$:

20.1 M$ (1957) x 1.49 = 30.0 M$ (1980)

4. SPECIFIC COSTS

This study utilizes specific costs for parametric analyses. The Shuttle volume and weight capabilities are 15 feet in diameter by 60 feet long (10,600 cubic feet) and 65,000 pounds to a low earth orbit (160 nautical miles). Specific costs for a dedicated user are then 2,830 $/cu ft and 462 $/lb:

$$\frac{\$30,000,000}{10,600 \text{ cu/ft}} = 2,830 \text{ \$/cu ft (dedicated user, 1980 \$)}$$

$$\frac{\$30,000,000}{65,000 \text{ lb}} = 462 \text{ \$/lb (dedicated user, 1980 \$)}$$

Resupply missions may not utilize the full Shuttle capability and hence would become user-shared missions. The specific costs for a user-shared misson increase due to the charge factor to load factor ratio of 1:0.75 specified by NASA (Figure 1). Hence, the specific costs for shared Shuttle usage increase by 33 percent:

$$\frac{\$30,000,000}{0.75 \times 10,600 \text{ cu ft}} = 3,744 \text{ \$/cu ft (shared user, 1980 \$)}$$

$$\frac{\$30,000,000}{0.75 \times 65,000 \text{ lb}} = 615 \text{ \$/lb (dedicated user, 1980 \$)}$$

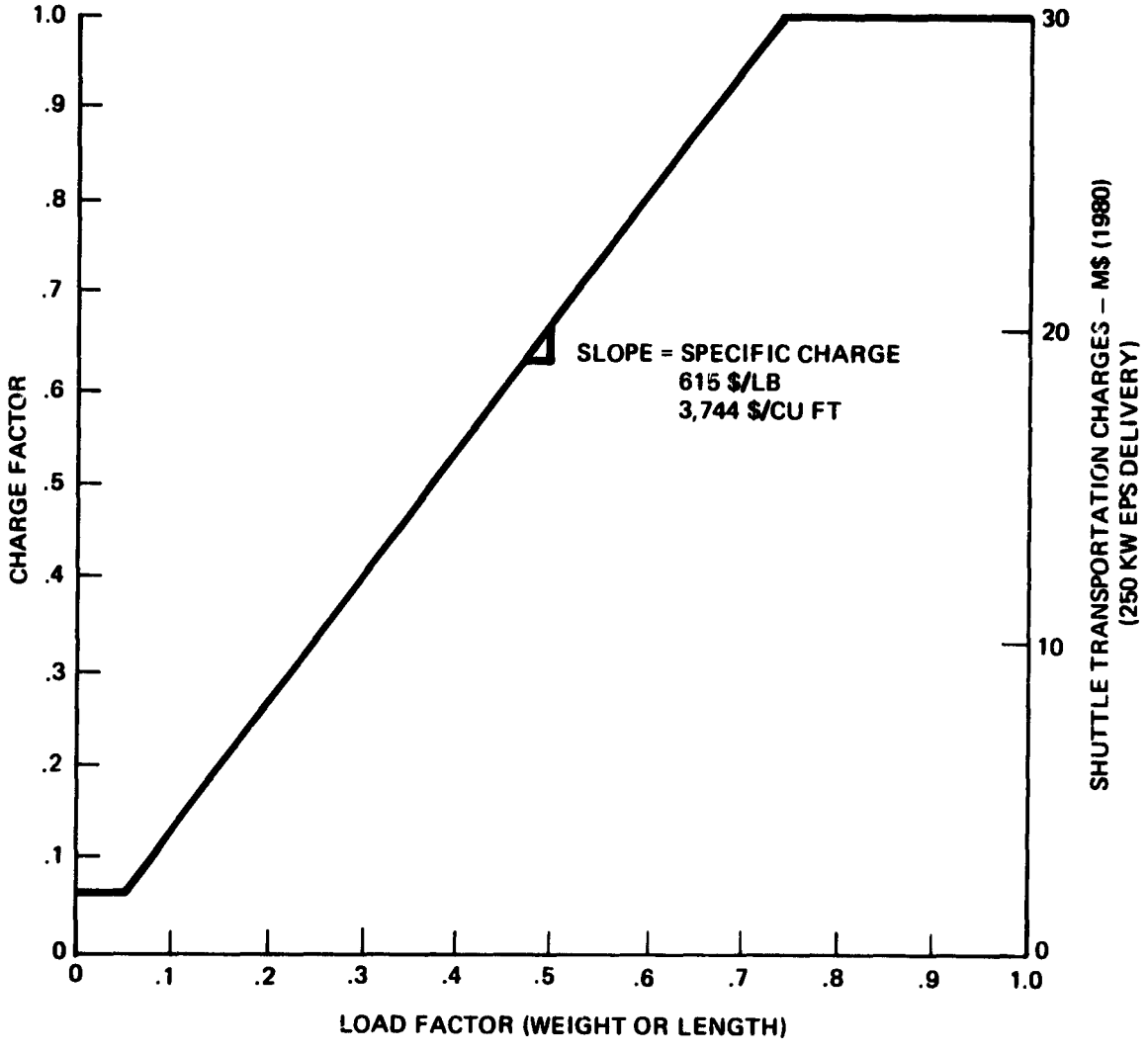

Figure 1. Shuttle Transportation Charges for Shared Use

The application of user-shared Shuttle launches incurs a substantial cost penalty. Therefore scenarios resulting in sharing are presumed avoided. A platform providing 250 kilowatts of payload power is presumed to have sufficient payload exchanges, resupply requirements (fuel, etc), and equipment replacements for failures and preventive maintenance that only dedicated missions are considered in this study.

5. ORBIT DELIVERY

The Shuttle capability to deliver weight into a circular orbit from Kennedy Space Center (KSC) declines as higher altitude orbits and/or other inclinations than 28.5 degrees are required (Figure 2). However, the basic launch cost of 30 M$ remains fixed except for the addition of orbital maneuvering subsystem (OMS) kits that cost approximately 3 million dollars each. Consequently, the specific cost ($/lb) for Shuttle transportation to higher orbits increases significantly with altitude (Figure 3) and dramatically above 600 nautical miles. For this study, a 160-nautical mile, 28.5-degree inclination, circular orbit is assumed and allows the full 65,000 pound delivery at minimum cost. Orbital altitudes to approximately 215 nautical miles with 28.5-degree inclination have essentially the same minimum cost.

6. CARGO VOLUME

The nominal Shuttle cargo bay is 15 feet in diameter by 60 feet long. However, this volume is reduced by EVA access clearances, the associated airlock, and any OMS kits installed (Figure 4). This can be a significant volume reduction for such items as solar arrays, gaseous hydrogen and oxygen tankage for fuel cells, etc. Therefore care must be exercised in coordinating the launch and deployment scenarios, the delivery altitude, and the payload volume requirement.

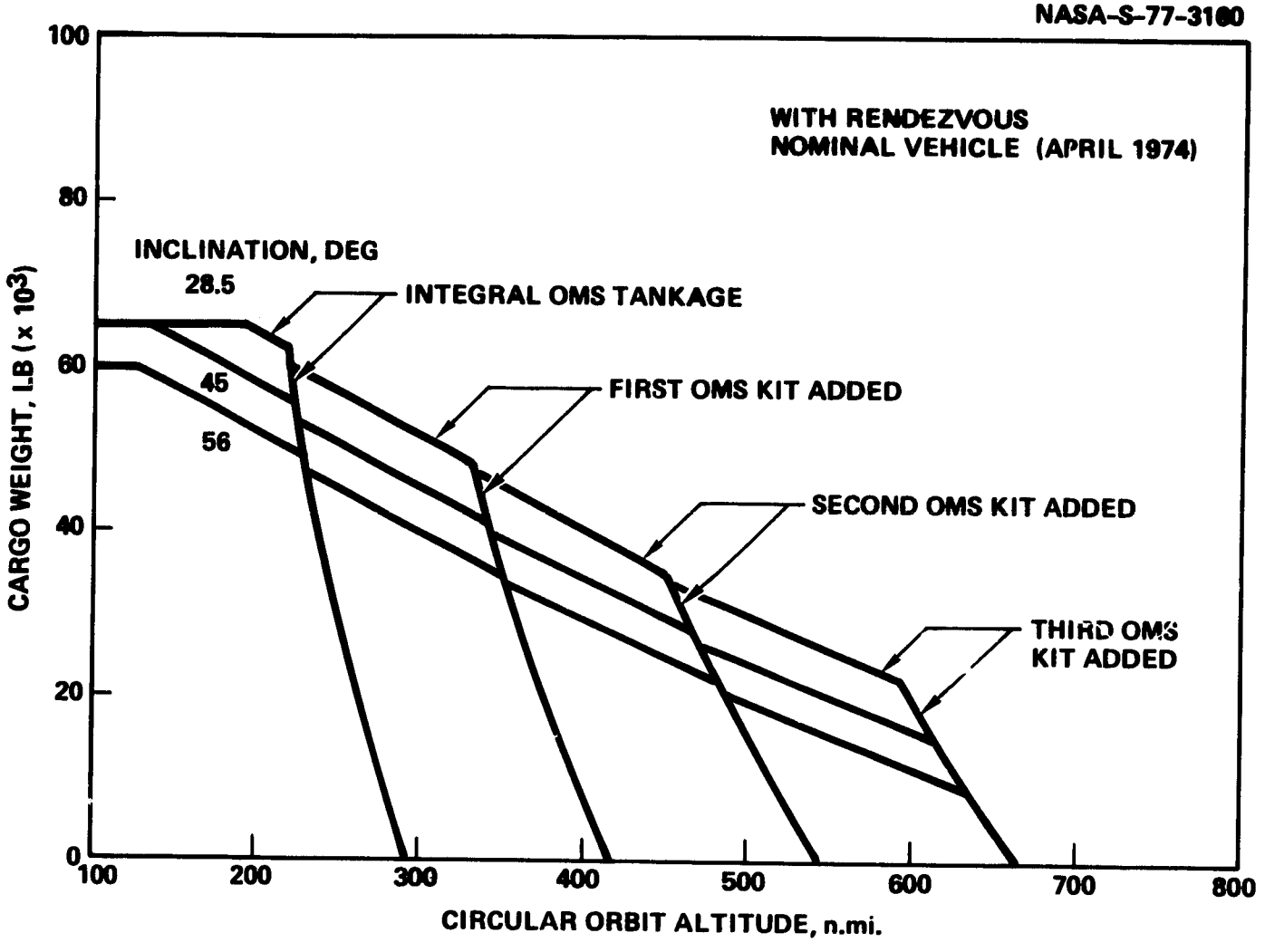

Figure 2. Higher Altitudes Reduce Shuttle Capability

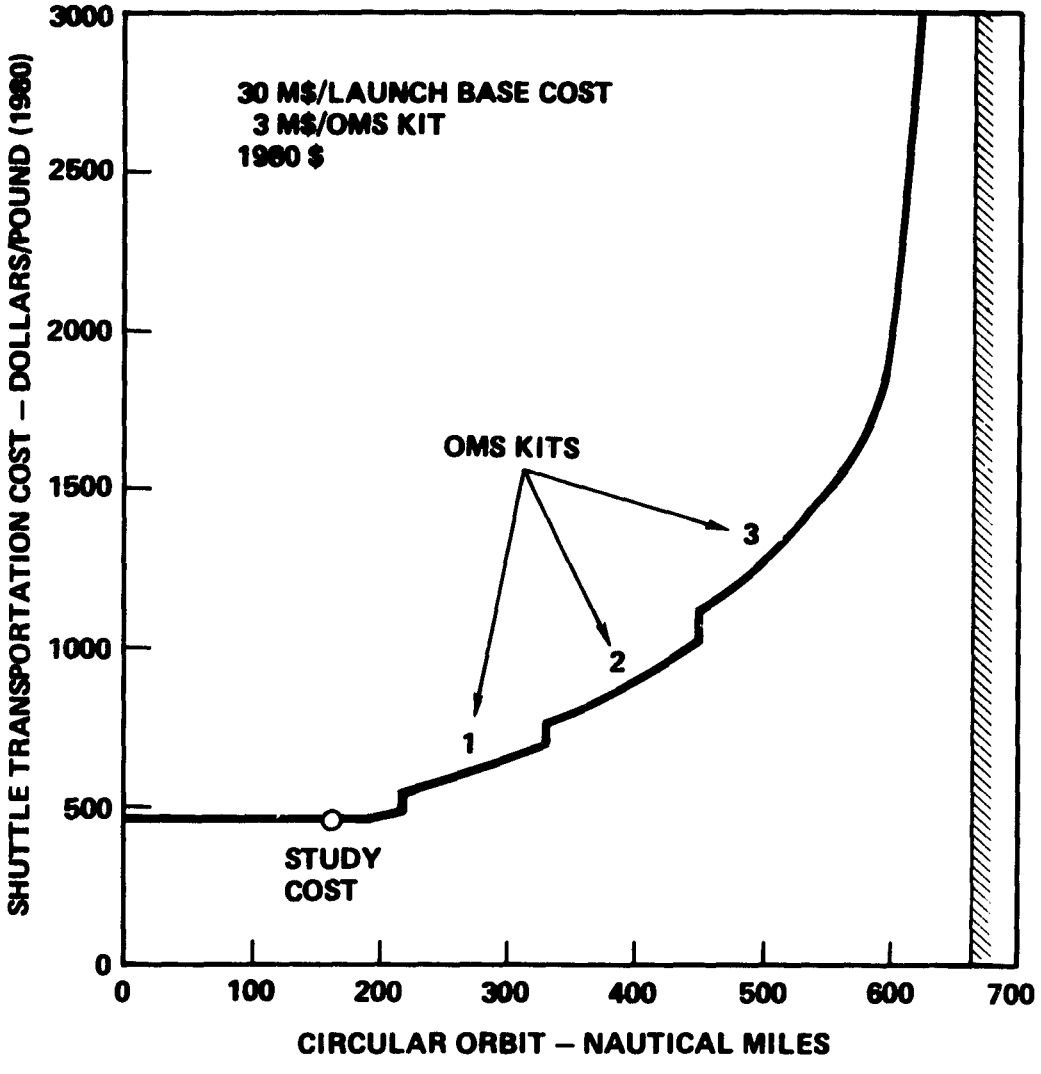

Figure 3. Shuttle Costs Increase Dramatically for Higher Altitude Delivery

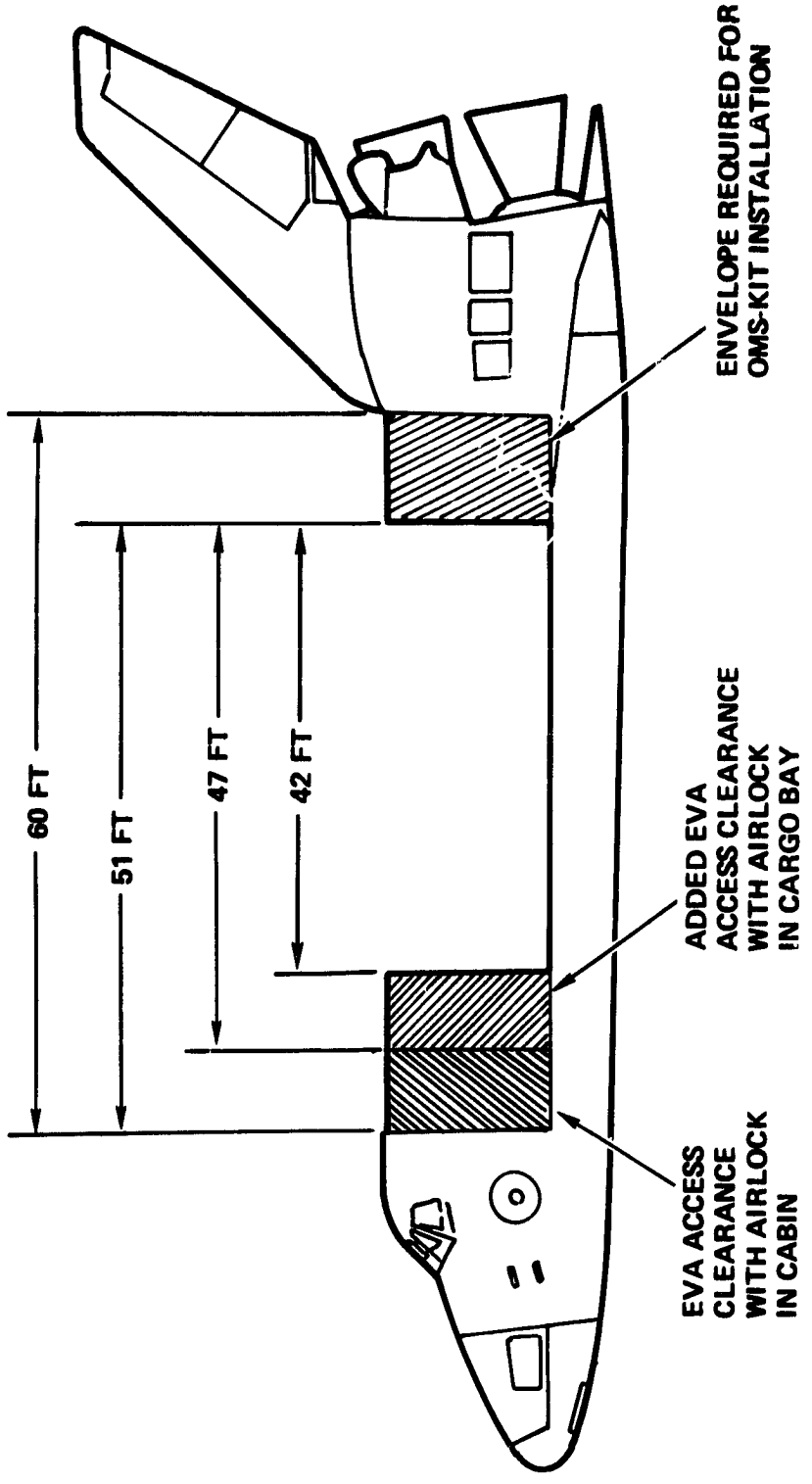

Figure 4. EVA and OMS Reduce Cargo Volume

APPENDIX C

OPTIMUM ORBITAL ALTITUDE

1. PROBLEM

Multihundred-kilowatt solar arrays in low earth orbits incur substantial orbital drag causing orbital velocity decay and altitude loss. Altitude maintenance propellant is required for velocity makeup to preclude orbital decay. Substantial amounts of propellant may be required depending upon the orbital altitude selected and the size of the solar array. This propellant requirement introduces a significant cost for low earth orbits [160 nautical miles (296 kilometers)] over an extended time period. Higher altitudes reduce the propellant cost, but increase the orbital delivery costs for initial satellite deployment, equipment replacement, and satellite payload delivery and retrieval. Evaluation of these opposing cost trends versus altitude indicates an optimum altitude selection near 215 nautical miles (~400 kilometers).

2. ANALYSIS

Shuttle transportation costs, developed in Appendix B, are based upon delivery to a 160 nautical mile (296 kilometer) orbit and result in a specific cost of 462 $/lb (1016 $/kg). Orbits above approximately 190 nautical miles (352 kilometers) reduce the Shuttle payload delivery weight (Figure 1). However, the launch costs remain fixed at 30 M$ per launch (1980 $) plus 3 M$ per orbital maneuvering subsystem kit (OMS kit) added to reach successively higher orbital altitudes. Specific costs increase accordingly with delivery altitude (Figure 2). This results in moderately increased Shuttle transportation costs to place the power subsystem in successively higher orbits (Figure 3), but satellite payloads also incur greater orbital delivery costs. A scenario of one Shuttle flight every 1 or 2 years delivers 2 or 1 million pounds of experiments into 160 nautical mile orbits over 30 years. These costs escalate accordingly (Figure 3) for orbits higher than 190 nautical miles (352 kilometers). The solar array for a 250-kilowatt electrical power subsystem utilizing nickel-hydrogen energy storage is expected to be approximately 690 kilowatts at the beginning of life. This solar array size is therefore selected to develop the altitude maintenance propellant weight and cost.

The daily propellant consumption for altitude maintenance (Figure 4) is taken from the Rockwell International study* of multikilowatt solar arrays. These curves are interpolated for the 700-kilowatt array. Daily propellant consumption is converted to a 30-year requirement accordingly:

Consumption in kg/day x 2.2 lb/kg x 365.25 days/yr x 30 yr.

Propellant manufacturing costs are neglected as miniscule compared to the Shuttle transportation costs of 462 $/lb minimum. The Shuttle delivery costs (Figure 2) are applied to the various 30-year propellant weights for delivery to the respective orbital altitudes (Figure 5). Maintenance of an orbital altitude below approximately 215 nautical miles (400 kilometers) becomes very expensive over 30 years.

A minimum exists in the sum of altitude maintenance propellant delivery cost and incremental cost for satellite, resupply, and experiment delivery to higher orbits (Figure 6). These cost minimums occur for orbital altitudes in the range of 215 to 270 nautical miles (400 to 500 kilometers). As the experiment delivery to orbit increases beyond 33,000 lb/yr (one million pounds over 30 years) the minimum sharpens and moves toward 215 nautical miles. Further, the 215 nautical mile circular orbit is essentially the limit of the cargo delivery capability of the basic Shuttle without additional OMS kits. Higher orbits, requiring OMS kits, significantly reduce the available cargo volume (length) in the Shuttle (Figure 7). Therefore, the 215 nautical mile altitude is considered an optimum cost altitude for the 30-year period considered in this study.

*SSD 80-0064, "Study of Multi-KW Solar Arrays for Earth Orbit Applications," Final Report dated May 15, 1980, by Rockwell International, Contract NAS8-32988.

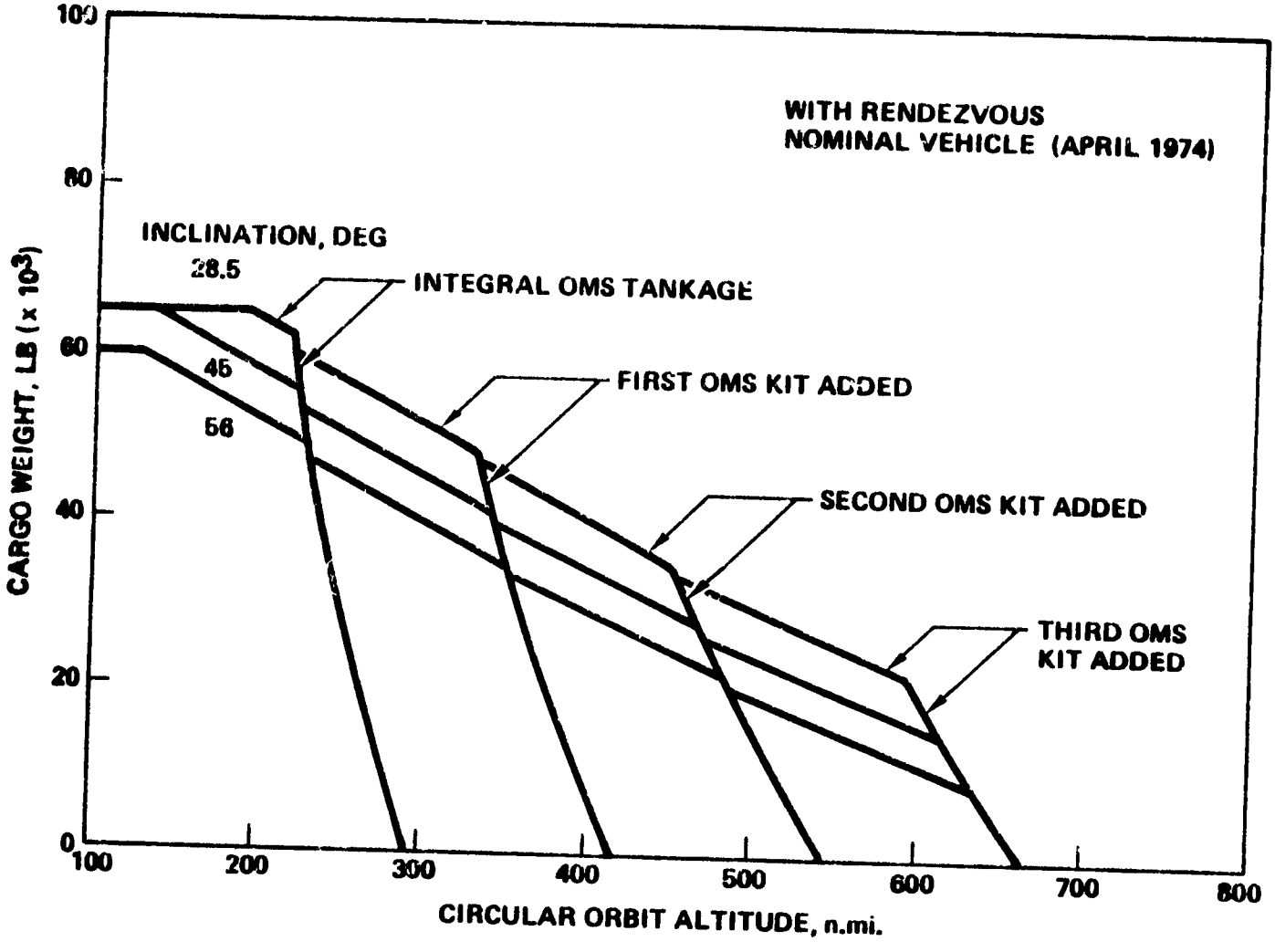

Figure 1. Higher Altitudes Reduce Shuttle Capability

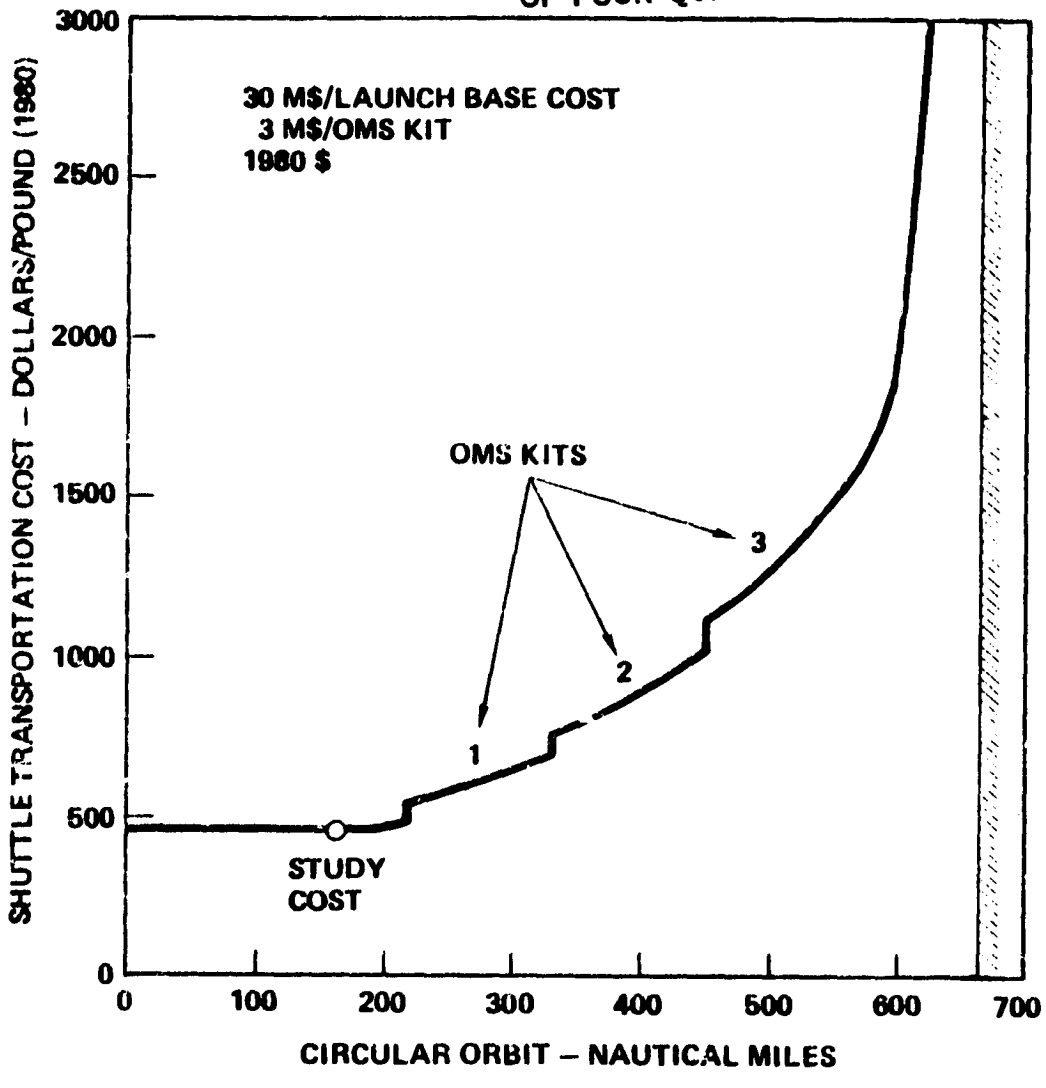

Figure 2. Shuttle Costs Increase Dramatically for Higher Altitude Delivery

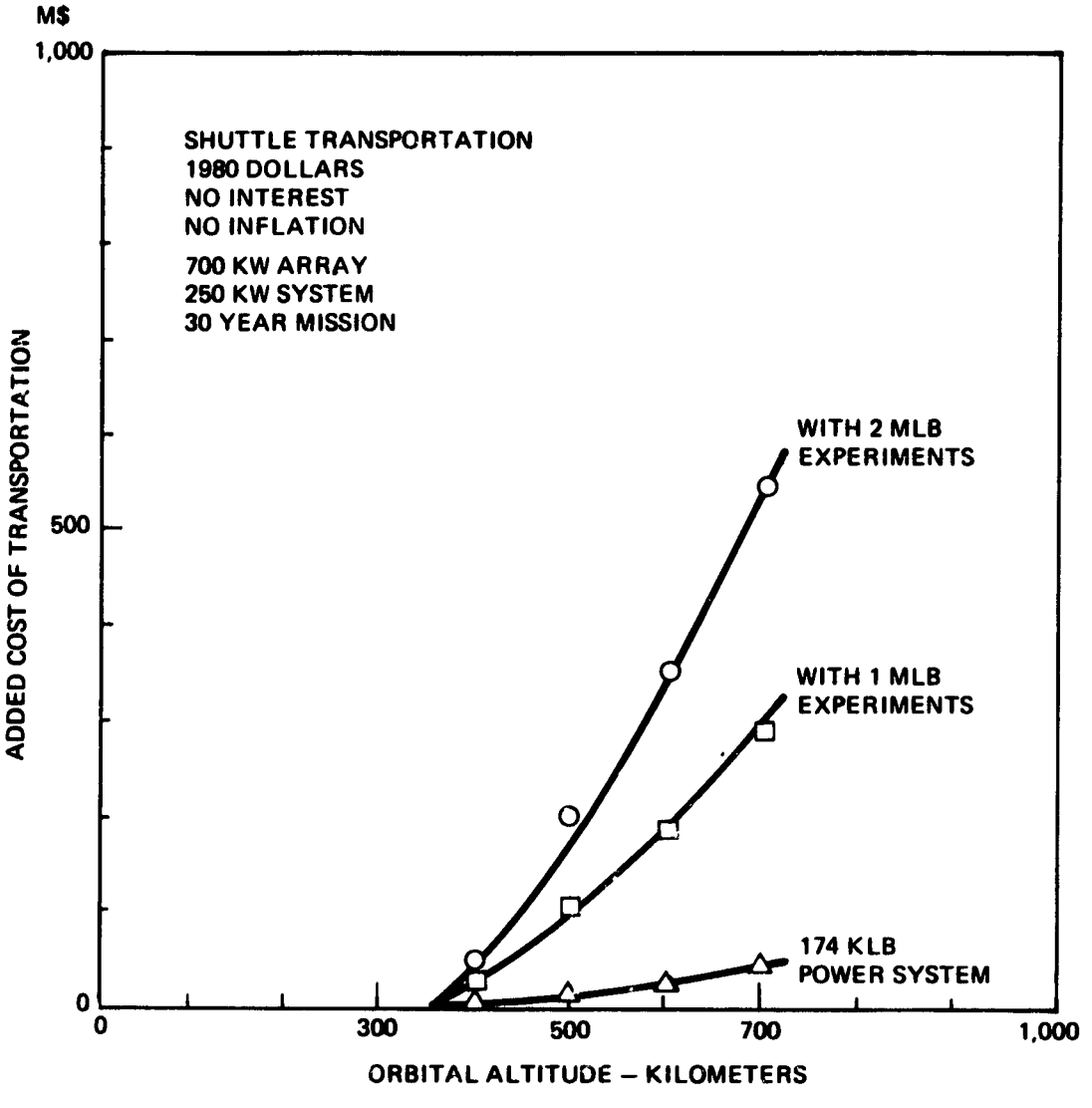

Figure 3. Higher Altitudes Increase Transportation Costs

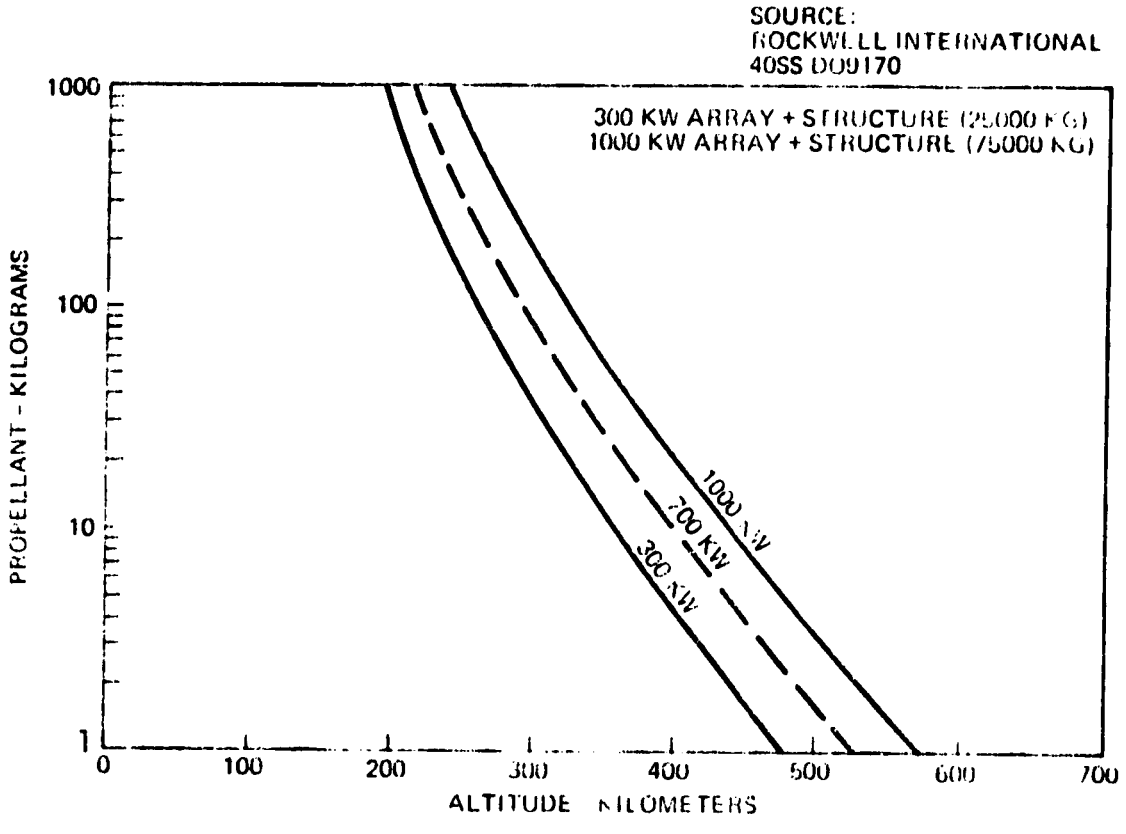

Figure 4. Daily Propellant Requirement

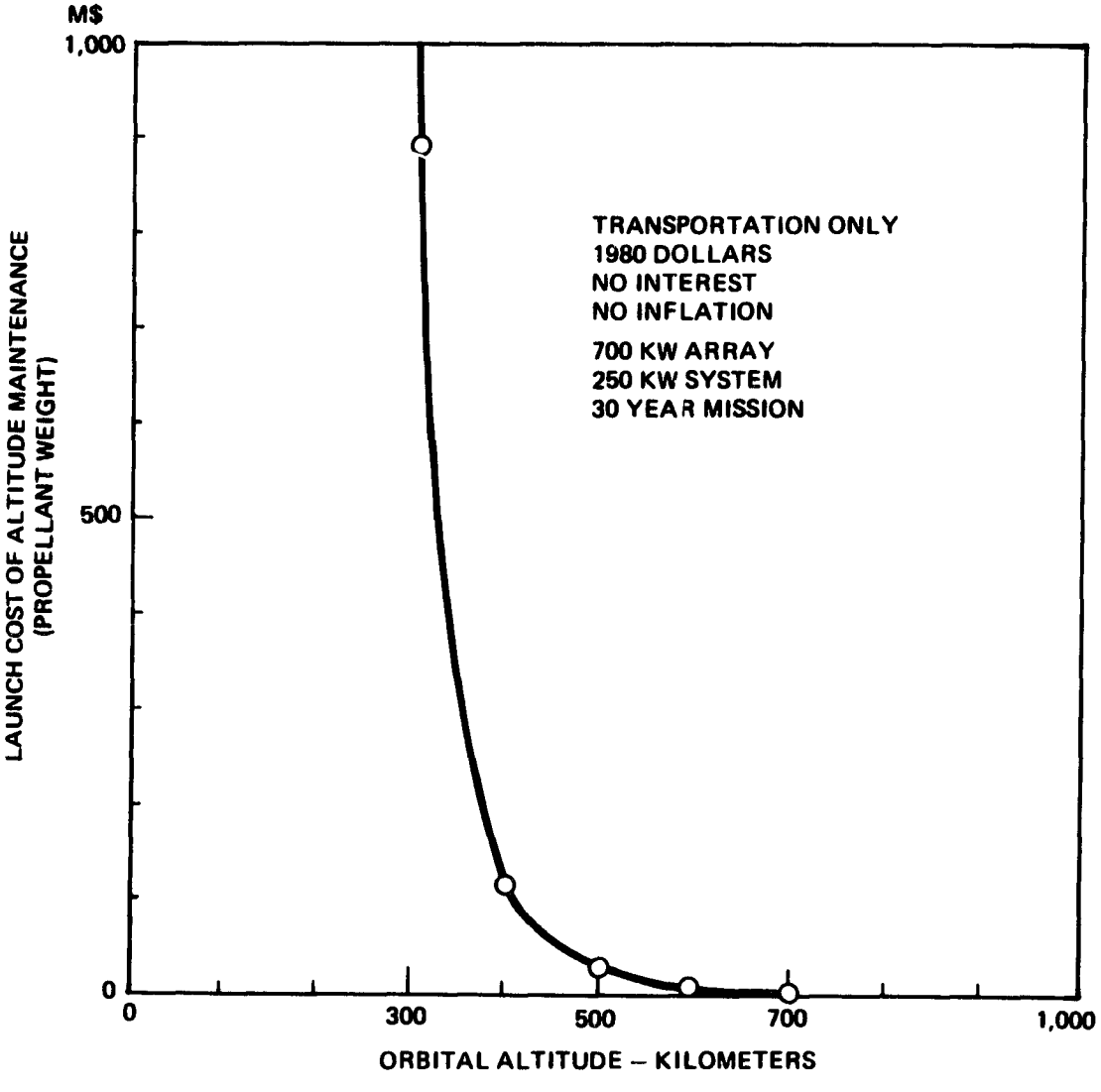

Figure 5. Low Orbit Maintenance Is Expensive

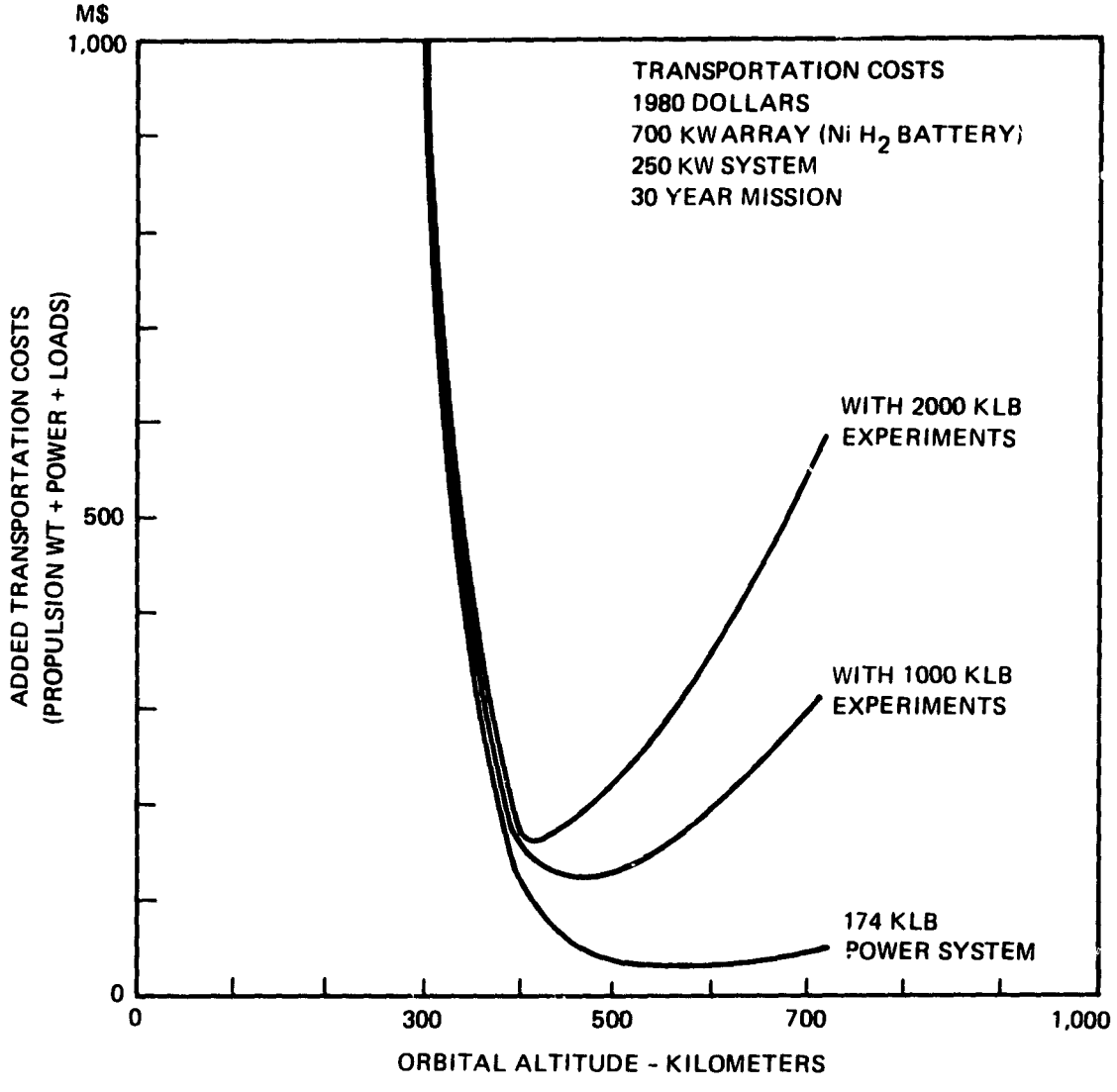

Figure 6. Optimum Altitude Near 400 km

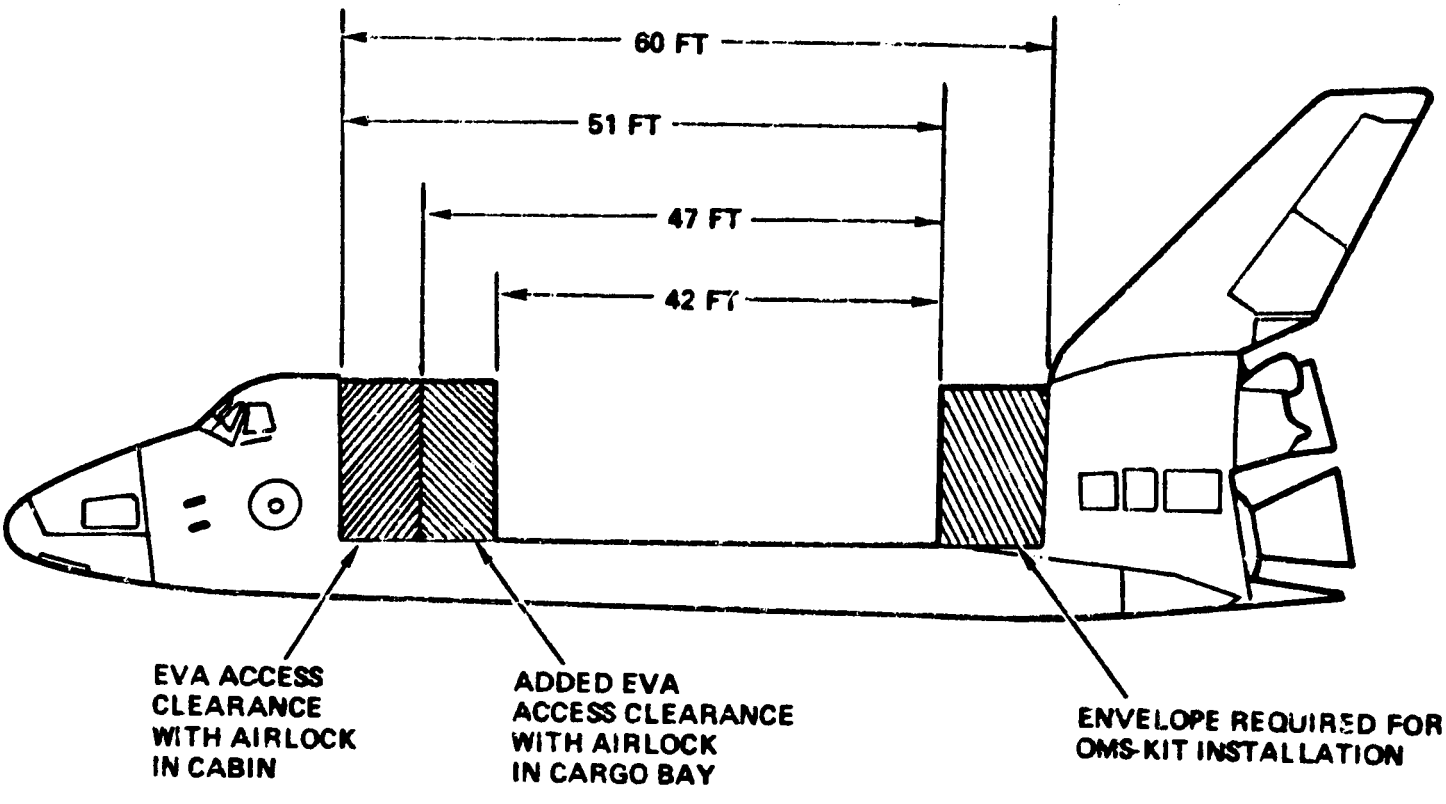

Figure 7. EVA and OMS Reduce Cargo Volume

APPENDIX D

OPTIMUM-COST CONDUCTOR ANALYSIS

The cost for electrical power transmission is composed of the conductor cost plus the incremental cost of power generation and energy storage to supply the transmission losses and thermal control to dissipate these losses. In addition, the power conversion equipment must be increased to handle the incremental power due to these losses. As conductor size is increased, transmission losses decrease, and an optimization exists. This optimization includes weight considerations as weight is translated into cost by the Shuttle transportation charge of 462 $/lb.

1. DERIVATION

The cost for electrical power transmission is the sum of five relatable terms:

$$C_{trans} = C_{wire} + C_{power_\Delta} + C_{energy_\Delta} + C_{thermal_\Delta} + C_{conv_\Delta}$$

where

C_{wire} = the cost of electrical power conductors.

C_{power_Δ} = the cost of the incremental increase in power generation (solar array) to supply the transmission losses.

C_{energy_Δ} = the cost of the incremental increase in energy storage capacity (battery) to supply the transmission energy losses during eclipse.

$C_{thermal_\Delta}$ = the cost of the incremental increase in thermal control equipment (radiators, plumbing, pumps) to dissipate the electrical transmission loss and the associated increase in energy storage thermal losses and conversion equipment losses.

C_{conv_Δ} = the cost of the incremental increase in power conversion/regulation equipment due to the increased load attributable to transmission conductor loss.

Each of these terms is complex but is related to the parameters of the transmission conductor under consideration (Figure D-1).

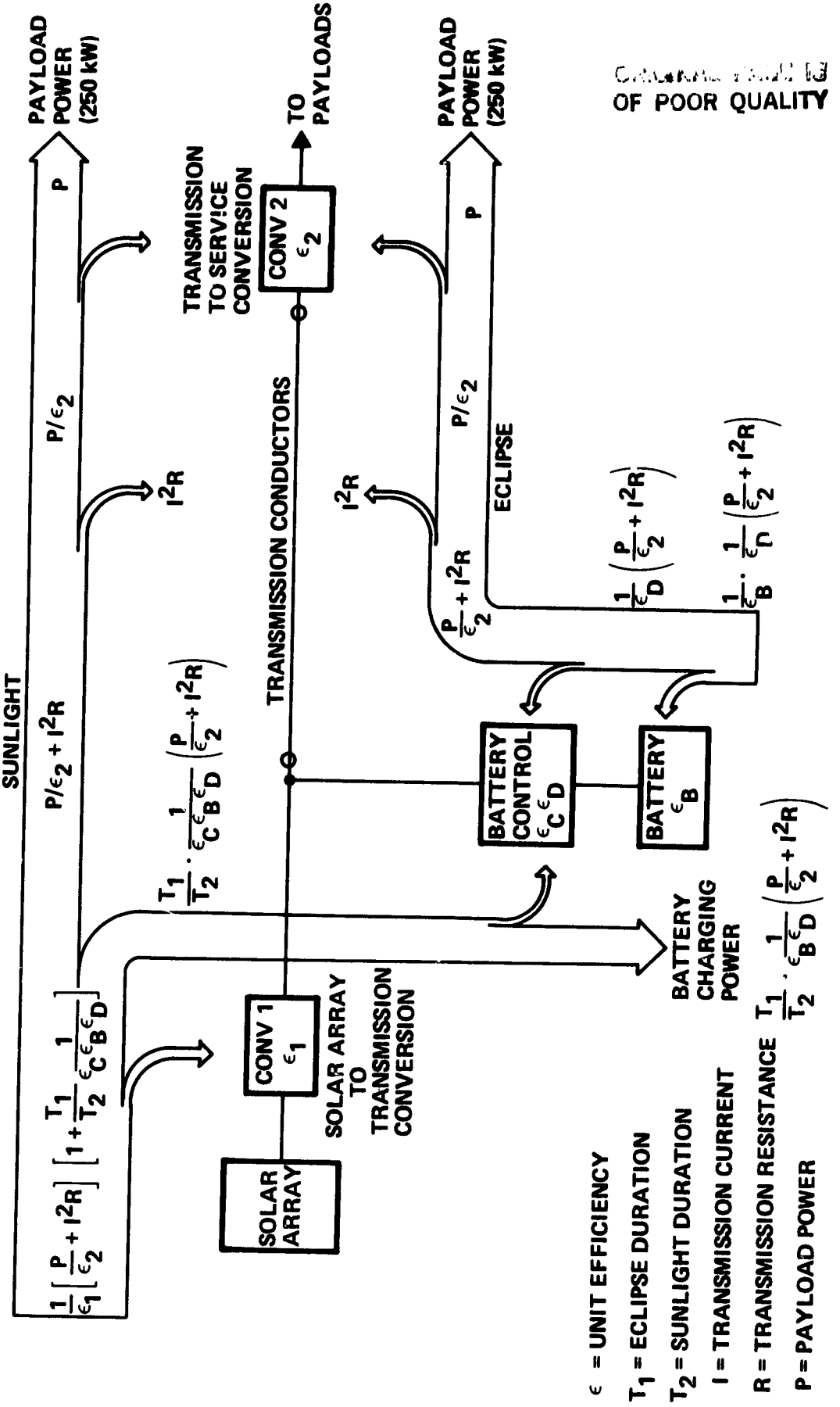

Figure D-1. Power Flow in Transmission Subsystem

1.1 Conductors

Transmission conductors for a 250-kilowatt system are expected to be large, possibly bus bars. Hence their cost is more relatable to structural elements, and therefore, size, weight, and material, rather than to harness costs of typical small satellites wherein connector and wire count are the significant parameters. The transmission conductor volume is the product of the total cross-sectional area (A) and the length of transmission (ℓ).* Multiplying this conductor volume by the density (σ) of the selected material yields the weight of the conductors. Applying the appropriate specific cost for conductor manufacture and Shuttle transportation produces the total conductor cost:

$$C_{wire} = (C_{MW} + C_L)\ \sigma A \ell = C_W\ \sigma A \ell, \text{ dollars}$$

where

C_W = specific wire cost, \$/lb

C_L = specific launch cost, 462 \$/lb

C_{MW} = specific cost to manufacture conductors, \$/lb

σ = material density, lb/cu ft

A = cross-section of conductor, sq ft

ℓ = length of conductor, feet.

The specific cost to manufacture conductors (C_{MW}) is considered a function of the material selected for the conductors. For example, C_{MW} for copper bars is ≈ 135 \$/lb, while for pure aluminum C_{MW} is ≈ 446 \$/lb.

*The transmission length, or conductor cross section must include the power return path.

1.2 Energy

During eclipse, the losses of the transmission conductors (Figure D-2) must be supplied by the energy storage subsystem and increase the requirement for energy storage capacity. The transmission energy losses during eclipse are directly proportional to the transmission line power loss (I^2R), and the eclipse time (T_1):

$$\text{Transmission energy losses} = \frac{I^2RT_1}{60} \text{ Wh, T in minutes}$$

The energy storage subsystem must also supply the losses for the efficiency of the battery discharge controller (ϵ_D) and the discharge losses within the battery and must provide an allowable depth of discharge (D) that is considerably less than one. These factors increase the required energy storage (battery) capacity by:

$$\text{Added energy storage required} = \frac{I^2RT_1}{60} \cdot \frac{1}{\epsilon_D} \cdot \frac{1}{\epsilon_B} \cdot \frac{1}{D} \text{ Wh}$$

where ϵ_B represents the electrochemical efficiency of the battery and charge method. This efficiency (ϵ_B) is effectively the discharge plateau voltage (1.20 volts per cell) divided by the charge voltage (1.45 volts per cell) for Ni-Cd or Ni-H_2 cells, and a further effective reduction due to the overcharge ratio (typically 1:1.05):

$$\epsilon_B = \frac{1.20}{1.45} \cdot \frac{1}{1.05} = 0.788$$

The current (I) identified herein (Figure D-2) is the transmission line current and hence is equal to the load power (P) increased by the transmission to service conversion efficiency (ϵ_2) and divided by the transmission line voltage (V):

$$I = \frac{P/\epsilon_2}{V} = \frac{P}{V\epsilon_2} \text{ amperes}$$

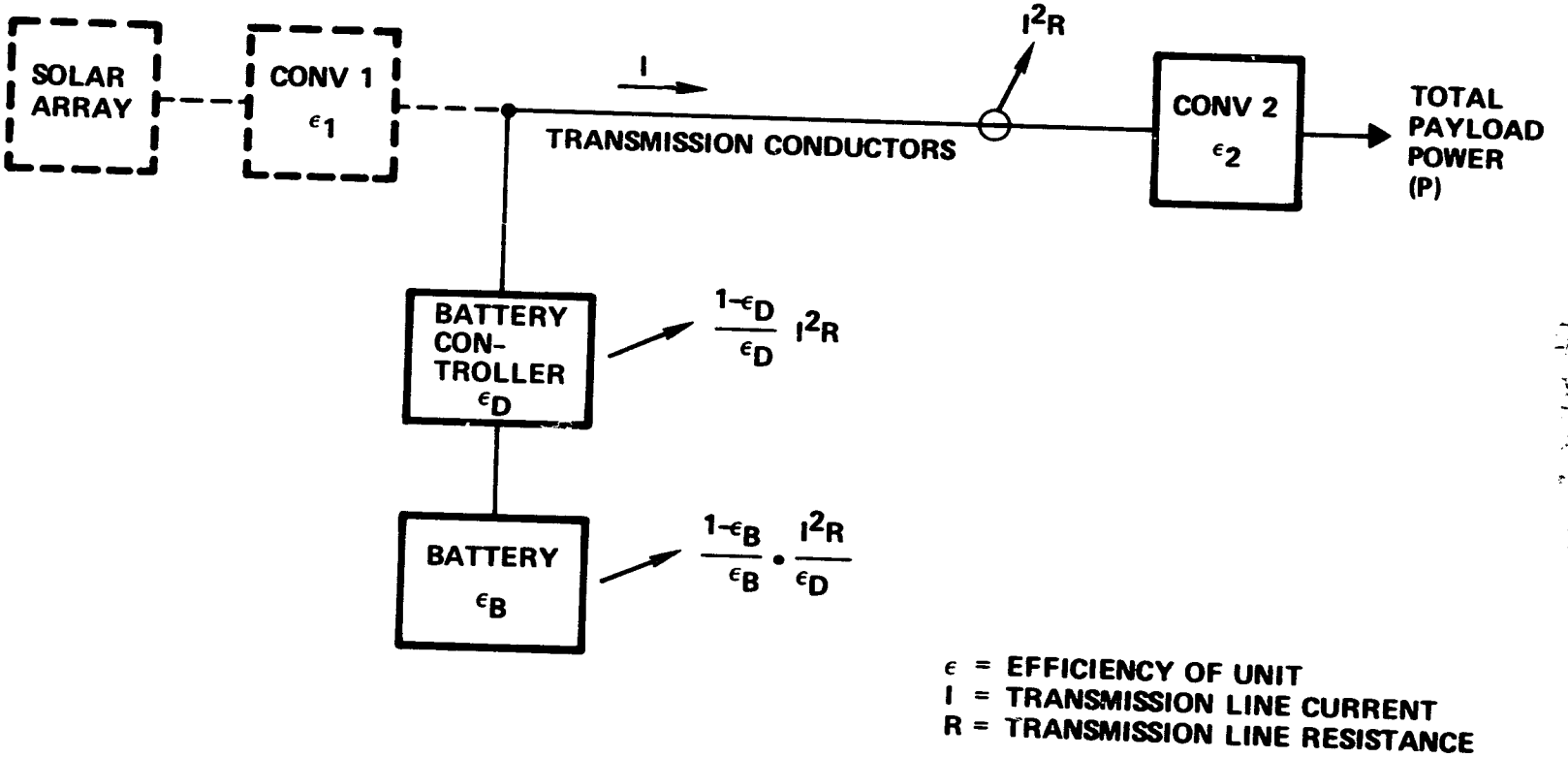

Figure D-2. Losses Attributable to Transmission Conductors (Eclipse)

The transmission conductor resistance proportional to the product of the conductor material resistivity (ρ) and length (ℓ) and inversely proportional to the cross-sectional area (A):

$$R = \left(\frac{\rho \ell}{A}\right)$$

Hence the increase in battery capacity due to transmission losses is:

$$\text{Battery capacity increase} = \left(\frac{P}{V\epsilon_2}\right)^2 \frac{\rho \ell}{A} \frac{T_1}{60} \frac{1}{\epsilon_D} \frac{1}{\epsilon_B} \frac{1}{D} \text{ Wh}$$

Multiplying this capacity by the specific costs for manufacturing and Shuttle transportation of batteries yields:

$$\text{Initial cost} = C_E \left(\frac{P}{V\epsilon_2}\right)^2 \frac{\rho \ell}{A} \frac{T_1}{60} \frac{1}{\epsilon_D \epsilon_B D} \text{ dollars}$$

where

C_E = the specific energy cost, \$/wh; $(C_{ME} + C_{LE})$

C_{ME} = the specific manufacturing cost, \$/Wh

C_{LE} = the specific launch cost, \$/Wh.

These values must be determined for each battery type considered. The battery is a life-limited device, and an additional factor must be added for replacement costs based upon an identified mean battery life (L_i). This produces the incremental cost for energy due to transmission losses over the satellite operational life (L_s) of:

$$C_{\text{energy}\Delta} = C_E \left(\frac{P}{V\epsilon_2}\right)^2 \frac{\rho \ell}{A} \frac{T_1}{60} \frac{1}{\epsilon_D \epsilon_B D} \left(1 + \frac{L_s}{L_i}\right) \text{ dollars}$$

1.3 Power

The area of the solar array must be increased to support the transmission conductor losses during the sunlight period and to recharge the battery incremental energy added to support transmission conductor losses during eclipse (Figure D-1). The direct losses (Figure D-3) to be supplied by the solar array are:

$$P_{loss} = I^2R = \left(\frac{P}{V\epsilon_2}\right)^2 \frac{\rho \ell}{A} \text{ watts}$$

where

P = load power, watts

ϵ_2 = transmission to service conversion efficiency

V = transmission line voltage

ρ = transmission conductor resistivity, Ω-ft

ℓ = transmission conductor length, feet

A = total conductor cross section, sq ft

The beginning-of-life solar array power necessary to support this power is increased by the solar-array-to-transmission conversion efficiency (ϵ_1) and the end-of-life degradation factor for the array (d):

$$P_{SA1} = \left(\frac{P}{V\epsilon_2}\right)^2 \frac{\rho \ell}{A} \cdot \frac{1}{\epsilon_1 d} \text{ watts}$$

The solar array indirect losses to be supplied via the battery subsystem are:

$$P_{loss} = \left(\frac{P}{V\epsilon_2}\right)^2 \frac{\rho \ell}{A} \cdot \frac{T_1}{60} \cdot \frac{1}{\epsilon_D \epsilon_B} \cdot \frac{60}{T_2} \cdot \frac{1}{\epsilon_C} \text{ watts}$$

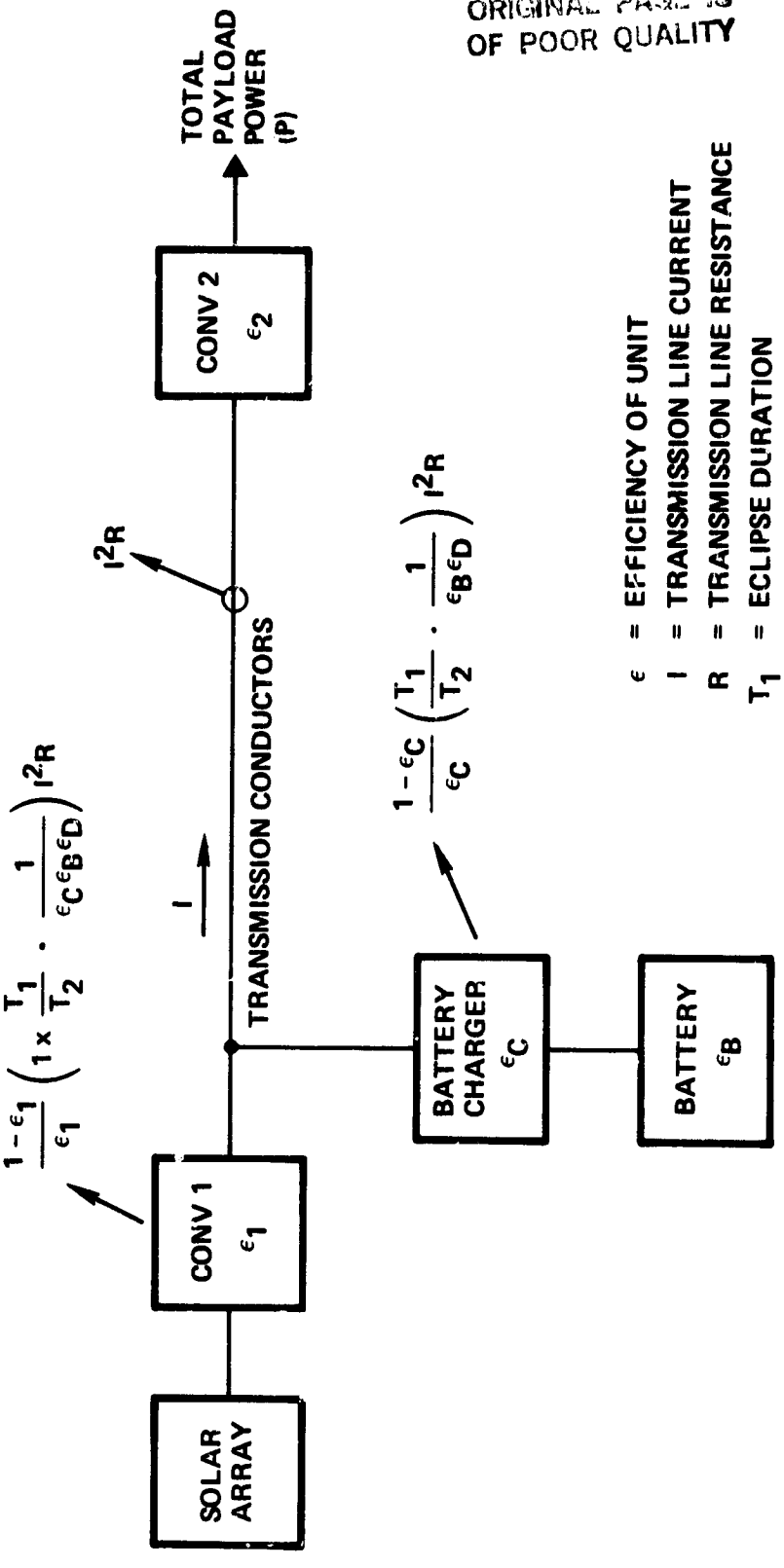

Figure D-3. Losses Attributable to Transmission Conductors (Sunlight)

where T_2 = sunlight duration in minutes and ϵ_c = the battery charger efficiency. Again, the beginning-of-life solar array power necessary to support this power is increased by the solar-array-to-transmission conversion efficiency (ϵ_1) and the end-of-life degradation factor for the array (d):

$$P_{SA2} = \left(\frac{P}{V\epsilon_2}\right)^2 \frac{\rho \ell}{A} \cdot \frac{T1}{T_2} \cdot \frac{1}{\epsilon_D \epsilon_B \epsilon_C} \cdot \frac{1}{\epsilon_1} \cdot \frac{1}{d} \text{ watts}$$

Summing these two terms, combining common factors, and applying the specific cost (C_{ps}) for solar array power yields the incremental cost of power generation for transmission losses:

$$C_{power_\Delta} = C_{ps} \left(\frac{P}{V\epsilon_2}\right)^2 \frac{\rho \ell}{A} \frac{1}{\epsilon_1 d} \left(1 + \frac{T_1}{T_2} \frac{1}{\epsilon_D \epsilon_B \epsilon_C}\right) \text{dollars}$$

1.4 Thermal

Electrical power system losses eventually become thermal subsystem heat inputs. The thermal subsystem must, therefore, dissipate these incremental losses from the electrical transmission components. These losses are the customary I^2R conductor loss plus the incremental increase in losses in the conversion and power handling equipment and in the battery on discharge and overcharge due to this additional transmission load of I^2R.

There are two separate and distinct sets of transmission loss levels. One level occurs during eclipse and is the sum of the transmission conductor loss, battery discharge controller incremental loss, and battery discharge (and overcharge) incremental loss (Figure D-2). The second level occurs during sunlight and is the sum of the transmission conductor loss, the battery charger incremental loss, and the incremental loss in solar-array-to-transmission line conversion (Figure D-3). These losses do not occur simultaneously. Hence, the thermal subsystem must be designed for the worst case aspects of each individual condition -- eclipse load and/or sunlight load.

During eclipse, there are three major sources of transmission conductor related losses (Figure D-2):

1) The conductor, I^2R = loss
2) The battery discharger, ϵ_D = efficiency
3) The battery discharge and overcharge, ϵ_B = effective efficiency.

The transmission line conductor loss (I^2R) is relatable to the load power (P), the transmission voltage (V), the transmission-to-service conversion efficiency (ϵ_2), the length (ℓ), cross-sectional area (A), and resistivity (ρ) of the conductors:

$$I^2R = \left(\frac{P/\epsilon_2}{V}\right)^2 \frac{\rho\ell}{A} \text{ watts}$$

The battery discharge controller (conversion and/or regulation) must handle an increased output power (over and above the payload requirement) equal to the transmission line loss. To accomplish this, the input power increases by the efficiency factor ($1/\epsilon_D$) of the discharge controller conversion/regulation equipment· I^2R/ϵ_D. The power loss in the discharge controller is then one minus the efficiency times the input power:

$$P_{\text{loss D}} = (1 - \epsilon_D)(I^2R/\epsilon_D) = \left(\frac{1 - \epsilon_D}{\epsilon_D}\right)\left(\frac{P}{V\epsilon_2}\right)^2 \frac{\rho\ell}{A} \text{ watts}$$

The battery produces heat during discharge due to the difference in the electrochemical voltage (1.45 volts/cell) and the output plateau voltage (1.20 volts/cell) - Ni-Cd or Ni-H_2 cells. In addition, the majority of the overcharge energy is returned in the form of heat from oxygen recombination during discharge. Hence, the effective efficiency (ϵ_B) previously derived for the battery is applicable to the losses on the discharge cycle:

$$\epsilon_B = \frac{1.20}{1.45} \times \frac{1}{1.05} = 0.788 \text{ for Ni-Cd or Ni-}H_2,$$

where 1.05 is the overcharge ratio.

The battery incremental output power for the transmission line loss of I^2R is increased to I^2R/ϵ_D by the efficiency of the battery discharge controller conversion/regulation equipment. The battery incremental input power is increased by the battery efficiency (ϵ_B) to: $I^2R/\epsilon_B\epsilon_D$. The battery incremental loss due to transmission line power loss is the difference in input and output powers:

$$P_{loss\ B} = \left(\frac{1-\epsilon_B}{\epsilon_B}\right)\left(\frac{1}{\epsilon_D}\right)\left(\frac{P}{V\epsilon_2}\right)^2 \frac{\rho\ell}{A} \text{ watts}$$

Eclipse losses are the sum of these increments (I^2R, $P_{loss\ D}$, $P_{loss\ B}$):

$$P_{loss\ eclipse} = \left(\frac{P}{V\epsilon_2}\right)^2 \frac{\rho\ell}{A}\left(1 + \frac{1-\epsilon_D}{\epsilon_D} + \frac{1-\epsilon_B}{\epsilon_B\epsilon_D}\right) \text{watts}$$

Note, however, that each of these loss terms affects the thermal subsystem in a different way. The I^2R term, $(P/V\epsilon_2)^2\ \rho\ell/A$, produces distributed heat over the transmission distance and is probably absorbed and radiated by the module structure. The battery discharger loss is an electronic loss and will increase the payload/electronic thermal radiator area and equipment (plumbing and pumps) accordingly. The battery discharge loss occurs within the battery. The battery is required to be one of the cooler equipment areas of the 250-kilowatt system, and this loss will require a significantly increased radiator area - proportionate to battery cooling requirements.

During sunlight, there are three major sources of transmission related losses (Figure D-3):

1) The conductor, I^2R

2) The battery charger, ϵ_C = efficiency

3) The solar array to transmission line conversion, ϵ_1 = efficiency.

The conductor loss (I^2R) is as previously derived:

$$I^2R = \left(\frac{P}{V\epsilon_2}\right)^2 \frac{\rho\ell}{A} \text{ watts}$$

The battery charger handles an output power level sufficient to replace the energy utilized during eclipse. Thus, the incremental power is equal to the I^2R conductor loss increased by the battery discharge controller efficiency (ϵ_D) and the battery effective efficiency (ϵ_B) and ratioed by the eclipse-to-sunlight times (T_1/T_2):

$$\text{Output power} = \frac{T_1}{T_2} \times \frac{1}{\epsilon_B \epsilon_D} \times I^2R \text{ watts}$$

The incremental loss in the battery charger is then:

$$P_{\text{loss C}} = \left(\frac{1-\epsilon_C}{\epsilon_C}\right)\left(\frac{T_1}{T_2}\right)\left(\frac{1}{\epsilon_B \epsilon_D}\right)\left(\frac{P}{V\epsilon_2}\right)^2 \frac{\rho \ell}{A} \text{ watts}$$

where ϵ_C is the battery changer efficiency.

The solar-array-to-transmission line conversion must simultaneously handle the incremental power of the transmission conductor loss (I^2R) and the incremental battery charging power from above. The incremental loss in the solar-array-to-transmission line conversion is then:

$$P_{\text{loss 1}} = \left(\frac{1-\epsilon_1}{\epsilon_1}\right)\left(1 + \frac{T_1}{T_2} \cdot \frac{1}{\epsilon_C \epsilon_B \epsilon_D}\right)\left(\frac{P}{V\epsilon_2}\right)^2 \frac{\rho \ell}{A} \text{ watts}$$

Sunlight losses are the sum of these increments:

$$P_{\text{loss sun}} = \left(\frac{P}{V\epsilon_2}\right)^2 \frac{\rho \ell}{A}\left[1 + \left(\frac{1-\epsilon_C}{\epsilon_C}\right)\left(\frac{T_1}{T_2}\frac{1}{\epsilon_B \epsilon_D}\right) + \left(\frac{1-\epsilon_1}{\epsilon_1}\right)\left(1 + \frac{T_1}{T_2}\frac{1}{\epsilon_C \epsilon_B \epsilon_D}\right)\right] \text{ watts}$$

Again note that the I^2R term, $(P/V\epsilon_2)^2\, \rho\ell/A$, produces distributed heat over the transmission distance and is probably absorbed and radiated by the module structure. The other two terms are an electronic loss and will increase the payload/electronic thermal radiator area and equipment accordingly. These two electronic losses are larger than the battery

discharge controller electronic loss during eclipse and become the size/cost determining factors:

$$\left(\frac{1-\epsilon_C}{\epsilon_C}\right)\left(\frac{T_1}{T_2}\,\frac{1}{\epsilon_B\epsilon_D}\right)+\left(\frac{1-\epsilon_1}{\epsilon_1}\right)\left(1+\frac{T_1}{T_2}\,\frac{1}{\epsilon_C\epsilon_B\epsilon_D}\right)>\frac{1-\epsilon_D}{\epsilon_D}$$

Thermal costs are then derived by applying the appropriate specific costs to each dominant term:

$$C_{\text{thermal}\ \Delta} = C_{TSW}\cdot I^2R + \qquad \text{[Conductor]}$$

$$C_{TSE}\cdot I^2R\left[\left(\frac{1-\epsilon_C}{\epsilon_C}\right)\left(\frac{T_1}{T_2}\,\frac{1}{\epsilon_B\epsilon_D}\right)+\left(\frac{1-\epsilon_1}{\epsilon_1}\right)1+\frac{T_1}{T_2}\,\frac{1}{\epsilon_C\epsilon_B\epsilon_D}\right]+ \qquad \text{[Electronics]}$$

$$C_{TSB}\cdot I^2R\left[\frac{1-\epsilon_B}{\epsilon_B}\left(\frac{1}{\epsilon_D}\right)\right]\text{dollars} \qquad \text{[Battery]}$$

where C_{TSW}, C_{TSE}, and C_{TSB}, are specific costs in \$/W.

1.5 Conversion

Three power conversion/regulation equipment areas must be increased in power capability to accommodate the transmission line loss:

1) Battery discharge controller, ΔP_D watts

2) Battery charger, ΔP_C watts

3) Solar-array-to-transmission line conversion, ΔP_1, watts.

The battery discharge controller power capability is increased directly by the transmission loss, I^2R:

$$\Delta P_D = I^2R = \left(\frac{P}{V\epsilon_2}\right)^2\frac{\rho\ell}{A}\ \text{watts}$$

The battery charger power rating is increased by the transmission line loss (I^2R) increased by the discharger efficiency (ϵ_D), the battery efficiency (ϵ_B), and the ratio of eclipse duration to sunlight duration (T_1/T_2):

$$\Delta P_C = I^2R \cdot \frac{1}{\epsilon_D} \cdot \frac{1}{\epsilon_B} \cdot \frac{T_1}{T_2} = \left(\frac{P}{V\epsilon_2}\right)^2 \frac{\rho \ell}{A}\left(\frac{T_1}{T_2}\frac{1}{\epsilon_B \epsilon_D}\right) \text{ watts}$$

The solar-array-to-transmission line conversion must simultaneously handle the incremental power for transmission conductor loss (I^2R) and the incremental battery charging power attributable to the transmission conductor loss during eclipse:

$$\Delta P_1 = I^2R + I^2R\left(\frac{T_1}{T_2}\frac{1}{\epsilon_D \epsilon_B \epsilon_C}\right) \text{ watts}$$

Multiplying these power increments by their respective specific costs ($/W) produces the incremental cost for power conversion equipment:

$$C_{conv\ \Delta} = C_{CSD} \cdot \Delta P_D + C_{CSC} \cdot \Delta P_C + C_{CS1} \cdot \Delta P_1 \text{ dollars}$$

$$= \left(\frac{P}{V\epsilon_2}\right)^2 \frac{\rho \ell}{A}\left(C_{CSD} + \frac{T_1 C_{CSC}}{T_2 \epsilon_B \epsilon_D} + C_{CS1} + \frac{T_1 C_{CS1}}{T_2 \epsilon_C \epsilon_B \epsilon_D}\right)$$

where C_{CSD}, C_{CSC}, and C_{CS1} are the respective specific costs of the conversion equipment.

2. OPTIMIZATION

Summing the derived terms for the costs of wire and incremental power, energy, thermal, and conversion equipment yields a complex but interesting equation:

$$C_{trans} = C_{wire} + C_{energy\Delta} + C_{power\Delta} + C_{thermal\Delta} + C_{conv\Delta}$$

$$C_{trans} = (C_{MW} + C_L)\,\sigma A \ell \qquad \text{[Wire]}$$

$$+ (C_{ME} + C_{LE}) \left(\frac{P}{V\epsilon_2}\right)^2 \frac{\rho \ell}{A} \frac{T_1}{60} \frac{1}{\epsilon_D \epsilon_B D} \left(1 + \frac{L_s}{L_i}\right) \qquad \text{[Energy]}$$

$$+ C_{PS} \left(\frac{P}{V\epsilon_2}\right)^2 \frac{\rho \ell}{A} \frac{1}{\epsilon_1 d} \left(1 + \frac{T_1}{T_2} \frac{1}{\epsilon_C \epsilon_B \epsilon_D}\right) \qquad \text{[Power]}$$

$$+ \left(\frac{P}{V\epsilon_2}\right)^2 \frac{\rho \ell}{A} \left[C_{TSW} + C_{TSB} \frac{(1-\epsilon_B)}{\epsilon_B \epsilon_D} + C_{TSE(Z)}\right] \qquad \text{[Thermal]}$$

$$+ \left(\frac{P}{V\epsilon_2}\right)^2 \frac{\rho \ell}{A} \left(C_{CSD} + \frac{T_1 C_{CSC}}{T_2 \epsilon_B \epsilon_D} + C_{CS1} + \frac{T_1 C_{CS1}}{T_2 \epsilon_C \epsilon_B \epsilon_D}\right) \qquad \text{[Conversion]}$$

where

$$Z = \left(\frac{1-\epsilon_C}{\epsilon_C}\right)\left(\frac{T_1}{T_2} \cdot \frac{1}{\epsilon_B \epsilon_D}\right) + \left(\frac{1-\epsilon_1}{\epsilon_1}\right)\left(1 + \frac{T_1}{T_2} \cdot \frac{1}{\epsilon_C \epsilon_B \epsilon_D}\right)$$

Simplifying the algebra:

$$C_{trans} = (C_{MW} + C_L)\,\sigma A \ell + \left(\frac{P}{V\epsilon_2}\right)^2 \frac{\rho \ell}{A} \qquad \text{[factor]}$$

where [factor] =

$$(C_{ME} + C_{LE}) \frac{T_1}{60\epsilon_B\epsilon_D D}\left(1 + \frac{L_s}{L_i}\right) \qquad \text{[Energy]}$$

$$+ \frac{C_{ps}}{\epsilon_1 d}\left(1 + \frac{T_1}{T_2\epsilon_C\epsilon_B\epsilon_D}\right) \qquad \text{[Power]}$$

$$+ C_{TSW} + \frac{C_{TSB}\,(1-\epsilon_B)}{\epsilon_B\epsilon_D} + C_{TSE}\left[\left(\frac{1-\epsilon_C}{\epsilon_C}\right)\frac{T_1}{T_2\epsilon_B\epsilon_D} + \left(\frac{1-\epsilon_1}{\epsilon_1}\right)\left(1 + \frac{T_1}{T_2\epsilon_C\epsilon_B\epsilon_D}\right)\right] \qquad \text{[Thermal]}$$

$$+ C_{CSD} + \frac{C_{CSC}\,T_1}{T_2\epsilon_B\epsilon_D} + C_{CS1}\left(1 + \frac{T_1}{T_2}\,\frac{1}{\epsilon_C\epsilon_B\epsilon_D}\right) \qquad \text{[Conversion]}$$

Note that [factor] is not a function of ℓ, P, A, ρ, σ, or V!
Differentiating with respect to A, setting the result equal to zero, and solving for A yields the optimum-cost cross-sectional area (A_o) for transmission conductors:

$$\frac{d(C_{trans})}{dA} = (C_{MW} + C_L)\,\sigma\ell - \left(\frac{P}{V\epsilon_2}\right)^2 \frac{\rho\ell}{A^2}[\text{factor}] = 0$$

$$A_o = \frac{P}{V\epsilon_2}\sqrt{\frac{\rho}{\sigma(C_{MW} + C_L)}\,[\text{factor}]}$$